# Strangeness Production in a Quark-Gluon Plasma

**D J Hislop**

25 October 1996



A thesis submitted in fulfilment of the
requirements for the degree of
**Doctor of Philosophy**
in the Department of Physics
University of Cape Town
Republic of South Africa

# Contents

# List of Tables

# Preamble

## 1 Introduction

Central collisions of heavy nuclei at ultrarelativistic energies are expected to lead to a quark-gluon plasma (deconfined quark matter). Theoretical arguments from lattice-QCD (quantum chromodynamics) simulations and finite temperature quantum field theory, predict that at sufficiently high temperatures, around 150 MeV, a phase transition from ordinary nuclear matter will lead to deconfined quarks. Since deconfined matter has a characteristic lifetime, $\tau$, of less than about 10fm/c ($3 \times 10^{-24}$ seconds), experiments will have to be able to find some distinctive remnants of this phase that can survive until the baryons and mesons are counted.

Already at the Brookhaven's Alternating Gradient Synchrotron (BNL-AGS) and the European Centre for Nuclear Research's Super Proton Synchrotron (CERN-SPS) second generation data are being produced ($Pb$ beams with a beam momentum of $150-160$ GeV$\cdot A$ in CERN and $Au$ beams with a beam momentum of $10-15$GeV$\cdot A$ at Brookhaven). It is expected that observing the production of photon and non-resonance lepton pairs will be the most direct way of 'seeing' the plasma. $J/\psi$ production, strangeness enhancement and the production of exotic structures (strangelets and MEMO's - Metastable Exotic Multistrange Objects) are also considered to be important.

We are particularly interested in strangeness production as a signature for the formation of a quark-gluon plasma. Relativistic Heavy Ion Collisions (RHIC's) have an observed enhanced strangeness production relative to nucleon-nucleon or nucleon-nucleus collisions at the same energy. The formation of a quark-gluon plasma (QGP) could explain this discovery, but so too could thermal models of hadron production.

Models of thermal production of strange particles in the hadronic sector are able to give a good fit to the ratios of strange particles ($K^+$, $K^-$, $K^o_s$, $\Lambda$, $\overline{\Lambda}$, $\Xi^-$, $\overline{\Xi^-}$, $\Omega^-$ and $\overline{\Omega^-}$) in the data. The predictions from thermal production impose severe restrictions on the limited number of thermodynamic parameters available. These parameters are accessible

experimentally and it is hoped they will help explain strangeness production.

Microscopically, the production of strange quarks could originate from QCD mechanisms producing strange quarks from gluon fusion, gluon decay and the annihilation of quark/antiquark pairs. Nonetheless the subtle effects of the thermal medium remain to be fully understood. We summarise some aspects of thermal field theory appropriate to this thesis in Chapter 2. Of particular importance are the Braaten-Pisarski resummation rules used to obtain the effective propagator and vertices of particles in a thermal medium. These rules show that the QCD coupling constant, $g$, is not a comprehensive enough expansion term. Due to the proliferation of diagrams in Thermal Field Theory, the Kobes-Semenoff rules are described because of their use in simplifying the calculation of rates. In Chapter 3 we outline the conventional perturbative QCD calculations of processes contributing to the production of strange quarks and plasmon decay into strange quarks with the intention of generalising these calculations to finite temperatures.

The aim of this thesis is to consider the evolution of strangeness from shortly after the initial collision to the little understood hadronisation phase, where thermodynamic models come into their own. Our simulation starts from a thermally equilibrated fireball composed of gluons (in thermal and chemical equilibrium) and with quarks far from chemical equilibrium. Using Bjorken's hydrodynamic scenario, we allow the gluons (and later quarks) to interact to produce a QGP. Of interest to us is the relative degree of chemical equilibrium of the strange quarks. The relative equilibrium is measured by a parameter, $\gamma_S$, which appears in the thermal hadron sector and quark models. If $\gamma_S = 1$, the strange quarks are in chemical equilibrium. Values of $\gamma_S$ less than one signify an undersaturation of strangeness phase space.

In this work we are not able to investigate the moment at which the hadron projectile and target disintegrate, nor are we able to probe the mechanism with which the quarks coalesce to form hadrons. We assume that a gluon plasma is formed and investigate the consequences of this assumption using QCD.

## 2 Outline

This thesis is arranged as follows:

**Chapter 1** notes that the production of strangeness measured at CERN and Brookhaven has two possible explanations. One is that strange quarks, being relatively light, are easily produced, creating an abundance of strange particles in the experiment. On the other hand, hadron gas models use only thermodynamics, strangeness neutrality and baryon number conservation to predict the same ratios. Both models need a parameter, $\gamma_S$, reflecting the relative departure from equilibrium of strangeness.

**Chapter 2** discusses the Cutkosky rules and their thermal field theory counterparts, the Kobes-Semenoff rules. The influence of the medium is brought into consideration through Braaten-Pisarski resummation.

In **Chapter 3** we use the Cutkosky rules to calculate the standard QCD quark production mechanisms. The intention is to eventually generalise these calculations to finite temperature. We then derive the rate of plasmon decay (gluons pick up finite masses and widths due to interactions with the medium), which was proposed by Tanguy Altherr and David Seibert [4, 7] to be another important mechanism for the production of strangeness.

In **Chapter 4** we use Bjorken's framework of one-dimensional hydrodynamic flow to study the evolution of a gluon plasma, through the production of quarks to a later stage, by which times hadrons should be prevalent. Of critical importance is the thermal equilibration time. We derive some analytic expressions for the proper time dependence of the chemical potential and temperature of the quark-gluon plasma.

**Chapter 5** concludes this thesis and sets out a program to be continued.

The **Appendices** summarise some useful data, notation and concepts with regard to make reading easier and to be used in continuing this research. Specifically the propagators and vertices of Thermal Field Theory (TFT) are listed as well as the cut propagators. Finally, at the end are listed **acknowledgments** and a **bibliography**.

# 3 Conclusion

The conclusion, demonstrated graphically on page 92, is that the saturation of the strange phase space is incomplete when the formation of hadrons should become significant. This lends credibility to the use of $\gamma_S$ in phenomenological models of hadrons and quarks.

This thesis also contains a brief survey of experimental data for strangeness ratios. There are also (model dependent) predicted values of the energy density ($\varepsilon$), pressure ($p$), temperature ($T$), chemical potential ($\mu$) and number density ($n$) for various scenarios. Analytic parameterisations of $\mu$ and $T$ as a function of proper time and mass are derived (page 74), as well as physical limits for this type of simulation.

In the chapters leading up to the pivotal chapter 4, we derive and record in detail results that would be needed to continue this study. Of particular importance are the Kobes-Semenoff and Braaten-Pisarski rules. Also intermediate steps in calculating different channels of strange quark production are recorded.

# Chapter 1

# A brief review of Phenomenology and Experiment

## 1.1 The Quark Gluon Plasma

Quarks are the basis of most models and theories in modern particle physics. In 1995 the mass of the top quark was established by the D0 [162] and CDF [163] collaborations at Fermilab. Despite the supporting weight of many theories and models an isolated quark has never been seen. The reasons for this are fundamental and crucial in casting light on questions about asymptotic freedom, confinement, the QCD phase transition and many other cornerstones of High Energy Particle physics. The hope and expectation is that in highly energetic collisions of heavy nuclei — relativistic heavy ion collisions or RHIC's — the vacuum state for strong interactions will be changed in such a way as to allow the propagation of free color charge. This should correspond to times of $10\mu s$ after the Big Bang.

Experimental results from RHIC's have been available for about ten years. Current experiments hover tantalisingly close to the phase transition from ordinary nuclear matter to a quark-gluon plasma. A quantitative interpretation of the reaction mechanism in a RHIC remains elusive; specifically the phase transition from a quark-gluon plasma to a phase characterised by hadronic interactions is needed. The unambiguous signature signifying the transition to a quark-gluon plasma has yet to be discerned.

Strangeness enhancement was advanced fifteen years ago as one possible signature for a quark-gluon plasma [116]. Experiments, at for example CERN SPS, show a strangeness enhancement of a factor of four relative to $p-p$ or $p-A$ reactions [105]. Significant success has been achieved at interpreting this result, but no unambiguous and decisive theory of RHIC's exists yet.

This chapter is arranged as follows: we do some order of magnitude calculations while reviewing some events of historical note. Experimental data is then recorded and used

in the investigation of thermal hadron models. The factor describing the deviation from chemical potential, $\gamma_S$, is introduced and its thermodynamic consistency justified. Finally we discuss the quark model from a thermodynamic perspective.

### 1.1.1 Relativistic Heavy Ion Collisions (RHIC's)

The following subsections introduce the lore of the Quark-Gluon Plasma.

#### A (brief) history of RHIC's

The history of RHIC's extends back to the 1950's when Fermi [164, 165] discussed the thermodynamics of $p - A$ collisions. He introduced the idea of stopping (in the centre of mass frame the target and projectile nuclei stop on colliding). Fermi identified three stages - Formation, Thermodynamic Equation of State/Expansion Hydrodynamics and Particle Production).

Other individuals who contributed were: Pomeranchuk [167], who introduced the freeze out temperature $T_f \simeq m_\pi$ and that there are far more pions than nucleons $N_\pi \gg N_{N,\overline{N}}$. Landau [166] developed relativistic hydrodynamics. Hagedorn [168] introduced the statistical bootstrap model by studying the density of states for higher hadron resonances at lower energies. He introduced a temperature, $T_H$, such that $T < T_H \simeq m_\pi$. This upper bound on the temperature was later explained in terms of a phase transition.

High energy relativistic heavy ion experimental programs began at the AGS and SPS accelerators in 1986-1987 after several years of planning.

#### Order of magnitude calculations

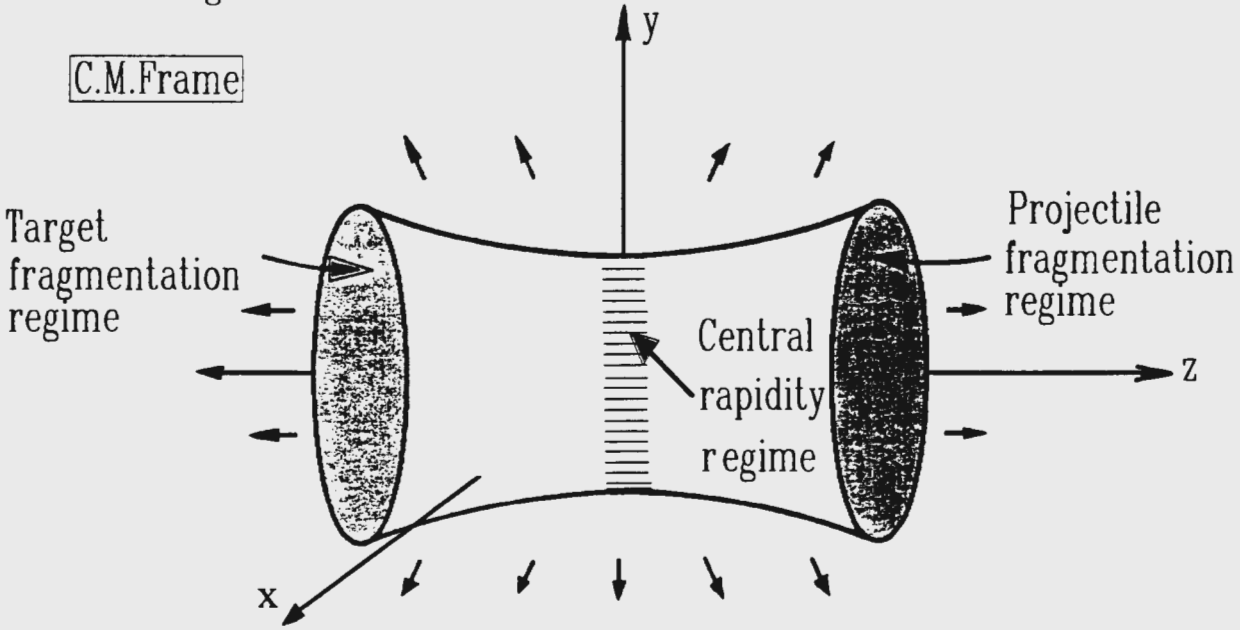


Figure 1.1.1: After a relativistic collision two pancakes recede...

It would be useful if we had some idea of the order of magnitude of the thermody-

namic quantities involved. Figure 1.1.1 represents a RHIC. The Lorentz contracted nuclei obliterate each other, and form a hot gas. The residual momentum stretches the gas in a longitudinal direction. The gas then hadronises and hadrons are detected. We will concentrate chiefly on $S-S$, $S-W$, $Au-Au$ and $Pb-Pb$ collisions at CERN-SPS ($\sqrt{s} = 17-20$ GeV·A) and BNL-AGS ($\sqrt{s} = 4-5$ GeV·A).

The energy at SPS for Sulphur is ($\sqrt{s} = 20$ GeV·A). Accordingly $E_{cm} = 10$ GeV·A, see appendix A.2 for the conversion between the different frames.

Hydrodynamic simulations are justified if the mean free path, $\lambda$, is much greater than the dynamics of the system. The mean free path is roughly given by $\lambda = \frac{1}{\rho\sigma}$. For nuclear matter $\rho = \frac{A}{V} = (0.15 - 0.2)$ nucleons/fm$^3$. The cross section for proton-proton collisions is $\sigma = (40-60)$mb. Since 1 fm$^2$ = 10 mb and assuming that in a RHIC both nuclei sit in the volume of one nucleus, then $\lambda \simeq (0.41 - 0.83)$ fm would be the mean free path of nucleons in the collision of two relativistic nuclei. Since we are contrasting this with a typical interaction length for strong reactions of 1 fm, we see that this is too small for hydrodynamic models, because the strong reaction will see the individual constituents of the nucleus, rather than allowing for collective effects. However we find that hydrodynamics are justified in RHIC's when we include relativistic effects.

Regarding the energy density we continue with the naive picture of all the kinetic energy being dumped into the volume of one nucleus. Using $\varepsilon = \frac{E_{cm}}{V}$ and the relation between volume and density used in the preceding paragraph, we find $\varepsilon = \frac{10A}{A/(0.15-0.2)} = (1.5 - 2)$ GeV/fm$^3$. We can compare this to that for protons (the proton mass is $m_p = 1$ GeV and charge radius is $r = 1$fm): $\varepsilon = E_{cm}/(\frac{4}{3}\pi r^3) \simeq 0.25$ GeV/fm$^3$.

Landau improved these simple results for a RHIC by assuming stopping in nucleus-nucleus collisions and using Lorentz contraction of the two nuclei. Using Lorentz contraction we obtain $\varepsilon = E_{cm}/(V \times m_p \cdot A/E_{cm}) = 20$ GeV/fm$^3$. This is probably an over-estimate. Bjorken [31] calculates $\varepsilon = A^{\frac{1}{3}} 0.5$ GeV/fm$^3$. $p$-$p$ collisions also lead to an increased energy density, but the initial volume, being that of a proton, is too localised.

The speed of sound is given by $v_s^2 = \frac{dP}{d\epsilon}$. Normally we work with a gas that is approximately massless and ideal. For this $\epsilon = 3p$ which implies that the speed of sound is $v_s = \frac{1}{\sqrt{3}}$. An estimate of the time taken for the hot compressed matter to cool by expanding to that of ordinary matter is done by noting that for the energy density to decrease from 4 GeV/fm$^3$ to 0.5 GeV/fm$^3$ the volume has to increase by a factor of 8. Therefore $\tau \sim 4$ fm is the time needed for the sound wave to travel over this volume for the increase to occur. Now $\lambda$ increasing by a factor of 8 is more promising from a thermodynamic point of view. We will assume that the use of thermodynamic and hydrodynamic equations are justified in RHIC's. We also do this under the assurances of the parton model calculation [65, 66, 67, 68].

The total lifetime of the fireball is about 8 fm, which should be compared with the hadronic timescale of 1 fm. The rapidity distribution of hadrons from a relativistic heavy ion collision is demonstrated in Figure A.1

**Timescale**

We supposed that the QGP goes through certain development stages. These values are listed in the next paragraph for argument sake only. Our values come from parton simulations [65, 66, 67, 68] and the results of Chapter 4.

In Figure 4.1 we have plotted schematically the trajectory of the projectile and target nuclei and the quark-gluon plasma. We list, in reverse chronological order, the following epochs, and some speculative times. We define t= $\tau = 0$ fm as the time when the two nuclei collide. The end of the hadronisation (the making of hadrons) epoch is characterised by $t_H \stackrel{?}{\approx} 10$ fm; the end of the quark-gluon plasma epoch by $t_Q \stackrel{?}{\approx} 4$ fm; $t_1 \stackrel{?}{\approx} 1$ fm corresponds to the chemical equilibration of the light quarks and the onset of the quark-gluon plasma; $t_0 \stackrel{?}{\approx} 0.05$ fm characterises the chemical equilibrium of gluons.

### 1.1.2 Strange particle production

Biró and Zimányi [25], Rafelski and Müller [116] and Hagedorn [168] were among the first to study the strange quark production in a quark-gluon plasma. Villalobos-Baillie notes "strangeness enhancement of a factor of 2-3 relative to $p + p$ reactions has been shown in many strangeness channels" [3]. The enhancement of strangeness [105] is a novel phenomenon because it persists through the quark-gluon plasma regime, if it exists, to the hadronic regime, whence strange hadrons decay weakly.

Strangeness production in a quark-gluon plasma is enhanced, because, relative to nucleon-nucleon collisions, it is easy to make strange quarks in a heat bath formed by the remnants of the obliteration of two big relativistic nuclei ($A - A$). However a detailed dynamical model is needed to account for the strangeness production.

Experimentally strangeness is enhanced in $A-A$ collisions over proton-proton ($p-p$) and proton-nucleus ($p - A$) collisions. There are many experiments measuring the production of particles from RHIC's - NA52, WA97 or NA38 at CERN-SPS or E802, E886 or E864 at BNL-AGS.

Laboratory energies at experiments at BNL-AGS are approximately 14 GeV·$A$ and CERN-SPS 200 GeV·$A$. Although the AGS produces true heavy ion collisions, the energy is lower than at SPS. There has been a steady convergence of the different thermodynamic parameters of data from BNL-AGS $Si$ and $Au$ beams, as well as NA35, NA36 and WA85/94.

Data is obtained from targets such as oxygen ($^{16}O$), aluminium ($^{27}Al$), silicon ($^{28}Si$), sulphur ($^{32}S$), copper ($^{64}Cu$), silver ($^{108}Ag$) and tungsten ($^{184}W$) targets. Data from lead

($^{208}Pb$) and gold ($^{197}Au$) beams are being analysed presently.

Since 1986 data from the AGS with $\sqrt{s} = 5$ GeV·A for $^{28}Si$ and SPS with $\sqrt{s} = 20$ GeV·A for $^{32}S$ has existed. Currently data is being processed for the $^{197}Au$ runs at AGS ($\sqrt{s} = 4$ GeV·A) and $^{207}Pb$ runs at SPS ($\sqrt{s} = 17$ GeV·A). If existing plans are met RHIC is expected to accelerate $^{197}Au$ with $\sqrt{s} = 200$ GeV·A in 1998, and LHC is expected to accelerate $^{208}Pb$ with $\sqrt{s} = 6200$ GeV·A in 2002.

### 1.1.3 Experimental Data

We focus on the results of four experimental collaborations measuring strange particle ratios: WA94, WA85, NA35 and NA36 (all from CERN). We record experiments which produce ratios of strange particles in Appendix B.3.

Data is measured in a certain rapidity and transverse momentum window. In Table 1.1 we have extrapolated the data from Appendix B.3 to cover the whole $p_T$ range. Also included in our program is the correction of the contribution of $\Sigma^o \to \Lambda + \gamma$ to the $\Lambda$ ratios.

**WA85: 1995 $S - W$ phase space corrected data**

| $\overline{\Lambda}/\Lambda$ | $\overline{\Xi^-}/\Xi^-$ | $\Xi^-/\Lambda$ | $\overline{\Xi^-}/\overline{\Lambda}$ | $\overline{\Omega^-}/\Omega^-$ |
|---|---|---|---|---|
| $0.200 \pm 0.010$ | $0.450 \pm 0.050$ | $0.082 \pm 0.005$ | $0.180 \pm 0.018$ | $0.570 \pm 0.410$ |

Table 1.1: Phase space corrected strange particle ratios

There are different scenarios to reproduce the experimental ratios of particles from RHIC's. We will discuss one of these, the quark model. First, however, it has been argued that it is possible to describe the data adequately with a thermal hadron gas [62]. Using only thermodynamic quantities and baryon number, strangeness and charge conservation, a description of the data can be found, within experimental error. We call this the hadron gas model.

## 1.2 Thermodynamic constraints of a hadron gas

An idea originating from R. Hagedorn [168] proposes that one possible scenario for the evolution of a RHIC assumes that hadron thermalisation takes place shortly after hadronisation and the system remains in thermal equilibrium until the hadrons produced in this system stop interacting and are measured [122]. In this case the experimentally observed particles will reflect the properties at freeze-out, irrespective of the history prior to the thermal hadron gas. (It is also possible for example, that the system expands too rapidly to

thermalise. In which case some relic of the quark-gluon plasma parameters will be carried by the hadrons.)

If thermalisation is achieved, and if it is not destroyed by subsequent possible non-equilibrium features, the produced hadrons should be observed in ratios determined by the thermodynamics of a system at freeze-out temperature and freeze out baryon density, [50]. Despite strange particles being in the minority compared to non-strange hadrons when counting particles emerging from a RHIC, we will focus on them in the following due to the considerable amount of experimental and theoretical interest in strangeness production in a RHIC.

### 1.2.1 Strangeness in a thermal hadron gas

From a thermal hadron gas [48, 50] strange particle ratios consistent with experiment have been demonstrated ([146, 147]). Closer examination reveals that the inclusion of a parameter, $\gamma_S$, [45] (now put on a theoretical footing ([134] and section 1.3.2)), giving a relative departure from chemical equilibrium of strange particles, must be included for the correct fit to the data. This parameter $\gamma_S$ has been explained from the perspective of a quark-gluon plasma [117] and is related to the strange quark fugacity [76, 130]. In general $\gamma_{\bar{S}} \neq {\gamma_S}^{-1}$ when the strange quarks are out of chemical equilibrium. Since we consider a strangeness neutral QGP, we use $\gamma_S = \gamma_{\bar{S}}$.

We show that a thermal hadron gas gives a good fit for the above data in Table 1.1. This is bad news for advocates of the quark-gluon plasma [116] because the hadron gas is extremely simple and does not refer to the creation of a quark-gluon plasma. This thermal hadron approach has a limited number of parameters ($\mu_B, \mu_S, \mu_Q$ and $T$), which can be compared directly to experiment, and that can give some indication as to the dynamics underlying the more complicated models depending on space and time.

The procedure is as follows: we only use three free parameters ($\mu_B, \mu_S$ and $T$) by dealing with (approximately) isospin symmetric $A - A$ collisions. Although it has been shown that the isospin quantum number does contribute significantly [62] in non-isospin symmetric $A - A$ collisions, the strange baryon ratios are still not correctly predicted by this work, indicating that this $\gamma_S$ factor may play a role in the strangeness sector. However, because non-strange baryons are produced far in excess of strange baryons, in models focusing on the non-strange sector this may be a minor correction.

If one starts by assigning a separate chemical potential to each meson and baryon, one finds that baryon and strangeness number conservation laws in particle reactions, relate each of these chemical potentials to linear combinations of $\mu_B$ and $\mu_S$. One finds that the baryonic and strange chemical potentials are non zero, because for a given strangeness, particles can have a different baryon number (e.g. $\Lambda$ and $K^o$).

By imposing strangeness neutrality

$$\sum_i n_s^i(\mu_B, \mu_S, T) - \sum_i n_{\bar{s}}^i(\mu_B, \mu_S, T) = 0 \tag{1.1}$$

and fixing the baryon number density,

$$\sum_j n_B^j(\mu_B, \mu_S, T) - \sum_j n_{\bar{B}}^j(\mu_B, \mu_S, T) = n_B, \tag{1.2}$$

we can to plot $\mu_B$ versus $\mu_S$ for various $T$'s. The $n_s^i$ are summed over strange meson and baryon states, and the $n_B^j$ over just baryon and antibaryon states. These quantities are calculated using the normal thermodynamic number density functions,

$$n_i(T, \mu_i) = \frac{\gamma_i}{2\pi^2} \int_0^\infty dk\, k^2\, f_\pm(E_i(k), \mu_i). \tag{1.3}$$

$\gamma_i$ is the degeneracy factor for spin and isospin. For example, in the Boltzmann limit (which is an excellent approximation in this temperature domain)

$$n_\Lambda = \frac{\gamma_\Lambda}{2\pi^2} \int_0^\infty dk\, k^2\, \exp(\frac{-E_\Lambda + \mu_B - \mu_S}{T}),$$

$$n_{\overline{\Lambda}} = \frac{\gamma_{\overline{\Lambda}}}{2\pi^2} \int_0^\infty dk\, k^2\, \exp(\frac{-E_{\overline{\Lambda}} - \mu_B + \mu_S}{T})$$

and

$$n_{K^0} = \frac{\gamma_{K^0}}{2\pi^2} \int_0^\infty dk\, k^2\, \exp(\frac{-E_{K^0} + \mu_S}{T}).$$

The immediate question on the upper bound on masses in the sums 1.1 and 1.2 are important. We use particles obtained from [107] up to about 2 GeV. The problem with the ignored infinite number of resonances is illustrated by comparing the 2 GeV tables with a much smaller table. We will return to this.

From 1.3 we have

$$\overline{\Lambda}/\Lambda = \exp\left[\frac{-2(\mu_B - \mu_S)}{T}\right]$$

and

$$\Xi^+/\Xi^- = \exp\left[\frac{2(-\mu_B + 2\mu_S)}{T}\right].$$

It is possible to obtain useful results by using an approximate expression to 1.3:

$$n_i = \frac{4\pi}{(2\pi)^3} e^{-\beta\mu_i}\, m_i^2\, T\, K_2(\frac{m_i}{T}) \simeq \frac{1}{(2\pi)^{\frac{3}{2}}} e^{-(m_i+\mu_i)/T}\, m_i^{\frac{3}{2}}\, T^{\frac{3}{2}}$$

which is valid for $m_i \gg T$. Therefore if we ignore contributions from resonance decays (we return to this in equation 1.9) we obtain the following examples

$$K^0/\overline{\Lambda} = \exp\left[-\frac{m_{K^0} - m_{\overline{\Lambda}}}{T}\right] \left(\frac{m_{K^0}}{m_{\overline{\Lambda}}}\right)^{\frac{3}{2}} \exp\left[\frac{\mu_B}{T}\right],$$

$$\Xi^-/\Lambda = \exp\left[-\frac{m_{\Xi^-} - m_\Lambda}{T}\right]\left(\frac{m_{\Xi^-}}{m_\Lambda}\right)^{\frac{3}{2}} \exp\left[\frac{-\mu_S}{T}\right],$$

$$\Xi^-/K^0 = \exp\left[-\frac{m_{\Xi^-} - m_{K^0}}{T}\right]\left(\frac{m_{\Xi^-}}{m_{K^0}}\right)^{\frac{3}{2}} \exp\left[\frac{\mu_B - 3\mu_S}{T}\right]$$

and

$$\Omega/\Lambda = 2\exp\left[-\frac{m_\Omega - m_\Lambda}{T}\right]\left(\frac{m_\Omega}{m_\Lambda}\right)^{\frac{3}{2}} \exp\left[\frac{-2\mu_S}{T}\right].$$

Let us assume for the moment that only protons, lambdas, kaons and their antiparticles are produced. The baryon chemical potential is fixed by baryon number conservation, equation 1.1, and is a positive, non zero number. Strangeness conservation, equation 1.2, gives us

$$\exp(\frac{-m_\Lambda + \mu_B - \mu_S}{T}) + \exp(\frac{-m_K - \mu_S}{T}) - \exp(\frac{-m_\Lambda - \mu_B + \mu_S}{T}) - \exp(\frac{-m_K + \mu_S}{T}) = 0.$$

Because of $\mu_B$'s size, and due to the fact $\mu_S$ should be positive to make this approximation work, we drop the two smallest terms and finally get

$$\exp(\frac{-m_\Lambda + \mu_B - \mu_S}{T}) - \exp(\frac{-m_K + \mu_S}{T}) = 0.$$

Hence $\mu_S = \frac{1}{2}(\mu_B - m_\Lambda + m_K)$.

On the other hand in a quark-gluon plasma, each of the quarks would contribute their chemical potential to the hadron during hadronisation (this is of course ignoring sea quarks). Therefore it is possible to relate the baryon and quark thermodynamic quantities: Because hadrons consist of three quarks

$$\mu_B = 3\mu_q \tag{1.4}$$

where

$$\mu_q = \frac{1}{2}(\mu_d + \mu_u) \simeq \mu_d \simeq \mu_u. \tag{1.5}$$

Further, for a strange baryon we have

$$\mu_B - \mu_S = 2\mu_q + \mu_s. \tag{1.6}$$

Because a strange quark has baryon number 1 and strangeness $-1$ (the minus is a convention)

$$\mu_s = \mu_B/3 - \mu_S. \tag{1.7}$$

This is consistent with the preceding equations.

To ensure strangeness neutrality in a quark-gluon plasma $n_s = n_{\bar{s}}$. This is possible only if $\mu_s = \mu_{\bar{s}} \equiv -\mu_s$. We then obtain from

$$\exp(\frac{-m_s + \mu_B/3 - \mu_S}{T}) = \exp(\frac{-m_s - \mu_B/3 + \mu_S}{T})$$

that $\mu_S = \mu_B/3$ or $\mu_s = 0$. In a quark-gluon plasma $\mu_B = 3\mu_S$. This simple link between the quark model and the hadron gas model would be necessary if the QGP existed.

It has been shown that there is a large contribution to the particle numbers from the decay products of heavier resonances. In fact the bulk of meson production occurs through resonance states at high $T$. To obtain the total number of a certain species of particle, we allow decays to contribute according to their branching ratios [107]. For example,

$$n_{\pi^+} = n_{\pi^+}^{THERMAL} + 0.285 n_\eta + \frac{2}{3} n_\rho + 1 n_\omega + 0.134 n_\phi + \frac{1}{3} n_{K^*} + \ldots . \tag{1.8}$$

Because different particles decay at different rates, it is possible to examine scenarios at different times, by taking relevant decay products with appropriate life times.

We examined three different tables; baryon octuplet and meson sextet table (Table 0), few decay products (Table 1)* and lots of decay products (Table 2)†. We plotted the mass versus degeneracy for Table 1 in Figure 1.2 and Table 0,1 and 2 are explicitly recorded in Appendix E.

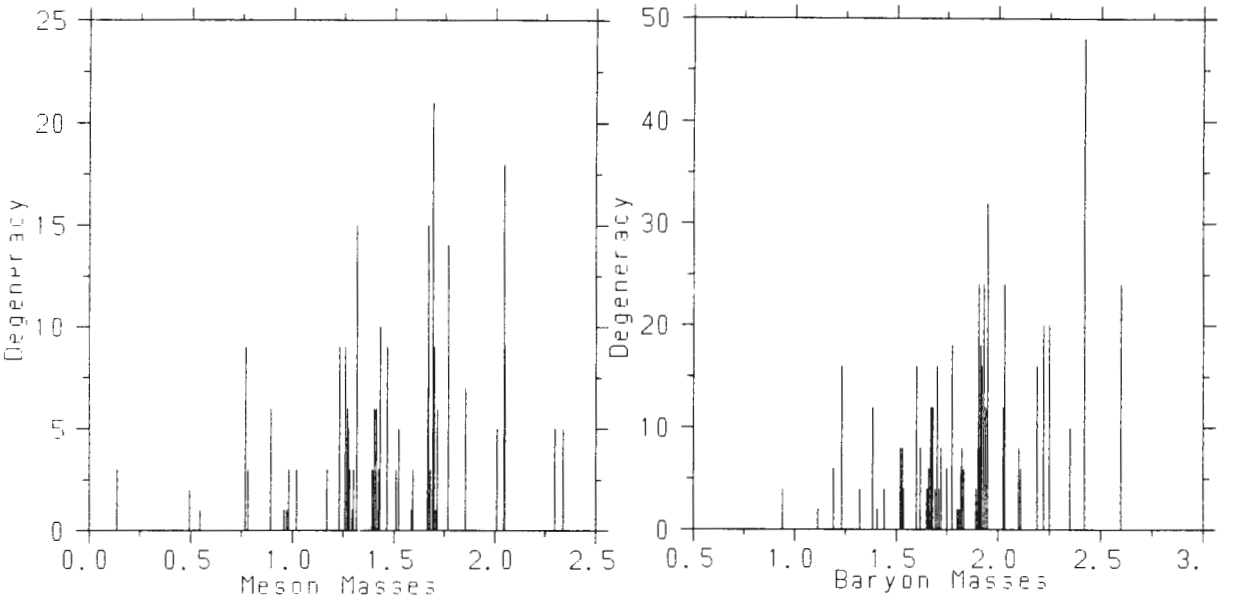


Figure 1.2.1 (Mesons) and Figure 1.2.2 (Baryons): Graphic representation of data from Table 1

Hagedorn [168] proposed a statistical bootsrap model to account for the higher masses which we have neglected. The mass distribution is given as $\rho(m) \propto m^{-3} \times \exp(\beta_H m)$. This relation and its derivation is analogous to Euler's partition theorem, in which the number of ways of writing an integer as a sum of smaller positive integers is given as $\tau(n) \sim n^{-1} \exp((2\pi/6)n)$ [126]. In the context of lower energies, Hagedorn concluded that the temperature should be less than $T_H = 1/\beta_H$ [126]. Cabibbo and Parisi (1975) observed

*Obtained from Detlov von Oertzen
†Obtained from Neven Bilić

that the hadronic density ceases to be meaningful for $T > T_H$, because the system undergoes a phase transition at this value, and hence higher temperatures are permissible. The Hagedorn temperature [168] has been found to be $T_H \sim m_\pi \sim 150MeV$. The thermodynamic constraints obtained from the particle ratios in this section are only weakly sensitive to the masses omitted from the continuum.

Returning to using the strangeness neutrality condition, it is possible to plot $\mu_S$ against $\mu_B$ for various values of $T$. It is particularly interesting to note that for $T \sim 200$ MeV one has [50] $\mu_S \sim \frac{1}{3}\mu_B$. This relation emerges naturally in a quark-gluon plasma.

We have at our disposal experimental data on the ratio of strange particles from RHIC's. The raw data is listed in appendix D.1 but must have a phase space correction included (see appendix B.2). This is because the data is measured in a certain rapidity and ($p_\perp$ or $m_\perp$) range. The extrapolated data are given in Table 1.1. It is essential to remove $\Sigma^0$ 'contamination' of the $\Lambda$ signal. This is because the $\Sigma^0$'s decay quickly ($c\tau_{\Sigma^0} < 1 \times 10^{-14}$s) into $\Lambda + \gamma$ ($c\tau_\Lambda = 3 \times 10^{-10}$s). The $\Lambda$ decay products of $\Sigma^0$ are indistinguishable from the weakly decaying thermal $\Lambda$'s.

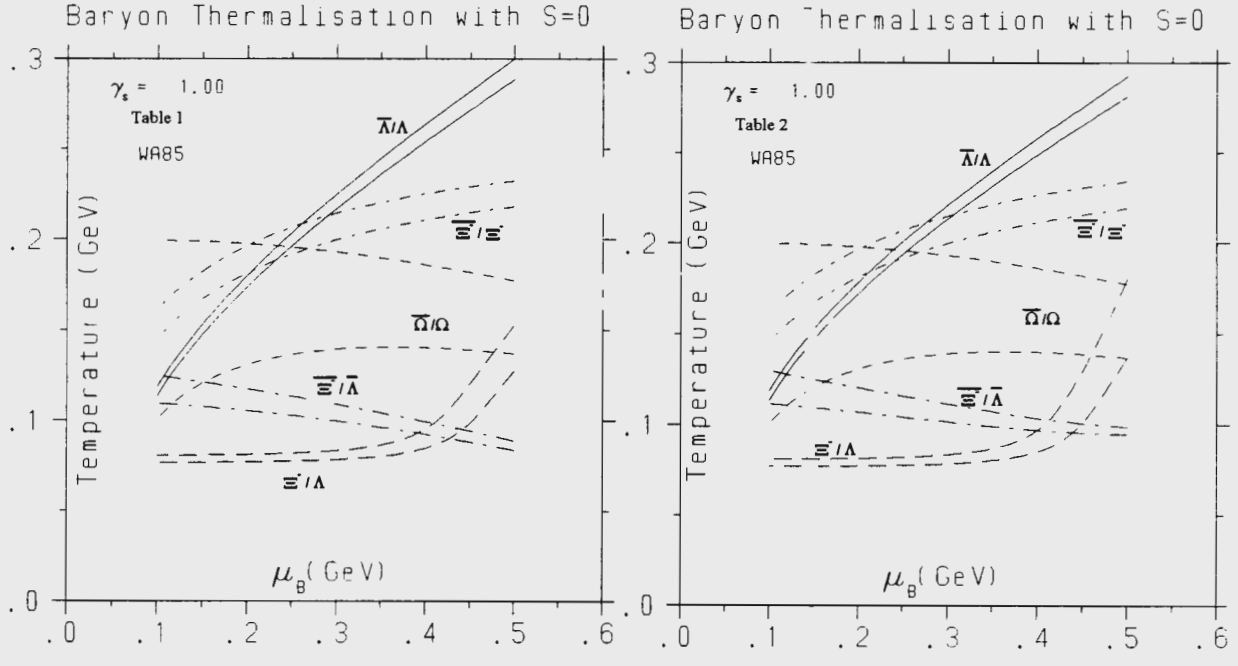


Figure 1.3.1 (Table 1) and Figure 1.3.2 (Table 2): $T$ versus $\mu_B$ for WA 85
The data used is obtained considering the upper and lower bounds of Table 1.1. The difference between the figures is due to different resonance contributions.

Using the data allows us to reduce the thermodynamic parameters by one. The plots in Figure 1.3 are obtained by finding a suitable value of $\mu_S$ consistent with experiment. We plot $T(\mu_S)$ and $\mu_B(\mu_S)$. We have two limits to consider because every ratio has an experimental error. This gives us a band that, if all the particles freeze-out with a common

temperature, should coincide at some point.

We note that there is no coincidence of the ratios in Figure 1.3. (In [57, 58] coincidence was obtained using experimental strange particle ratios available in Quark Matter 91. These data were subsequently corrected in Quark Matter 93.) If all the particle species froze out of the expanding hadron gas simultaneously we would have expected them to have the same temperature and chemical potentials. The above results are familiar from the literature [51]. There are slight discrepancies in precise values of the thermodynamic variables in the literature. This is due to different decay products being incorporated into the equation 1.8 (which, if done consistently, characterises freeze-out at different times).

### 1.2.2 Deviation from strange chemical equilibrium

Figures 1.3a and 1.3b are corrected by the inclusion of a factor to parametrise relative chemical equilibrium, $\gamma_S^{|S|}$. This is a multiplicative factor to the particle ratios. This is when all the particles are thermally and chemically equilibrated and the relative abundance of strange hadrons have had time to maximise their entropy but the overall strangeness is suppressed relative to its equilibrium value. The number density of equation 1.3 now can be approximated by

$$n_i(T,\mu_i) = \frac{\gamma_S^{|S_i|}\gamma_i}{2\pi^2}\int_0^\infty dk\, k^2\, f_\pm(E_i(k),\mu_i). \tag{1.9}$$

$S$ is the strangeness number. Equation 1.9 is now used in 1.1 and 1.2. We repeated the above but this time using this factor.

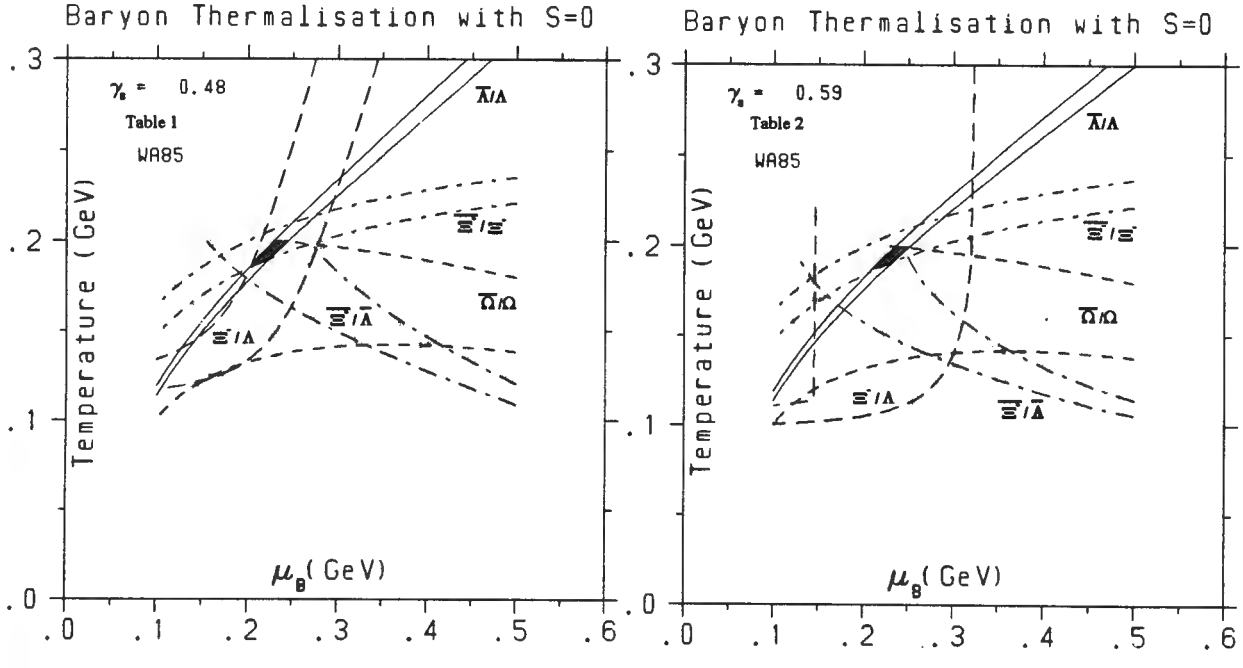


Figure 1.4.1 (Table 1) and Figure 1.4.2 (Table 2): $T$ versus $\mu_B$ for WA 85

Here we have included a $\gamma_S = 0.48$ and $\gamma_S = 0.59$ respectively. The marked region in the above curves have $\mu_B \simeq 0.225$ GeV, $T \simeq 0.190$ GeV and $\mu_S \simeq 0.070$ GeV. We will find that the $\gamma_S$ factor is between 0.5 and 0.7, depending on the experiment, and the data table used. Cleymans [50] estimates thermodynamic variables in RHIC's with $\mu_B$ =250-300MeV, $\mu_S$ =100MeV and $T$ =200MeV. The final state does not show chemical equilibration, with the $\Xi/\Lambda$ ratio about 30% too small for this to have occurred. Rafelski [121] quotes $\gamma_S$ as being $0.75 \pm 0.15$.

### Transverse flow

The temperature measured in experiments and the temperature for freeze-out may not be the same due to the plasma expanding transversely. In the transverse mass spectra of strange (anti)baryons the inverse slope parameter is found to be typically 232 $\pm$ 5 MeV. Transverse flow causes Doppler shift of the form: $T = T_f\sqrt{\frac{1+\beta}{1-\beta}}$ ,where ($\frac{v}{c} = \beta = 0.3$) and $T_f$ is the freeze-out temperature.

It is possible to include finite volume corrections to the particle number density [49]. This is frequently done in terms of hard-sphere pictures modelling hadron repulsion.

### Thermodynamic consistency

One of the important considerations is thermodynamic consistency [‡]. Significant work has been done in this regard, especially around entropy production and the second law of thermodynamics. In this section, and in the later sections using Bjorken's hydrodynamic equations, it is tempting to make the masses temperature dependent or make the chemical potential rapidity dependent, which seem like physically reasonable improvements. We have avoided such measures in order to obey the second law of thermodynamics $d\epsilon = T\,ds + \mu\,dn - dp$.

Although it would be possible to add a physically acceptable temperature dependence, thermodynamic consistency needs to be retained. A simple illustration of this point is in order: The thermodynamic relation ($\epsilon = T\,s + \mu\,n - p$ ) should be inviolate. If we use $s(T,\mu) = \frac{\partial p(T,\mu)}{\partial T}|_\mu$ and then assume for the time being that $\mu = 0$ we get a strict condition that $\epsilon = T\frac{dp}{dT} - p$. Now if, for simplicity's sake

$$p(T) \propto \int \frac{k^4}{w^*}\exp(-w^*/T), \qquad \epsilon(T) \propto \int k^2\,w^*\exp(-w^*/T) \text{ and } w(T)^{*2} = k^2 + m(T)^2$$

then we can see that the thermodynamic condition leads to a constraint on the form of $f(m(T),T) = 0$ which severely limits the $T$ dependence of $m$. In fact in most cases $\frac{dm(T)}{dT} = 0$.

[‡]Thanks to Mark Gorenstein for pointing this out

## 1.3 Quark-gluon plasma model

Assuming a quark-gluon plasma does exist, the QGP fireball is expected to last for $(2-4)\times 10^{-24}$ seconds. Until now there has been no reference to the quarks and gluons apart form the coincidental $\mu_S = \frac{1}{3}\mu_B$.

In the quark model, each of the quarks is assigned a chemical potential. Then the thermodynamic properties of hadrons are completely described by their $SU_F(3)$ quark content. Therefore, for a $\Lambda$, having $u+d+s$ quarks, we would have

$$\mu_\Lambda = \mu_u + \mu_d + \mu_s.$$

Strangeness phase space may not be saturated and $\gamma_S$ may be introduced into quantities with strange quarks. This is done by including a prefactor of $\gamma_S$ for every strange quark **and** strange anti-quark. This has to do with the occupancy of strangeness phase space affecting strange quarks and anti-quarks similarly. We return to a rigorous discussion of this in the next section.

The examples of the hadron model now become

$$K^0/\overline{\Lambda} = \exp\left[-\frac{m_{K^0}-m_{\overline{\Lambda}}}{T}\right]\left(\frac{m_{K^0}}{m_{\overline{\Lambda}}}\right)^{\frac{3}{2}}\exp\left[\frac{2\mu_d+\mu_u}{T}\right],$$

$$\overline{\Lambda}/\Lambda = \exp\left[\frac{-2(\mu_u+\mu_d+\mu_s)}{T}\right],$$

$$\Xi^-/\Lambda = \gamma_S\exp\left[-\frac{m_{\Xi^-}-m_\Lambda}{T}\right]\left(\frac{m_{\Xi^-}}{m_\Lambda}\right)^{\frac{3}{2}}\exp\left[\frac{\mu_s-\mu_u}{T}\right],$$

$$\Xi^-/K^0 = \gamma_S\exp\left[-\frac{m_{\Xi^-}-m_{K^0}}{T}\right]\left(\frac{m_{\Xi^-}}{m_{K^0}}\right)^{\frac{3}{2}}\exp\left[3\frac{3\mu_s}{T}\right],$$

$$\Omega/\Lambda = 2\,\gamma_S^2\exp\left[-\frac{m_\Omega-m_\Lambda}{T}\right]\left(\frac{m_\Omega}{m_\Lambda}\right)^{\frac{3}{2}}\exp\left[\frac{-\mu_u-\mu_d+2\mu_s}{T}\right]$$

and

$$\Xi^+/\Xi^- = \exp\left[\frac{-2(\mu_d+2\mu_s)}{T}\right].$$

### 1.3.1 Strangeness in a QGP

The quark model provides the basis of the next chapter. The original proposal by Rafelski and Müller [116] was followed by extensive discussions in the literature [4, 5, 25, 26, 98, 96]. It is the intention of the following chapters to investigate on a microscopic level the formation of strangeness, and to show that the $\gamma_S$ factor emerges naturally from this, at least within a model. It is not the intention of this work to weigh the merits or demerits of the hadron gas and quark-gluon plasma scenarios.

### 1.3.2 Thermodynamic Consistency of $\gamma_S$

It is commonly agreed that fireballs resulting from collisions between heavy ions establish a thermal equilibrium, and at least a relative chemical equilibrium. The thermodynamics of relative chemical equilibrium, treated heuristically until now, have been rigorously established by C. Slotta et al [134]. We briefly review this proof.

Absolute chemical equilibrium of strange particle is not established due to the large mass of $s - \overline{s}$ pairs. This means that there are insufficient strange quarks to fill the available phase space, but strangeness is distributed among the available strange hadron channels by maximising the entropy. A new thermodynamic quantity, $\gamma_S$, parametrises this. The abundance of hadrons is then regulated by another fugacity term, $\gamma_S^{|S|}$, where $|S|$ counts the number of strange or anti-strange quarks in the respective hadron species

In general, the equilibrium solution, of an ideal gas is obtained by maximising the entropy, within a number of constraints, such as energy, baryon number, strangeness and charge conservation. However, if different species equilibrate chemically at different times, then a parameter can be introduced.

In general the entropy is defined as

$$\mathcal{S} = -\sum_{k\,\Delta V} \int d\omega \left(f_k \ln f_k - \theta_k \left(1 - \theta_k f_k\right) \ln\left(1 - \theta_k f_k\right)\right) \tag{1.10}$$

where $f_k$ is a Bose-Einstein or Fermi-Dirac distribution function, $\theta_k = 1(-1)$ for baryons (mesons) and $\int_{\Delta V} d\omega = \frac{1}{(2\pi)^3} \int d^3x \int d^3p$. The additional constraints in the Grand Canonical Ensemble are the average thermal energy, charge and strangeness:

$$< E >= \sum_k \int d\omega\, E_k\, f_k, \qquad <Q>= \sum_k \int d\omega\, q_k\, f_k \;\text{ and }\; <S>= -\sum_k \int d\omega\, s_k\, f_k$$

Partially saturated strange phase space is introduced through a new constraint

$$<|S|>= -\sum_k \int d\omega\, |s_k|\, f_k.$$

$< |S| >$ and $< S >$ can be specified independently. Another way of expressing $< |S| >$ is using $\sum_k < |S_k| >^{Eq} \xi_k$. In these terms $\xi_k$ can be understood to be $\xi_k = \frac{f_k(E,\mu)}{f_k(E,\mu=0)}$ which, in the Boltzmann limit tends to $\exp(\mu\,\beta)$. Accordingly, if there are no strange quarks ($\mu = -\infty$) then $\xi_k = 0$ or if strange space is saturated ($\mu = 0$) then $\xi_k = 1$.

The usual prescription in obtaining the distribution functions $f_k(E,\mu)$ is to minimise the functional $\mathcal{S}[f_k]$ using the Lagrange multipliers $\beta, \nu_q, \nu_s$ and $\sigma$. Here $\sigma$ is for the new constraint on strangeness. One obtains

$$f_k(E,\mu) = \frac{1}{\exp(\beta\, E + \nu_q\, q_k + \nu_s\, s_k + \sigma\, |s_k|) + \theta_k} \tag{1.11}$$

Inserting 1.11 into 1.10 gives

$$\mathcal{S} = \beta < E > + \sum_k (\nu_q q_k + \nu_s s_k) < N_k > + \ln \mathcal{Z} + \sum_k \sigma |s_k| < N_k >$$

where $< N_k >= \sum_k \int d\omega \; f_k$. $\ln \mathcal{Z}$ is the generating functional for all thermodynamic quantities.

If $\alpha_k = \nu_q q_k + \nu_s s_k + \sigma |s_k|$ then

$$< E >= -\frac{\partial}{\partial \beta} \ln \mathcal{Z}|_{\alpha_k, V},$$

$$< N_k >= -\frac{\partial}{\partial \alpha_k} \ln \mathcal{Z}|_{\beta, V}$$

and

$$p = T \frac{\partial}{\partial V} \ln \mathcal{Z}|_{\alpha_k, T}.$$

As expected $\alpha_k = -\frac{\mu_k}{T}$ and $\beta = \frac{1}{T}$. Returning to the Boltzmann approximation $\xi_k = \exp(\sigma \beta |s_k|) = \gamma_S^{|s_k|}$. This suppression factor has no influence on other thermodynamic quantities apart from entropy: If $\mathcal{S} = \sum_k \mathcal{S}_k$ then each component receives an additional $-|s_k| \ln \gamma_S \; < N_k >$.

## 1.4 Strangeness as a QGP signature?

A great many questions remain open in relativistic heavy ion collisions. If a quark-gluon plasma is created, a number of questions relating to the phase transition remain. This impacts on the considerations of this chapter because strong changes in the thermodynamic quantities are expected if the phase transition is first order.

In the newest heavy ion collisions at the AGS (2.5 GeV·$A$ in the centre of mass system) and SPS (10 GeV·$A$ in the centre of mass system) RHIC's are seemingly not transparent [113] despite a considerable amount of longitudinal non-thermal flow.

The equilibration rate for strange quarks in a quark-gluon plasma is fast compared to the equilibration rate for mesons in a hadron gas. Therefore hadron gas models are brought into question. Non-equilibrium effects are also expected to play an important role towards the enhancement of strangeness which may vindicate the validity of the hadron gas. Non-equilibrium effects are dependent on specific models, and this makes theoretical comparison difficult. The question as to the equilibrium rate will decide on whether the quark or hadron model is correct.

As to the prognosis of strangeness as a signature of the Quark Gluon Plasma: it is still believed to be important, but other signatures, such as direct lepton production, are believed to be stronger candidates. The quark model for strangeness is shadowed by the thermal hadron gas model.

It is remarkable that the quark-gluon plasma remains elusive after fifteen years. Perhaps in the next generation of colliders, these experiments will cross over the phase transition. It is believed that current experiments are on the edge of the hadron/quark-gluon phase.

# Chapter 2

# Cutting rules and Braaten-Pisarski resummation

**Introduction**

In this chapter we move away from phenomenology, and develop ideas of microscopic QCD in a thermal medium that will be used in the next chapter to calculate the rate of production of strange quarks in a (quark-)gluon plasma. In the beginning calculations of strange quark production were done in a vacuum [116]. Thermal distribution functions were added post-facto into expressions for rates [98]. Developing the perturbative QCD calculations more rigorously at finite temperature has led to claims by T. Altherr and D. Seibert that gluon decay is as important as the above processes [4, 7, 26]. In this chapter, we will record key results of conventional field theory, needed to generalise the "$T = 0$" perturbative QCD results. The leading order calculation has been done [22].

This chapter is structured as follows. In the first section we discuss the Cutkosky rules of conventional QCD at "$T = 0$". The next section introduces thermal field theory. The finite temperature analogue to the Cutkosky rules, the Kobes-Semenoff rules, are then examined and finally Braaten-Pisarski resummation is summarised.

## 2.1 Perturbative QCD

We want to calculate the formation rate of strange quarks. We would like to isolate the most important perturbative channels of strangeness formation. The channels that are known at this stage are gluon fusion ($gg \to s\bar{s}$) and quark annihilation ($q\bar{q} \to s\bar{s}$). The question as to what the contribution of the non-perturbative sector is, remains open. In the next chapter we investigate gluon decay, where perturbative QCD is used, but with propagators and vertices resummed due to the effects of the thermal medium. The above processes are represented in terms of their Feynman diagrams as

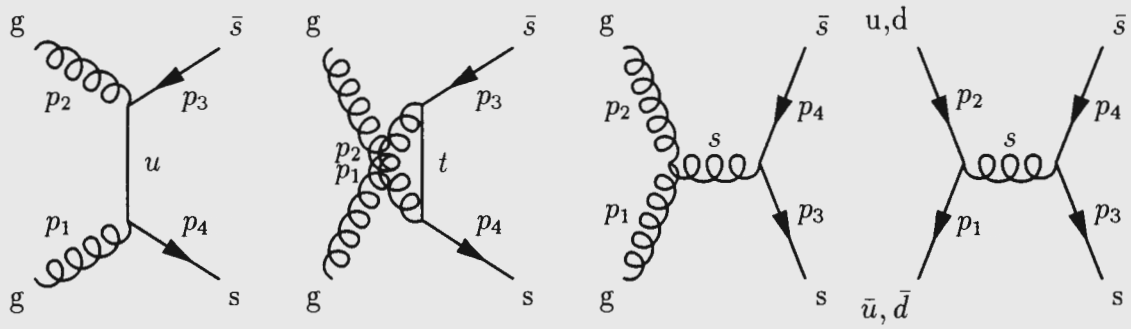


Figure 2.1: Gluon fusion $u-$, $t-$ and $s-$ channels and quark annihilation

They have been calculated in [25, 26, 28, 54, 98, 116]. We outline their derivation again but use the Cutkosky rules to go directly to the rate whereas in for example [98], the matrix element has been calculated and then squared. At finite temperature the Cutkosky rules, or rather their finite temperature generalisation, reduce the number of graphs to be evaluated quite considerably. Bearing in mind the procedure we would follow at finite temperature, we review the calculation for perturbative QCD.

### 2.1.1 Cutkosky Rules

The Cutkosky rules [55] are used to simplify the calculation of the imaginary component of a Feynman diagram representing a certain process. The imaginary components of Feynman diagrams are helpful, because the optical theorem equation A.5, obtained from imposing the unitarity condition, is a relation between the cross section or rate of a certain process, and the imaginary component of a particular matrix element of the process, (see Appendix A.4).

The Cutkosky rules state that the imaginary part of any process is proportional to the sum of all 'cut' graphs. To "cut" a graph means that a line must be drawn through the propagators of a Feynman diagram and depending whether or not a propagator was cut by this line, or on what side the vertex or propagator falls, determines the graphs analytic structure. The line has a "shadow" and "sun" side to ensure energy conservation. In the expression for the matrix element all 'cut' propagators must be replaced with expressions for "cut" propagators, given in Appendix C.1. Similarly all the vertices falling in the shadowed region (or circled vertices) must likewise be replaced from the table. This increases the number of terms to be evaluated, but a few of the terms are immediately seen to be zero because of energy conservation and the terms remaining are simpler, in the sense that the integrations are simpler. The Cutkosky rules ensure that the phase space factors are correct and are essential at finite temperature, due to the increase in Feynman diagrams.

Rigorous derivations of the Cutkosky rules appear in [77] and [144]. We use the standard notation of 't Hooft and Veltman [144] in describing the rules. Through the use of two

worked examples appropriate for this thesis, we illustrate the Cutkosky rules. What follows is intended to be read with 't Hooft and Veltman's Diagrammar [144]. All that is assumed in the following is that the Feynman diagrams can be sufficiently regulated so that no divergences occur and that the propagator can be decomposed into two parts

$$\Delta(x) = \Theta(x_0)\,\Delta^+(x) + \Theta(-x_0)\,\Delta^-(x),$$

where the $\Delta^\pm$ are defined in terms of the density function

$$\Delta^\pm(x) = \frac{1}{(2\pi)^3}\int d^4k\, e^{ikx}\Theta(\pm k_0)\,\rho(k^2). \tag{2.1}$$

We mainly limit ourself to the case of bare propagators.

### Quark Annihilation

The following is the first example of the use of Cutkosky rules. We want to evaluate the rate of quark fusion. The optical theorem, Appendix A.4, implies that we must evaluate the following diagram:

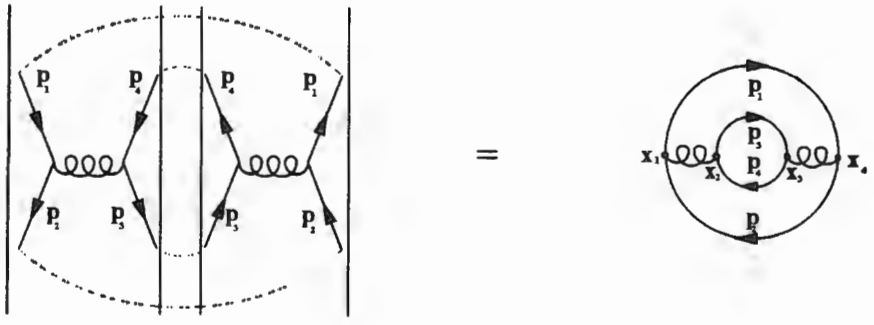

Figure 2.2: The diagram needed to evaluate the rate of quark fusion using the Cutkosky rules.

This diagram is obtained by multiplying the matrix element by its conjugate, and joining the inside and outside propagators according to the Optical Theorem prescription. (Time and energy flow from left to right in all Feynman diagrams.) The $x$ labels the vertices, and $p$ labels the momenta. In the notation of 't Hooft and Veltman [144] and Kobes and Semenoff [83] we write down a generic function, $F(x)$, related to this Feynman diagram. $F(x)$ is defined in terms of $\Delta(x)$ functions, which are generic expressions for propagators. At this stage there is no need to distinguish whether they are spin 0, $\frac{1}{2}$ or 1 propagators. For a free spin zero field we have

$$\Delta(x) = \frac{1}{i(2\pi)^4}\int d^4k \frac{e^{ikx}}{k^2 - m^2 + i\epsilon}$$

and for a free spin half propagator

$$\Delta(x) = \frac{1}{i(2\pi)^4}\int d^4k \frac{e^{ikx}\,(\not{k}+m)}{k^2-m^2+i\epsilon}.$$

The propagators need not be free. All we need is equation 2.1 and the equation preceding it to be sufficient to develop rules for the non-free case. In the spirit of 't Hooft and Veltman we define a function $F(x)$

$$\begin{aligned} F(x_1,x_2,x_3,x_4) = \Delta(x_4-x_1)\,\Delta(x_4-x_1)\,g\,\Delta(x_1-x_2)\times \\ g\,\Delta(x_2-x_3)\,g\,\Delta(x_2-x_3)\,\Delta(x_3-x_4)\,g \end{aligned} \tag{2.2}$$

The $g$'s and $\Delta$'s are generic vertices and propagators. The cutting rules say that

$$\begin{aligned} F(x_1,x_2,x_3,x_4) - F(\underline{x_1},\underline{x_2},\underline{x_3},\underline{x_4}) &\equiv 2\,\mathrm{Im}\,F(x_1,x_2,x_3,x_4) \\ &= \sum_{Underlinings}{}' F(x_1,x_2,x_3,x_4) \end{aligned} \tag{2.3}$$

By 'underlining' we mean the following: All possible combinations of the $x_n$ must be underlined or not underlined. Each possibility is summed, although it is immediately possible to see that some of the terms are zero. The permissible diagrams are best expressed graphically. From the remaining terms, rules are defined relating them to $F(x_n)$. Each of the remaining terms will be easier to calculate than the original $F(x_n)$.

Graphically, underlining corresponds to circling a vertex. Any vertex may be circled, as long as the circlings form a connected region on the right of the graph. Due to the connectedness of the circlings, a line can be drawn through the graph from top to bottom. This line makes the graph look as though it has been cut. Cutting is a consequence of the direction of energy flow coming in at the left and out at the right. We shall see that each propagator is modified by the cut in a certain way. The cut propagators, defined in Appendix C.1, must be replaced by $\Delta^{\pm}$ depending on whether the momentum of a cut propagator runs from left or right. The cut propagators have theta functions ensuring the correct direction of energy flow. Also depending on whether a propagator or vertex falls to the left or right of a cut (the right is called the shadowed region, and is symbolically marked as such - see the right-hand side of Figure 2.3) introduces small modifications to these quantities. Shadowed propagators must be replaced by $\Delta^*$, and shadowed vertices, $g \to -g$. These rules are reiterated in Appendix C.3.

Continuing with the ideas of 't Hooft ([144]) applied to this example, we now get

$$\begin{aligned} \sum_{Underlinings}{}' F(x_1,x_2,x_3,x_4) = {} & F(\underline{x_1},x_2,x_3,x_4) + F(x_1,\underline{x_2},x_3,x_4) + F(x_1,x_2,\underline{x_3},x_4) + \\ & F(x_1,x_2,x_3,\underline{x_4}) + F(\underline{x_1},\underline{x_2},x_3,x_4) + F(\underline{x_1},x_2,\underline{x_3},x_4) + F(\underline{x_1},x_2,x_3,\underline{x_4}) + \\ & F(\underline{x_1},\underline{x_2},\underline{x_3},x_4) + F(\underline{x_1},\underline{x_2},x_3,\underline{x_4}) + F(x_1,\underline{x_2},\underline{x_3},x_4) + F(x_1,\underline{x_2},x_3,\underline{x_4}) + \\ & F(x_1,\underline{x_2},\underline{x_3},\underline{x_4}) + F(x_1,x_2,\underline{x_3},\underline{x_4}). \end{aligned} \tag{2.4}$$

In the above the cuttings obviously exclude the 'no-cutting' case, and 'all-cut' case because they appear on the left of equation 2.3.

As mentioned we can discard some of the above as violating the cutting rule. This can be seen graphically in that the circled vertices do not form a connected region with the outgoing or right hand lines/propagators. Accordingly $F(\underline{x_1}, x_2, x_3, x_4)$, $F(x_1, \underline{x_2}, x_3, x_4)$, $F(x_{1,2}, \underline{x_3}, x_4)$, $F(\underline{x_1}, \underline{x_2}, x_3, x_4)$, $F(\underline{x_1}, x_2, \underline{x_3}, x_4)$, $F(\underline{x_1}, x_2, x_3, \underline{x_4})$, $F(\underline{x_1}, \underline{x_2}, \underline{x_3}, x_4)$, $F(\underline{x_1}, \underline{x_2}, x_3, \underline{x_4})$, $F(x_1, \underline{x_2}, \underline{x_3}, x_4)$ and $F(x_1, \underline{x_2}, x_3, \underline{x_4})$ all go for this reason. All that remains is

$$\sum_{Underlinings}{}' F(x_1, x_2, x_3, x_4) = F(x_1, x_2, x_3, \underline{x_4}) + F(x_1, x_2, \underline{x_3}, \underline{x_4}) + F(x_1, \underline{x_2}, \underline{x_3}, \underline{x_4}), \quad (2.5)$$

which can be represented graphically as

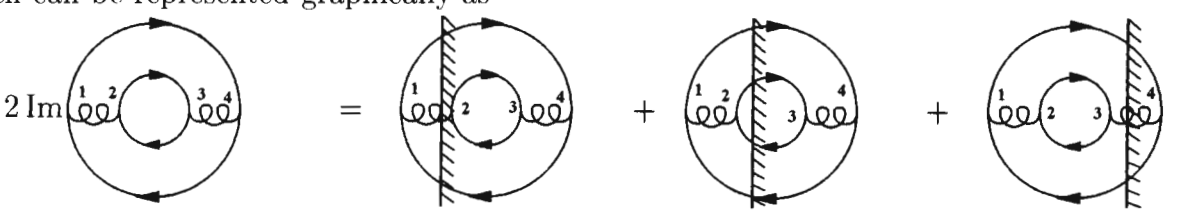


Figure 2.3: The graphical representation of equation 2.3

In Figure 2.3 the numbers at the vertices label the space coordinates $x_n$ and each graph has an analogue in equation 2.5. The "Underlinings" term of 2.5 and Imaginary term of Figure 2.3 are related using equation 2.3. Graphs, like 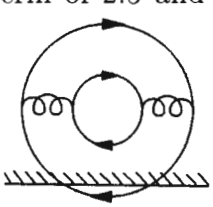 , are seen to be zero due to conflicting $\theta$ functions introduced by the cutting.

It is easier to look at energy momentum conservation in momentum space. This we do using the Fourier transformed expressions, and then look up the expressions for cut propagators or circled vertices in Appendix C.3. Before doing this we can further reduce the number of graphs - the first and last graphs of Figure 2.3 will be zero when we integrate the initial and final states to get the rate, because the gluon is massless. Finally, after all the zero contribution cuts have been removed, we obtain for equation 2.3, using Appendix C.3

$$\begin{aligned} 2\,\mathrm{Im}\,F(x_1, x_2, x_3, x_4) \;=\; & F(x_1, x_2, \underline{x_3}, \underline{x_4}) = \tilde{\Delta}^-(x_4 - x_1)\,\tilde{\Delta}^+(x_1 - x_4)\; g\,\tilde{\Delta}(x_1 - x_2)\; g\; \times \\ & \tilde{\Delta}^-(x_2 - x_3)\,(-g)\,\tilde{\Delta}^+(x_3 - x_2)\;\tilde{\Delta}^*(x_3 + x_4)\;(-g). \end{aligned} \quad (2.6)$$

Hence, all we need calculate the rate is the second graph of Figure 2.3 or equation 2.6. In momentum space equation 2.6 becomes

$$2\,\mathrm{Im}\,F(p_1, p_2, p_3, p_4) = \tilde{\Delta}^-(p_4)\,\tilde{\Delta}^+(p_3)\; g\,\tilde{\Delta}(p_4 + p_3)\; g\,\tilde{\Delta}^-(p_2)\;(-g)\,\tilde{\Delta}^+(p_1)\;\tilde{\Delta}^*(p_2 + p_1)\;(-g)$$

where $\tilde{\Delta}(p)$ is the Fourier transformed $\Delta(x)$ and $p_n$ are the propagator momenta of Figure 2.5 or equation 2.8.

We then look up the twiddle vertices and propagators in Appendix C.1, and this then gives us the matrix element squared. To make a connection with the $T$-matrix, we need to integrate the (internal) momenta of expression 2.6. Next, to obtain the rate we must first consider the optical theorem (section A.4 and equation A.5), from which we see that we have just calculated the requisite imaginary (Im) part. Hence

$$\begin{aligned} \text{Im} <q\bar{q}|T|q\bar{q}>= \frac{1}{2}\int dp_1\, dp_2\, dp_3\, dp_4\, \tilde{\Delta}^-(p_4)\, \tilde{\Delta}^+(p_3)\; g \;\times \\ \tilde{\Delta}(p_4+p_3)\; g\, \tilde{\Delta}^-(p_2)\; (-g)\; \tilde{\Delta}^+(p_1)\; \tilde{\Delta}^*(p_2+p_1)\; (-g). \end{aligned} \tag{2.7}$$

By $dp$ we mean $d^4p$. In fact, we will soon have statistical distribution factors multiplying the measures as well. This equation for the rate has been derived in the same sense as the cross-section. However the integration over $p_1$ and $p_2$ may lad to infinite quantities. We will return to this point from the perspective of thermal field theory. Graphically the rate is simply

$$R_{q\bar{q}\to Q\bar{Q}} = \frac{1}{2}$$

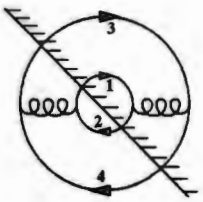


. (2.8)

In future we drop the half, because there are two ways of joining the external lines (i.e. the top left 'outgoing' line, can either be identified with the top right 'incoming' line or bottom right 'outgoing' line). We will evaluate equation 2.8 in the next section. If we had decided to calculate the cross sections, we would have not closed the incoming with the outgoing fermion lines.

### Gluon Fusion

Our second example is to evaluate the rate for gluon fusion. Without going through the analogous steps of the previous example, we find that we have to evaluate the following:

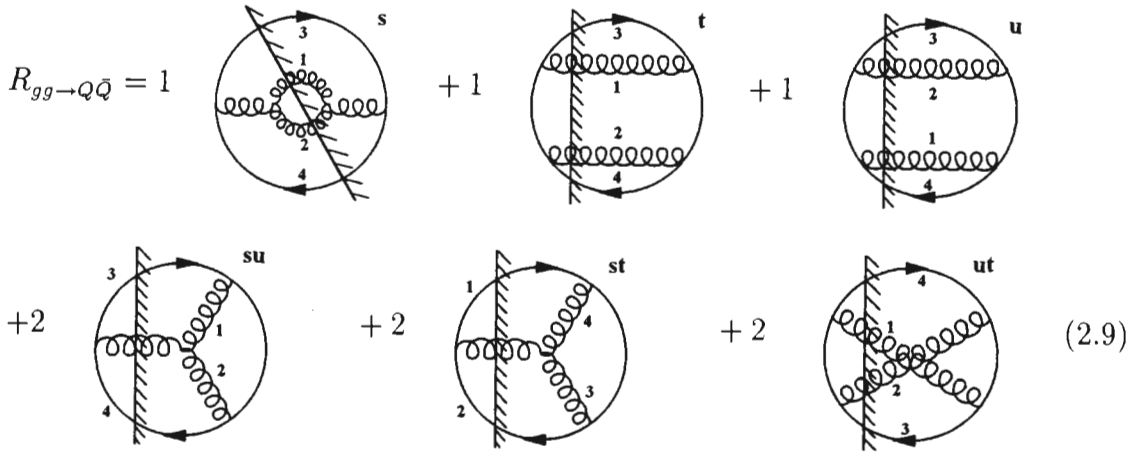


(2.9)

There are cross terms ($su$, $st$ and $ut$) from squaring the matrix element, to be taken into account. Note that the preceding diagrams are representative of various different geometries, all with the same topology. For example, diagram 1 of equation 2.9 may be drawn as

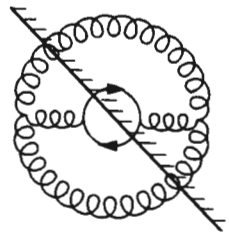

Figure 2.4: Equivalent geometries

The only tricky thing we need to consider, that goes beyond the normal application of the Cutkosky rules, are phase space factors, loosely represented by $dp$, which we discuss again in section (2.1.2). In the quark-gluon plasma the phase space factors will be weighted with a thermal equilibrium distribution function (Bose-Einstein or Fermi-Dirac). This is an ad-hoc way of introducing the effect of the medium on the rate. These phase space factors emerge 'naturally' in the finite temperature formalism (which is the whole point of introducing the formalism).

The Cutkosky rules, summarised in Appendix C.3, tell us how to evaluate the imaginary part of Feynman diagrams. We do this in the next chapter.

### 2.1.2 Thermal factors

We must address is the phase space factors mentioned earlier.

In a thermal medium we must take into account the availability of gluons and quarks to

allowing a reaction, and Pauli blocking, prohibiting a reaction. This we add by hand, although it emerges naturally in the finite temperature formalism and in the Kobes-Semenoff rules.

For quarks, the Pauli blocking term is $(1 - f_{FD})$, where $f_{FD}$ are Fermi Dirac statistics (thermal equilibrium is assumed, but more about this later). The gluons get an enhancement factor of $(1 + f_{BE})$ where $f_{BE}$ are Bose-Einstein statistics.

These statistical factors are automatically introduced with the Kobes-Semenoff rules.

**Pauli Blocking:**

As more quarks and anti-quarks are produced so they progressively reduce the available phase space through the Pauli Exclusion principle. Assuming that the produced quarks are rapidly thermalised, then their momentum distributions can be represented by the usual Fermi Dirac distribution function $f_{FD} = \frac{1}{e^{\beta(E-\mu)}+1}$.

It [116] has been concluded that Pauli blocking does not have a significant effect on the results of [98] in the $gg \to s\bar{s}$ and $q\bar{q} \to s\bar{s}$. It is then possible to further evaluate some of the integrals to follow in this section analytically. At the expense of accelerating the numerical integration we rather leave the Pauli blocking terms in because we will be using the distribution functions with a wide domain of parameters ($T$ and $\mu$).

With these considerations, the rates of equation 2.9 become

$$\begin{aligned} R^{loss}_{gg\to s\bar{s}} &= \int \frac{d^3p_1}{(2\pi)^3 2E_1}\frac{d^3p_2}{(2\pi)^3 2E_2}\frac{d^3p_3}{(2\pi)^3 2E_3}\frac{d^3p_4}{(2\pi)^3 2E_4}(2\pi)^4\delta(p_1+p_2-p_3-p_4)\times \\ &\quad f_{BE}(E_1)\, f_{BE}(E_2)\,(1-f_{FD}(E_3))\,(1-f_{FD}(E_4))\sum|\mathcal{M}(gg\to s\bar{s})|^2 \end{aligned} \tag{2.10}$$

and

$$\begin{aligned} R^{gain}_{s\bar{s}\to gg} &= \int \frac{d^3p_1}{(2\pi)^3 2E_1}\frac{d^3p_2}{(2\pi)^3 2E_2}\frac{d^3p_3}{(2\pi)^3 2E_3}\frac{d^3p_4}{(2\pi)^3 2E_4}(2\pi)^4\delta(p_1+p_2-p_3-p_4)\times \\ &\quad f_{FD}(E_3)\, f_{FD}(E_4)\,(1+f_{BE}(E_1))\,(1+f_{BE}(E_2))\sum|\mathcal{M}(s\bar{s}\to gg)|^2. \end{aligned} \tag{2.11}$$

and a similar expression for quark annihilation equation 2.8.

**Distribution functions:** The Bose-Einstein and Fermi Dirac momentum space distribution functions are $f_{(BE=+)} = \left(e^{\beta(E-\mu)}-1\right)^{-1}$ and $f_{(FD=-)} = \left(e^{\beta(E-\mu)}+1\right)^{-1}$. These distribution functions however only hold when the system is in thermal equilibrium. Accordingly, as $T \to \infty$ (or $\tau \to 0$ and $\mu \to -\infty$) then these functions are no longer valid, as witnessed by results to follow in section 4.3.2.

Also the distribution functions can not be taken seriously for the momentum $k \gg T$. This is due to the long equilibrium time (due to the long mean free path) for high momentum

particles which can be done by comparing the thermal relaxation time to the expansion time.

For numerical reasons we find it easier to use $f'_{\pm}(E,\mu)$ defined by

$$f_{\pm}(E,\mu) = \frac{1}{(e^{\beta(E-\mu)} \mp 1)} = e^{-\beta E}\frac{e^{\beta\mu}}{(1 \mp e^{-\beta(E-\mu)})} = e^{-\beta E} f'_{\pm}(E,\mu). \tag{2.12}$$

The other useful formula we use is

$$1 \mp f_{\pm} = \exp(\beta(E-\mu)) f_{\pm}.$$

With the help of this equation we can express all the rates in the form of

$$\delta R_{x_1x_2\leftrightarrow y_1y_2} = \delta R_{x_1x_2\rightarrow y_1y_2} - \delta R_{x_1x_2\leftarrow y_1y_2} = (\exp\beta(\mu_{x_1}+\mu_{x_2}) - \exp\beta(\mu_{y_1}+\mu_{y_2}))R^*_{x_1x_2\leftrightarrow y_1y_2}.$$

The second term,$R^*$, only weakly depends on $\mu$, for the domain of interest. It has the functional form $R^* = \int dp_1\, dp_2\, dp_3\, dp_4\, \mathcal{M}\, f_{\pm} \times f_{\pm} \times f_{\pm} \times f_{\pm}$.

If we are considering gluon fusion, then $\mu_{x_1} = \mu_{x_2} = 0$ because we assume that gluons have reached chemical equilibrium in our simulation. We will see in the next chapter that for $\mu_{x_3} = \mu_{x_4} = \mu = -\infty$ the associated number densities are zero but the rate, as a function of $\mu$, is at a maximum. If we consider only strange quarks and have them produced in pairs then from $n_s = n_{\bar{s}}$ we have $\mu_s = \mu_{\bar{s}}$. Chemical equilibrium is determined by the minimum of the Gibbs Free Energy $G = \mu_s n_s + \mu_{\bar{s}} n_{\bar{s}}$ . Since we have $n_s = n_{\bar{s}}$ then $\frac{dG}{dn_s} = 0$ gives $\mu_s = -\mu_{\bar{s}}$ and hence $\mu_s = 0$.

The statistical factors can be included in the rates in a more rigorous way using thermal field theory.

## 2.2 Thermal Field Theory

### Introduction

We have outlined the production rates of strange quarks in a gluon plasma by perturbative QCD in the zero temperature formalism. However, the medium has only been alluded too in a trivial way. The most recent understanding of a quark-gluon plasma predicts that from a medium dominated by gluons, with a possibly non-perturbatively generated mass, heavier quarks are formed. This now necessitates a consistent finite temperature field theory. Besides bulk thermodynamic quantities that have been studied using TFT, phase transitions and other dynamical quantities are of interests.

Thermal Field Theory arises by noting the similarity between the partition function (the thermodynamic trace over all quantum states)

$$\mathcal{Z} = \mathrm{Tr}\left[\exp\left(-\beta H\right)\right] = \sum_{i=0} <\varphi^{(i)} \mid \exp\left(\beta H\right) \mid \varphi^{(i)}> \tag{2.13}$$

and the propagator

$$S_{T=0}(x,y) = <0|\mathrm{T}[\varphi(x),\varphi(y)]|0> \quad (2.14)$$

$$= <\varphi_f \mid \exp[-i(t_f - t_i)H] \mid \varphi_i> . \quad (2.15)$$

Assuming $x^0 > y^0$, equation 2.14 is obtained from equation 2.13 by using $\exp(i\,t_i\,H)|\varphi_i>= |0>$. The propagator is generalised to include temperature by

$$S_{T\neq 0}(x,y) = \mathrm{Tr}\,[\exp(-\beta H)\mathrm{T}[\varphi(x),\varphi(y)]] \quad (2.16)$$

$$= <\varphi_f \mid \exp[-i(t_f - t_i + i\beta)H] \mid \varphi_i> /\mathcal{Z}. \quad (2.17)$$

In the Path Integral representation 2.14 becomes

$$\int [d\pi] \int_{\varphi(\vec{x},t_i)=\varphi(t_i)}^{\varphi(\vec{x},t_f)=\varphi(t_f)} [d\varphi]\, \exp[i \int_{t_i}^{t_f} dt \int d^3x \left(\pi(x)\frac{\partial\varphi(x)}{\partial t} - \mathcal{H}(\pi(x),\varphi(x))\right). \quad (2.18)$$

$\pi(x)$ is the momentum conjugate to the field variable $\varphi(x)$. $\mathcal{H}$ is a functional of $\pi(x)$ and $\varphi(x)$ .

Equation 2.18 has a similar generalisation but the integration will now go from $t = \tau = t_f - t_i$ to $t = \tau - i\beta$. The contour joining $\tau$ to $\tau - i\beta$ can be generalised to a contour monotonic in the imaginary variable in $\mathcal{C}$. Two choices of contour are of interest [10]: The simplest choice, a vertical line joining $\tau$ and $\tau - i\beta$, gives the Imaginary Time Formalism (ITF). This can be analytically continued to the real time [60]. Otherwise, by choosing the contour with a segment on the real axis we get a $2 \times 2$ matrix structure for the propagator [87] with real time. There is a parameter, $\sigma$, which is the intermediate value of the contour. This is often fixed at $\sigma = \frac{\beta}{2}$. From this we get a $2 \times 2$ structure of the propagator, the Real Time Formalism (RTF). The $1-2$, $2-1$ and $2-2$ components represent 'ghost' fields. It has been shown that another way of looking at the structure of the propagator is in terms of advanced and retarded propagators. The $1-1$ component is physical. It corresponds with the analytically continued Imaginary Time Formalism and the conventional QCD results. This $2\times 2$ propagator resolves ambiguous delinquent products of delta functions that emerge from the analytically continued Imaginary Time Formalism.

Because the Lagrangian is Lorentz invariant, it is most often used in TFT. Thermal field theory is renormalisable, provided the conventional field theory is. Infra-red divergences are more difficult to understand, however they are not considered further here.

### Thermal Field Theory Formalism

We will mainly use the Real Time Formalism, because we will be needing a real time in calculating dynamical quantities. We have at our disposal the one component propagator prescription of Dolan and Jackiw [60], but because we will be multiplying propagators, to

avoid ambiguous products of delta functions we will use the $2 \times 2$ Real Time Formalism. This doubles the degrees of freedom on internal lines, giving rise to 'ghost' lines, or advanced and retarded propagators.

The rules for the $2 \times 2$ Real time formalism are in Appendix C.2.

## 2.3 Kobes-Semenoff Rules

The Kobes-Semenoff rules are the thermal field theory equivalents to the Cutkosky rules. They are of use because in some cases it is of interest to calculate the imaginary part of a Feynman graph, such as in calculating spectral functions, dispersion relations, decay due to Landau damping of the propagator and cross section or rates.

The Cutkosky rules of conventional Field Theory were generalised in 1984 and 1985 in two papers by Kobes and Semenoff [83, 84]. The rules consist of a general set and a set with a narrower application. The latter are of use here.

We have already outlined the Cutkosky rules by applying them to specific cases (see section 2.1.1). The notion of cutting a Feynman graph does not carry through for finite temperatures. Nonetheless, the Kobes-Semenoff rules are still labour saving. The Kobes-Semenoff rules use the $2 \times 2$ real-time formalism, because analytically continuing the imaginary time formalism is difficult for $(n > 2)$-point functions.

The derivation of Kobes and Semenoff follows that of [144] follow directly from the notation of section 2.1.1 and can be compared to the Cutkosky rules in Appendix C.3 and section 2. We do not repeat the discussion of section 2, because of the close analogy with what follows. We must however note that the idea of cutting does not extend to finite temperature and therefore every modified diagram contributes. For the Cutkosky rules, by examining the connectivity of the circling/cutting, we could disregard diagrams.

### 2.3.1 Kobes-Semenoff Rules - arbitrary vertices

We use $\Delta_{ij}(k)$ as a generic expression for $D^{ab}, D^{ab}_{\mu\nu}$ or $S^{ab}$ in [83]. Given in Appendix C2 is the cut propagator $\Delta^{\pm}$.

The cutting rules then say that to evaluate the imaginary part of a diagram $F(x_1, ...x_n)$ we have to sum over all possible internal vertices first, and then take the imaginary part of each diagram. This means that for $n$ vertices we have to evaluate $2^n$ diagrams. This process is exactly the same as for conventional QCD, except that we cannot use the notion of cutting.

- for a 1-1/2-2 propagator
  - leave $i\Delta_{11}(x-y)$ or $i\Delta_{22}(x-y)$ unchanged if neither $x$ nor $y$ is underlined;

  - replace $i\Delta_{11}(x-y)$ or $i\Delta_{22}(x-y)$ by $\Delta^{+}(x-y)$ or $i\Delta^{-}(x-y)$ if $x$ but not $y$ is underlined;
  - replace $i\Delta_{11}(x-y)$ or $i\Delta_{22}(x-y)$ by $\Delta^{-}(x-y)$ or $i\Delta^{+}(x-y)$ if $y$ but not $x$ is underlined;
  - replace $i\Delta_{11}(x-y)$ or $i\Delta_{22}(x-y)$ by $\Delta_{22}(x-y)$ or $i\Delta_{11}(x-y)$ if $x$ and $y$ are underlined;

- The $1-2$ and $2-1$ propagators are left unchanged in all cases;
- Reverse the sign of the vertex of either type 1 or 2 when it is underlined.

All possible combinations of internal vertices must be considered. These rules must be applied to each possible configuration in turn.

In momentum space these rules are

- for a $1-1$ or $2-2$ propagator
  - leave $i\Delta_{11}(k)$ or $i\Delta_{22}(k)$ unchanged if neither of the vertices are circled;
  - replace $i\Delta_{11}(k)$ or $i\Delta_{22}(k)$ by $\Delta^{+}(k)$ or $i\Delta^{-}(k)$ if $k$ flows from an uncircled vertex to a circled one;
  - replace $i\Delta_{11}(k)$ or $i\Delta_{22}(k)$ by $\Delta^{+}(k)$ or $i\Delta^{-}(k)$ if $k$ flows from a circled vertex to an uncircled one;
  - replace $i\Delta_{11}(k)$ or $i\Delta_{22}(k)$ by $\Delta_{22}(k)$ or $i\Delta_{11}(k)$ if $k$ both vertices are circled;

- The $1-2$ and $2-1$ propagators are left unchanged in all cases;
- Reverse the sign of the vertex of either type 1 or 2 when it is underlined.

### 2.3.2 Kobes-Semenoff Rules - external vertices

The above rules can be made specific to the case where all the external legs are physical particle lines. This reduces the sum over internal vertices and cut diagrams considerably [84].

Consider an amputated diagram corresponding to $F(y_1,..,y_l,z_1,..,z_p)$, namely $\mathcal{F}(y_1,..,y_l,z_1,..,z_p)$. If there are $p$ vertices that are internal and $k$ vertices with external lines attached to them, then a naive use of the rules would mean we would have to sum over all internal vertices $G(y_1,..,y_l,z_1,..,z_p)=\sum_{z_i\in(1,2)}\mathcal{F}(y_1,..,y_l,z_1,..,z_p)$. A simpler expression is for the Imaginary part of $G$ is

$$\mathrm{Im}G=\frac{1}{2}[G(y,z)+G^{*}(y,z)]=-\frac{1}{2}\sum_{(y),z}F_{<}(y_1,..,y_l,z_1,..,z_p)=-\frac{1}{2}\sum_{(y),z}F_{>}(y_1,..,y_l,z_1,..,z_p).$$

we sum over all possible ways of underlining the internal $z$ vertices, but sum only over those terms that include both underlined and non-underlined vertices. We will now find how to calculate $F_<$ and $F_>$.

Although the previous Kobes-Semenoff rules are straight forward, they lead to a proliferation of terms. Unlike conventional QCD every term contributes. We will try and reduce the graphs. The procedure involves removing any reference to vertices through the rules

- $\Delta_{11}(x-y) = \Delta(x-y)$
- $\Delta_{12}(x-y) = i\Delta^-(x^0 - y^0 + \frac{1}{2}i\beta, \vec{x}-\vec{y})$ which becomes in momentum space $i\Delta_{12}(p) = \exp(\beta p_0/2)\, i\Delta^-(p)$
- $\Delta_{21}(x-y) = i\Delta^+(x^0 - y^0 - \frac{1}{2}i\beta, \vec{x}-\vec{y})$ which becomes in momentum space $i\Delta_{21}(p) = \exp(-\beta p_0/2)\, i\Delta^+(p)$
- $\Delta_{22}(x-y) = \tilde{\Delta}(x-y)$

The $\Delta$ is the same as before, and $i\tilde{\Delta}(x) = -i\Delta^*(x)$. By confounding the vertex summation and the diagram summation, one is able to reduce the number of terms substantially. The rules are now defined for either one of two possible functions, $F_<(x_1, .., x_n)$ and $F_>(x_1, .., x_n)$, called the largest time and smallest time relations. For underlined points the following must be done:

- for a $\Delta(x-y)$ propagator
  - leave $i\Delta(x-y)$ unchanged if neither $x$ nor $y$ is underlined;
  - for $F_>$ or $F_<$ replace $\Delta(x-y)$ by $\Delta^+(x-y)$ or $i\Delta^-(x-y)$ if $x$ but not $y$ is underlined;
  - for $F_>$ or $F_<$ replace $\Delta(x-y)$ by $\Delta^-(x-y)$ or $i\Delta^+(x-y)$ if $y$ but not $x$ is underlined;
  - replace $i\Delta(x-y)$ by $\tilde{\Delta}(x-y)$ if $x$ and $y$ are underlined;
- The sign of underlined vertices must be reversed.

In momentum space these rules are

- for a $i\Delta(k)$ propagator
  - leave $i\Delta(k)$ unchanged if neither vertex is underlined;
  - for $F_>$ or $F_<$ replace $\Delta(k)$ by $\Delta^+(k)$ or $i\Delta^-(k)$ if $k$ flows from a non-underlined to an underlined vertex;

- for $F_>$ or $F_<$ replace $\Delta(k)$ by $\Delta^-(k)$ or $i\Delta^+(k)$ if $k$ flows from an underlined to a non-underlined vertex;
- replace $i\Delta(k)$ by $-i\Delta^*(k)$ if both vertices are underlined;

- The sign of underlined vertices must be reversed.

These rules do not support the notion of cutting. We do not use these rules further directly, but they would be vital in extending the calculations of Chapter 2 to finite temperature.

## 2.4 Braaten-Pisarski Resummation

When introducing the rules for Braaten Pisarski resummation we will use the mixed representation of the imaginary time formalism, because it is simpler than the real time formalism and because we do not need any explicit time dependence. The mixed representation uses $\tau$ and $k$ for the independent variables. In the following, $P$ or $p$ is the external momenta, and $K$ or $k$ the internal momenta of the hot thermal loop.

### A simple example

In hot scalar theories (because it is hot we can disregard the mass) such as $(\lambda\phi)^4$ theory, the only diagram contributing to order $\lambda$ is the tadpole graph, ie . We will show briefly that the self-energy ($\Sigma$) of this tadpole is proportional to $\lambda T^2$.

**Mixed Representation of Propagator:** To proceed we need the $\Delta(\tau, k)$ propagator in $(\lambda\phi)^4$ theory. To evaluate $\Delta(\tau, k)$ we must go back to the Fourier transform

$$\Delta(\tau, k) = T \sum_{j=-\infty}^{\infty} e^{i k_0 \tau} \Delta(k_0, k). \tag{2.19}$$

$k_0$ is the usual Matsubarra frequency, $k_0 = 2\pi j T$ for bosons and $k_0 = \pi(2j+1)T$ for fermions. We also need $\Delta(k_0, k) = 1/(k_0^2 + k^2)$. For this section we use the Euclidean metric, appropriate for the ITF.

To make progress the sum is replaced with a contour integral that sums the argument, the above expression, at the infinite number of poles corresponding to appropriate values for $k_0$. The contour is then deformed in such a way as to contribute nothing to the integral, but to isolate a finite number of new poles that are easily evaluated.

$$\Delta(\tau, k) = T \sum_{j=-\infty}^{\infty} \sum_{k_0 = 2\pi j T} \exp(i k_0 \tau) \frac{1}{k_0^2 + k^2} = \frac{-1}{2\pi i} \int_{C_1} \exp(i k_0 \tau) \frac{1}{k_0^2 + k^2} \frac{dk_0}{\exp(i k_0 / T) - 1}$$

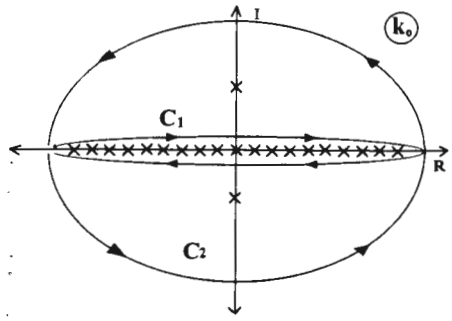


Figure 2.5: Contour for Summation

This has poles along the real axis at $k_0/T = 2\pi j$ and at $k_0 = \pm ik$. The contour $C_1$, the inside lens like loop, and $C_2$, the outside loop that will be brought to infinity, are also indicated. The integral along $C_1 + C_2 = 0$. Accordingly

$$\begin{aligned}\Delta(\tau,k) &= \frac{T}{2\pi i}\int_{C_2}\exp(ik_0\tau)\frac{1}{k_0^2+k^2}\frac{dk_0}{\exp(ik_0/T)-1}\\ &= \frac{1}{2\pi i}\int_{C_2}\exp(ik_0\tau)\left(\frac{1}{k_0-ik}-\frac{1}{k_0+ik}\right)\frac{1}{2k}\frac{dk_0}{\exp(ik_0/T)-1}\\ &= T\left(\frac{\exp(-k\tau)}{\exp(-k/T)-1}-\frac{\exp(k\tau)}{\exp(k/T)-1}\right)\frac{1}{2k}\end{aligned}$$

This gives for bosons

$$\Delta_-(\tau,k) = \frac{1}{2k}\left((1+n_-(k))\,e^{-k\tau}+n_-(k)\,e^{k\tau}\right),$$

and for fermions

$$\Delta_+(\tau,k) = \frac{i\not{K}}{2k}\left((1-n_+(k))\,e^{-k\tau}-n_+(k)\,e^{k\tau}\right),$$

where $n_\pm(k) = 1/\left(e^{k/T}\pm 1\right)$ is the Bose-Einstein$(-)$ or Fermi-Dirac$(+)$ distribution functions. We can invert the relation using

$$\Delta(k_0,k) = \int_0^{\frac{1}{T}} d\tau\, e^{i\,k_0\,\tau}\,\Delta(\tau,k). \tag{2.20}$$

$(\lambda\phi)^4$**Theory** We look at the tadpole diagram for bosons illustrated earlier as an example. This is the simplest diagram:

$$\mathrm{Tr}\Delta(K) = T\,\lambda\int\frac{d^3k}{(2\pi)^3}\sum_{\substack{j=-\infty\\ k^0=2\pi\,j\,T}}^{\infty}\Delta(k^0,k). \tag{2.21}$$

Using 2.20 in 2.21, then evaluating the $k_o$ summation which gives $\delta(k_o)$ then finally doing the integration gives

$$\mathrm{Tr}\Delta(K) = T\,\lambda\int\frac{d^3k}{(2\pi)^3}\frac{1}{2k}(1+2\,n(k)).$$

The first term is divergent but is removed during renormalisation. The second integral can be done and $\mathrm{Tr}\Delta(K) = \frac{\lambda}{12}T^2$. Relabeling the vertex $\lambda = g^2$ means that $m \propto gT$. Summing all these contributions to the propagator ($D$) into an effective propagator ($i\mathcal{D}$) can be done using Dyson's equation:

$$i\mathcal{D} = iD + iD(-i\Sigma)i\mathcal{D}$$

or graphically expanding the self-referential $\mathcal{D}$

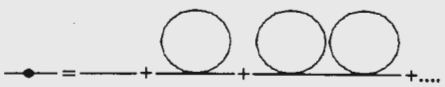

If $D \to \Delta$ and $i\Sigma \to \mathrm{Tr}\Delta(k)$ then this can be solved

$$i\mathcal{D} = \frac{1}{p^2 - m^2 - \Sigma + i\epsilon}.$$

That the thermal medium induces a mass is a well known result going back decades to Silin. This is all Braaten-Pisarski summation amounts to in scalar theory. The nice surprise is that this result can be generalised to gauge theories. Here, we do not have simple scalars, but functions that depend upon external momentum in a complicated way. The functions are also similar in QED and QCD.

**Introduction**

In perturbative calculations, such as in calculating the damping rate, expansions based solely on the power of $g$, the dimensionless coupling constant of QCD leads to problems such as gauge dependent physical results and solutions dependent on the number of terms in the expansion. This is due to terms in the expansion of the same order as those been retained, being omitted, because in hot gauge theories the usual connection between order of the loop expansion and powers of $g$ is effectively lost. In 1989 Braaten and Pisarski [36] determined a systematic procedure of exhaustively finding all diagrams of the same magnitude and summing them into effective propagators and vertices.

In the following discussion, and in fact in the whole thesis, we are working in a hot medium with gluons and deconfined quarks . Roughly speaking we expect the constituent particles to have $p \simeq T$ and we have $g < 1$. If $p \simeq gT$ then it is termed **soft**, otherwise if $p \simeq T$ it is termed **hard**. In thermal gauge theories, closed loops with hard internal momenta need to be added to propagators and vertices with soft momenta. These loops are called Hard Thermal Loops (HTL's). Ordinary perturbation theory applies to propagators or vertices with hard momenta but effective vertices and propagators are required when all external lines have soft momenta.

HTL's consist of one loop corrections of order $g^2T^2/P^2$ times the corresponding tree amplitude, where $P$ is the momentum characteristic of the external line. If the external leg is hard, then they are $g^2$ times smaller than the tree amplitude. If the external momentum

is soft, then $g^2T^2/P^2 \to 1$, and the Hard Thermal Loop is as important as the tree diagram. Accordingly, hard thermal loops of the same 'order' need to be resummed. Braaten-Pisarski show how to identify hard thermal loops and establish an exhaustive list of them. They further show how they must be resummed.

HTL's are ultraviolet finite (if the $T = 0$ field theory is) and gauge independent. No general proof exists of this gauge invariance but have been calculated in the Feynman Gauge and Coulomb Gauge and found to be the same. They satisfy Ward-like identities. If all the momenta going into a vertex are soft then an effective vertex is needed.

### 2.4.1 Hard Thermal Loops

The hard thermal loops in non-Abelian gauge theories were first computed by Weldon and Klimov [148]. We will come back to these in section 3.2.1.

Central to Braaten Pisarski Resummation is that Hot Gluon Loops (HTL's) contribute to the same order as the equivalent tree diagram. HTL's arise from the part of the integration over closed loops that is hard, and all other momenta are soft.

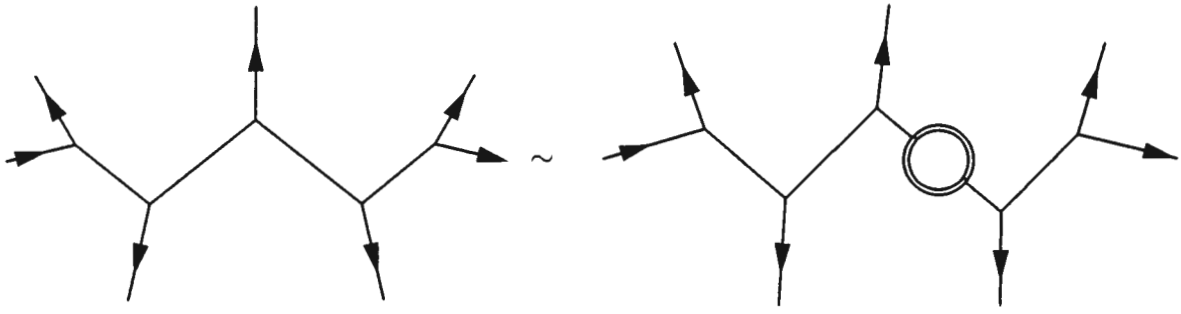

Figure 2.6: Equivalent $N = 7$-point tree diagrams.

In the accompanying tree diagram in Figure 2.6, the double circle represents a HTL listed below. Therefore disregarding the last diagram as being of order $g^2$ smaller than the first tree diagram leads to errors in such quantities as the damping rate.

Before continuing we list all possible Hot Thermal Loops. In the Coulomb and Feynman gauges (in which we work) HTL's are produced by an extremely small subset of loops. Despite there being more diagrams in other non-covariant gauges, when the sum of all the one loop diagrams contributing to a certain amplitude are added, the sum is the same for that for the Coulomb and Feynman gauges.

We get four generic kinds of Hot Thermal Loops. Referring to Figure 3.2. First the $N$-gluon amplitudes - gluon loops (1a), ghost loops (1b) and quark loops (3). Then the HTL between a quark pair and $N-2$ gluons (2). Tadpole diagrams may be considered to be a fifth (4).

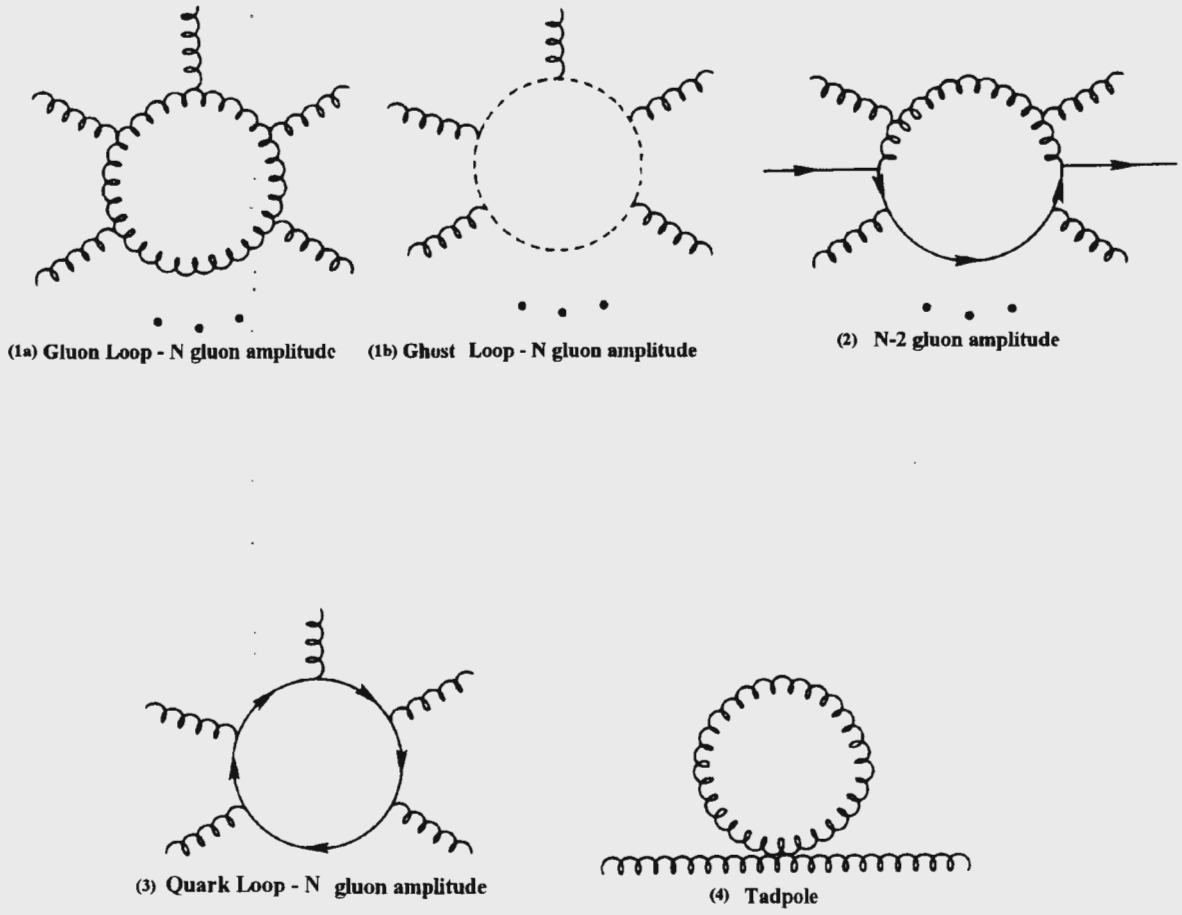


Figure 2.7: The only Hot Thermal Loops in QCD

In non-abelian gauge theories these are the only integrals to develope Hard Thermal Loops.

The ghost contribute only to the same order as the other graphs when all the propagators are internal.

### 2.4.2 Extracting Hard Thermal Loops

We outline a method of identifying hard thermal loops.

#### Power-Counting

These loops were isolated by Braaten and Pisarski [33]. They developed a way of power counting to isolate the HTL's. Essentially the idea is to use the Imaginary Time Formalism, but with propagators in a form where the 'time' component is explicit, see equation 2.19.

The power-counting rules for the $k_0, k$ expressions are

- $\int d^3k$ gets $T^3$
- the summation over $k_0$ and first propagator contributes $1/T$

- every additional propagator gives $\frac{1}{PT}$
- Powers of $K$ gets $T$, powers of $P$ reduces the order for HTL's because they give $P$
- For integrals with 2 or more fermion or boson propagators only, the power count gets an additional $P/T$ from cancellation of distribution functions.

### 2.4.3 Resummation

Until now we have discussed how to isolate HTL's. We have shown that if one has a propagator with soft momentum, there are a few other diagrams that are of the same effective order. These diagrams must now be summed into an effective propagator. This propagator must be used in calculations whenever (parts of the integration over) momenta are soft.

We have suppressed color factors in consistency with [36]. These factors enter the summed and unsummed quantities in the same way. In other words Braaten-Pisarski resummation does not affect them. Resummed quantities, indicated with a delta function, are obtained by Braaten-Pisarski resummation. These quantities are linear combinations of the Legendre functions of the second kind, $Q_n(z)$. Resummed quantities are graphically indicated by a filled circle.

**Effective Propagators:**

**Plasmino:** The only possible contribution to the quark self-energy is given below. The resummed quark propagator is often called a plasmino. The ambiguity in the sign with [33] is due to the convention employed by those authors, and not used here. The approximation sign is to remind one that the external momenta are soft and internal momenta are hard. We give the HTL part of the summation ($\delta\Sigma(P)$, $\delta\Pi_{\mu\nu}(P)$ and $\delta\Lambda_{\mu\nu\ldots}(P)$) later. The plasmino propagator is ${}^*S(P) = S(P) - \delta\Sigma(P)$.


Figure 2.8: Plasmino

**Plasmon:** The effective propagator for gluons (frequently called a plasmon) consists of the bare propagator, the gluon and quark loops (self energies sandwiched between external propagators) and the tadpole. As mentioned earlier the ghost is of a smaller effective order in $g$ because it is on external lines.

Explicitly, the effective gluon propagator in the Coulomb gauge is

$$^*D_C^{00}(K) =^* D_l(K)\,,\ ^*D_C^{0i}(K) = 0 \text{ and } ^*D_C^{ij}(K) = (\delta^{ij} - \frac{k^i\,k^j}{k^2})^*D_t(K)$$

where

$$^*D_{t,l}(K) = \frac{1}{K^2 - \Pi_{t,l}}. \tag{2.22}$$

The plasmon propagator is $^*D_{\mu\nu}(K) = D_{\mu\nu}(K) - \delta\Pi_{\mu\nu}(K)$.

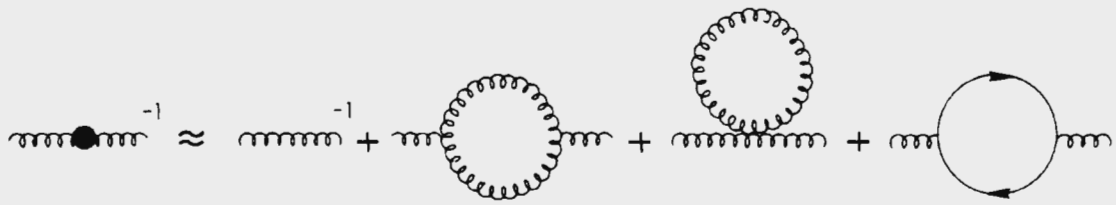


Figure 2.9: Plasmon

**Effective Vertices:**

The effective vertices are obtained by adding the HTL to the bare vertex.

**Three-gluon vertex:** The 3-gluon vertex is $^*\Lambda_{\mu\nu\lambda}(P,Q,R) = \Lambda_{\mu\nu\lambda}(P,Q,R) + \delta\,\Lambda_{\mu\nu\lambda}(P,Q,R)$.

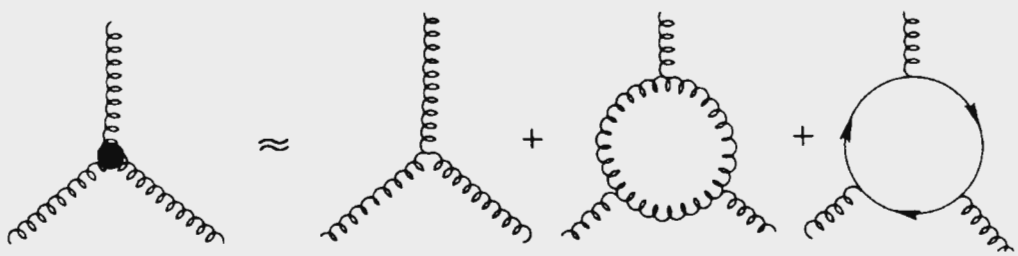


Figure 2.10: 3-gluon vertex

**Quark-gluon vertex:** The quark-gluon vertex is given as ${}^*\Lambda_\mu(P,Q,R) = \gamma_\mu + \delta\,\Lambda_\mu(P,Q,R)$.

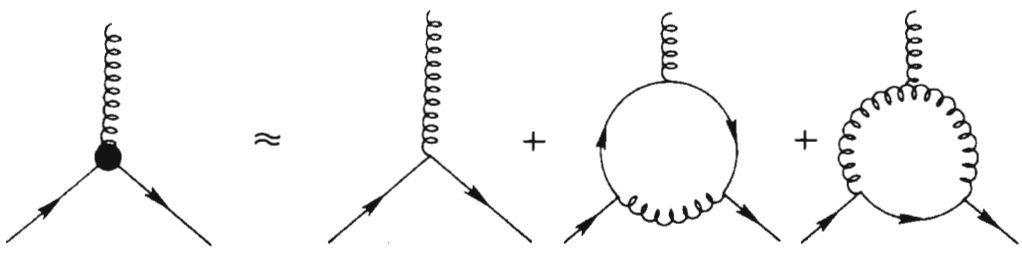

Figure 2.11: Quark-gluon vertex

**Four-Gluon vertex:** Although we do not use the 4-gluon vertex except in the tadpole diagram we record it The 4-gluon vertex is - ${}^*\Lambda_{\mu\nu\lambda\sigma}(P,Q,R,S) = \Lambda_{\mu\nu\lambda\sigma}(P,Q,R,S) + \delta\,\Lambda_{\mu\nu\lambda\sigma}(P,Q,R,S)$.

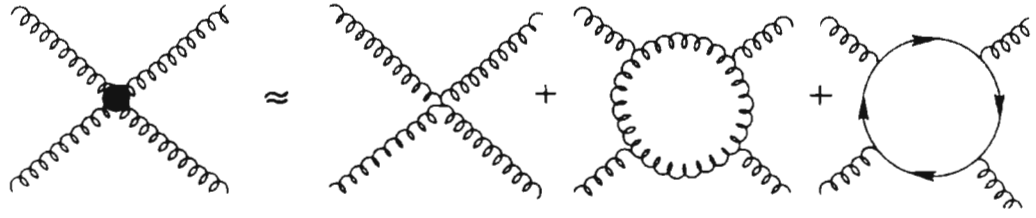

Figure 2.12: 4-Gluon vertex

**Two-quark-two-gluon vertex:** Finally, we have a vertex with no bare analogue. This vertex is represented as ${}^*\Lambda_{\mu\nu}(P,Q,R,S) = \delta\,\Lambda_{\mu\nu}(P,Q,R,S)$. The effective propagator is obtained directly be inversion.

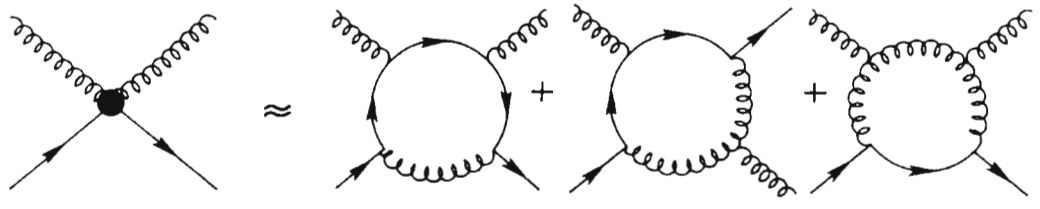

Figure 2.13: 2-quark - 2-gluon vertex

**Ward Identities, Gauge invariance:**

The Hard Thermal Loops obey Ward like identities. In general at finite temperature, vertices and propagators do not have this property. They are exactly the same as they would be for the zero temperature case, except they are starred. The Ward identities become important for writing down the effective propagator for gluons.

# Chapter 3

# QCD mechanisms for the formation of strangeness

### Outline

Microscopic mechanisms of strangeness production in a quark gluon plasma were introduced by T. S. Biró and J. Zimányi [25] in 1982. Shortly thereafter J. Rafelski and B. Müller [116] added the dominant channel of gluon-gluon fusion (see also [98]). The additional mechanism of gluon decay was shown by Altherr and Seibert [4, 7, 22] in 1994 to contribute significantly to the production of strange quarks.

We use the Cutkosky rules to write down the rate of quark annihilation and gluon fusion. In the next section, the polarisation of the vacuum, self energy, damping rate and dispersion relations are presented and examined because they are needed for gluon decay. The intention of this chapter, calculating the rate of gluon decay, is then finally investigated.

We will show that gluon decay is an important (but non-leading) process in strangeness production. We will investigate the contribution of the next order effects of thermal field theory, i.e. thermal corrections to the "$T = 0$" perturbative QCD rates.

We assume that the energy density is sufficiently large to allow the formation of a quark-gluon plasma. For the present highest energy range of $\sqrt{s} = 20$ GeV$\cdot A$ non-perturbative QCD is not negligible. At $\sqrt{s} = 200$ GeV $\cdot A$ the Parton Cascade Model can be used [66, 67].

The intention is to record here important results used in later work, and that will have to be used to extend this work. An obvious program yet to be performed is to continue the above conventional calculations of chapter 2.1 to finite temperature. In this thesis Braaten-Pisarski and Kobes-Semenoff are used explicitly only once or twice. We shall however show that Braaten-Pisarski resummation underlies gluon decay, and Kobes-Semenoff rules are used to calculate the polarisation tensor and will be indispensable in extending these calculations to higher order. We will calculate the decay rate of a plasmon (a gluon with a thermally induced mass and width) and show that it is as important as gluon annihilation to the formation of strangeness. Gluon fusion and quark annihilation, calculated at finite

temperatures, are the next most important in order contributing to strangeness production. In addition infra-red divergences in the production rates of massless quarks are addressed by including effects of the medium.

## 3.1 Rates calculated from the Cutkosky Rules

We now write down the correct Feynman diagrams to calculate the rates, articulate the diagrams in mathematical terms according to the Feynman and Cutkosky rules, and do some obvious simplifications. The next step is to further simplify the expressions by evaluating as many of their integrals as possible. We outline some of the intermediate step in the Appendix D.1. Unless we make some approximations, we cannot remove all the integrals. The remaining integrals we write in a way useful for numerical Gauss-Laguerre and Gauss-Legendre integration.

### 3.1.1 Quark Annihilation

We will now use equation (2.7 or 2.8) to evaluate the rate of quark annihilation. The corresponding fully labelled Feynman diagram is

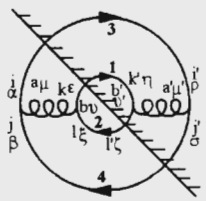


Figure 3.1: Rate of quark annihilation

$p_n$ are labelled in the figure as simply $n$. We suppress the $+i\epsilon$ prescription in the following section and take $dp$ to be $d^4p$ and appropriate statistical factors, obtained from the Kobes-Semenoff rules, or using some prescription for incoming or outgoing fermions or bosons.

$$
\begin{aligned}
R_{q\bar{q}\to s\bar{s}} = \left(\frac{(-1)^2(2\pi)^4}{(2\pi)^{12}}\right) \int dp_1\, dp_2\, dp_3\, dp_4 \left[\theta(p_4^0)\,\delta(p_4^2 - m_s^2)\,(-\not{p}_4 - m)_{\sigma\beta}\,\delta_{jj'}\right] \times \\
\left[\left(ig\gamma^{\mu}_{\beta\alpha}\right)\, T^a_{ij}\right] \left[\theta(p_3^0)\,\delta(p_3^2 - m_s^2)\,(\not{p}_3 - m)_{\alpha\rho}\,\delta_{i'i}\right] \left[\frac{ig_{\mu\nu}\,\delta_{ab}}{(p_3+p_4)^2}\right] \left[\left(ig\gamma^{\nu}_{\epsilon\xi}\right)\, T^b_{kl}\right] \times \\
\left[\theta(p_2^0)\,\delta(p_2^2 - m_s^2)\,(-\not{p}_2 - m)_{\xi\zeta}\,\delta_{ll'}\right] \left[\left(-ig\gamma^{\nu'}_{\zeta\eta}\right)\, T^{b'}_{l'k'}\right] \left[\theta(p_1^0)\,\delta(p_1^2 - m_s^2)\,(\not{p}_1 - m)_{\eta\epsilon}\,\delta_{kk'}\right] \\
\times \left[\frac{-ig_{\mu'\nu'}\,\delta_{b'a'}}{(p_1+p_2)^2}\right] \left[\left(-ig\gamma^{\mu'}_{\rho\sigma}\right)\, T^{a'}_{i'j'}\right] \delta^4(p_1 + p_2 - p_3 - p_4). \qquad (3.1)
\end{aligned}
$$

This can be further simplified to

$$
R_{q\bar{q}\to s\bar{s}} = -\frac{g^4}{(2\pi)^8} \int dp_1\, dp_2\, dp_3\, dp_4\, T^a_{ij}\, T^a_{kl}\, T^b_{lk}\, T^b_{ij}\, \frac{1}{s^2} \times \delta^4(p_1 + p_2 - p_3 - p_4)
$$

$$\times \mathrm{Tr}\left[(\not{p}_2 + m)\ \gamma^\mu\ (\not{p}_1 - m)\ \gamma_\nu\right]\ \mathrm{Tr}\left[(\not{p}_4 + m)\ \gamma^\nu\ (\not{p}_3 - m)\ \gamma_\mu\right]. \tag{3.2}$$

The delta functions and theta functions have now been absorbed into the measures using $d^4p\,\theta(p^0)\,\delta(p^2-m^2) = \frac{d^3p}{2E}$. The color factors can be evaluated by first using equation C.12 or C.13 and evaluating the resulting product of delta functions. The answer is $T^a_{ij}\,T^a_{kl}\,T^b_{lk}\,T^b_{ji} = 2$. The traces are evaluated by multiplying out each bracket, commuting and contracting the $\gamma^\mu$ matrices using equation C.4 and C.5. This diagram is evaluated further in Appendix D.1. The final answer is ([54, 98])

$$\begin{aligned} R_{q\bar{q}\to s\bar{s}} &= -\frac{g^4}{(2\pi)^8}\int dp_1\,dp_2\,dp_3\,dp_4\,\delta(p_1+p_2-p_3-p_4)\times \\ 2\times 8 &\times \frac{(m^2+M^2-t)^2+(m^2+M^2-u)^2+2(M^2+m^2)s}{s^2}. \end{aligned} \tag{3.3}$$

When comparing the above result with that in the literature, an average has to be taken over initial states and isospin factors.

### 3.1.2 Gluon fusion

The final step is to evaluate the gluon fusion processes of equation 2.9.

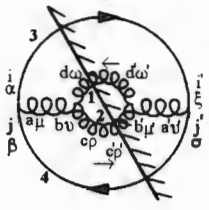


Figure 3.2: Gluon fusion -$s$-channel

We need to include a factor of $\frac{1}{2}$ because of the Bose-Einstein nature of gluons. The arrow over the gluon indicates momentum flow.

$$\begin{aligned} R^s_{gg\to s\bar{s}} = &\left(\frac{(-1)(2\pi)^4}{2(2\pi)^{12}}\right)\int dp_1\,dp_2\,dp_3\,dp_4\,\left[\theta(p_4^0)\,\delta(p_4^2-m_s^2)\ (-\not{p}_4-m)_{\sigma\beta}\,\delta_{jj'}\right]\left[\left(ig\gamma^\mu_{\beta\alpha}\right)\,T^a_{ij}\right] \\ &\times\left[\frac{-ig_{\mu\nu}\,\delta_{ab}}{(p_3+p_4)^2}\right]\left[(g\,f_{dbc})\left[g^{\omega\rho}(p_2-p_1)^\nu+(-p_1-p_4-p_3)^\omega g^{\nu\rho}+(p_4+p_3-p_2)^\nu g^{\rho\omega}\right]\right]\times \\ &\left[-ig_{\omega\omega'}\,\delta_{dd'}\,\theta(p_1^0)\,\delta(p_1^2)\right]\left[-ig_{\rho\rho'}\,\delta_{cc'}\,\theta(p_2^0)\,\delta(p_2^2)\right]\left[(-g\,f_{d'c'b'})\right]\delta^4(p_1+p_2-p_3-p_4)\times \\ &\left[g^{\omega'\rho'}(-p_2+p_1)^{\nu'}+(p_1+p_4+p_3)^{\omega'}g^{\nu'\rho'}+(-p_4-p_3+p_2)^{\nu'}g^{\rho'\omega'}\right]\times \\ &\left[\frac{-ig_{\mu'\nu'}\,\delta_{b'a'}}{(p_1+p_2)^2}\right]\left[\left(-ig\gamma^{\mu'}_{\xi\sigma}\right)\,T^{a'}_{i'j'}\right]\left[\theta(p_3^0)\,\delta(p_3^2-m_s^2)\ (\not{p}_3-m)_{\alpha\xi}\,\delta_{i'i}\right]. \end{aligned} \tag{3.4}$$

This can be simplified using

$$R^s_{gg\to s\bar{s}} = \frac{g^4}{2(2\pi)^8}\int dp_1\,dp_2\,dp_3\,dp_4\;(\not{p}_4+m)_{\sigma\beta}\;((\gamma_\nu)_{\beta\alpha})\;\frac{1}{s^s}\,T^b_{ij}\,T^a_{ij}\,f_{dbc}f_{dca}\times$$
$$(\not{p}_3+m)_{\alpha\xi}\;g_{\mu\nu}\;[g^{\omega\rho}(p_2-p_1)^\nu+(-p_1-p_4-p_3)^\omega g^{\nu\rho}+(p_4+p_3-p_2)^\nu g^{\rho\omega}]\times$$
$$\left[g^{\omega\rho}(-p_2+p_1)^{\nu'}+(p_1+p_4+p_3)^\omega g^{\nu'\rho}+(-p_4-p_3+p_2)^{\nu'}g^{\rho\omega}\right]((\gamma_{\nu'})_{\xi\sigma})\,. \qquad (3.5)$$

We have not recorded the intermediate steps to evaluating the matrix element squared

$$R^s_{gg\to s\bar{s}} = -\frac{g^4}{2(2\pi)^8}\int dp_1\,dp_2\,dp_3\,dp_4\,3\times 8^2\,\frac{(m^2-t)\,(m^2-u)}{s^2}\delta(p_1+p_2-p_3-p_4). \qquad (3.6)$$

Unfortunately we have unwanted longitudinal gluon degrees of freedom which we remove using ghosts. The following diagram needs to be subtracted:

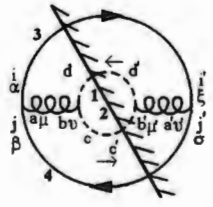


Figure 3.3: Ghost

$$R_{ghost} = \left(\frac{(-1)(2\pi)^4}{2(2\pi)^{12}}\right)\int dp_1\,dp_2\,dp_3\,dp_4\,\left[(-\not{p}_4-m)_{\sigma\beta}\,\delta_{jj'}\theta(p_4^0)\,\delta(p_4^2-m_s^2)\right]\left[\left(ig\gamma^\mu_{\beta\alpha}\right)\,T^a_{ij}\right]$$
$$\times\left[(\not{p}_3-m)_{\alpha\xi}\,\delta_{i'i}\theta(p_3^0)\,\delta(p_3^2-m_s^2)\right]\left[\frac{-ig_{\mu\nu}\,\delta_{ab}}{(p_3+p_4)^2}\right][(g\,f_{dbc})\,[p^\nu_{1\to 2}]]\left[(-i\delta_{dd'})\,\theta(p_4^0)\,\delta(p_1^2)\right]$$
$$\times\left[(-i\delta_{cc'})\,\theta(p_4^0)\,\delta(p_1^2)\right]\left[(-g\,f_{d'c'b'})\,\left[p^{\nu'}_{2\to 1}\right]\right]\left[\frac{-ig_{\mu'\nu'}\,\delta_{b'a'}}{(p_1+p_2)^2}\right]\left[\left(-ig\gamma^{\mu'}_{\xi\sigma}\right)\,T^{a'}_{i'j'}\right]. \qquad (3.7)$$

What we mean by $f(p_{2\to 1},p_{1\to 2})$ is $f(p_1,p_2)+f(p_2,p_1)$. For both the $s$-channel gluon fusion term and its ghost we have to evaluate $T^b_{ij}\,T^a_{ji}\,f_{dbc}\,f_{dca}$. We do this using equation C.16 and obtain $-\frac{1}{2}3\cdot 3$. We will return to the ghost expressions in the subsection (3.1.2). Evaluating the $t$- and $u$- matrix elements is straight-forward because all we have to do is swap the momentum labels $p_1 \leftrightarrow p_2$.

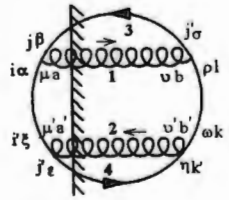


Figure 3.4: Gluon fusion - $t$ and $u$ - channels

$$R^t_{gg\to ss} = \frac{-1}{2(2\pi)^{12-4}} \int dp_1\, dp_2\, dp_3\, dp_4\, \theta(p_3^0)\, \delta(p_3^2 - m_s^2)\, (-\not{p}_3 - m)_{\sigma\beta}\, \delta_{jj'} \left(ig\gamma^\mu_{\alpha\beta}\right) T^a_{ij} \times \quad (3.8)$$
$$\frac{(\not{p}_1 - \not{p}_3 - m)_{\alpha\xi}}{(p_1 - p_3)^2 - m^2} \delta_{i'i} \left(-ig_{\mu\nu}\, \delta_{ab} \theta(p_4^0)\, \delta(p_1^2)\right) \left(-ig\gamma^\nu_{\rho\sigma}\right) T^b_{j'l} \frac{(\not{p}_2 - \not{p}_4 - m)_{\rho\omega}}{(p_2 - p_4)^2 - m^2} \delta_{lk} \times$$
$$\left(-ig\gamma^\nu_{\omega\eta}\right) T^{b'}_{kk'} \theta(p_4^0)\, \delta(p_4^2 - m_s^2)\, (\not{p}_4 - m)_{\eta\epsilon} \delta_{j'k'} \left(-ig_{\mu'\nu'}\, \delta_{b'a'} \theta(p_4^0)\, \delta(p_2^2)\right) \left(-ig\gamma^{\mu'}_{\epsilon\xi}\right) T^{a'}_{i'j'},$$

and

$$R^u_{gg\to ss} = \frac{-1}{2(2\pi)^{12-4}} \int dp_1\, dp_2\, dp_3\, dp_4\, \theta(p_3^0)\, \delta(p_3^2 - m_s^2)\, (-\not{p}_3 - m)_{\sigma\beta}\, \delta_{jj'} \left(ig\gamma^\mu_{\alpha\beta}\right) T^a_{ij} \times \quad (3.9)$$
$$\frac{(\not{p}_2 - \not{p}_3 - m)_{\alpha\xi}}{(p_2 - p_3)^2 - m^2} \delta_{i'i} \left(-ig_{\mu\nu}\, \delta_{ab} \theta(p_4^0)\, \delta(p_1^2)\right) \left(-ig\gamma^\nu_{\rho\sigma}\right) T^b_{j'l} \frac{(\not{p}_1 - \not{p}_4 - m)_{\rho\omega}}{(p_1 - p_4)^2 - m^2} \delta_{lk} \times$$
$$\left(-ig\gamma^\nu_{\omega\eta}\right) T^{b'}_{kk'} \theta(p_4^0)\, \delta(p_4^2 - m_s^2)\, (\not{p}_4 - m)_{\eta\epsilon} \delta_{j'k'} \left(-ig_{\mu'\nu'}\, \delta_{b'a'} \theta(p_4^0)\, \delta(p_2^2)\right) \left(-ig\gamma^{\mu'}_{\epsilon\xi}\right) T^{a'}_{i'j'}.$$

Evaluating these gives

$$R^t_{gg\to s\bar{s}} = -\frac{g^4}{2(2\pi)^8} \int dp_1\, dp_2\, dp_3\, dp_4\, \frac{2 \cdot 8^2}{3} \frac{(m^2 - t)(m^2 - u) - 2m^2(m^2 + t)}{(m^2 - t)^2},$$

and

$$R^u_{gg\to s\bar{s}} = -\frac{g^4}{2(2\pi)^8} \int dp_1\, dp_2\, dp_3\, dp_4\, \frac{2 \cdot 8^2}{3} \frac{(m^2 - t)(m^2 - u) - 2m^2(m^2 + u)}{(m^2 - u)^2}.$$

The final diagrams to evaluate are the cross terms. Fortunately, of the six remaining, three have a matching diagram due to relations like $|\mathcal{M}_a \mathcal{M}_b^*| = |\mathcal{M}_a^* \mathcal{M}_b|$. This leaves three diagrams. In addition we have two diagrams that are the same, but for momentum labels. For brevity we include only one; to get the other simply swap $p_1$ with $p_3$, $p_4$ with $p_1$,$p_3$ with $p_2$ and $p_2$ with $p_4$.

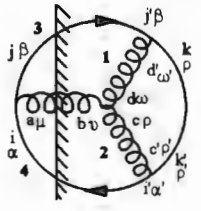


Figure 3.5: Gluon fusion - cross channels $su^* + s^*u$

$$R^{s^*u+u^*s}_{gg\to s\bar{s}} = \left(\frac{(-2)(2\pi)^4}{2(2\pi)^{12}}\right) \int dp_1\, dp_2\, dp_3\, dp_4\, \theta(p_4^0)\, \delta(p_4^2 - m_s^2)\, (-\not{p}_4 - m)_{\beta'\beta}\, \delta_{jj'} \left(ig\gamma^\mu_{\beta\alpha}\right)$$
$$T^a_{ij} \times \theta(p_4^0)\, \delta(p_4^2 - m_s^2)\, (\not{p}_3 - m)_{\alpha\alpha'}\, \delta_{i'i} \left(-ig_{\mu\nu}\, \delta_{ab} \theta(p_3^0 - p_4^0)\, \delta(p_4 - p_3)^2\right) (g\, f_{dbc}) \times$$
$$[g^{\omega\rho}(p_2 - p_1)^\nu + (-p_1 - p_4 - p_3)^\omega g^{\nu\rho} + (p_4 + p_3 - p_2)^\nu g^{\rho\omega}] \frac{(-ig_{\omega\omega'}\delta_{dd'})}{p_1^2} \times$$
$$\frac{(-ig_{\sigma\sigma'}\delta_{cc'})}{p_2^2} \left(-ig\gamma^{\omega'}_{\rho\beta}\right) T^{d'}_{kj'} \frac{(\not{p}_3 + \not{p}_4 - m)_{\rho\rho'}}{(p_3 + p_4)^2 - m^2} (\delta_{d'c'}) \left(-ig\gamma^{\sigma'}_{\alpha'\rho'}\right) T^{a'}_{i'j'}. \quad (3.10)$$

Evaluating these gives

$$R^{2st}_{gg\to s\bar{s}} = -\frac{g^4}{(2\pi)^8}\int dp_1\, dp_2\, dp_3\, dp_4\, 96\frac{(m^2-t)\,(m^2-u)-(u-t)}{(m^2-t)\,s},$$

and

$$R^{2su}_{gg\to s\bar{s}} = -\frac{g^4}{(2\pi)^8}\int dp_1\, dp_2\, dp_3\, dp_4\, 96\frac{(m^2-t)\,(m^2-u)-(t-u)}{(m^2-u)\,s}.$$

The last diagram is the $u$ cross $t$ graph

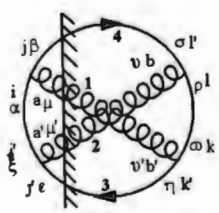


Figure 3.6: Gluon fusion - cross channel $ut^* + u^*t$

$$\begin{aligned} R^{u^*t+t^*u}_{gg\to ss} = &\left(\frac{(-1)(2\pi)^4}{2(2\pi)^{12}}\right)\int dp_1\, dp_2\, dp_3\, dp_4\ (-\not{p}_3 - m)_{\sigma\beta}\,\delta_{jl'}\,\left(ig\gamma^{\mu}_{\alpha\beta}\right)\,T^a_{ij}\times \\ &\frac{(\not{p}_1 - \not{p}_3 - m)_{\alpha\xi}}{(p_1-p_3)^2-m^2}\delta_{i'i}\,(-ig_{\mu\nu'}\,\delta_{ab'})\,\left(-ig\gamma^{\nu}_{\omega\eta}\right)\,T^{b'}_{kk'}\,\frac{(\not{p}_1 - \not{p}_4 - m)_{\rho\omega}}{(p_1-p_4)^2-m^2}\delta_{lk}\ \times \\ &\left(-ig\gamma^{\nu}_{\rho\sigma}\right)\,T^b_{j'l}\,(\not{p}_4 - m)_{\eta\epsilon}\,\delta_{j'k'}\,(-ig_{\mu'\nu}\,\delta_{ba'})\,\left(-ig\gamma^{\mu'}_{\epsilon\xi}\right)\,T^{a'}_{i'j'}, \end{aligned} \tag{3.11}$$

Evaluating these gives

$$R^{tu}_{gg\to s\bar{s}} = -\frac{g^4}{(2\pi)^8}\int dp_1\, dp_2\, dp_3\, dp_4\, 24^2\,\frac{32}{3}\frac{m^2\,(s-4m^2)}{(m^2-t)\,(m^2-u)}.$$

These expressions have been further evaluated, and the answers are given in [98]. We also record the correct expressions in equations 3.13 to 3.14. On repeating the calculation of [98] we reach agreement for the gluon fusion, but differ with them by a factor of 2 for quark annihilation. In fact their work has a discrepancy. We indicate this in the plot in Figure 3.7.

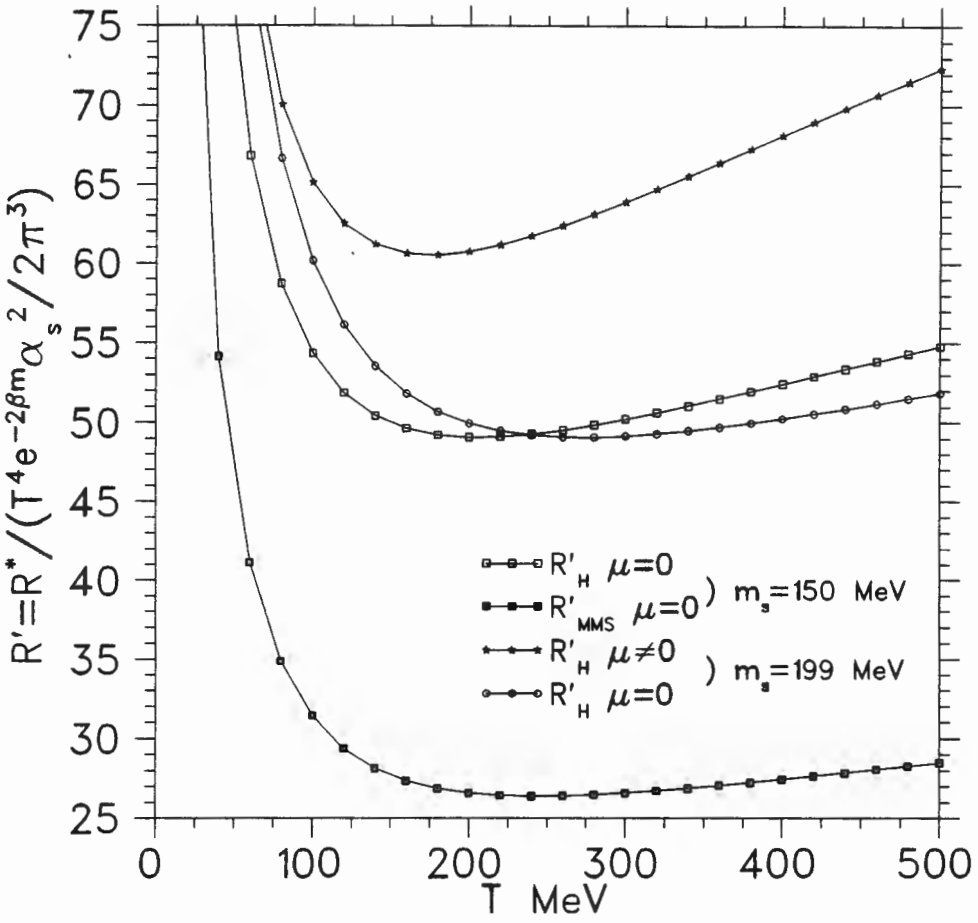


Figure 3.7: A comparison of rates of quark production.

The filled squares correspond exactly to the result of [98] if we divide their expression for gluon fusion by 2. We have, however, found that there is an extra factor of $\frac{1}{2}$ in the expression for their quark annihilation process and so the graph in this paper is not correct. Using the correct expression for the quark annihilation and not including the spurious $\frac{1}{2}$ in gluon fusion (which is correctly given in the paper) we get the open squares. The open circles give the correct results for the mass we use (199MeV as opposed to 150MeV), and we have included a parameterisation of the chemical potential in the starred graph.

### Ghosts, Projection Operators and Gauges

**Ghosts:** We briefly outline the role of ghosts in removing the unphysical longitudinal polarisations for the massless case. In the literature, the transversality condition ( $p_\mu F^{\mu\nu}(p) = 0$ ) is used to remove the longitudinal degrees of freedom by explicitly multiplying the polarisation tensors with momentum dependent expressions. In our approach this fortuitous turn of events is not possible due to the polarisation tensors not entering the

expressions obtained using the Cutkosky rules, because we do not have any external lines.

In general there are two ways of dealing with the unwanted degrees of freedom, namely ghosts ([138]) and a non-covariant approach. In the non-covariant approach we use the explicit expression for the sum over polarisation states (see equation C.9)

$$\sum_{\zeta} \epsilon_{\mu}(\zeta, k)\, \epsilon_{\nu}(\zeta, k) = P_{\mu\nu}(k) \tag{3.12}$$

There are however a lot of different equivalent expressions for the transverse projection operator, $P_{\mu\nu}(k)$.

In this case, the product of cut gluon lines is replaced by $P_{\mu\nu}$ to remove the longitudinal degree of freedom. This approach is explicitly non-covariant and is not used here. There is a theorem which is often used to get around this non-covariance - the theorem states that $\sum_{\zeta} \epsilon_{\mu}(\zeta, k)\, \epsilon_{\nu}(\zeta, k)\, F^{\mu\nu}$ can be simply replaced by $-\sum_{\zeta} g_{\mu\nu}\, F^{\mu\nu}$, as long as $F^{\mu\nu}$ obeys the transversality condition, $p_{\mu} F^{\mu\nu}(p) = 0$.

This is true for Abelian fields, but in QCD this transversality condition does not hold due to the color factors. The better way to remove these unphysical longitudinal degrees of freedom is to subtract ghost terms (3.7). The ghost contribution is to cancel effects of non-physical degrees of freedom of gauge fields.

As an illustration, if the matrix element squared is evaluated in 3.6, (in this discussion we will take $m = 0$) one obtains $\sum^{T+L} |M|^2 = \frac{1}{2} 3 \cdot 8 \cdot 4 g^4 \frac{1}{s^2} \left[ -4s^2 - 2t\,u - \frac{7}{2}(t^2 + u^2 - s^2) \right]$. Evaluating the ghost gives $\sum^{Ghost} |M|^2 = -\frac{3}{2} \cdot 8 \cdot 4 g^4 \frac{1}{s^2} [4s^2]$. And adding the two gives $\sum^{T} |M|^2 = \frac{1}{2} 3 \cdot 8 \cdot 4 g^4 \frac{1}{s^2} [-2t\,u]$ as required in equation 3.6.

**Projection Operators:** Since we will be using projection operators later, we define them. If $u_{\mu}$ is the velocity of the plasma, $K^{\mu} = (\omega, \vec{k})$ and $k = \sqrt{(\vec{k}^2)}$ then the (non-covariant) transverse projection operator is

$$P_{\mu\nu} = g_{\mu\nu} - u_{\mu}\, u_{\nu} + \frac{(K_{\mu} - \omega\, u_{\mu})(K_{\nu} - \omega\, u_{\nu})}{k^2}$$

and the longitudinal projection operator is

$$Q_{\mu\nu} = -\frac{(k^2\, u_{\mu} + \omega(K_{\mu} - \omega\, u_{\mu}))(k^2\, u_{\nu} + \omega(K_{\nu} - \omega\, u_{\nu}))}{K^2\, k^2}.$$

**Propagators:** In the Coulomb Gauge, with gauge parameter $\xi_C$ the gluon propagator is, in the notation of the preceding paragraph,

$$\Delta_{00}(K) = \frac{1}{k^2} + \xi_C \frac{(k^0)^2}{k^4},\ \Delta_{0i}(K) = \xi_C \frac{k^0\, k^i}{k^4} \text{ and } \Delta_{ij}(K) = \Delta^{tr}_{ij}(K) + \xi_C \frac{k^j\, k^i}{k^4}$$

where the transverse propagator is $\Delta^{tr}_{ij}(K) = (\delta^{ij} - \frac{k^i\, k^j}{k^2}) \Delta(K)$ and $\Delta(K) = 1/K^2$.

The Covariant Gauge has

$$\Delta_{\mu\nu}(K) = g_{\mu\nu}\,\Delta(K) - \xi\,K^{\mu}\,K^{\nu}\,\Delta^2(K).$$

The strict Coulomb and Feynman gauges have $\xi_C$ and $\xi$ zero.

### 3.1.3 Steps leading to the calculation of Rates

The rates as calculated by [22] and [98] are given below in a form ready for computation. All our variables are dimensionless (except $T$ and $\mu$). Variables with dimension, such as mass, are divided by $T$; $M = \frac{m_s}{T}$ and $m = \frac{m_{u,d}}{T}$. We also have noted the corrections in the expressions given in [98]. We write the equations for the rates in the form where the integrals over the finite domain can be evaluated using Gauss-Legendre integration and over the infinite domain using Gauss-Laguerre integration.

The light quark contribution to the formation of more massive quarks is [98]

$$\begin{aligned}\delta R_{q\bar{q}\to Q\bar{Q}} &= \left(e^{(2\beta\mu_q)} - e^{(2\beta\mu_s)}\right)\frac{\alpha_S^2}{\pi^3}e^{(-2\beta M)}T^4\int_0^{\infty}dz\int_0^1 du\int_0^1 dx\int_0^1 dy\,u^2e^{-z}\times \\ &\quad f'_+(\frac{q_o}{2}+p_o,\mu_q)\times f'_+(\frac{q_o}{2}-p_o,\mu_q)\,f'_+(\frac{q_o}{2}+p'_o,\mu_s)\,f'_+(\frac{q_o}{2}-p'_o,\mu_s)\times \\ &\quad \sqrt{1-4\frac{m^2}{s}}\sqrt{1-4\frac{M^2}{s}}\,(z(z+4M))^{\frac{3}{2}}\,\frac{D}{s^2} \qquad (3.13)\end{aligned}$$

where

$$D = s^2\left(1+\left[\frac{(1-y^2)(1-x^2)}{2}+x^2y^2\right]\left(1-4\frac{m^2}{s}\right)\left(1-4\frac{M^2}{s}\right)+\frac{4(m^2+M^2)}{s}\right). \qquad (3.14)$$

Our integration variables are related to the variables used previously by $q_o = z + 2M$ , $q = (q_o^2 - 4M^2)^{\frac{1}{2}}$ , $s = q_o^2 + q^2$ , $p_o = \frac{q}{2}\left(1-\frac{4m^2}{s}\right)^{\frac{1}{2}}x$ and $p'_o = -\frac{q}{2}\left(1-\frac{4M^2}{s}\right)^{\frac{1}{2}}y$. The definition of the primed distribution functions given above, see equation 2.12. Because we will need to know the rate of $s\bar{s} \leftrightarrow c\bar{c}$ in our simulation, we have a term for the mass of the light quarks, $m = m_q/T$.

The dominant mechanism for the production of massive quarks is gluon fusion, via the $s-$, $t-$ and $u-$ channels [98].

$$\begin{aligned}\delta R_{gg\to Q\bar{Q}} &= \left(1-e^{(2\beta\mu)}\right)\frac{\alpha_S^2}{(2\pi^3)}e^{(-2\beta M)}\,T^4\int_0^{\infty}dz\int_0^1 dv\int_0^1 dx\int_0^1 dy\,u^2e^{-z}\times \\ &\quad \sqrt{1-4\frac{M^2}{s}}\,(z(z+4M))^{\frac{3}{2}}\times\left[A+B\times\left(\frac{1}{K_+}+\frac{1}{K_-}\right)+C\times\left(\frac{\Delta_+}{K_+^3}+\frac{\Delta_-}{K_-^3}\right)\right] \\ &\quad \times f'_-(\frac{q_o}{2}+p_o,0)\times f'_-(\frac{q_o}{2}-p_o,0)\times f'_+(\frac{q_o}{2}+p_o,\mu)\times f'_+(\frac{q_o}{2}-p_o,\mu) \qquad (3.15)\end{aligned}$$

where

$$A = 3\left(1-\left[(1-y^2)(1-x^2)/2+x^2y^2\right]\left(1-4\frac{M^2}{s}\right)-\frac{34}{3}-24\frac{M^2}{s}\right) \qquad (3.16)$$

$$B = \frac{16}{3}\left(1 + 4\frac{M^2}{s} + \frac{M^4}{s^2}\right) \text{ and } C = -\frac{128}{3}\frac{M^4}{s^2}, \tag{3.17}$$

$$K_\pm = \sqrt{1 - (1 - y^2 - x^2)\left(1 - 4\frac{M^2}{s}\right)} \pm 2xy\sqrt{1 - 4\frac{M^2}{s}} \tag{3.18}$$

and

$$\Delta_\pm = 1 \pm \sqrt{1 - 4\frac{M^2}{s}}xy. \tag{3.19}$$

## 3.2 Requisite resummation functions

In this penultimate section we will exhibit quantities, alluded to previously by the Braaten-Pisarski rules, that will be used in calculating the gluon decay rate.

### $2 \times 2$ Real Time Formalism

We deal with the meaning of self-energy and polarisation in the $2 \times 2$ Real Time Formalism now. Concentrating on the scalar field (the spin-$\frac{1}{2}$ and boson field follows naturally). The spectral representation of the full scalar propagator is

$$i\mathcal{D}^{ab}(p) = \int_0^\infty d\omega\, \rho(\omega, \overrightarrow{p})\, i\, D^{ab}(p_0, \omega) \tag{3.20}$$

where $\rho(\omega, \overrightarrow{p})$ is the thermal spectral function and $i\, D^{ab}(p_0, \omega)$ is the free scalar propagator. Note that from the structure of the free scalar propagator [83], Appendix C.3 and equation 3.20 we conclude that

$$i\mathcal{D}^{ab}(p) = U(\beta, p) \begin{bmatrix} -i\mathcal{D} & 0 \\ 0 & i\mathcal{D}^* \end{bmatrix} U(\beta, p).$$

The important result that follows from Dyson's equation,

$$i\mathcal{D}^{ab} = i\, D^{ab} + i\, D^{ac}\left(-i\Sigma^{cd}\right) i\mathcal{D}^{db},$$

is the expression for the self energy,

$$i\Sigma^{ab}(p) = U^{-1}(\beta, p) \begin{bmatrix} -i\Sigma & 0 \\ 0 & i\Sigma^* \end{bmatrix} U^{-1}(\beta, p).$$

This allows us to write $i\mathcal{D} = \frac{i}{p^2 - m^2 - \Sigma + i\varepsilon}$ as well as the relations $\Sigma_{12} = \Sigma_{21} = -i\tanh(2\theta)\mathrm{Im}\,\Sigma_{11}$, $\Sigma_{22} = -\Sigma_{11}^*$, $\mathrm{Re}\Sigma = \mathrm{Re}\Sigma_{11}$ and $\mathrm{Im}\Sigma = \mathrm{sech}(2\theta)\mathrm{Im}\Sigma_{11} = \varepsilon(p_0)\tanh(\frac{1}{2}\beta p_0)\,\mathrm{Im}\Sigma_{11}$ ($\theta$ is defined in appendix C.1). We see that knowledge of $\Sigma_{11}$ is enough to determine all the components of $\Sigma^{ab}(p)$. (Needing to calculate $\Sigma_{11}$ justifies the use of the second set of Kobes-Semenoff cutting rules.)

A similar result for the fermions also holds. As before we have

$$-i\Sigma^{ab}(p) = V^{-1}(\beta, p, \mu) \begin{bmatrix} -i\Sigma & 0 \\ 0 & i\Sigma^* \end{bmatrix} V^{-1}(\beta, p, \mu)$$

(which allows us to write $iS = \frac{i}{\not{p}-m-\Sigma+i\epsilon}$) as well as the relations
$i\Sigma_{12} = -i\,e^{(-\beta\,\mu)}\Sigma_{21} = -i\,\varepsilon(p_0)\,\exp(-\beta\,\mu/2)\tanh(2\varphi)\mathrm{Im}\Sigma_{11}$,
$i\Sigma_{22} = -i\Sigma_{11}^{*}$, $\mathrm{Re}\Sigma = \mathrm{Re}\Sigma_{11}$ and
$\mathrm{Im}\Sigma = \sec(2\varphi)\,\mathrm{Im}\Sigma_{11} = \varepsilon(p_0)\,\tanh(\frac{1}{2}\beta p_0)\,\mathrm{Im}\Sigma_{11}$.

### 3.2.1 Calculating the Polarisation and Self-Energy

In [33], [83] and [148] the self-energy and polarisation of a gluon and fermion are calculated. What is of interest are the three different approaches. Weldon uses the imaginary-time formalism; Braaten-Pisarski show that the contribution to the self-energy comes from HTL's; Kobes-Semenoff calculate the self-energy in the real-time formalism, using specially devised rules to simplify the process.

#### Polarisation

The polarisation of the vacuum adds a term to the inverse gluon propagator, demonstrating the interaction of the gluon with the Dirac sea. The polarisation tensor is defined as $\Pi_{\mu\nu} = \int d^4x\, e^{ikx} < T[J_\mu(x), J_\nu(0)] >$. $J_\mu(x) = \bar{\psi}(x)\,\gamma_\mu\,\psi(x)$ is the current. By substituting it into $\Pi_{\mu\nu}$ it can be recast in terms accessible from the Feynman diagram point of view,

$$\Pi_{\mu\nu} = \int d^4x\, e^{ikx} < T[\gamma_\mu\, S(x)\,\gamma_\nu\, S(-x)] > .$$

The polarisation can be shown to satisfy $P^\mu\,\Pi_{\mu\nu}(P) = 0$ due to current conservation. Due to the plasma providing a privileged rest frame, the polarisation tensor can be broken into the longitudinal and transverse propagating mode, both of which are physical. This means that $\Pi_{\mu\nu} = P_{\mu\nu}\Pi_T + Q_{\mu\nu}\Pi_L$, where $P_{\mu\nu}$ and $Q_{\mu\nu}$ are the transverse and longitudinal projection operators defined in [148].

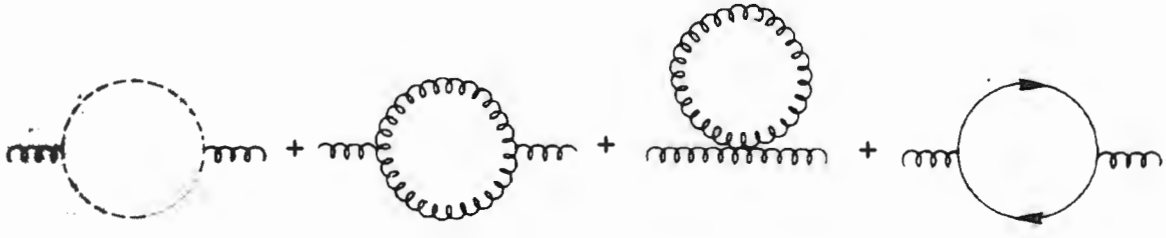

Figure 3.8: Diagrams contributing to the polarisation

Using the resummed propagators of Chapter 2, we find that we have to evaluate one quark loop, one gluon loop and its ghost and one tadpole diagram.

$$\Pi_{\mu\nu}(Q) = ig^2\,N_f \int \frac{d^4p}{(2\pi)^4}\,\mathrm{Tr}[\gamma_\mu\, S(p+Q)\,\gamma_\nu\, S(p)] + \ldots \qquad (3.21)$$

where $S$ are the temperature dependent fermion propagators. $\Pi^{T,L}(Q)$ are obtained by contraction with $g^{\mu\nu}$ and the plasma velocity $u^{\mu}$:

$$\Pi^{L}(Q) = -\frac{Q^2}{q^2} u^{\mu}\, u^{\nu}\, \Pi_{\mu\nu}(Q) \text{ and } \Pi^{T}(Q) = -\frac{1}{2}\Pi_{L}(Q) + \frac{1}{2} g^{\mu\nu}\, \Pi_{\mu\nu}(Q).$$

$\Pi_{\mu\nu}(Q)$ is defined by

$$\Pi_{00}(Q) = \Pi_{L}(Q), \qquad \Pi_{0i}(Q) = -\frac{q^0\, q^i}{q^2}\Pi_{L}(Q)$$

$$\text{and } \Pi_{ij}(Q) = \left(\delta^{ij} - \frac{q^0\, q^i}{q^2}\Pi_{L}(Q) + \frac{(q^0)^2\, q^i\, q^j}{q^4}\Pi_{L}(Q)\right).$$

The real transverse and longitudinal parts of the gluon self energy in the high temperature limit are given respectively by [148]

$$\mathrm{Re}\Pi_{T}(q_0, q) = \frac{3}{2} m_g^2 \left[\frac{q_0^2}{q^2} + \left(1 - \frac{q_0^2}{q^2}\right)\frac{q_0}{2q} \ln\frac{q_0 + q}{q_0 - q}\right], \tag{3.22}$$

and

$$\mathrm{Re}\Pi_{L}(q_0, q) = \frac{3}{2} m_g^2 \left(1 - \frac{q_0^2}{q^2}\right)\left[2 - \frac{q_0}{q} \ln\frac{q_0 + q}{q_0 - q}\right]. \tag{3.23}$$

$m_g = gT\sqrt{\frac{2N_c + N_f}{18}}$ ($N_f$ is the number of light flavors of quark) is the gluon mass induced by the thermal medium. The two polarisations are related

$$\mathrm{Re}\Pi_{L}(q_0, q) = 2\frac{3}{2} m_g^2 - 2 \times \mathrm{Re}\Pi_{T}(q_0, q).$$

These functions are plotted in figures 3.11 and 3.12. These graphs are plotted along the mass shell, ie $\omega^2 = q^2 + \mathrm{Re}\Pi_{T,L}$. We also have a three dimensional representation of the transverse case (Figure 3.9a). For the $q = 0$ axis is constant, $\mathrm{Re}\Pi_T = m_g$ and for $\omega = q$ $\mathrm{Re}\Pi_T = \frac{3}{2} m_g$. Another way of plotting $\mathrm{Re}\Pi_{T,L}$ is in terms of a variable $x = \omega/k$ (Figure 3.9b).

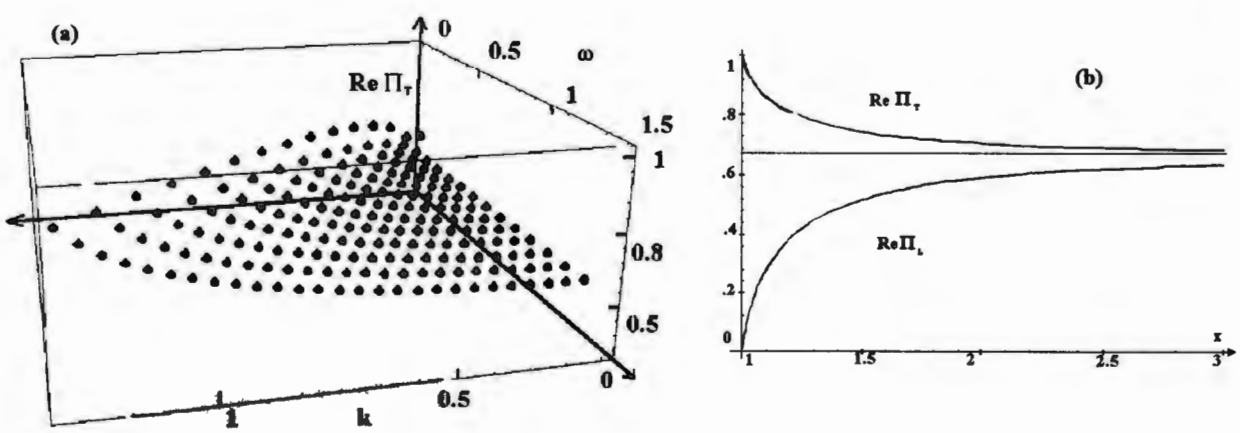


Figure 3.9: (a) - $\mathrm{Re}\Pi_T(\omega, k)$ and (b) - $\mathrm{Re}\Pi_{T,L}(x)$

**HTL's:** Braaten and Pisarski calculated the transverse polarisation in terms of hot thermal loops. (They included the ghost to remove the longitudinal degrees of freedom.) We can see that this is possible if we appreciate that the loops in Figure 3.8 can be divided into two sets, one where the loop momentum is hard, and one where it is soft. We know that the soft momenta will contribute to a lower order. Accordingly it is the hard thermal loops that contribute dominantly to the polarisation. We do not give their results here, because in their paper they leave it in a form to be integrated out. However they maintain that their result is consistent with that recorded above.

$\delta\Pi_{L,T}(p^o, p)$ can be defined in terms of Legendre functions of

$$\delta\Pi_L(q^o, q) = 3m_g^2\, Q_1(\frac{iq_o}{q})$$

and

$$\delta\Pi_T(q^o, q) = \frac{3}{5}m_g^2\left[Q_3(\frac{iq_o}{q}) - Q_1(\frac{iq_o}{q}) - \frac{5}{3}\right].$$

**Self Energy of the Fermion**

The self energy of a fermion in a thermal medium has been calculated by [83] and [150].

Figure 3.10: Self Energy of a quark

This quantity has been calculated by [83], [33] and [148]. It is also used in a paper by [115], where plasmino decay is analysed.

### 3.2.2 Dispersion relations

Plotted in Figure 3.11 and 3.12 are graphs of the dispersion relation for the transverse and longitudinal modes of a gluon. The dispersion relations are obtained from the poles of the propagator $1/(Q^2 - \Pi(Q))$. Using $Q^\mu = (\omega + i\gamma, \vec{q})$ and finding the poles of the propagator gives the equation

$$\omega_{T,L}^2 = q^2 - \mathrm{Re}\Pi_{T,L}. \tag{3.24}$$

The imaginary part of the dispersion relation is related to gluon damping and in the Feynman gauge goes as

$$2\gamma_{T,L}\,\omega = \mathrm{Im}\,\Pi_{T,L}. \tag{3.25}$$

We will come to this in section 3.2.3. The transverse gluons and plasmons have the same rest mass,

$$m_g^2 = (N_C + \frac{N_F}{2})\frac{g^2T^2}{9}, \tag{3.26}$$

(a quantity determined at $q = 0$) because $\Pi(P)$ must be smooth as $\vec{q} \to 0$.

In Figure 3.11 we plot some transverse properties of a gluon. We also plot the longitudinal dispersion relation and the residue of the propagator is plotted for later reference. Figure 3.12 is the same, but for the longitudinal case.

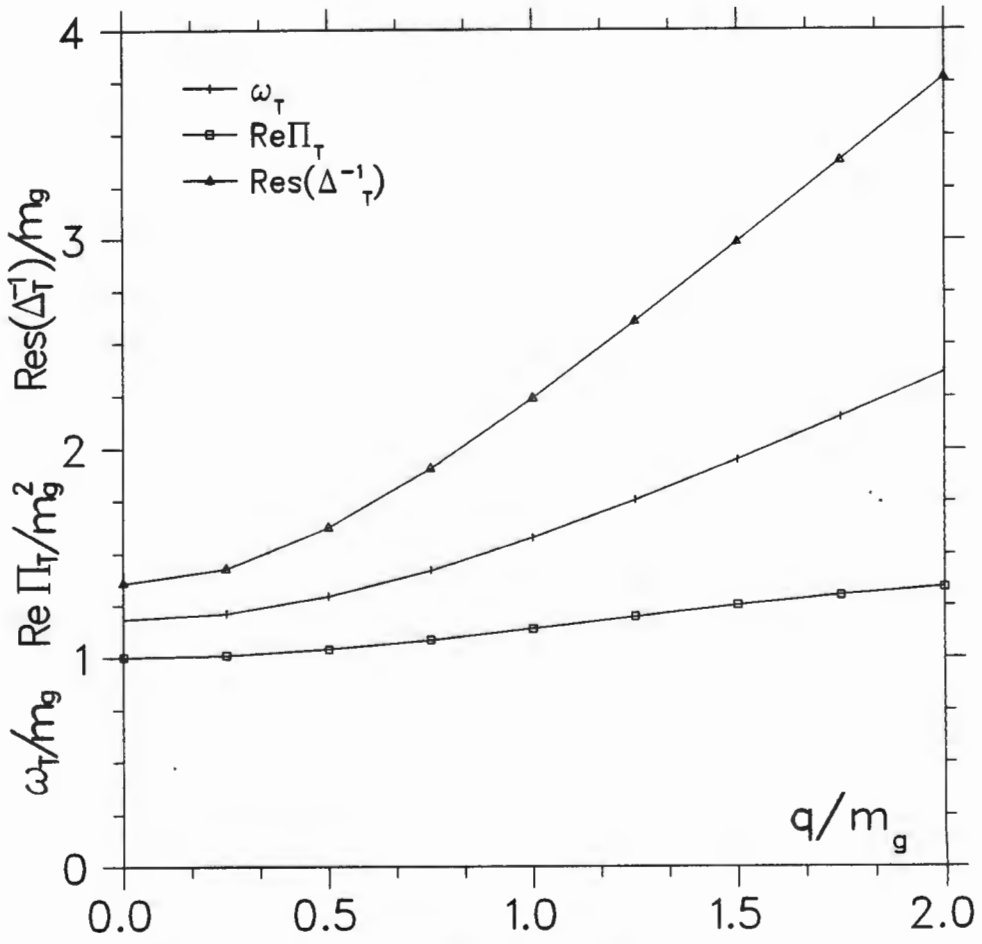


Figure 3.11: Transverse properties of a gluon

### 3.2.3 Gluon Damping

The damping rate determines how quickly a system near chemical equilibrium approaches it. It is the difference between the production and absorption rate of a particle. The controversy of the gluon damping rate in perturbative QCD at high temperature was solved by Braaten and Pisarski [38]. They successfully managed to add all the contributions to this quantity to the correct order and show that it was gauge invariant. The damping rate

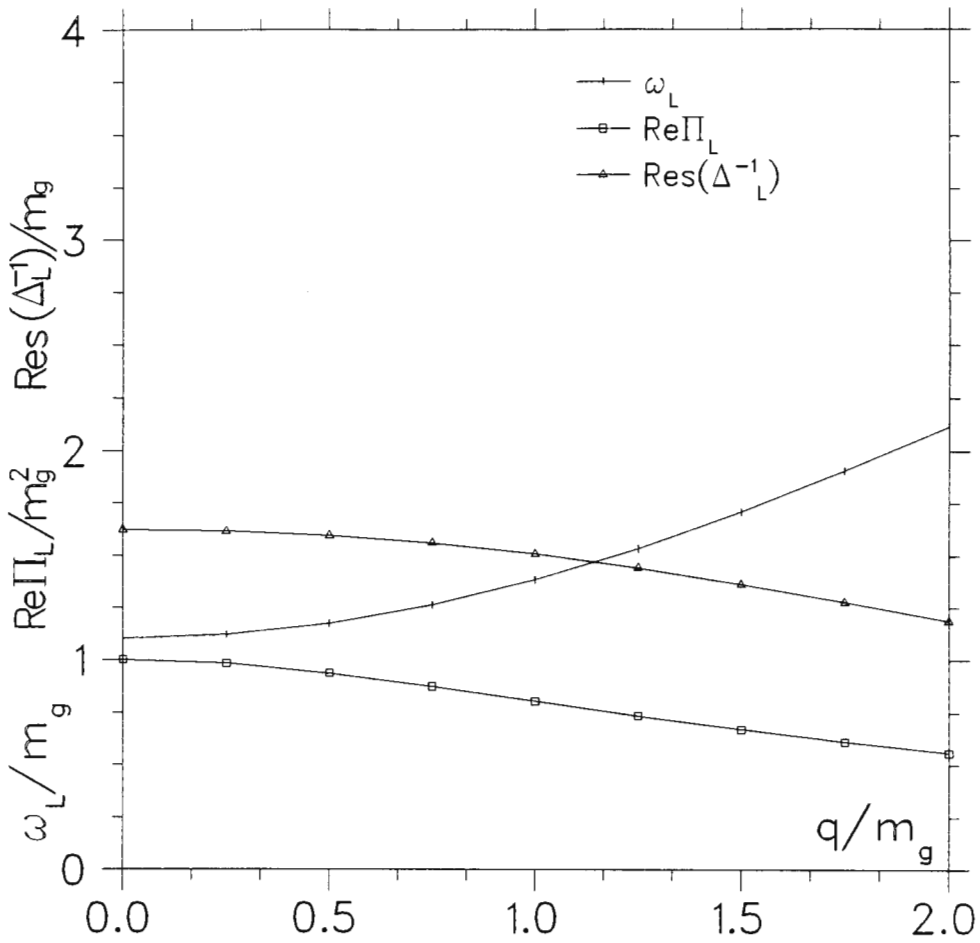


Figure 3.12: Longitudinal properties of a gluon

can only be calculated correctly using hard thermal loops. It is expected to be of order $g^2 T$, but depends on how fast the quasi-particle (ie effective resummed propagator) is moving though the medium.

Calculating the damping rate of the plasmon was one of the first successes of Braaten-Pisarski resummation.

The effective inverse gluon propagator in the Coulomb gauge is

$$D_{\mu\nu}(Q)^{-1} = Q^2\delta_{\mu\nu} - Q_\mu Q_\nu - \delta\Pi_{\mu\nu}(Q) -^* \Pi_{\mu\nu}(Q) + \frac{1}{\xi_c} p^i p^j \delta_{\mu i}\delta_{\nu j} \tag{3.27}$$

where $\delta\Pi_{\mu\nu}(Q)$, mentioned earlier, is the contribution from hard thermal loops to the polarisation of the gluon and ${}^*\Pi_{\mu\nu}(Q)$ is the next order correction in the effective polarisation needed to extract the damping coefficient. At soft momenta $\delta\Pi_{\mu\nu}(Q) \simeq (gT)^2$. The effective polarisation is a perturbative correction ${}^*\Pi_{\mu\nu}(Q) \simeq g(gT)^2$. The imaginary part of ${}^*\Pi_{\mu\nu}(Q)$ contributes to the gluon damping.

$\delta\Pi_{\mu\nu}(Q)$ is the quantity first computed by Silin [169] and later by Klimov [170] and Weldon [148]. The propagators are as in equation 2.22. In the strict Coulomb gauge,

$\xi_c = 0$, the only non-zero components of the propagator are $\Delta^{*C}_{oo} = (Q^2 - \delta\Pi_L(Q))^{-1}$ and $\Delta^{*C}_{ij}(Q) = (\delta_{ij} - q_i q_j)(q^2 - \delta\Pi_T(Q))^{-1}$.

The effective polarisation ${}^*\Pi_{\mu\nu}(Q)$ is more complicated, satisfying the less restrictive Ward identity $Q^\mu\, {}^*\Pi_{\mu\nu}(Q)\, Q^\nu = 0$. This implies that it depends on three scalar functions,

$$ {}^*\Pi_{oo}(Q) =^* \Pi_L(q^o, q) \tag{3.28} $$

$$ {}^*\Pi_{oi}(Q) = -\frac{q_o q_i}{q^2}\,[{}^*\Pi_L(q^o, q) +^* \Pi'_L(q^o, q)] \tag{3.29} $$

$$ {}^*\Pi_{ij}(Q) = (\delta_{ij} - \frac{q_i q_j}{q^2})\,{}^*\Pi_T(q^o, q) + \frac{q_i q_j (q^o)^2}{q^4}\,[{}^*\Pi_L(q^o, q) + 2{}^*\Pi'_L(q^o, q)] \tag{3.30} $$

Fortunately, in finding the propagator we find that , ${}^*\Pi'_L(q^o, q)$ does not contribute in this gauge. Accordingly the complete gluon propagator is the same form as the effective propagator $\Delta^{*C}_{oo} = (Q^2 - [{}^*\Pi_L(Q) + \delta\Pi_L(Q)])^{-1}$ and
$\Delta^{*C}_{ij}(Q) = (\delta_{ij} - q_i q_j)(q^2 - [{}^*\Pi_T(q^o, q) + \delta\Pi_T(Q)])^{-1}$.

The dispersion relation for transverse gluons is $\omega_T^2 - q^2 = -\delta\Pi_T -^* \Pi_T$ and for plasmons is $q^2 = \delta\Pi_L +^* \Pi_L$. The damping rate comes from the imaginary part of $q_o = \omega + i\gamma$. Separating the previous equations into a real and imaginary part gives equation 3.25. For zero momentum, $\omega = m_g$, we then obtain to the lowest order

$$ \gamma_T(0) = \frac{1}{2m_g}\mathrm{Im}{}^*\Pi_T(m_g, 0^+) \tag{3.31} $$

and

$$ \gamma_L(0) = \frac{1}{2m_g}\lim_{q\to 0}(\frac{m_g^2}{q^2}\mathrm{Im}{}^*\Pi_L(m_g, 0^+)). \tag{3.32} $$

We expect $\gamma_L(0) = \gamma_T(0)$ because for a particle at rest we would not expect to be able to distinguish between longitudinal and transverse gluons.

The following diagrammatically illustrates the contributing loops. Note that the ghost enters now, but it is not resummed.

Figure 3.13.

In the above ${}^*\Pi^{\mu\nu}(P) =^* \Pi^{\mu\nu}_{3g}(P) +^* \Pi^{\mu\nu}_{4g}(P) +^* \Pi^{\mu\nu}_{gh}(P)$. The above expression is evaluated using the effective vertices and propagators of Braaten and Pisarski (in fact, calculating

the damping rate is why they developed the theory). The expression is extremely complex, but can be reduced to angular integrals. An approximate answer that is readily obtained is

$$\gamma_T(0) = \gamma_L(0) = +a\frac{g^2\,T\,N_C}{24\pi}$$

where $a$ is obtained numerically using spectral densities obtained through expressions of the form of equation 3.20

$${}^*\Delta(k^0,k) = \int_0^{1/T} d\tau\, \exp(i\,k_0\,\tau) \int_{-\infty}^{\infty} d\omega\, {}^*\rho(\omega,k)\,(1+n(\omega))\,e^{-\omega\tau}.$$

For zero momentum

$${}^*\rho(\omega,0) = \frac{1}{2m_g}\left(\delta(\omega-m_g)+\delta(\omega+m_g)\right).$$

The value for $a$ is $a = 6.63538$. The significance of the "+" is that the quark-gluon plasma is thermodynamically stable.

A closed expression for the damping rate, derived by Pisarski [109], in the limit where $m_{mag} \gg \gamma$ , is

$$\gamma = \frac{g^2 N_C T}{8\pi}\left[\ln\left(\frac{m_g^2}{m_{mag}^2 + 2m_{mag}\gamma}\right) + 1.09681...\right]. \tag{3.33}$$

In [22] it is shown that this limit is indeed valid, despite Pisarski's concerns [109].

The magnetic mass is a basic non-perturbative feature of the high temperature plasma phase of QCD. The magnetic mass plays an important role in the infra-red regime. The magnetic mass at high temperature is of the form

$$m_{mag} = c_N\, g^2 T \tag{3.34}$$

where $c_N$ is a number depending on the gauge group and cannot be calculated by a perturbation expansion. Lattice estimates [24, 59] for SU(2) giving

$$c_2 = 0.27 \pm 0.03 \tag{3.35}$$

have been confirmed by recent SU(2) semiclassical calculations [27]. However Kalashnikov uses $m_{mag}^{SU(2)} = 0.24 g^2 T\sqrt{(\log(g^{-2})}$. The most recent lattice calculation for SU(2) electric and magnetic screening masses * [82] is

$$m_e(T) = 2.484(52)T \;\text{ and }\; m_m(T) = 0.466(15)g^2(T)T.$$

So far no reliable estimate exists for SU(3) [71]. The best one can do is extrapolate the SU(2) value using [56]

$$c_3 = \frac{N_C}{2}c_2 \tag{3.36}$$

*This result is not used, recently been submitted for publication

Expanding the log in (3.33) in powers of $\gamma/m_{mag}$ and retaining only the leading terms one finds

$$\gamma = (1+\eta)^{-1}\frac{g^2 N_C T}{8\pi}\left[\ln\left(\frac{m_g^2}{m_{mag}^2}\right) + 1.09681...\right]. \tag{3.37}$$

$\eta = 0$ if we keep the leading log term only. If the next-to-leading term is included then

$$\eta = \frac{N_C}{4\pi c_N}. \tag{3.38}$$

The approximation is well justified if one uses the expression (3.37) in the range $1 < g < 2.5$.

## 3.3 Gluon decay rate

We finally get to what we have been aiming to do, namely calculate the rate of gluon decay.

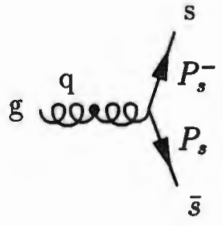


Figure 3.14: Gluon Decay

**Introduction:** It has been claimed that the process $g^* \to \bar{q}q$ dominates for a wide range of quark masses [4, 7]. We show that the rate of gluon decay is of the same order as the gluon fusion, but not greater than it. Normally, the gluon cannot decay into a strange quark-antiquark pair because its thermal mass is too low. Even for the optimistic case where one takes the coupling constant $g = 2$ in a plasma with two massless quarks, the gluon mass is given to lowest order in perturbation theory by

$$m_g = \frac{2}{3}gT. \tag{3.39}$$

The important observation by Altherr and Seibert [4] is that in addition to acquiring a thermal mass of the order $g^2T$ [110] gluons also acquire a width determined by the large damping rate. This is the reason why thermal gluon decay into a heavy quark-antiquark pair is allowed, even though the gluon mass is below the threshold for strange pair production.

### Gluon Propagator

The effective gluon propagator at finite temperature in the Feynman gauge is given by [148]

$$iD^{ab}_{\mu\nu}(q_0, q) = -i\delta^{ab}[P_{\mu\nu}\Delta_T(q_0, q) + Q_{\mu\nu}\Delta_L(q_0, q)], \tag{3.40}$$

where the transverse and longitudinal projectors have been previously defined.

$$\Delta_{T,L}(q_0, q) = \frac{1}{Q^2 - \Pi_{T,L}(q_0, q)} \tag{3.41}$$

where $Q^2 \equiv q_0^2 - q^2$.

If a pole is located at

$$q_0 = \omega_{T,L} + i\gamma_{T,L} \tag{3.42}$$

then the imaginary shift of the pole $\gamma_{T,L}$ is related to the imaginary part of the self energy through equation 3.25, 3.31 and 3.32

$$\gamma_{T,L} = \mathrm{Res}(\Delta_{T,L})\mathrm{Im}\,\Pi_{T,L}, \tag{3.43}$$

where $\mathrm{Res}(\Delta)$ is the residue of the propagator given by

$$\mathrm{Res}(\Delta_{T,L})^{-1} = \left.\frac{\partial \Delta_{T,L}^{-1}}{\partial q_0}\right|_{\omega_{T,L}}. \tag{3.44}$$

This we verify by differentiating equation 3.41

$$\frac{\partial}{\partial q_o}\frac{(q_o - \omega - i\gamma)^2}{q_o^2 - q^2 - \Pi}.$$

After inverting this we take the limit $q_o \to \omega + i\gamma$ (we ignore $T, L$ for the time being) and then use L'Hospital's rule twice. Some fortunate cancellations give us the desired result.

Using expression 3.22 and 3.23 we can remove the tricky log functions, and rewrite the residues in terms of $\omega_{T,L}$ and $q$

$$\mathrm{Res}(\Delta_T)^{-1} = -\omega_T + \frac{q^2}{\omega_T} + \frac{3m_g^2\omega_T}{\omega_T^2 - q^2} \text{ and} \tag{3.45}$$

$$\mathrm{Res}(\Delta_L)^{-1} = -\omega_L + \frac{q^2}{\omega_L} + \frac{3m_g^2}{\omega_L}. \tag{3.46}$$

The residues are plotted in Figures 3.11 and 3.12. Thus we can write (3.41) as

$$\Delta_{T,L}(Q) = \frac{Q^2 - \mathrm{Re}\Pi_{T,L}}{(Q^2 - \mathrm{Re}\Pi_{T,L})^2 + \mathrm{Res}(\Delta_{T,L})^{-2}\gamma_{T,L}^2} + \frac{i\mathrm{Res}(\Delta_{T,L})^{-1}\gamma_{T,L}}{(Q^2 - \mathrm{Re}\Pi_{T,L})^2 + \mathrm{Res}(\Delta_{T,L})^{-2}\gamma_{T,L}^2}. \tag{3.47}$$

The imaginary part of this expression will be used to replace the mass-shell $\delta$-function for thermal gluons.

The imaginary part of the pole in (3.42) gives the damping rate of the plasma oscillations [15, 110].

### 3.3.1 Calculation of the $g^* \to s\bar{s}$ rates

Using the Kobes-Semenoff rules we need to evaluate only

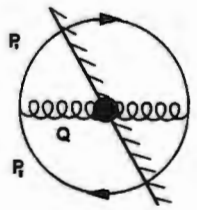


Figure 3.15: The rate of Gluon Decay

The vertex is external. Hence we need only use $1-1$ propagators. The cut propagator corresponds to a gluon in a medium.

$$R_{g\to s\bar{s}} = \int \frac{d^3q}{(2\pi)^3 2E_g}\frac{d^3p_s}{(2\pi)^3 2E_s}\frac{d^3p_{\bar{s}}}{(2\pi)^3 2E_{\bar{s}}}(2\pi)^4\delta(Q-P_s-P_{\bar{s}})\times f_-(E_g)(1-f_+(E_s))(1-f_+(E_{\bar{s}}))|\mathcal{M}(g\to s\bar{s})|^2. \tag{3.48}$$

Implicitly we have summed over all colors and polarizations of the gluons and the final state quark-antiquark pair. We have included the Pauli blocking factors although, as long as the density of strange quarks is well below one, Pauli blocking does not play a significant role. Following Matsui, McLerran and Svetitsky [98] we can investigate the evolution process in terms of the relaxation time determined near equilibrium. Therefore we have to evaluate the rates (3.48) at $\mu = 0$, i. e. when quarks are in both thermal and chemical equilibrium. Thermal field theory calculations become fully legitimate in this way. In particular, we can use the thermal quark mass given by [149]

$$m_s^2(T) = m_s^2(0) + \frac{g^2T^2}{6} \tag{3.49}$$

and the thermal gluon mass (3.26)

$$m_g^2 = (N_C + 2N_F)\frac{g^2T^2}{18}.$$

The thermal gluon decay, also discussed by Altherr and Seibert [4, 7], can be calculated similarly as in Appendix D.1. We first replace the integrations over $q$, $p_s$ and $p_{\bar{s}}$ by

$$\frac{d^3q}{2E_g} = d^4Q\,\delta(Q^2-m_g^2)\theta(q_0) \tag{3.50}$$

$$\frac{d^3p_s}{2E_s}\frac{d^3p_{\bar{s}}}{2E_{\bar{s}}} = d^4P_s\,\delta(P_s^2-m_s^2)\theta(p_s^0)\,d^4P_{\bar{s}}\,\delta(P_{\bar{s}}^2-m_s^2)\theta(p_{\bar{s}}^0) \tag{3.51}$$

and change variables

$$Q = P_s + P_{\bar{s}} \text{ and } P = \frac{1}{2}(P_s - P_{\bar{s}}). \tag{3.52}$$

Next we explicitly choose $Q^\mu = (q_0, 0, 0, q)$ and $P^\mu = (p_0, p\sin\theta, p\cos\theta)$. The product of the delta functions in 3.51 now are

$$\delta(\frac{Q^2}{4} + \frac{QP}{2} + P^2 - m_s^2)\,\delta(\frac{Q^2}{4} - \frac{QP}{2} + P^2 - m_s^2).$$

Now use is made of an identity between the products of delta functions that

$$\delta\left(A(x)+B(x)\right)\delta A\left((x)-B(x)\right)=\frac{1}{2}\delta\left(A(x)\right)\,\delta\left(B(x)\right).$$

This gives for the above

$$\frac{1}{4p^2\,q}\delta\left(p-(\frac{q^2}{4}+p_0^2-m_s^2)^{\frac{1}{2}}\right)\,\delta\left(\cos\theta-\frac{p_0\,q_0}{pq}\right).$$

After eliminating the integrals over $d^4Q'$ and $d^3p$ using the Dirac delta functions we find

$$R_{g\to s\bar{s}} = \frac{1}{4(2\pi)^4}\int d^4Q\,\delta(Q^2-m_g^2)\frac{1}{q}\,f_-(q_0)\times\int dp_0\,(1-f_+(\tfrac{1}{2}q_0+p_0))\times$$
$$(1-f_+(\tfrac{1}{2}q_0-p_0))|\mathcal{M}(g\to s\bar{s})|^2\Bigg|_{\substack{\cos\theta=\frac{p_0\,q_0}{p\,q}\\ p=(p_0^2+\frac{q^2}{4}-m_s^2)^{\frac{1}{2}}}} \qquad (3.53)$$

where the integration space is restricted by the following kinematical constraints:

$$q_0>2m_s,\quad 0<q<(q_0^2-4m_s^2)^{1/2},\quad p_0^2<\frac{q^2}{4}\left(1-\frac{4m_s^2}{Q^2}\right). \qquad (3.54)$$

It immediately follows that $R_{g\to s\bar{s}}=0$ if $m_g<2m_s$. At the relevant temperatures the thermal gluon mass is not high enough to allow for decay into a strange quark pair. It is only because of its width that the gluon decays. To take this into account the $\delta$-function is replaced by a function, similar to a Breit-Wigner resonance.

### Matrix Element

The matrix element squared is given by applying the optical theorem to Figure 3.14 and using the Kobes-Semenoff rules. This is represented in Figure 3.15

$$\sum_{a,\zeta}|\mathcal{M}(g\to s\bar{s})|^2=-g^2\mathrm{Tr}[(\not{P}_s+m_s)\gamma_\mu(\not{P}_{\bar{s}}-m_s)\gamma^\nu]\,(P_{\mu\nu}+Q_{\mu\nu}). \qquad (3.55)$$

Here we have suppressed the color factors $T^a_{ij}\,T^b_{ij}\,\delta^{ab}=\frac{3}{2}$. Since the frame of the quark-gluon plasma introduces a preferred direction, it is furthermore necessary to distinguish between the transverse and the longitudinal components of the gluons. Simplifying the above we get

$$\sum_{a,\zeta}|\mathcal{M}(g\to s\bar{s})|^2=-4g^2[p_s^\mu\,p_{\bar{s}}^\nu+p_s^\nu\,p_{\bar{s}}^\mu-p_s\,p_{\bar{s}}\,g^{\mu\nu}]\,(P_{\mu\nu}+Q_{\mu\nu}).. \qquad (3.56)$$

Evaluating the transverse case further as an example. In the rest frame the transverse projection operator is $P^{ij}=-(\delta^{ij}-\frac{q^i\,q^j}{q^2})$, $P^{00}=0$. It is easily seen that $P^{\mu\nu}\,g^{\mu\nu}=2$ and

$$P^{\mu\nu}\,p_s^\mu p_{\bar{s}}^\nu=-(p_s\,p_{\bar{s}}-p_s\cdot q\,p_{\bar{s}}\cdot q/q^2)=-p_s\,p_{\bar{s}}(1-\cos^2\theta).$$

Finally, we must use $\cos\theta = \frac{q_0 p_0}{pq}$ obtained from the delta function.

We find for the transverse and longitudinal cases that

$$|\mathcal{M}_T(g \to s\bar{s})|^2 = 8g^2[4m_s^2 + Q^2(1 + 4\frac{p_0^2}{q^2})], \tag{3.57}$$

$$|\mathcal{M}_L(g \to s\bar{s})|^2 = 8g^2Q^2(1 - 4\frac{p_0^2}{q^2}). \tag{3.58}$$

Adding the two gives

$$\sum |\mathcal{M}(g \to s\bar{s})|^2 = 16g^2(2m_s^2 + Q^2). \tag{3.59}$$

### Breit Wigner Distribution

The Breit Wigner distribution is an approximation needed to take the plasmon distribution function into account. Summing over multi-gluon initial and final states is a non-trivial problem. Also, the time dependence of the gluon density in the sum is needed to reflect the time development of the thermal mass.

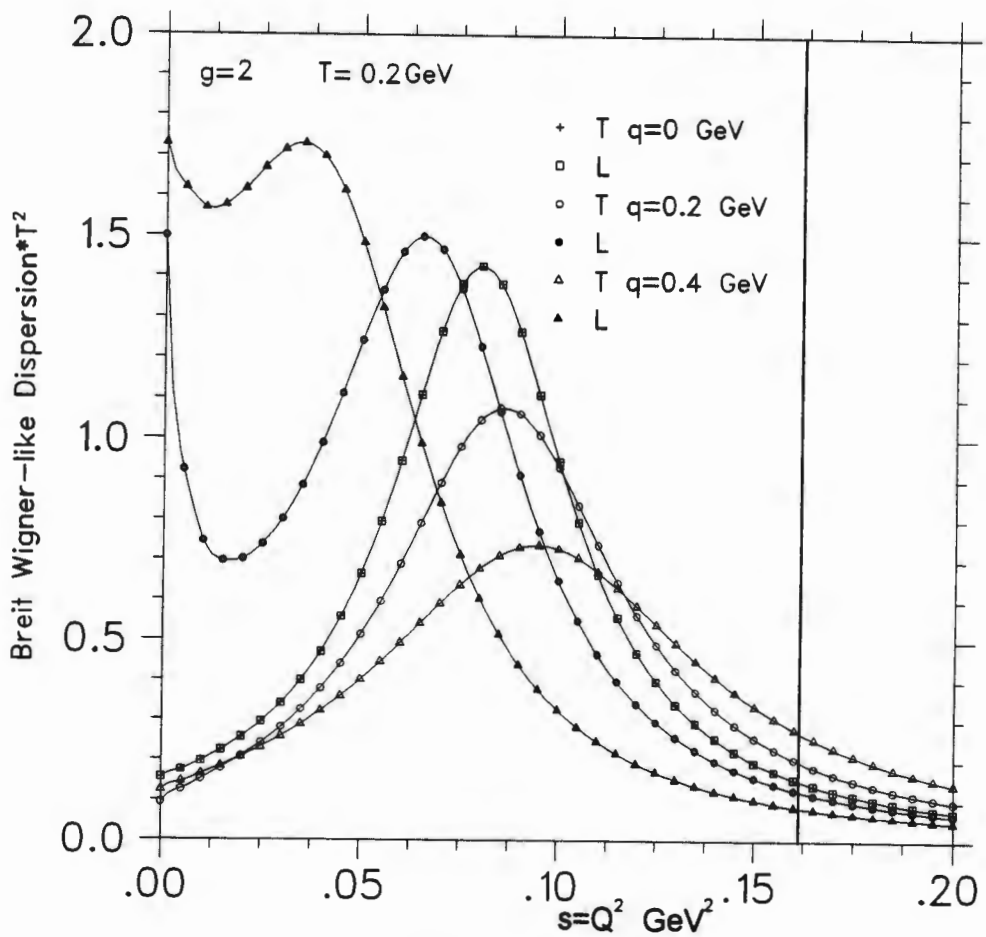


Figure 3.16: Transverse and Longitudinal Breit Wigner Distribution Functions

In the case of a narrow resonance the width of the resonance is related to the imaginary shift of the pole in the propagator in the complex $q_0$ plane

$$\frac{1}{q_0^2 - (\sqrt{q^2+m^2} + i\gamma)^2} \approx \frac{1}{Q^2 - m^2} + \frac{i2\sqrt{q^2+m^2}\,\gamma}{(Q^2-m^2)^2 + 4(q^2+m^2)\gamma^2} \tag{3.60}$$

which in the limit $\gamma \to 0$ yields the standard free particle propagator

$$\frac{1}{Q^2 - m^2 - i\epsilon} = \mathcal{P}\frac{1}{Q^2-m^2} + i\pi\delta(Q^2-m^2). \tag{3.61}$$

Thus for a Breit-Wigner resonance with width $\Gamma = \gamma/2$ the mass-shell $\delta$-function should be replaced by

$$\delta(Q^2-m^2) \to \frac{1}{\pi}\frac{\sqrt{q^2+m^2}\,\Gamma}{(Q^2-m^2)^2 + (q^2+m^2)\Gamma^2}\ . \tag{3.62}$$

This simple prescription cannot be directly applied to the case of thermal gluons because the location of the pole is determined by complicated dispersion relations (3.24, 3.22 and 3.23) for transverse and longitudinal gluons. Instead of (3.62) we use (3.47) to obtain

$$\delta(Q^2-m_g^2) \to \frac{1}{\pi}\frac{\mathrm{Res}(\Delta_{T,L})^{-1}\gamma_{T,L}}{(Q^2 - \mathrm{Re}\Pi_{T,L})^2 + \mathrm{Res}(\Delta_{T,L})^{-2}\gamma_{T,L}^2}. \tag{3.63}$$

The transverse and longitudinal Breit-Wigner-like distributions are shown in Figure 3.16. for three different values of the momentum $q$. One can clearly see the peak corresponding to the thermal gluon mass. This peak levels off as one increases the value of $q$. Also shown is a vertical line corresponding to the strange quark production threshold $4m_s^2$, where we have taken $m_s$ to be 0.2 GeV [107]. Note that this threshold is in the tail of the distribution. Only the part to the right of this line contributes to strange quark production.

By making use of (3.63) and (3.57,3.58) we find from (3.53)

$$\begin{aligned} R^T_{g\to s\bar{s}} \;=\; & \frac{g^2}{2\pi^4}\int_{2m_s}^{\infty} dq_0\, f_-(q_0) \int_0^{\sqrt{q_0^2-4m_s^2}} dq\, q \int_{-\frac{q}{2}\sqrt{1-\frac{4m_s^2}{Q^2}}}^{\frac{q}{2}\sqrt{1-\frac{4m_s^2}{Q^2}}} dp_0 \times \\ & \Big(1 - f_+(\tfrac{1}{2}q_0 + p_0)\Big)\Big(1 - f_+(\tfrac{1}{2}q_0 - p_0)\Big) \times \\ & \frac{\mathrm{Res}(\Delta_T)^{-1}\gamma_T}{(Q^2 - \mathrm{Re}\Pi_T)^2 + \mathrm{Res}(\Delta_T)^{-2}\gamma_T^2}[4m_s^2 + Q^2(1 + 4\frac{p_0^2}{q^2})], \end{aligned} \tag{3.64}$$

and a similar expression for $R^L_{g\to s\bar{s}}$ . The production rate due to gluon decay is given by the sum

$$R_{g\to s\bar{s}} = R^T_{g\to s\bar{s}} + R^L_{g\to s\bar{s}}. \tag{3.65}$$

We use the full high temperature expressions for $\mathrm{Re}\Pi_{T,L}$ given by (3.34,3.35) and numerically solve the dispersion relations (3.25) in order to determine $\mathrm{Res}(\Delta_{T,L})$ from (3.45,3.46).

We use $\gamma \equiv \gamma_T \approx \gamma_L$ which is estimated using (3.37).

The contribution from thermal gluons as calculated in [7] and corrected in [22] is

$$\delta R^{T,L}_{g^*\to q\bar{q}} = \left(1-e^{2\beta\mu}\right)\frac{g^2}{(2\pi^4)}T^4\int_{2m_s}^{\infty}dq_o\int_0^{\sqrt{q_o^2-4m_s^2}}dqq\int_{-\frac{q}{2}\sqrt{1-\frac{4m_s^2}{Q^2}}}^{\frac{q}{2}\sqrt{1-\frac{4m_s^2}{Q^2}}}dp_o\times$$
$$\frac{\mathrm{Res}(\Delta_{T,L})^{-1}\gamma_{T,L}}{(Q^2-\mathrm{Re}\Pi_{T,L})^2+(\mathrm{Res}(\Delta_{T,L})^{-1}\gamma_{T,L})^2}\left(4m_s^2+Q^2\left(1+4\frac{p_o^2}{q^2}\right)\right)\quad e^{-q_o}\times$$
$$f_-(q_o,0)\times f_+(\frac{q_o}{2}+p_o,\mu)\times f_+(\frac{q_o}{2}-p_o,\mu). \tag{3.66}$$

We have

$$\delta R_{g^*\to Q\bar{Q}} = \delta R^T_{g^*\to Q\bar{Q}} + \delta R^L_{g^*\to Q\bar{Q}}. \tag{3.67}$$

The rates for different processes are depicted in Figure 3.17.

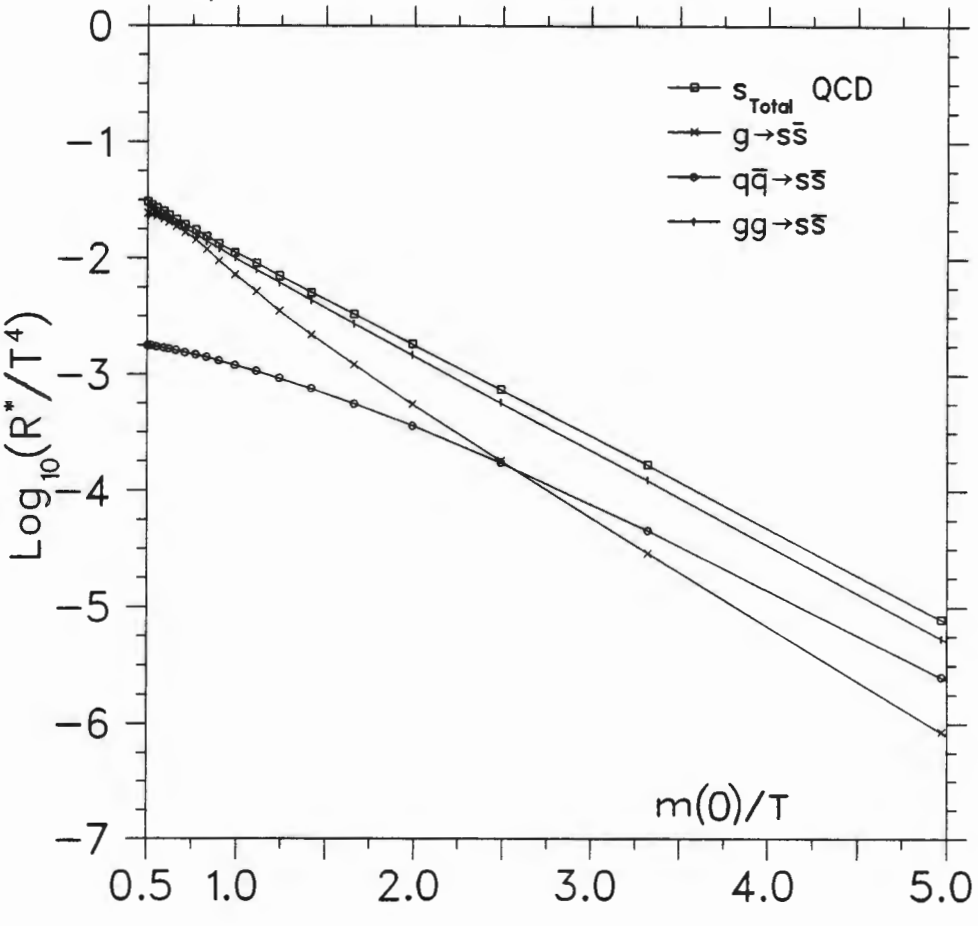


Figure 3.17: $\delta R$ vs $m_s/T$

Our numerical calculation of the thermal gluon decay is done using equations (3.64,3.65) with (3.22,3.23,3.45,3.46) and (3.37). We calculate the rates for quark-antiquark annihilation and gluon fusion by making use of equations 3.13 and 3.15 in reference [98]. We fix

the QCD running coupling constant at the value $g = 2$ because the temperature during the time evolution is almost constant and the effect on the running coupling constant is negligible.

In our figure the quark mass is kept fixed. In reference [22] it varies with temperature according to (3.49). In both cases we find that gluon fusion dominates everywhere. The gluon decay process is comparable to the gluon fusion when $T$ becomes very large. Had we used $g = 1$ instead of $g = 2$ the difference between the gluon decay rates with the different parameterisations of the width would not be so pronounced (about 30-50% for $g = 1$ compared to 70-80% for $g = 2$).

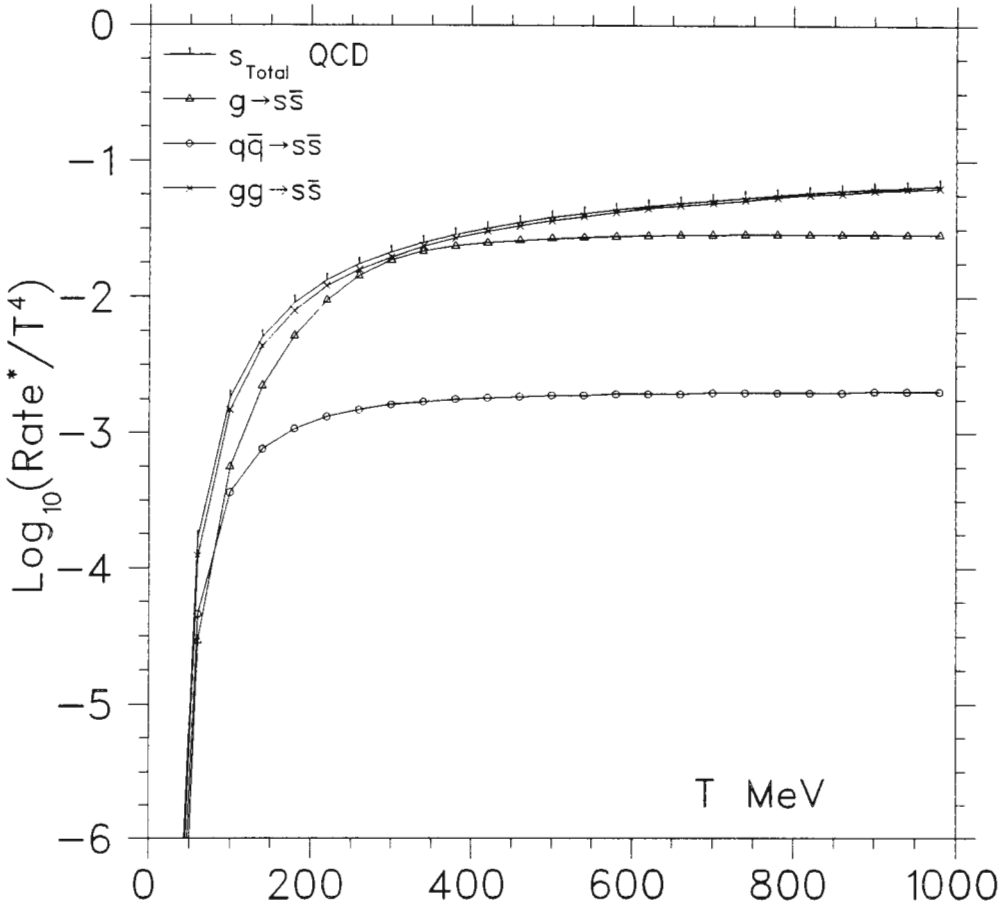


Figure 3.18 $\delta R$ versus $T$

We replot the Figure 3.17 in 3.18, but with $T$ as the independent variable.

### 3.3.2 Calculations of the next order

A more complete calculation should also include thermal gluons and resummed propagators in the gluon fusion process. For the present analysis this is not necessary because the next

order will be of a lower magnitude.

Gluon fusion with massless gluons and *nonzero* $m_s$ is of the order $\alpha_S^2$. Including the thermal gluon mass would lead to the following corrections

$$R_{gg\to s\bar{s}} \sim \alpha_S^2(1 + a\frac{m_g^2}{T^2} + b\frac{m_g^2}{m_s^2} + ..) \tag{3.68}$$

with $m_g^2 \sim \alpha_S$. If the thermal width is included there will be additional corrections

$$R_{gg\to s\bar{s}} \sim \alpha_S^2(1 + ... + c\frac{\gamma^2}{T^2} + d\frac{\gamma^2}{m_s^2} + ..) \tag{3.69}$$

with $\gamma \sim \alpha_S \log \alpha_S$. (The above expression is obtained using the available dimensionful quantities.) Constants $a, b, c, d$ can be calculated using, for example, the amplitude square given in [26]. Thus, the corrections coming from the gluon thermal mass are of the order $\alpha_S^3$ and those from the width are $\alpha_S^4(\log \alpha_S)^2$.

On the other hand, gluon decay is of the order $\alpha_S^2(\log \alpha_S)$ which can be seen from (3.64) and therefore it is legitimate to compare gluon decay to gluon fusion calculated to lowest order. Moreover, including the above mentioned corrections would be consistent only if one also includes other $\alpha_S^3$ contributions.

The production of massless quarks is another matter. In that case the above corrections contribute to lowest order and one needs the resummation program for the gluon fusion process. In addition the resummation is believed to cure a kinematic divergence of the type $\ln(Q^2/m_q^2)$ [54] as discussed by Altherr and Seibert [5]. However, this program goes beyond the aim of our work.

### Comments regarding Gluon Decay

In calculating the rate of gluon decay use was made of the Braaten-Pisarski resummation scheme. This is strictly valid only when $gT << T$ which is clearly not the case here, since we use $g = 2$. Unfortunately this is the case with most applications of QCD at finite temperatures. Secondly the magnetic mass has been introduced although only very limited knowledge is available. It has been used to calculate the damping rate of a thermal gluon inside a plasma. In comparison to the calculations of references [4, 5] we keep the standard form of the Breit-Wigner distribution. The consequence of this is that the rate for high masses is reduced, while for low masses it is enhanced.

**Double counting:** Due to the resummation of the gluon propagator, we now consider the possibility of double counting. Expanding Figure 3.14 using the expression for the propagator in Figure 2.9 we see that the gluon loop contributing to the gluon propagator could also contribute to the $s$-channel of gluon fusion. This problem is resolved by considering

the different parts of the phase space occupied by the two different processes. The virtual gluon in the gluon fusion process must have energy $\sqrt{s} > 2m_s$, to be above threshold. If one remembers that the gluon loop is hard and the external momentum must be soft to increase the effective order (we are using an HTL then), the virtual photon that decays into two strange particles must have $P \approx gT$. Therefore we only have problems if $gT > 2m_s$. The Breit Wigner distribution allows gluon decay below mass threshold and so with $g \ll 1$ we are safe.

## 3.4 Conclusion

The rate of $gg \to i\bar{i}$ has not been properly calculated in perturbative thermal QCD. It is expected that hard thermal loops will screen divergences of the type $\frac{1}{m}$ as $m \to 0$. We see that for light quarks we will have to take care of double counting.

Conversely, looking at Figure 3.16 we see that it is a small tail of the distribution function above the mass threshold that contributes to gluon decay. Gluon decay for up and down quarks will be far greater than for strange quarks due to this threshold. The question as to whether the infra-red screening in gluon fusion will damp this rate sufficiently to allow gluon decay to become dominant for light quarks is an open question.

In chapters 2 and 3 we have outlined in some detail considerations that would have to be made in calculating the next order of TFT's contribution to strange quark production. This has not been done yet, but would prove to be an important, though challenging, exercise.

# Chapter 4

# Hydrodynamic Expansion of a Gluon Gas

**Introduction.** From the remnants of a Relativistic Heavy Ion Collision, the dynamic processes are to be reconstructed. We have discussed the evolution of the hadron phase of the RHIC in Chapter 1. QCD and effective QCD were used to investigate microscopic snapshots of a hot quark-gluon plasma. In this chapter we will discuss a model in which we can study the evolution of a gluon plasma to a quark-gluon plasma. The questions of the mechanism of the transition from a QGP to a baryon gas, and from two relativistic nuclear pancakes to a gluon gas are beyond the scope of this model, but are important phases in the wake of a RHIC.

We now discuss the hydrodynamic expansion of a gluon gas with a QCD quark creation mechanism. Until now we have had no knowledge of the correct $T$ and $\mu$, or their dependence on each other. We will first introduce Bjorken's hydrodynamic equations. The initial conditions are briefly discussed as well as analytic solutions. The next goal is to simulate a gluon plasma's evolution, through a quark-gluon plasma phase, until a later time. We discuss the role of gluons, thermodynamic consistency and the inclusion of heavier quarks (charm and above).

The mechanism used to create quarks from gluons is discussed in [4], [22] and [98]. The purpose of this simulation is to investigate the conclusions of [67] but in the same vein as in [4]. The question that we answer is to what extent strange quarks approach chemical equilibrium. In [7] a similar approach is taken. However it is of interest to consider why the heavy quarks in this paper diverge and this paper uses approximate expressions over the whole range of $T$ and $\mu$ which may not be admissible. Finally, it is of interest to see the effects of the chemical potential on the rates.

# 4.1 Bjorken's Hydrodynamic Model

**Introduction:** The relativistic hydrodynamic model of Bjorken is applied to the evolution of a gluon plasma, from the preequilibrium nucleus-nucleus collision to a later stage in which hadrons are expected to dominate. Chemical equilibration of the quark species is approached through the production of quarks by perturbative (first order) gluon annihilation, gluon fusion, light quark annihilation and non-perturbative gluon decay processes. Important thermodynamic aspects are particularly interesting, notably the relative departure from chemical equilibrium of the heavier quarks, the number of charmed, bottom and top quarks and appropriate time, energy density and number density scales for such a plasma. This model has a few simple analytic solutions, and the numerical results can be compared with numerous (more complicated) models. We have some confidence in the assumptions of our model due to the results of the parton simulation [68].

## 4.1.1 Thermodynamic Definitions

We use the standard thermodynamic expressions for $n_i$, $\varepsilon$ and $p$. We will discuss their validity in the next section.

From the covariant definition of the energy tensor

$$T^{\mu\nu} = \sum_i^n \int_{-\infty}^{\infty} \frac{d^3k}{(2\pi)^3 E} k^\mu k^\nu f_\pm(E_i(k), \mu_i) = -g^{\mu\nu} p + (\varepsilon + p) u^\mu u^\nu \tag{4.1}$$

($n$ is over all degrees of freedom, $E_i^2 = m_i^2 + k^2$ and $f_\pm$ is the standard Bose-Einstein or Fermi-Dirac distribution function) and number density

$$n_i^\mu = \gamma_i \int \frac{d^3k}{(2\pi)^3 E_i} k^\mu f_\pm(k, m_i, \mu_i) = n_i(T, \mu)\, u^\mu \tag{4.2}$$

where $\gamma_i$ is a degeneracy factor. We are able to extract $\varepsilon(T, \mu)$, $p(T, \mu)$ and $n_i(T, \mu)$, by contracting the above expressions with suitable tensors $g^{\mu\nu}$ and $u^\mu u^\nu$ . Hence

$$n_i(T, \mu_i) = \frac{\gamma_i}{2\,\pi^2} \int_0^\infty dk\, k^2\, f_\pm(E_i(k), \mu_i),$$

$$\varepsilon(T, \mu_i) = \frac{1}{2\,\pi^2} \sum_i^n \gamma_i \int_0^\infty dk\, k^2\, E_i\; f_\pm(E_i(k), \mu_i)$$

and

$$p(T, \mu_i) = \frac{1}{6\,\pi^2} \sum_i^n \gamma_i \int_0^\infty dk \frac{k^4}{E_i}\; f_\pm(E_i(k), \mu_i).$$

Because gluons in equilibrium have $\mu = 0$ they only enter the equations in the energy density and pressure. We can explicitly do the integration over the gluon degrees of freedom and obtain

$$\varepsilon(T, \mu_i) = \frac{(N_c^2 - 1)\pi^2}{15} T^4 + \frac{2N_c}{\pi^2} \sum_i^n \int_0^\infty dk\, k^2\, E_i\; f_+(E_i(k), \mu_i) \tag{4.3}$$

and

$$p(T,\mu_i) = \frac{(N_c^2-1)\pi^2}{45}T^4 + \frac{2\,N_c}{3\,\pi^2}\sum_i^n \int_0^\infty dk \frac{k^4}{E_i}\; f_+(E_i(k),\mu_i) \tag{4.4}$$

where $\gamma = 2 \times 2 \times N_c$ = spin $\times$ color and $i$ runs over the quark and anti-quark flavors.

### 4.1.2 Bjorken's Hydrodynamic Equations

Bjorken [31] proposed an extremely simple set of equations to model the hydrodynamic expansion of a relativistic gas. He assumed that thermodynamic quantities were independent of rapidity. His derivation also assumed one spatial dimension. These assumptions are pivotal for the model and it would be of interest to see how they can be relaxed [20]. We know for example that the first assumption is only approximately true in $p$-$p$ collisions.

#### Derivation of Bjorken's equations

For an ideal fluid where interactions are weak, we get energy-momentum conservation

$$\partial_\mu T^{\mu\nu}(x) = 0 \tag{4.5}$$

and number density

$$\partial_\mu n^\mu(x) = R_{gain} - R_{loss} = \delta R. \tag{4.6}$$

After contracting equation 4.5 with $u^\nu$ we simplify

$$\begin{aligned} u_\nu\,\partial_\mu\,T^{\mu\nu}(x) &= -u_\nu\partial^\nu p + \partial_\mu(\varepsilon+p)u^\mu u_\nu u^\nu + (\varepsilon+p)\left((\partial_\mu u^\mu)u_\nu u^\nu + u^\mu u_\nu \partial_\mu u^\nu\right) \\ &= \partial_\mu\left(\varepsilon\right)u^\mu + (\varepsilon+p)\left(\partial_\mu u^\mu\right) = 0. \end{aligned}$$

Here we have used the property that since $u^\mu u_\mu = 1$ then

$$0 = u^\mu\partial_\mu\left(u^\nu u_\nu\right) = u^\mu u_\nu\partial_\mu u^\nu + u^\mu u^\nu\partial_\mu u_\nu = 2u^\mu u_\nu\partial_\mu u^\nu.$$

To make further progress we need the fluid velocity $u^\mu = (\cosh y, 0, 0, \sinh y)$ and we need to change our space variables to $x^\mu = (\tau\cosh y, 0, 0, \tau\sinh y)$. From this it can be shown that

$$\partial^\mu u_\mu = \frac{1}{\tau}$$

and

$$u_\mu\partial^\mu = \frac{\partial}{\partial\tau}.$$

The first of Bjorken's equations follows immediately

$$\frac{d\varepsilon}{d\tau} = -\frac{(\varepsilon+p)}{\tau}. \tag{4.7}$$

The other equations are derived using

$$\partial^{\mu}\left(n_B\, u_{\mu}\right) = \delta R \Rightarrow \partial^{0}\left(n_B\, u_0\right) + \partial^{z}\left(n_B\, u_z\right) = \delta R. \tag{4.8}$$

Scale invariance, $n_B(\mu(\tau), T(\tau))$, allows us to drop one term. Hence

$$\frac{dn_i}{d\tau} = -\frac{n_i}{\tau} + \delta R_i. \tag{4.9}$$

Here $i = u\,, d\,, s\,, c\,, b$ and $t$ quarks and anti-quarks. $\tau$ is the proper time, $t$ the real time and $z$ the spatial dimension: $\tau = \sqrt{t^2 - z^2}$ and $y = \frac{1}{2}\ln\frac{t+z}{t-z}$.

In Figure 4.1 is drawn the space-time diagram of a RHIC, as well as important epochs in the history of a RHIC. The proper time, $\tau$, is appropriate for Bjorken's model.

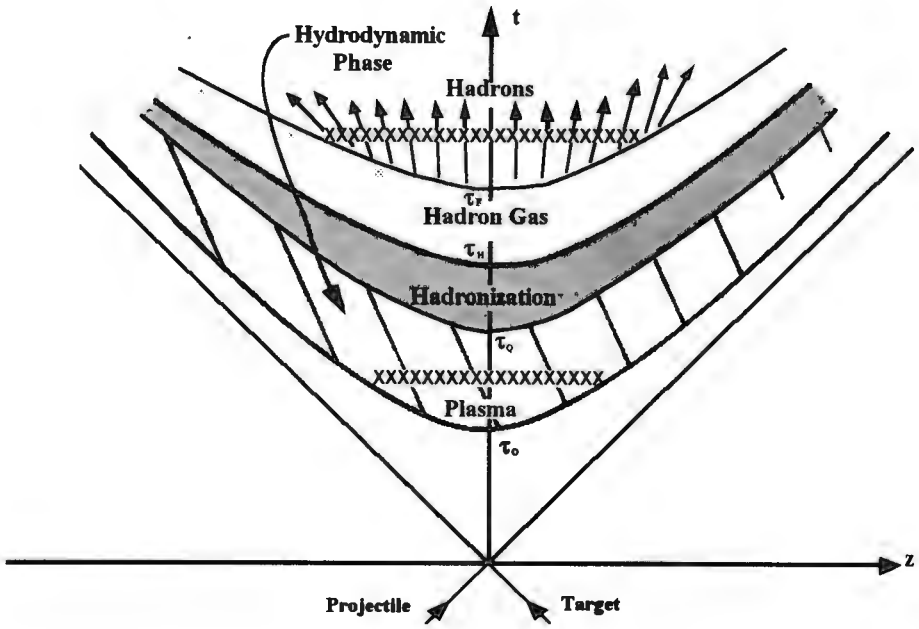


Figure 4.1: The space time evolution of a relativistic heavy ion collision in the cm frame. The origin corresponds to the coincidence of the centre of mass of the nuclei. The nuclei follow aproximately the $t = \pm z$ line. The initial and final values may be represented by the $xxx$'s. The initial conditions we use in the Bjorken model are along the $\tau_0$ hyperbola.

The first observed problem with the above figure is that, because of the use of proper time, if we limit the initial condition to a finite part of the light cone, we find difficulties in linking the initial values by a time-like trajectory. We have indicated our initial value $\tau_0$, which implies an infinite plasma. Also, experimental evidence concludes that radial flow may not be negligible. Acknowledging these criticisms, Bjorken's equations provide us with a first approximation of the evolution of a (quark-) gluon plasma.

We have allowed for the possibility that the baryon number of the colliding nuclei need not reside only in the receding beam fronts. We parameterize this by

$$n_i(T, \mu_i) - n_{\bar{i}}(T, \mu_{\bar{i}}) = B_i/(\sigma\tau) \tag{4.10}$$

for $i = u, d$. $B_i$ is the 'valence' number of quarks of species $i$ in the pre-fragmentation baryons, $\sigma \sim constant$ is the cross section of the baryons and $\tau$ is the proper time. For $Pb - Pb$ $B_{up} = 332$ and $B_{down} = 289$. For simplicity, we take $\sigma = 4\pi R^2$. We get $R$ from ordinary nuclear matter $\rho = \rho_0 = \frac{4}{3} A\pi R^3$, where $\rho_0 = 0.17/fm^3$. This relates the chemical potential of quarks and antiquarks to the temperature. (The plasma is assumed to expand at near the speed of light.)

Since $n_i(T, \mu_i) = n_{\bar{i}}(T, \mu_{\bar{i}})$ for strange, charm, bottom and top to ensure strangeness, charm conservation we have $\mu_i = \mu_{\bar{i}}$. This implies that if we have six quarks and six anti-quarks, we only need eight chemical potentials - $\mu_u, \mu_{\bar{u}}, \mu_d, \mu_{\bar{d}}, \mu_s, \mu_c, \mu_b$ and $\mu_t$.

Now using

$$\frac{df}{d\tau} = \frac{\partial f}{\partial T}\frac{dT}{d\tau} + \sum_i^n \frac{\partial f}{\partial \mu_i}\frac{d\mu_i}{d\tau} \tag{4.11}$$

we obtain an $(n+1) \times (n+1)$ matrix that can now be applied to equations 4.7 and 4.9. We can then invert this matrix to obtain $dT/d\tau$ and $d\mu/d\tau$ and then use standard numerical algorithms to evolve this ordinary differential equation (ODE) over time. For example we consider initially only up, down and strange quarks, and therefore a $4 \times 4$ matrix. To include anti-particles, assuming particle number conservation ensures that the chemical potentials are equal for all three quarks, we need to include an extra '2' per particle in **final** expression for $\varepsilon$ and $p$.

$$\begin{bmatrix} a_1 & b_1 & 0 & 0 \\ a_2 & 0 & b_2 & 0 \\ a_3 & 0 & 0 & b_3 \\ c & d_1 & d_2 & d_3 \end{bmatrix} \begin{bmatrix} dT/d\tau \\ d\mu_u/d\tau \\ d\mu_d/d\tau \\ d\mu_s/d\tau \end{bmatrix} = \begin{bmatrix} e_1 \\ e_2 \\ e_3 \\ f \end{bmatrix}$$

where

$$\begin{array}{lll} a_i = \partial n_i/\partial T, & b_i = b_{ij}\delta_{ij} = \partial n_i/\partial \mu_j \delta_{ij} = \partial n_i/\partial \mu_i, & c = \partial \varepsilon/\partial T, \\ d_i = \partial \varepsilon/\partial \mu_i, & e_i = -n_i/\tau + \delta R_i \text{ and} & f = -(\varepsilon + p)/\tau. \end{array} \tag{4.12}$$

We can invert this matrix and the solution to this system of equations is

$$\begin{bmatrix} dT/d\tau \\ d\mu_u/d\tau \\ d\mu_d/d\tau \\ d\mu_s/d\tau \end{bmatrix} = \begin{bmatrix} a_1 & b_1 & 0 & 0 \\ a_2 & 0 & b_2 & 0 \\ a_3 & 0 & 0 & b_3 \\ c & d_1 & d_2 & d_3 \end{bmatrix}^{-1} \begin{bmatrix} e_1 \\ e_2 \\ e_3 \\ f \end{bmatrix} \tag{4.13}$$

Explicitly this becomes

$$\begin{bmatrix} dT/d\tau \\ d\mu_u/d\tau \\ d\mu_d/d\tau \\ d\mu_s/d\tau \end{bmatrix} = \begin{bmatrix} b_2b_3d_1/D & b_1b_3d_2/D & b_1b_2d_3/D & -b_1b_2b_3/D \\ A/D & -a_1b_3d_2/D & -a1b_2d_3/D & a1b_2b_3/D \\ -a_2b_3d_1/D & B/D & -a2b_1d_3/D & a_2b_1b_3/D \\ -a_3b_2d_1/D & -a_3b_1d_2/D & C/D & a_3b_1b_2/D \end{bmatrix} \begin{bmatrix} e_1 \\ e_2 \\ e_3 \\ f \end{bmatrix} \tag{4.14}$$

using $A = -b_2b_3c + a_2b_3d_2 + a_3b_2d_3$, $B = -b_1b_3c + a_1b_3d_1 + a_3b_1d_3$, $C = -b_1b_2c + a_1b_2d_1 + a_2b_1d_2$

and $D = -b_1b_2b_3c + a_1b_2b_3d_1 + a_2b_1b_3d_2 + a_3b_1b_2d_3$. Finally we get

$$\begin{bmatrix} dT/d\tau \\ d\mu_u/d\tau \\ d\mu_d/d\tau \\ d\mu_s/d\tau \end{bmatrix} = \begin{bmatrix} b_2b_3d_1e_1 + b_1b_3d_2e_2 + b_1b_3d_2e_3 - b_1b_2b_3e_4 \\ Ae_1 - a_1b_3d_2e_2 - a_1b_2d_3e_3 + a_1b_2b_3e_4 \\ -a_2b_3d_1e_1 + Be_2 + -a_2b_1d_3e_3 + a_2b_1b_3e_4 \\ -a_3b_2d_1e_1 - a_3b_1d_2e_2 + Ce_3 + a_3b_1b_2e_4 \end{bmatrix} \div D. \qquad (4.15)$$

We have found that the analytic expression for the matrix for the case of one quark and anti-quark with the same chemical potential reduces to that for one quark only. Similarly the matrix for the case of three quarks with two quarks equal to their anti quarks, reduces to the case of three distinct quarks. Physically this is trivial but it gives us a good numeric tool. It turns out that we need only include an additional 2 before the summation in the definitions of $\varepsilon$ , $p$ and $\partial\varepsilon/\partial T$ (and not $n_i, \partial\varepsilon/\partial\mu_i$ and $\delta R_i$ ) to include effects of anti-quarks.

### 4.1.3 Implementation

We now write a program to evaluate each of the $a_i$ , $b_i$ , $c$ , $d_i$ , $e_i$ and $f$ for a certain $\mu_i^o$, $T^o$ and $\tau^o$. Then from the definition of the derivative $f'(x) = \lim_{\delta x \to 0} \frac{f(x+\delta x) - f(x)}{\delta x}$ we extrapolate using Euler's method

$$f(x + \delta x) = f(x) + \delta x\, f'(x)$$

the next value of $\mu_i$ and $T$ for some later value of $\tau = \tau^o + \delta\tau$ determined by the program. We then repeat this process using our new-found values of $\mu_i$, $T$ and $\tau$ for $\mu_i^o$, $T^o$ and $\tau^o$.

Rather than using *Euler's* method (which is slow and unstable) we used the *Runge-Kutta-$\mathcal{O}(4)$* method the *Runge-Kutta-$\mathcal{O}(4)$ with variable step size* and *Bulirsch-Stoer* methods [106]. The bottle-neck in the computation was calculating the rates - we decided not to approximate our expressions. A typical calculation of the rates involves 8 Gauss-Laguerre or Gauss-Legendre points, integrated $2 \times 4$ times for $(2 \times 2 + 4)$ quarks $= 8 \times 8 \times 8^4 = 262144$ calculations.

We do the simulation for the simplest case, and slowly build up our scenario to include the full set of physically relevant mechanisms. We are also able to check the numerical validity of our results by comparing them with approximate analytic solutions.

## 4.2 Approximate Solutions

### 4.2.1 Light Quark approximation

Before getting involved in numerical solutions, we can solve this system of equations for certain simple cases. We can do this exactly for the massless one particle case. We obtain that $T$ and $\mu$ go as $\tau^{\frac{1}{3}}$, and $T/\mu$ is set by the initial condition. Identical results are obtained in a gluon plasma.

In exactly the same way as for this case, but this time taking the first **3** terms of the Taylor Expansion we can solve approximately for the case of $m \neq 0$.

For example, in equation 4.1.1, with the degeneracy factor $\gamma = 2 \cdot 3$ (spin $\times$ color) we get

$$\begin{aligned} n &= \gamma \int \frac{4\pi}{(2\pi)^3} \frac{k^2}{e^{\beta(E-\mu)}+1}\, dk = \frac{3T^3}{\pi^2} \int \frac{u^2 du}{e^{(\sqrt{u^2+(m/T)^2}-\beta\,\mu)}+1} \\ &= \frac{3T^3}{\pi^2} \int u^2\, du \sum_{k=1}^{\infty} (-1)^{(k+1)} \left(e^{(\sqrt{u^2+(m/T)^2}-\beta\,\mu)}\right)^k \end{aligned} \tag{4.16}$$

using $u = q/m$ and then expressing the Fermi-Dirac integral as a sum. In the Boltzmann approximation this becomes

$$= \frac{3T^3}{\pi^2} \int_0^{\infty} u^2\, du\, e^{-(\sqrt{u^2+(m/T)^2}-\beta\,\mu)} = \frac{3m^3}{\pi^2} \int_1^{\infty} \sqrt{(z^2-1)}\, z\, dz\, e^{-z\,m/T+\beta\,\mu}$$

where $(m/T)^2 z^2 = u^2 + (m/T)^2$. Doing a Taylor expansion of $(z^2-1)^{\frac{1}{2}}$ for large $z$ (valid if mass is small with respect to $T$),

$$n(T,\mu) = \frac{3m^3}{\pi^2} \int_1^{\infty} (z^2 - \frac{1}{2} - \frac{1}{8z^2} + \ldots) e^{(-z\,m/T+\beta\,\mu)}\, dz.$$

Now integrating by parts the first two terms gives

$$n(T,\mu) = \frac{3.2\,T^3}{\pi^2} \left(1 + \frac{m}{T} + \frac{1}{4}\frac{m^2}{T} + \mathcal{O}(\frac{m^3}{T})\right) e^{\beta(\mu-m)}.$$

Defining a common term

$$\mathcal{N} = \frac{3}{\pi^2} e^{\frac{-m+\mu}{T}} \tag{4.17}$$

we obtain

$$n(T,\mu) \approx 2\mathcal{N} \left(T^3 + mT^2 + \frac{m^2 T}{4}\right) = \mathcal{N}\frac{T}{2}(m+2\,T)^2. \tag{4.18}$$

Doing a similar Taylor expansion for $\varepsilon(T,\mu)$ and $p(T,\mu)$, but keeping four terms in the series, leads to

$$\varepsilon = \mathcal{N}\left(6 + 6\frac{m}{T} + \frac{5}{2}\frac{m^2}{T^2} + \frac{1}{2}\frac{m^3}{T^3} + \mathcal{O}(\frac{m^4}{T^4})\right) T^4 \approx \frac{\mathcal{N}T}{2}(m+2\,T)\left(m^2 + 3\,m\,T + 6\,T^2\right) \tag{4.19}$$

and

$$p = \mathcal{N}\left(2 + 2\frac{m}{T} + \frac{1}{2}\frac{m^2}{T^2} - \frac{1}{6}\frac{m^3}{T^3} + \mathcal{O}(\frac{m^4}{T^4})\right) T^4 \approx \mathcal{N}\left(2\,T^4 + 2\,m\,T^3 + \frac{m^2\,T^2}{2} - \frac{m^3\,T}{6}\right). \tag{4.20}$$

Using the above expressions 4.18, 4.19 and 4.20, and the definitions of 4.12 we calculate to at least $\mathcal{O}(\frac{m^3}{T^3})$ the following terms for large T:

$$a = \frac{\mathcal{N}}{2\,T}(m+2\,T)\left(m^2 + 3\,m\,T + 6\,T^2 - \mu\,(m+2\,T)\right) + \mathcal{N}\cdot\mathcal{O}(\frac{m^4}{T^4}), \tag{4.21}$$

$$b = 2\mathcal{N}\left(T^2 + m\,T + \frac{m^2}{4}\right) + \mathcal{N}\cdot\mathcal{O}(\frac{m^4}{T^4}), \tag{4.22}$$

$$c = \tfrac{\mathcal{N}}{2T}\,(m^4 + 6\,m^3\,T + 22\,m^2\,T^2 + 48\,m\,T^3 + 48\,T^4 - \mu(m^3 + 5\,m^2\,T + 12\,m\,T^2 + 12\,T^3)) + \mathcal{N}\cdot\mathcal{O}(\tfrac{m^5}{T^5}), \tag{4.23}$$

$$d = \mathcal{N}\left(6T^3 + 6\,m\,T^2 + \frac{5\,m^2\,T}{2} + \frac{m^3}{2}\right) + \mathcal{N}\cdot\mathcal{O}(\frac{m^4}{T}), \tag{4.24}$$

$$e = \frac{-2\mathcal{N}}{\tau}\left(T^3 + \frac{m^2\,T}{4} + m\,T^2\right) + \mathcal{N}\cdot\mathcal{O}(\frac{m^3}{T^3}), \tag{4.25}$$

and

$$f = \frac{-\mathcal{N}T}{3\,\tau}\left(m^3 + 9\,m^2\,T + 24\,m\,T^2 + 24\,T^3\right) + \mathcal{N}\cdot\mathcal{O}(\frac{m^4}{T^4}). \tag{4.26}$$

We will also need the denominator

$$D = a\,d - b\,c = \frac{-\mathcal{N}^2}{8\,T^4}(m + 2\,T)^2\,\left(m^2 + 12\,m\,T + 12\,T^2\right) + \mathcal{N}^2\cdot\mathcal{O}(\frac{m^5}{T^5}). \tag{4.27}$$

Accordingly, using an expression analogous to equation 4.15 we get

$$\frac{d\mu}{d\tau} = \frac{-\,(m^5 - 12\,m^3\,T^2 - 24\,m^2\,T^3\mu(-m^4 + m^3\,T + 18\,m^2\,T^2 + 36\,m\,T^3 + 24\,T^4)\,) + \mathcal{O}(6)}{(3\,T\,(m + 2\,T)\,(m^2 + 12\,m\,T + 12\,T^2) + \mathcal{O}(4))\,\tau} \tag{4.28}$$

and

$$\frac{dT}{d\tau} = \frac{m^3 - 3\,m^2\,T - 12\,m\,T^2 - 12\,T^3 + \mathcal{O}(4)}{(3\,(m^2 + 12\,m\,T + 12\,T^2) + \mathcal{O}(3))\,\tau}. \tag{4.29}$$

By disregarding terms in equation 4.28 of order $(m/T)^5$ (when comparing this expression to others, we must remember the terms in the denominator) we get, by writing down terms dependent and independent of $\mu$ apart,

$$\frac{d\mu}{d\tau} = \frac{4\,m^2\,T + \mathcal{O}(3)}{(m^2 + 12\,m\,T + 12\,T^2 + \mathcal{O}(3))\,\tau} - \mu\frac{(m + 2\,T)^2 + \mathcal{O}(3)}{(m^2 + 12\,m\,T + 12\,T^2 + \mathcal{O}(3))\,\tau}. \tag{4.30}$$

Now using $\frac{m}{x} = 2\,T$ and $u = \mu/(2m)$ we get

$$\frac{du}{d\tau}(x) = \frac{-u + x - 2\,u\,x - u\,x^2 + \mathcal{O}(3)}{\tau(3 + 6\,x + x^2 + \mathcal{O}(3))} = \frac{x + \mathcal{O}(2)}{\tau(3 + 6x + x^2 + \mathcal{O}(3))} - u\frac{(1 + x)^2 + \mathcal{O}(3)}{\tau(3 + 6x + x^2 + \mathcal{O}(3))}. \tag{4.31}$$

We can do a similar transformation to $dT/d\tau$

$$\frac{dT}{d\tau}(x) = \frac{m\,(-3 - 6\,x - 3\,x^2 + 2\,x^3 + \mathcal{O}(4))}{6\,x\,(3 + 6\,x + x^2) + \mathcal{O}(4)}. \tag{4.32}$$

The $-3$ in equation 4.32 corresponds to the term of $\mathcal{O}(\frac{m^3}{T^3})$ in equation 4.29, which we disregard to be consistent with the order of $\mu$. Factorising gives

$$\frac{dT}{d\tau}(x) = \frac{-\left(m\,(1+x)^2 + \mathcal{O}(3)\right)}{\tau\,\left(2\,x\,\left(3+6\,x+x^2\right) + \mathcal{O}(4)\right)}. \tag{4.33}$$

Now replacing $dT$ with $\frac{-m\,dx}{2\,x^2}$

$$\frac{dx}{d\tau}(x) = \frac{x\,(1+x)^2 + \mathcal{O}(4)}{\tau\,\left(\left(3+6\,x+x^2\right) + \mathcal{O}(3)\right)}. \tag{4.34}$$

The problem now is to correctly expand out the above and group terms of the same order. This we do by noting that if we write the above as $\frac{g(3)+\mathcal{O}(4)}{f(2)+\mathcal{O}(3)}$ where $f$ and $g$ refer to the polynomial expressions of order 2 and 3 in the denominator and numerator, respectively, then this becomes $\frac{1}{f(2)}\frac{g(3)+\mathcal{O}(4)}{1+\mathcal{O}(3)/f(2)}$ where $\mathcal{O}(3)/f(2)$ is of order $\mathcal{O}(1)$ which is a number less than 1 in this approximation. Doing a Taylor series, this becomes $\frac{1}{f(2)}\left(g(3)+\mathcal{O}(4)\right)\left(1-\mathcal{O}(3)/f(2)\right) = \frac{1}{f(2)^2}\left(g(3)+\mathcal{O}(4)\right)\left(f(2)-\mathcal{O}(3)\right)$. This goes as

$$\begin{aligned} &\frac{1}{f(2)^2} \qquad \left(g(3)\,f(2) - \mathcal{O}(3)\,g(3) + \mathcal{O}(4)\,f(2) - \mathcal{O}(4)\,\mathcal{O}(3)\right) \\ &\qquad \rightarrow \quad \frac{g(3)}{f(2)} + \left(\mathcal{O}(3+2-2) + \mathcal{O}(3+3-2) + \mathcal{O}(4+3-2)\right). \end{aligned} \tag{4.35}$$

The first term is of order 1 and the other terms are then negligible. So we solve

$$\frac{dx}{d\tau}(x) = \frac{x\,(1+x)^2}{\tau\,\left(\left(3+6\,x+x^2\right)\right)}$$

. We can solve this using standard techniques and obtain

$$\tau = \frac{\lambda}{T(2T+m)^2} e^{\frac{4T}{2T+m}}. \tag{4.36}$$

$\lambda$ is the integration constant. We know this expression is only valid to order 1, so the exponential is spurious in the sense that it is only approximately valid, and is removed by a Taylor approximation. Hence

$$\tau = \frac{\lambda}{T(2T+m)^2}\left(1+\frac{4T}{2T+m}\right) = \frac{\lambda}{T^3}\left(\frac{1}{(1+\frac{m}{2T})^2} + \frac{2}{(1+\frac{m}{2T})^3}\right). \tag{4.37}$$

The limiting case of $m \rightarrow 0$ is as expected:

$$\tau = \frac{\lambda}{T^3}. \tag{4.38}$$

Equation 4.37 can be inverted using techniques for cubic (or quartic) roots, but nothing significant is gained because the resulting expression is a complicated sum of fractional exponents.

Unfortunately we cannot simply solve for $\mu$ as a function of $\tau$, but we can obtain $\mu(T)$. By dividing equation 4.31 by equation 4.34 we find, after correctly having extricated the highest order terms, that we have to integrate

$$\frac{du}{dx} = \frac{-u + x - 2\,u\,x - u\,x^2}{x\,(1+x)^2} = \frac{1}{(1+x)^2} - \frac{u}{x}. \tag{4.39}$$

This we can solve simply, using the same arguments as before to get rid of the higher order terms, getting

$$\mu = -\lambda' T + \frac{2T}{1+\frac{m}{2T}} + 2T\log(\frac{m}{2T}+1). \tag{4.40}$$

Using the correct order implies

$$\mu = -\lambda' T + \frac{2T}{1+\frac{m}{2T}} + m.$$

This leads to

$$\frac{\mu - m}{T} = \frac{2}{1+\frac{m}{2T}} - \lambda'. \tag{4.41}$$

$\lambda'$ is the integration constant (in our simulation it would typically by a large positive number). Equation 4.40 is correct in the limit $m \to 0$ .

### 4.2.2 Heavy Quark approximation

In much the same way as for the light quark we can find $\mu(\tau)$ and $T(\tau)$ for heavier quarks. "Heavier" means that $m > p$; since we are in a plasma $p \approx T$ and therefore we expect the mass to be larger than the temperature in this limit. As before we can derive the following thermodynamic quantities:

$$n = \frac{\gamma}{(2\pi)^{\frac{3}{2}}}\exp(\frac{\mu - m}{T})(mT)^{\frac{3}{2}},$$

$$\varepsilon = \frac{\gamma}{(2\pi)^{\frac{3}{2}}}\exp(\frac{\mu - m}{T})(mT)^{\frac{3}{2}}(m + \frac{3}{2}T)$$

and

$$p = \frac{\gamma}{(2\pi)^{\frac{3}{2}}}\exp(\frac{\mu - m}{T})(mT)^{\frac{3}{2}}(T - \frac{5T^2}{2m}).$$

Using these expressions we calculate the coefficients

$a = \frac{\partial n}{\partial T} = \mathcal{N}(\frac{3}{2} + \frac{m-\mu}{T})$, $b = \frac{\partial n}{\partial \mu} = \mathcal{N}$, $c = \frac{\partial \varepsilon}{\partial T} = \mathcal{N}(\frac{m(m-\mu)}{T} - \frac{3}{2}\mu + 3m + \frac{15}{4}T)$,

$d = \frac{\partial \varepsilon}{\partial \mu} = \mathcal{N}(\frac{3}{2}T + m)$, $e = \frac{-n}{\tau} = -\mathcal{N}\frac{T}{\tau}$ and $f = \frac{\varepsilon + p}{\tau} = -\mathcal{N}\frac{T}{\tau}(m + \frac{5}{2}T - \frac{5}{2}\frac{T^2}{m})$ where $\mathcal{N} = \frac{\gamma}{(2\pi)^{\frac{3}{2}}}\exp\frac{\mu-m}{T}m^{\frac{3}{2}}T^{\frac{1}{2}}$. The denominator is $D = ad - bc = \mathcal{N}^2(-\frac{3}{2}T)$ and we obtain after some algebra that

$$\frac{dT}{d\tau} = \frac{-2T}{3\tau}(1 - \frac{5T}{2m})$$

and

$$\frac{d\mu}{d\tau} = \frac{-2T}{3\tau}\left(\frac{5}{2} - \frac{m}{T} + \frac{15T}{4m} + \frac{\mu}{T}(1 - \frac{5T}{2m})\right).$$

We can solve these differential equations:

$$T = \begin{cases} \frac{1}{\frac{5}{2}m + \Lambda\tau^{\frac{2}{3}}} & \text{for } \frac{T}{m} < \frac{2}{5} \\ \frac{1}{\frac{5}{2}m - \Lambda\tau^{\frac{2}{3}}} & \text{for } \frac{T}{m} > \frac{2}{5} \end{cases} \tag{4.42}$$

and

$$\frac{\mu}{T} = \begin{cases} \frac{m}{T} + \frac{3}{2}\ln(\frac{2m}{m-5T}) - \lambda' & \text{for } \frac{T}{m} < \frac{2}{5} \\ \frac{m}{T} + \ln(\frac{m}{T}(\frac{5}{2} - \frac{m}{T})) - \lambda' & \text{for } \frac{T}{m} > \frac{2}{5} \end{cases} \tag{4.43}$$

(Once again $\lambda$ and $\lambda'$ are integration constants. In the sense that $p \approx T$, this approximation is valid where $m > T$, and we accordingly only pay attention to the $\frac{T}{m} < \frac{2}{5}$ case. We are considering temperatures of $200 - 1000$MeV, and therefore, in this limit we are considering charmed quarks and heavier. For the same reason as for the light quark approximation, the logarithm is an artefact and must be approximated. This yields

$$\frac{\mu}{T} = \frac{m}{T} + \frac{15\,T}{2m} - \lambda''. \tag{4.44}$$

We note that for our model $\lambda''$ is very negative. Assuming that charmed quarks are eventually produced, there will be correspondingly few, and therefore the temperature of the plasma will be determined by the gluons and light quarks. Accordingly using the parametrisation of the temperature of $T \sim \tau^{-\frac{1}{3}}$ in the chemical potential we find the proper time dependence of the chemical potential of heavy quarks.

## 4.3 The numerical simulation - an overview

### 4.3.1 Naive results

Having obtained the rates in Chapters 2 and 3 we now use these as the $\delta R$ term and allow our system to expand using Bjorken's hydrodynamic expansion in one dimension.

We would like to establish whether $\mu \to 0$ as $T \to 0$, and, if so, what the characteristic time is. A quantity worth considering is $n_i(\mu_i, T)/n_i^o$ where $n_i^o = n_i(\mu_i = 0, T)$. It can easily be seen from 4.11 that

$$\frac{d(n_i/n_i^o)}{d\tau} = \frac{\delta R_i}{n_i^o}; \tag{4.45}$$

this is a very useful way of testing the numerical correctness of the solution.

It can be shown that $\frac{dn_s}{dt} = A(1 - \left[\frac{n_s(t)}{n_s(\infty)}\right]^2)$ leads to $n_s = n_s(\infty)\tanh(t/\tau)$ where $\tau = n_s(\infty)/A$. $A$ is related to $\delta R$. Therefore we would expect the number density to tend to the equilibrium density as $t$ tends to infinity.

A further numerical check we used was that the simulation had to be symmetric; having started from $\mu_i^o$ , $T^o$ and $\tau^o$ and after a certain number of iterations reached $\mu_i^*$ , $T^*$ and $\tau^*$ we expect to be able to reverse the hydrodynamic simulation.

For the case of $\delta R_i = 0$ Bjorken's hydrodynamic equations can be solved exactly for $\varepsilon = 3p$ . This is the case of an ultrarelativistic/massless gas. One gets the following useful parametrisation of the results obtained earlier:

$$T(\tau) = T_o \left(\frac{\tau_o}{\tau}\right)^{\frac{1}{3}}, \quad s(\tau) = s_o \left(\frac{\tau_o}{\tau}\right)^{1}, \quad n_i(\tau) = n_i^o \left(\frac{\tau_o}{\tau}\right)^{1} \text{ and } \varepsilon(\tau) = \varepsilon_o \left(\frac{\tau_o}{\tau}\right)^{\frac{4}{3}}. \quad (4.46)$$

This should be contrasted with the parametrisation of the results of Geiger and Kapusta [67] who use the parton model:

$$T(\tau) = 950 \left(\frac{\tau_0}{\tau}\right)^{0.3} \text{MeV}, \; s(\tau) = 1800 \left(\frac{\tau_0}{\tau}\right)^{0.85} \text{fm}^{-3}, \; n(\tau) = 565 \left(\frac{\tau_0}{\tau}\right)^{0.9} \text{fm}^{-3},$$

$$\varepsilon(\tau) = 1300 \left(\frac{\tau_0}{\tau}\right)^{1.15} \text{GeV/fm}^3 \text{ and } p(\tau) = 580 \left(\frac{\tau_0}{\tau}\right)^{1.25} \text{GeV/fm}^3.$$

We have $\tau_0 = 0.05$fm in the last parametrisation.

### 4.3.2 A note of caution

What follows is an explanation of an unphysical feature of the numerical solutions we will encounter later. These problems can be understood with the following analytic result. For our purposes we can set $m = 0$. Of particular interest is what happens at $\tau \to 0$. Right from the outset we know that the equilibrium statistics will break down here; we would like to establish where the hydrodynamic equations break down. Repeating the above, but this time allowing $\delta R \neq 0$ gives a result of the form

$$\frac{d\mu}{d\tau} = -\frac{\mu}{3\tau} - (4 - \frac{\mu}{T}) \left(e^{-\beta\mu} - e^{\beta u}\right) T^2 \Lambda(T, \mu)$$

$\Lambda$ is very weakly dependent on $\mu$ in the sense that it varies slowly between 0.5 and 1. and so we treat it as a constant. Similarly

$$\frac{dT}{d\tau} = -\frac{T}{3\tau} - \left(e^{-\beta u} - e^{\beta u}\right) T^2 \Lambda'(T, \mu)$$

Physically, for $\tau \to 0$ we have $\mu \to -\infty$. There are badly diverging terms in the above two equations; $e^{-\beta\mu}$ diverges fastest. Admittedly $\beta \to 0$ but $\mu \to -\infty$ *faster* because we expect that $n(\tau = 0) = 0$. Taking the terms that diverge the fastest of the above two equations we consider $d\mu/d\tau = -(4 - \mu/T)e^{-\mu/T}T^2\Lambda$ and $dT/d\tau = -e^{-\mu/T}T^2\Lambda'$. Dividing these two expressions gives

$$\frac{dT}{d\mu} = \frac{T}{\mu - 4T} \Rightarrow \mu = -4T \log T + c'T \quad (4.47)$$

which from a numerical point of view has quite drastic implications: Instead of $n \overset{\tau\to\infty}{\to} T^3 \sim \frac{1}{\tau}$ we get instead $n \overset{\tau\longrightarrow 0}{\longrightarrow} \frac{1}{T} \sim \tau^{\frac{1}{3}}$. This exponential in the differential leads to additional numerical difficulties - once the function reaches this regime terms diverge rapidly, and small step sizes are necessary. New distribution functions that reflect a departure from thermal equilibrium are needed in this limit.

### 4.3.3 Initial Conditions

We start the simulations with only 'valence' quarks. Because of the physical reasons discussed in connection with the distribution functions, we are not able to start the simulation at $\tau = 0$ but later at $\tau = 0.05$ fm. Having decided on $\tau$ we can fix the rest of the initial conditions to give the approximate energy density, which we calculate by saying that all the available energy of the two obliterated nuclei is dumped in the volume of a nucleus. It is easy to calculate that the appropriate temperature should be around $T \approx 1000$ MeV because the energy density gets mainly contributions from gluons. We use the initial energy density corresponding to values obtained at SPS ($\varepsilon \sim 20\text{GeV/fm}^3$) or RHIC ($\varepsilon \sim 2000\text{GeV/fm}^3$) We must remember that our energy density calculations are extremely rough.

The initial chemical potentials present more of a problem - numerically speaking at $\tau \to -\infty$, $\mu$ will increase exponentially. We solved this problem by making the step size of the ODE solver small enough to bring the solution (ie $\mu$) into better behaved bounds. This explains why the number density rises from zero to a bigger number, before ordinary Bjorken expansion sets in. (See the following figures in this chapter.)

The central regime is probably neutral, the excess baryons being carried off in the target and projectile regimes. Our approximation of the baryon number being homogeneously distributed throughout the plasma is probably wrong, but provides an interesting extreme. Until we know the dependence of $\mu$ and $\mu_{\bar{i}}$ on $T$ we cannot solve relation 4.10; however we need only solve it for the initial temperature because quark number conservation embodied in the Bjorken equations will hold. We use the fact that once we have set the baryon number, this must be conserved throughout the evolution of the plasma, to check the numerical accuracy of the program.

The first five simulations do not give realistic energy densities because we chose no gluons in the simulation to bring out details in the quark sector. In the results given in Table 4.6 we find typical values for the energy density in the rest of the simulation of $\varepsilon = 560$ GeV/fm$^3$ at $\tau_0 = 0.05$ fm.

#### Thermodynamic Equilibrium

The thermal equilibration time in High Energy Heavy Ion Collisions for quarks and gluons has been estimated [133]. First gluons equilibrate thermally in $\tau_g \sim \frac{1}{2}$fm while the

equilibration of quarks needs $\tau_q \sim 2$ fm.

| | $T_g$ MeV | $\tau_g$fm/c | $T_q$ MeV | $\tau_q$fm/c |
|---|---|---|---|---|
| RHIC | 500 | 0.30 | 200 | 2 |
| LHC | 660 | 0.25 | 260 | 1.7 |

Table 4.1: Initial gluonic and quark temperatures and equilibration times

Discussed earlier were numerical difficulties encountered with the heavier quarks. We note [132] the long time for heavier quarks to reach thermal equilibrium.

| | $\tau_g$ fm/c | $\tau_{u,d}^{TH}$ fm/c | $\tau_s^{TH}$ fm/c | $\tau_c^{TH}$ fm/c | $\tau_b^{TH}$ fm/c | $\tau_{QGP}^{TH}$ fm/c |
|---|---|---|---|---|---|---|
| RHIC | 0.30 | 1.0 | 1.2 | 2.6 | 17.5 | 9.0 |
| LHC | 0.25 | 0.7 | 0.8 | 1.6 | 7.5 | 17.5 |

Table 4.2: Initial gluonic and quark thermal equilibration times

In conclusion, the initial conditions of the plasma are not readily available. We use a value of $\tau = 0.05$fm and $T = 950$MeV to be consistent with [4, 65] and allow the program to find numerically stable initial conditions in $\mu$ for the start of the simulation. Fortunately, the results of the simulation are not strongly dependent on the initial $\mu$.

Strictly speaking we should have

$$\alpha_s = \frac{g^2}{4\pi} = \frac{12\pi}{(33 - 2N_f)\ln\frac{\bar{Q}^2}{\Lambda^2}}$$

with $\Lambda \approx 300$MeV is the renormalisation scale, $N_f$ is the number of flavors and $\bar{Q}^2 \simeq m(T)^2 + 9T^2$ is the mean momentum transfer. $g$ is accordingly temperature dependent, leading to the thermodynamic problems alluded to earlier. Due to the very weak dependence on $T$, we set $g = 2$.

### Fokker-Plank equation

The heavier quarks could be included in our simulation by using the correct pre-equilibrium distribution functions [2], considering only the central rapidity window and assuming that quarks execute a random Brownian motion in a gluon bath in the pre-equilibrium fireball. Further, if the sea quarks carry a negligible amount of the initial momentum, then the relativistic Fokker-Plank equation can be used to provide the needed pre-equilibrium thermal distribution functions.

$$\frac{\partial f}{\partial \tau} = \frac{\partial}{\partial p_z}\left(\frac{a_p\, p_z\, f}{\sqrt{p_z^2 + m_T^2}}\right) + D_F \frac{\partial^2 f}{\partial p_z^2}$$

where $a_p$ is the friction constant and $D_F$ is the diffusion coefficient ($= a_p T$). The coefficients $a_p$ and $D_F$ are critical in the behaviour of the solution. $a_p$ is obtained from $dE/dx$. From experiment $a_p \sim \alpha\tau^{(-\frac{2}{3})}$. The boundary conditions are firstly that each parton has sharp longitudinal momentum in the z-plane and that there are no infinitely fast quarks.

$$f_i(p_z,\tau) \stackrel{\tau\to\tau_g}{\longrightarrow} \Delta_i\,\delta(p_z) \text{ and } f_i(p_z,\tau) \stackrel{|p_z|\to\infty}{\longrightarrow} 0.$$

$\Delta_i$ is taken from parton model calculations of the central rapidity density. The Fokker-Plank equation can be solved subject to the initial conditions. The answer for heavy quarks is

$$f(p,\tau) = f(p_z,\tau)\frac{1}{\pi\mu^2}\exp(-p_T^2/\mu^2).$$

$f(p_z,\tau)$ is obtained using an integrating factor, to get

$$f(p_z,\tau) = \frac{1}{\sqrt{\pi\,A(\tau)}}\exp[-p_z^2/A(\tau)]$$

and the integrating factor $A(\tau)$ can be found using the usual prescription and matching the boundary conditions to be

$$\begin{aligned} A(\tau) &= 4\left[\int_{\tau_g}^{\tau} D_F(\tau')\exp\left(\frac{2}{m_T}\int_{t_g}^{\tau'} a_p(\tau'')\,d\tau''\right)d\tau'\right] \\ &\times \exp\left(\frac{-2}{m_T}\int_{\tau_g}^{\tau} a_p(\tau')\,d\tau'\right)\times\exp\left(\left[1-\frac{-2}{m_T}\int_{\tau_g}^{\tau'} a_p(\tau')\,d\tau'\right)\right]. \end{aligned} \tag{4.48}$$

Here $m_T = \sqrt{m_{eff}^2 + p_T^2}$ also has a contribution due to the thermal mass through $m_{eff} = m_{current} + m_{thermal}$.

The distribution function so obtained can be substituted into the expressions for the rates, in place of our Fermi-Dirac distributions, and the hydrodynamic simulation repeated. However, the validity of the Bjorken model becomes questionable, and thermodynamic consistency remains to be proved.

## 4.4 Hydrodynamic simulation with $\delta R = 0$

In order to get the feel of the physics, numerous different simulations have been done. We will start with no gluons or QCD interactions for the cases of one massless type of quark and anti-quark, three massless types of quarks and anti-quarks and then six massless quarks and anti-quarks. Gluons will then be added for these three cases, then the correct constituent mass, and then up/down and anti-up/anti-down quarks will be distinguished. With these last three results we will investigate the scenario of quarks being created from a quark-gluon plasma for various initial conditions.

Our goal is to investigate the abundance and relative abundance of quarks at some later time characterised by the formation of baryons.

In order to represent the data we have presented either a log fit for the thermodynamic data or else we have plots. The parameters $a$ and $b$ given in the tables fit $\log y = a \times \log \tau + b$. $r$ is also given, where $-1 \leq r \leq 1$. $y$ can be one of $\varepsilon$, $p$, $\mu$,$n$ or $T$. The correlation parameter, $r$, has its normal statistical meaning, giving the statistical fit of the data to a line: $r = 1$ signals absolute linearity with a positive gradient, $r = -1$ absolute linearity with a negative gradient, and the closer $r$ is to zero the lower the correlation of the data to a line.

**Computing:** The simulation was done on a DEC-Alpha RISC. A typical calculation took between 12 hours and 2 days of CPU time. The algorithm was written in Fortran 77. Other authors approximated some of the integrals in calculating the rates but we decided against this because the approximations are only valid for specific $T$ and $\mu$, and we were not sure into which regime the simulation would force us.

After inputting the physical parameters (mass, coupling constant $g$, $N_c$ and $N_f$), initial conditions ($\tau, \mu$ and T) and numerical parameters, the derivatives were calculated for the matrix elements $a_i, b_i, c, d_i, e_i$ and $f$ using the initial values. In evaluating $e_i$ the rates of Chapter 2 were numerically evaluated - this was an extremely time consuming part of the program. The temperature was needed to evaluate the rates as well as the chemical potentials of the outgoing and incoming quarks, if applicable. For the up and down quarks the chemical potential need not have been the same, if we maintained a small baryon number. Gauss-Laguerre and Gauss-Legendre integration were used here.

We used the Burlisch-Stoer algorithm to solve the Ordinary Differential Equation (ODE). This was by far the fastest and numerically most stable algorithm . It steps the temperature and chemical potential, as well as works out the optimal next step in our independent variable, the proper time. As is evident from the plots, the spacing of the steps along the independent variable is irregular. This is a feature of the algorithm; it takes small step sizes if the function changes faster than some tolerance, but takes as big a step size as possible when the function under consideration is flat. Once the new values of $T$ and $\mu$ have been calculated, they are used to recalculate elements of the matrix. This process iterates until the final $\tau$.

A pedantic note on units is now necessary: temperature and chemical potential are measured in MeV and the proper time in Fermi(fm). Hence, for example, $T = \exp a\,\tau^b$ should be read as $T = T_0 \exp(a)\,(\frac{\tau}{\tau_0})^b$ where $T_0 = MeV$ and $\tau_0$ =fm. The constants for the other thermodynamic terms are $\varepsilon_0 = 1\text{MeV}^4$, $p_0$ =MeV$^4$, $\mu_0$ =MeV and $n_0$ =MeV$^3$. These are not convenient units for the densities. The conversion from MeV to fm is obtained using 197 MeV·fm$= \hbar \cdot c = 1$.

### 4.4.1 $m = 0$ and no gluons

We now record the results of the simulation. Since, in most cases there is no difference between quarks and anti-quarks, we only record the values of the quarks.

We develop the simulation from a simple example, to a fully fledged simulation.

#### One quark

This problem can be solved analytically using Bjorken's equations for an ultrarelativistic quark, see equation 4.46. Comparison wit numerical results gives us confidence that the program is correct. As expected we find $\varepsilon = 3\,p$ and using the values for $a$ and $b$ in the table to parametrise $T$ and $\mu$ we obtain the correct parametrisation of $n(\tau)$ as given in equation 4.18. Because we have a quark/antiquark pair, we must remember to include a factor of 2 in expressions 4.19 and 4.20.

We record the results of the numerical solution in Table 4.3 to ease comparison with later work. This enables us to compare our results to those of [65]. Throughout the following sections, unless otherwise stated, we use the following initial conditions: $\tau^o = 0.050$fm, $T^o = 950.00$ MeV, $\mu^o = -28105$ MeV. After running the simulation the final values at $\tau = 4$fm are $T = 220.48$MeV and $\mu = -6522.59$ MeV. The negative in the log of the

| $\log y$ | a | b | $-1 \leq r \leq 1$ |
|---|---|---|---|
| $\log T$ | -1/3 | 5.85788 | -1. |
| $\log \varepsilon$ | -4/3 | -4.85861 | -1. |
| $\log p$ | -4/3 | -5.95723 | -1. |
| $\log -\mu$ | -1/3 | 9.24513 | -1. |
| $\log n$ | -1. | -12.50826 | -1. |

Table 4.3: 1 quark: $\delta R = 0, m = 0$ and no gluons

chemical potential labeled in the table is due to the chemical potential being negative. The meaning of $a$ and $b$ is that $\log y = a \log \tau + b$ as mentioned on page 81.

Due to the large negative value of the chemical potential, the number density remains almost negligible. However, since we can immediately solve Bjorken's number-density equation when $\delta R = 0$, we expect the coefficient of $\tau$ in this expression to be $-1$. This is what we obtain, despite the smallness of the number density. From expression 4.45, we see that if $\delta R = 0$, we have $\frac{n(\mu,T)}{n(0,T)} = constant$. This gives us a way of testing our numerical solutions for the $\delta R = 0$ case and gives us a useful way of looking at the approach to chemical equilibrium.

### 3 quarks and antiquarks

As, before these results can be obtained either by directly solving Bjorken's equations, or alternatively using our numerical algorithm. As before we record these values, see Table 4.4. Since all three quarks enter the equations indistinguishably, we only record one set of values. A feature that will be found to persist is that $T$ and $\mu$ (both intensive quantities) are not strongly dependent on the existence of other species of quark or gluon. We expect that $\varepsilon_3 = 3\varepsilon_1$ and $p_3 = 3p_1$.

The initial conditions now include $\mu^o = -28105$ MeV. These initial conditions are arbitrary in the sense that the relevant constraint was that we want to start the simulation with no quarks. We could have used a more negative chemical potential. For consistency with later work, we use the previous values.

The final values of the simulation at $\tau = 4$fm are $T = 220.48$MeV and $\mu = -6522.59$ MeV. We find that the temperature does not deviate according to the flavor species and composition of the quark-gluon gas. That the chemical potentials (and indeed other intensive quantities) are the same is not surprising, but that they are identical to the previous case is remarkable. We will encounter this again.

| $\log y =$ | a | b | $-1 \leq r \leq 1$ |
|---|---|---|---|
| $\log T$ | -1/3 | 5.85788 | -1. |
| $\log \varepsilon$ | -4/3 | -3.76000 | -1. |
| $\log p$ | -4/3 | -4.85861 | -1. |
| $\log -\mu$ | -1/3 | 9.24513 | -1. |
| $\log n$ | -1. | -12.50826 | -1. |

Table 4.4: 3 quarks: $\delta R = 0, m = 0$ and no gluons

### 4 quarks and antiquarks

The arguments of the previous case carry through exactly. We find that $\varepsilon_6 = 6\varepsilon_1$. Since all six quarks appear identically, we only look at the values of one, see Table 4.5. The initial conditions for the chemical potentials of the new quarks introduced into this simulation are $\mu^o = -28105$ MeV. The final values at $\tau = 4$fm are not surprisingly in the light of the earlier simulation $T = 220.48$MeV and $\mu = -6522.59$ MeV.

## 4.4.2 $m = 0$ and gluons

We will find for the following that the only change from the previous section is that the energy density and pressure change. We only look at the one quark case since the quark contribution to the energy density is completely swamped by that of the gluons for our initial values.

| $\log y =$ | a | b | $-1 \leq r \leq 1$ |
|---|---|---|---|
| $\log T$ | -1/3 | 5.85788 | -1. |
| $\log \varepsilon$ | -4/3 | -3.06685 | -1. |
| $\log p$ | -4/3 | -4.16547 | -1. |
| $\log -\mu$ | -1/3 | 9.24513 | -1. |
| $\log n$ | -1. | -12.50826 | -1. |

Table 4.5: 6 quarks: $\delta R = 0, m = 0$ and no gluons

**One quark and antiquark**

As before, since quark and anti-quark are indistinguishable, we only record the data for one quark, see Table 4.6. We note, using 4.3 and 4.4 and the parameterizations of $T$ and $\mu$, that gluons are essentially the only contributors to the energy density. Our initial conditions are exactly as before $\tau^o = 0.050$fm, $T^o = 950.00MeV$ and $\mu^o = -28105$ MeV. Despite the addition of gluons the final values of the intensive quantities at $\tau = 4$fm ($T = 220.48$MeV and $\mu = -6522.59$ MeV) are unchanged. The energy density and pressure only reflect the contribution of the gluons, the contribution of the quarks being negligible. Because we

| $\log y =$ | a | b | $-1 \leq r \leq 1$ |
|---|---|---|---|
| $\log T$ | -1/3 | 5.85788 | -1. |
| $\log \varepsilon$ | -4/3 | 25.09239 | -1. |
| $\log p$ | -4/3 | 23.99378 | -1. |
| $\log -\mu$ | -1/3 | 9.24513 | -1. |
| $\log n$ | -1. | -12.50826 | -1. |

Table 4.6: 1 quark: $\delta R = 0, m = 0$ and gluons

start the simulation with as few quarks as possible, the energy density equation fixes the temperature. However the integration constant for $T$ is not fixed by the energy density, but by the initial time. The power of $\tau$ is determined by the relation between pressure and energy density, and is therefore a reflection of the properties of the gas. In all our simulations, the initial conditions and the 'physics' remain the same, and so we would accordingly expect the temperature to remain more or less unchanged. The temperature only begins to reflect the changes in composition of the gas when the mass of the quarks becomes large, or the number of quarks present at the beginning of the simulation is allowed to increase.

Because the addition of gluons does not change the intensive properties ($T$ and $\mu$), $n(T, \mu)$ is unchanged from the massless case.

### 4.4.3 $m \neq 0$ and gluons

In the following sections we use the current mass of quarks as contained in [107]. The use of the current mass reflects the fact that gluons and quarks have been deconfined to constitute an (almost) ideal gas.

#### Strange quark and antiquark

Now we have one massive quark and antiquark ($m_s$=199MeV) - the gluons are part of the simulation. See Table 4.7. The initial conditions are as before, at $\tau^o = 0.050$fm, $T^o = 950.00MeV$ and $\mu_u^o = -28105$ MeV.

The final values (at $\tau = 4$fm, $T = 220.48$MeV and $\mu = -6486.85$ MeV) reflect the fact that the chemical potentials only are significant in the number density equation.

| $\log y =$ | a | b | $-1 \leq r \leq 1$ |
|---|---|---|---|
| $\log T$ | -1/3 | 5.85788 | -1. |
| $\log \varepsilon$ | -4/3 | 25.09239 | -1. |
| $\log p$ | -4/3 | 23.99378 | -1. |
| $\log -\mu_s$ | -0.33391 | 9.24362 | -1. |
| $\log n_s$ | -1. | -12.51900 | -1. |

Table 4.7: Strange quark: $\delta R = 0$ and gluons

Not surprisingly, only the chemical potential changes from the massless case. We find in general that the heavier the quark, the more the number density is suppressed.

#### Up, Down and Strange quarks and antiquarks

| $\log y =$ | a | b | $-1 \leq r \leq 1$ |
|---|---|---|---|
| $\log T$ | -1/3 | 5.85788 | -1. |
| $\log \varepsilon$ | -4/3 | 25.09239 | -1. |
| $\log p$ | -4/3 | 23.99378 | -1. |
| $\log -\mu_u$ | -1/3 | 9.24512 | -1. |
| $\log n_u$ | -1. | -12.50827 | -1. |
| $\log -\mu_d$ | -1/3 | 9.24512 | -1. |
| $\log n_d$ | -1. | -12.50827 | -1. |
| $\log -\mu_s$ | -0.33439 | 9.24230 | -1. |
| $\log n_s$ | -1. | -12.51900 | -1. |

Table 4.8: Up, down and strange quarks: $\delta R = 0$ and gluons

We use $m_u = 5.6$ MeV and $m_d = 9.9$ MeV to obtain Table 4.8. The initial conditions are as expected at $\tau^o = 0.050$fm, $T^o = 950.00$ MeV and $\mu_u^o = \mu_{\bar{u}}^o = \mu_d^o = \mu_{\bar{d}}^o = \mu_s^o = \mu_{\bar{s}}^o = -28105$MeV.

The final values calculated at $\tau = 4$fm are $T = 220.48$MeV and $\mu_u = -6522.56$, $\mu_d = -6522.49$ and $\mu_s = -6486.85$ MeV. We note that the chemical potential for strange quarks is smaller than that for light quarks at the end of the simulation. From the solutions in section 4.43 and equation 4.47 we find that the chemical potential tends to zero faster for the more massive case than the less massive cases. This is the opposite of what we will find when we allow quarks to be created.

It is now apparent that the simple $\frac{1}{3}$ law for the chemical potential no longer holds for the massive case. This is the result of the ultra-relativistic relation $\epsilon = 3p$ being lifted.

### Up, Down, Strange and Charmed quarks and antiquarks

We now use the following mass for the charmed quark $m_c = 1300$MeV to obtain Table 4.9. The initial conditions are as before, and the final values at $\tau = 4$fm are $T = 220.48$MeV and $\mu_u = -6522.56$MeV, $\mu_d = -6522.49$MeV, $\mu_s = -6486.85$MeV and $\mu_c = -5850.23$MeV. There is a slight departure from linearity in the behaviour of the logarithms of the charmed

| $\log y =$ | a | b | $-1 \leq r \leq 1$ |
|---|---|---|---|
| $\log T$ | -1/3 | 5.85788 | -1. |
| $\log \varepsilon$ | -4/3 | 25.09239 | -1. |
| $\log p$ | -4/3 | 23.99378 | -1. |
| $\log -\mu_u$ | -1/3 | 9.24512 | -1. |
| $\log n_u$ | -1. | -12.50827 | -1. |
| $\log -\mu_d$ | -1/3 | 9.24512 | -1. |
| $\log n_d$ | -1. | -12.50828 | -1. |
| $\log -\mu_s$ | -0.33439 | 9.24230 | -1. |
| $\log n_s$ | -1. | -12.51900 | -1. |
| $\log -\mu_c$ | -0.35519 | 9.18555 | -0.99986 |
| $\log n_c$ | -1. | -12.86795 | -1. |

Table 4.9: Up, down, strange and charm quarks: $\delta R = 0$ and gluons

chemical potential.

### Top quark and antiquark

| $\log y =$ | a | b | $-1 \leq r \leq 1$ |
|---|---|---|---|
| $\log T$ | -1/3 | 5.85788 | -1. |
| $\log \varepsilon$ | -4/3 | 25.09239 | -1. |
| $\log p$ | -4/3 | 23.99378 | -1. |
| $\log -\mu_t$ | 0.42024 | 11.12040 | 0.37919 |
| $\log n_t$ | -1.01207 | -185.73251 | -0.99999 |

Table 4.10: Top quark: $\delta R = 0$ and gluons

In table 4.10 we once again come to the unexpected behavior of the heavier quarks as functions of $\tau$. Here we examine the top and anti-top quark only. We do this despite the fact we know that the Fermi-Dirac distribution functions are inappropriate for this case, there being no thermal equilibrium. The mass we use is $m_t = 171500$ MeV and the initial conditions are as before. The final values at $\tau = 0.307$ fm are $T = 518.77$ MeV and $\mu_c = +62026.00$ MeV respectively. We have to stop the simulation at this point due to extreme numerical divergences.

The temperature, energy density, pressure and number density behave pretty much as expected, and fairly well ($r \approx -1$). However the chemical potential has a behavior that is far from pure exponential. We look at equation 4.44 and see that the chemical potential tends to $m_t$ as $T \to 0$. We can calculate the value at which $T$ crosses the $x$-axis, namely $T = 314$ MeV. Beyond this the numerical solutions overflow.

### 4.4.4 $m \neq 0$, $\mu_u \neq \mu_{\bar{u}}$, $\mu_d \neq \mu_{\bar{d}}$ and gluons

By carefully choosing the chemical potentials for the up and down quarks, a positive baryon number can be maintained. We use that for S-S, ie $B_{\text{up,down}} = 2$ nuclei $\times$ (A=32) $\times$ 3 quarks /(isospin=2) = 198. This is according to the equation 4.10.

#### Up, Down and Strange quarks and antiquarks

| $\log y =$ | a | b | $-1 \leq r \leq 1$ |
|---|---|---|---|
| $\log T$ | -1/3 | 5.85788 | -1. |
| $\log \varepsilon$ | -4/3 | 25.28513 | -1. |
| $\log p$ | -4/3 | 24.18649 | -1. |
| $\log -\mu_u$ | -0.33336 | 6.00895 | -1. |
| $\log n_u$ | -1. | 15.87627 | -1. |
| $\log -\mu_{\bar{u}}$ | -1/3 | 9.24512 | -1. |
| $\log n_{\bar{u}}$ | -1. | -12.50827 | -1. |
| $\log -\mu_d$ | -0.33341 | 6.00882 | -1. |
| $\log n_d$ | -1. | 15.87625 | -1. |
| $\log -\mu_{\bar{d}}$ | -1/3 | 9.24511 | -1. |
| $\log n_{\bar{d}}$ | -1. | -12.50828 | -1. |
| $\log -\mu_s$ | -0.33439 | 9.24230 | -0.99989 |
| $\log n_s$ | -1. | -12.51900 | -1. |
| $\log -\mu_{\bar{s}}$ | -0.33439 | 9.24230 | -1. |
| $\log n_{\bar{s}}$ | -1. | -12.51900 | -1. |

Table 4.11: Up, down and strange quarks: $\delta R = 0$, $\mu_u \neq \mu_{\bar{u}}$, $\mu_d \neq \mu_{\bar{d}}$ and gluons

See Table 4.11. The initial conditions are $\tau^o = 0.050$fm, $T^o = 950.00 MeV$ and $\mu_u^o = -1105$ MeV, $\mu_{\bar{u}}^o = -28105$MeV, $\mu_d^o = -1105$MeV,$\mu_{\bar{d}}^o = -28105$MeV, $\mu_s^o = -28105$MeV

and $\mu_{\bar{s}}^o = -28105$MeV. These conditions will start the simulation with a small baryon excess. The thermodynamics are guaranteed to maintain this excess. Physically, if we start with a certain baryon number, we will end with the same number of baryons.

Final values at $\tau = 4$fm are $T = 220.47$MeV and $\mu_u = -256.41$MeV, $\mu_{\bar{u}} = -6522.52$MeV, $\mu_d = -256.35$MeV, $\mu_{\bar{d}} = -6522.45$ MeV, $\mu_s = -6486.82$ MeV and $\mu_{\bar{s}} = -6486.82$ MeV.

### Up, down, strange and charm quarks and antiquarks

For the last in our series of simple simulations we include the charm quark. See Table 4.12. The initial conditions at $\tau^o = 0.050$fm are $T^o = 220.48MeV$, $\mu_u^o = -1105$MeV, $\mu_{\bar{u}}^o = -28105$MeV,$\mu_d^o = -1105$MeV, $\mu_{\bar{d}}^o = -28105$MeV, $\mu_s^o = -28105$ MeV, $\mu_{\bar{s}}^o = -28105$ MeV. $\mu_c^o = -28105$ MeV and $\mu_{\bar{c}}^o = -28105$ MeV.

The final values at $\tau = 4$fm are $T = 220.47$MeV and $\mu_u = -256.41$MeV, $\mu_{\bar{u}} = -6522.52$MeV, $\mu_d = -256.35$MeV, $\mu_{\bar{d}} = -6522.45$ MeV, $\mu_s = -6486.82$ MeV and $\mu_c = -5850.19$ MeV respectively.

| $\log y =$ | a | b | $-1 \leq r \leq 1$ |
|---|---|---|---|
| $\log T$ | -1/3 | 5.85788 | -1. |
| $\log \varepsilon$ | -4/3 | 25.28513 | -1. |
| $\log p$ | -4/3 | 24.18649 | -1. |
| $\log -\mu_u$ | -0.33336 | 6.00895 | -1. |
| $\log n_u$ | -1. | 15.87627 | -1. |
| $\log -\mu_{\bar{u}}$ | -1/3 | 9.24512 | -1. |
| $\log n_{\bar{u}}$ | -1. | -12.50827 | -1. |
| $\log -\mu_d$ | -0.33341 | 6.00882 | -1. |
| $\log n_d$ | -1. | 15.87625 | -1. |
| $\log -\mu_{\bar{d}}$ | -1/3 | 9.24511 | -1. |
| $\log n_{\bar{d}}$ | -1. | -12.50828 | -1. |
| $\log -\mu_s$ | -0.33439 | 9.24230 | -1. |
| $\log n_s$ | -1. | -12.51900 | -1. |
| $\log -\mu_c$ | -0.35519 | 9.18555 | -0.99986 |
| $\log n_c$ | -1. | -12.86795 | -1. |

Table 4.12: Up, down, strange and charm quarks: $\delta R = 0$, $\mu_u \neq \mu_{\bar{u}}$, $\mu_d \neq \mu_{\bar{d}}$ and gluons

We see that the addition of the charmed quark hardly affects $\varepsilon, p$ and $T$, and accordingly the chemical potentials for the lighter quarks remain unchanged from the previous simulation.

This completes the simple simulation. We have established how pure Bjorken expansion drives $\mu$ and $T$. We have now got a simple parametrisation of the thermodynamic quantities obtained from a one dimensional Bjorken expansion.

## 4.5 Hydrodynamic simulation with $\delta R \neq 0$

Until now we have been laying groundwork. We now come to the central results. Since we now know the effects of a pure expansion on a plasma, we turn to the question of the effects of the production of quarks. The previous sections established the effects of longitudinal expansion on the thermodynamic properties of the plasma.

We now use the rates as listed or calculated in equations 3.13, 3.15 and 3.66. We include this as $\delta R$ in equation 4.9. By including the rates we greatly increase CPU time. Typical calculations took six to forty eight hours of CPU time or up to three days.

Our conclusions are that the initial conditions $T_0$ at $\tau_0$ set the coefficient of $T = T_0(\tau/\tau_0)^b$ and that the relation between $\varepsilon$ and $p$ determines $b$. This means that $b$ reflects properties of constituents of the plasma. The chemical potential is set by $n(\mu(\tau_0))$. The powers of $\varepsilon, p, n, \mu$ and $T$ are very close to the massless case, namely $(-\frac{4}{3}, -\frac{4}{3}, -1, -\frac{1}{3}$ and $-\frac{1}{3})$. Quarks more massive than charm no longer fall into this scenario.

In the following sections we represent the data graphically.

### 4.5.1 Strange quark/anti-quark

The initial conditions are as before ($\tau^o = 0.050$fm, $m_s = 199$ MeV, $\mu_s^o = -28105$ MeV and $T^o = 950$ MeV).

The final values at $\tau = 4.0$fm are $T = 210.6$MeV and $\mu_s = -90.26$ MeV, see table 4.13.

| $\log y =$ | a | b | $-1 \leq r \leq 1$ |
|---|---|---|---|
| $\log T$ | -0.34317 | 5.82969 | -0.99999 |
| $\log \varepsilon$ | -1.29756 | 25.19561 | -1. |
| $\log p$ | -1.30213 | 24.08488 | -1. |
| $\log -\mu_s$ | -0.97761 | 5.77749 | -0.97456 |
| $\log n_s$ | 0.87048 | 15.86717 | 0.28488 |

Table 4.13: Strange quark: $\delta R \neq 0$ and gluons

The indicated points in Figure 4.1.1 correspond to some of the numerical steps. We recognise the deviation of $\log n(\tau)$ from linearity in Figure 4.1.1 is due to our initial chemical potential, which effectively initially put the quark number to zero. We have outlined in section 4.3.2 the reason why the log of the number density starts from negative infinity. However after a very short time, quarks have been produced: after about 0.75fm the derivative is tending towards $-1$, the case of pure Bjorken expansion. Due to the bad correlation, we see the exponential parametrisation is inappropriate. We examine the rate of quark creation in Figure 4.1.5.

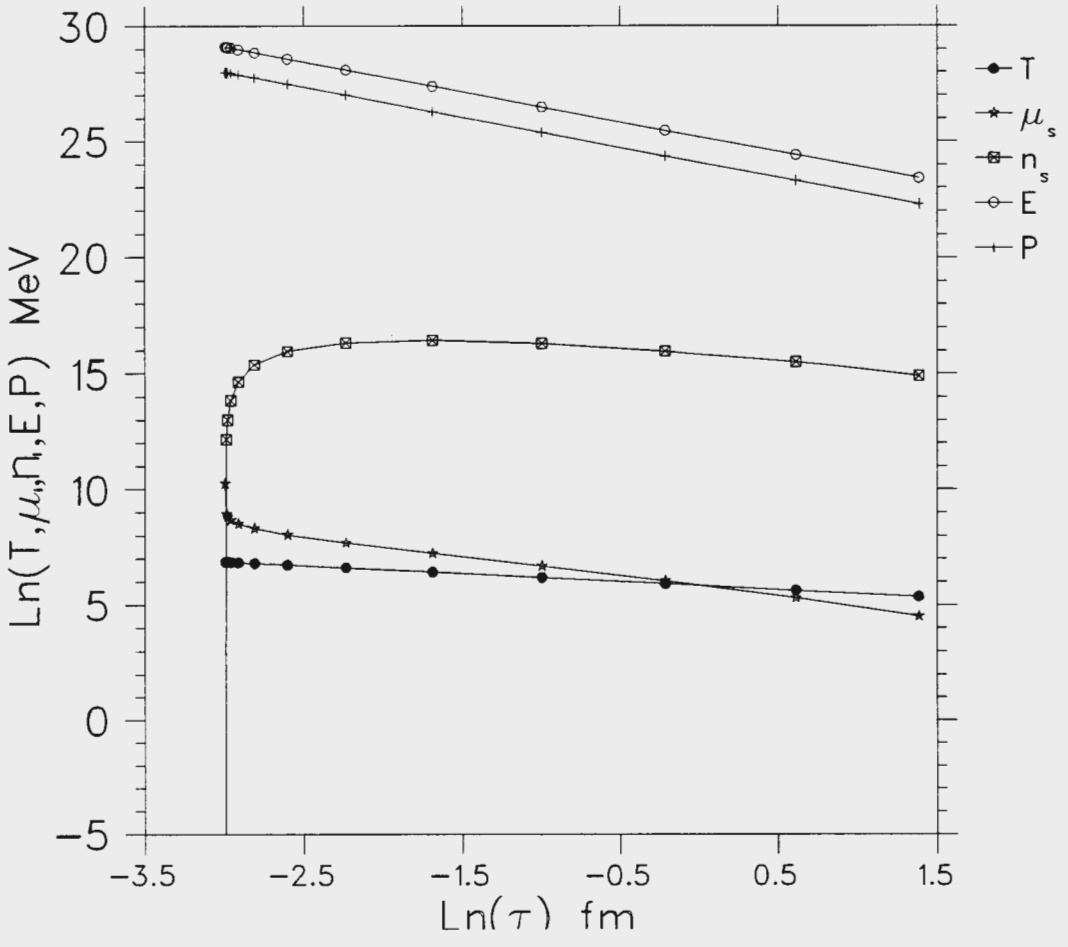


Figure 4.1.1: Log ($T, n, \varepsilon, p$ and $\mu$) versus $\log \tau$

We also note that the temperature has scarcely changed from the case in which no quarks were created, because the gluon contribution dominates the energy density and the pressure (hence we find that the log of these quantities is almost linear). Another noticeable feature is the chemical potential. We have plotted the log of the absolute value: we see that the chemical potential changes quickly from negative infinity to a value which changes at a lower rate. However, the chemical potential does not return to a value of $-\frac{1}{3}$.

It would be of considerable interest to study the formation of quarks in more detail. Specifically examining quark formation with different initial conditions, and looking at non-equilibrium effects (thermal and chemical.) We return to this in Figures 4.1.4 and 4.1.5. Reasons for the explosive increase in the quark number lie in more detailed models of the dynamics.

We could have reversed the chronological order of our simulation, but then we would have had to decide on the correct numerical conditions. This would have defeated the objective, to establish the veracity of $\gamma_S$.

We would have expected the chemical potential to have a gradient of $-\frac{1}{3}$, but instead it

is closer to $-1$. Because the temperature is essentially fixed by the gluons, the chemical potential varies to increase the number of quarks, as demanded by the rate equation. (Because there is available energy, quark/antiquark pairs can be created). Because of Pauli blocking, we see that the chemical potential tends to zero as expected. The chemical potential is plotted in Figure 4.1.2.

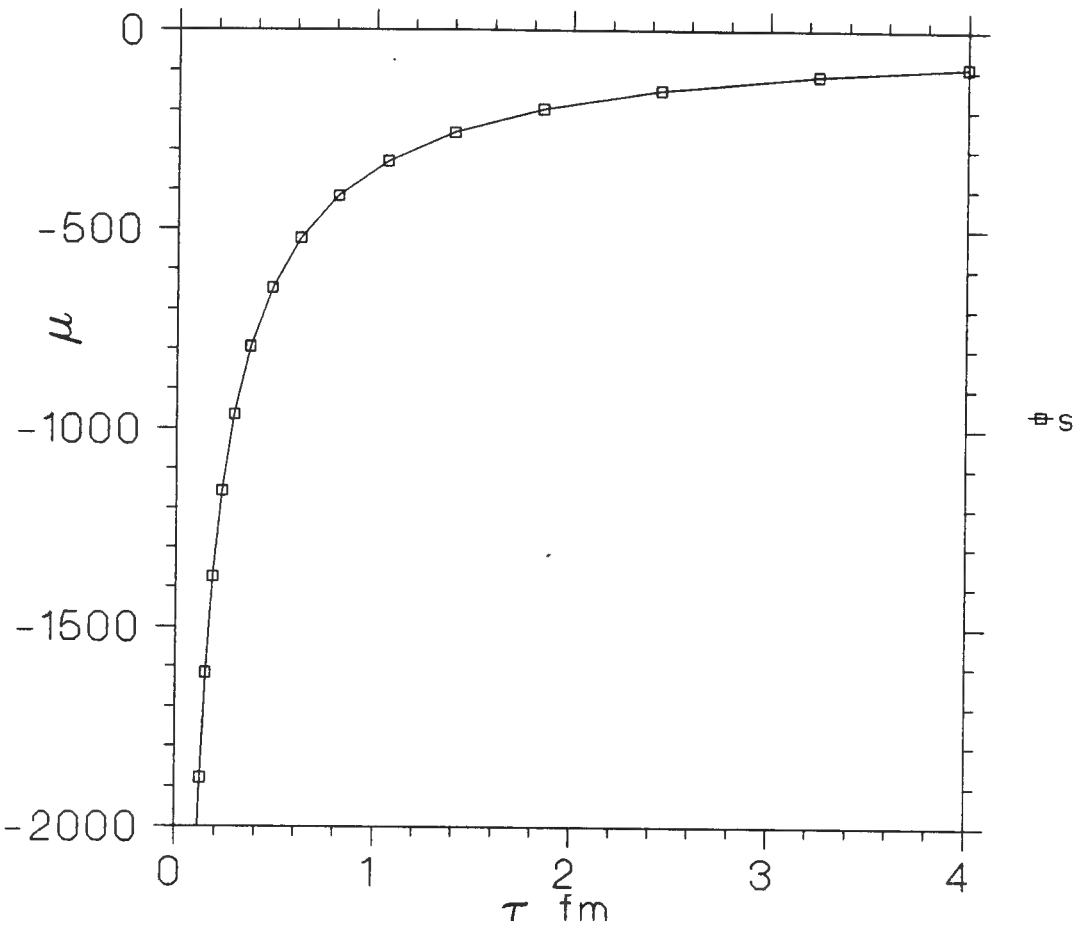


Figure 4.1.2: Chemical Potential as a function of proper time.

More interesting is the graph in Figure 4.1.3 of

$$\frac{n(\tau)}{n_0(\tau)} = \frac{n(T(\tau), \mu(\tau))}{n(T(\tau), \mu = 0)}$$

which shows that at the onset of the baryon phase, some time after 4fm, the number of strange quarks is far from the expected equilibrium value. We say that we are at equilibrium if $\frac{n(\mu,T)}{n(0,T)} = 1$. However, an additional feature has to be considered before we can say that we have obtained chemical equilibrium ($\mu$=0 is not sufficient). This is the chemical equilibrium time, $n_i^o/R_i$, must be smaller than the timescale of interactions affecting species $i$. If this is true then $\mu$ tends to zero rapidly. Nonetheless this ratio gives us a useful way of looking at the approach to chemical equilibrium.

By the time of the onset of the baryon phase, we see that the strange quarks are quite

far from chemical equilibrium. We can read off that at about 4 fm, we have $\gamma_S = 0.63$ - however, the precise value depends on the value of the time of the onset of the baryon phase. This result depends on the Bjorken hydrodynamics to give $T(\tau)$ and $\mu(\tau)$. Another assumption is that, to leading order, we have included all the most important processes contributing to strangeness production in $\delta R$.

It is apparent that $\gamma_S$ is dependent on $\tau$ and the initial conditions. Although it tends to unity, it does so very slowly. Looking at the correlation in Table 4.13 we see that the exponential fit is only approximate, and therefore $\mu_s$ probably tends towards some other value.

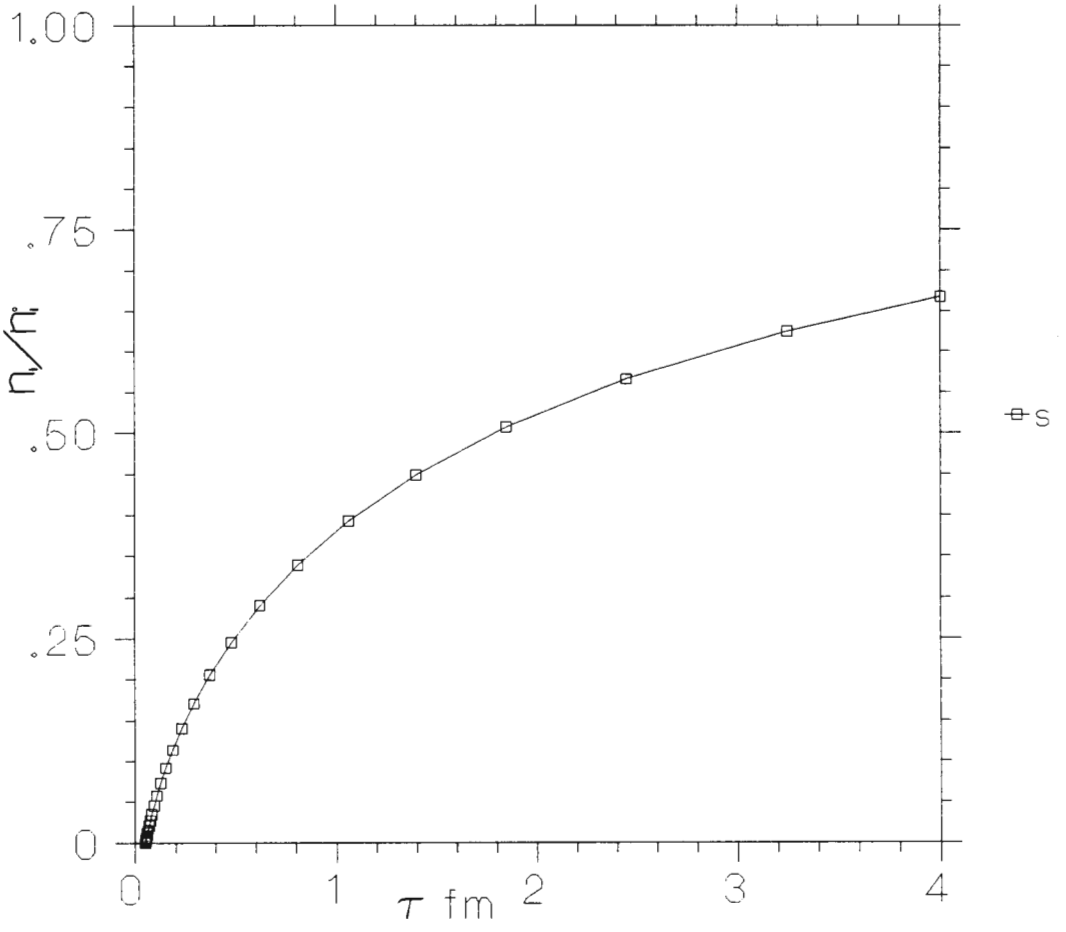


Figure 4.1.3: $n(\tau)/n_0(\tau)$ versus $\tau$

The question of how the inclusion of the other quarks affects the result that we are still far from chemical equilibrium at the onset of the baryon phase remains to be answered. Also the sensitivity of this result on the initial conditions and how the light quarks behave remains.

Plotted in the Figure 4.1.4 is the equivalent of Figure 3.20, but this time with the 'real' rate, ie the chemical potential depends on temperature, and is not set to zero as done previously. We see that using the appropriate chemical potential does not significantly

alter the reduced rate as plotted earlier, because, effects of the chemical potential are exponentially suppressed. Also, we are plotting the 'reduced rate', in which the exponential dependence on $\mu$ has been factored out.

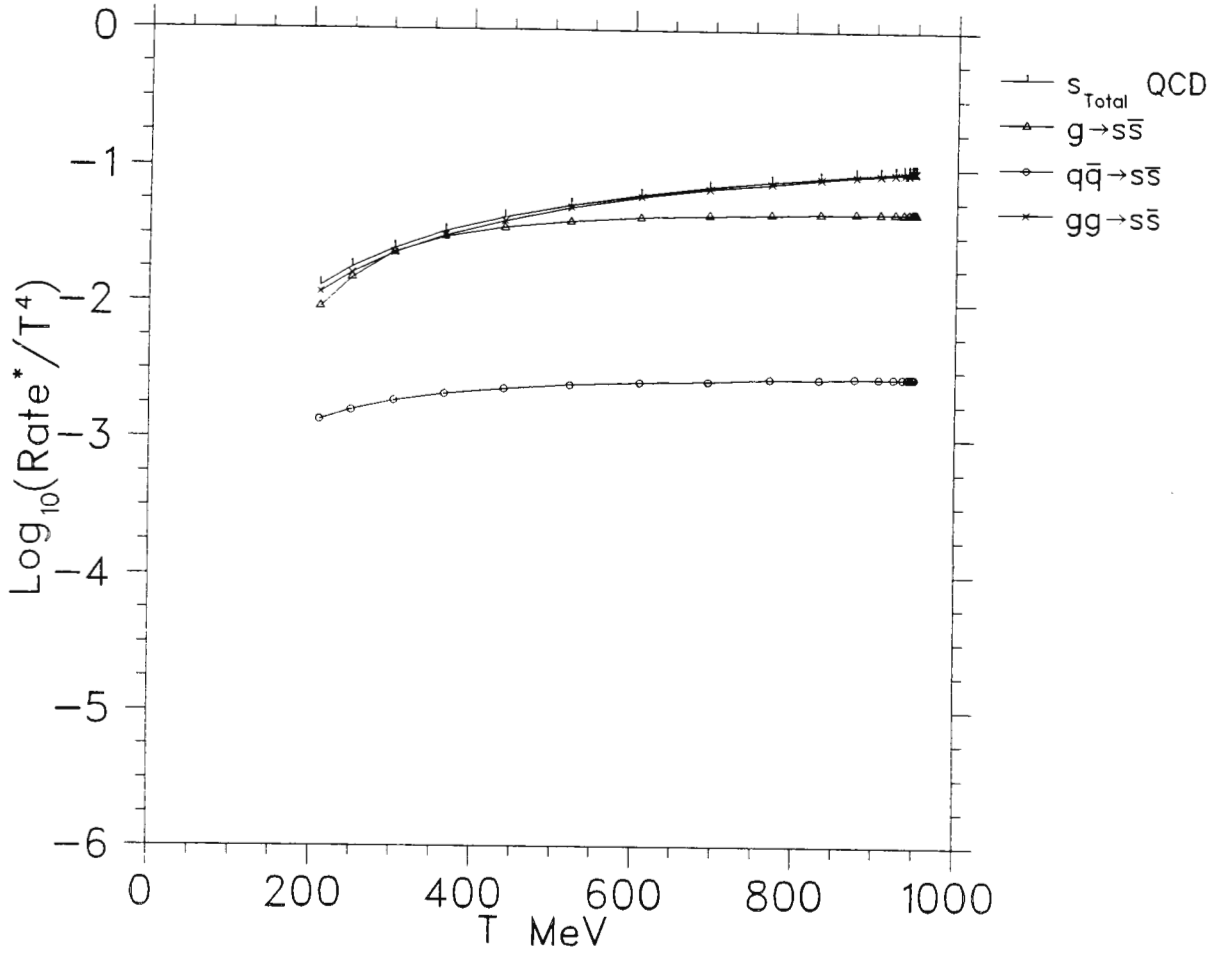


Figure 4.1.4: Log $R^*/T^4$ versus $T$

The only difference between Figure 3.20 and Figure 4.1.4 is at higher $T$. Noticeable is that at $T \simeq 300$MeV gluon decay and gluon fusion are approximately equal, but that at $T \simeq 1000$MeV there is a 35% difference. This is due to the Breit-Wigner distribution of chapter 3 being proportional to $1/T^2$.

We know that the differential on the left of equation 4.9 depends on $\frac{n(\tau)}{\tau}$ and $\delta R(\tau)$. We know how $\frac{n(\tau)}{n_0(\tau)}$ behaves, so it is of interest to consider $\frac{\delta R(\tau)\times\tau}{n_0(\tau)}$ in Figure 4.1.5. Figure 4.1.5 shows the importance of the quark creation term, relative to the number density term. As expected the value stays below one, showing that this and $\frac{n(\tau)}{n_0(\tau)}$ in the number equation are of comparable magnitude. At the onset of the hadron phase, the quark creation term is reduced, but is not negligible.

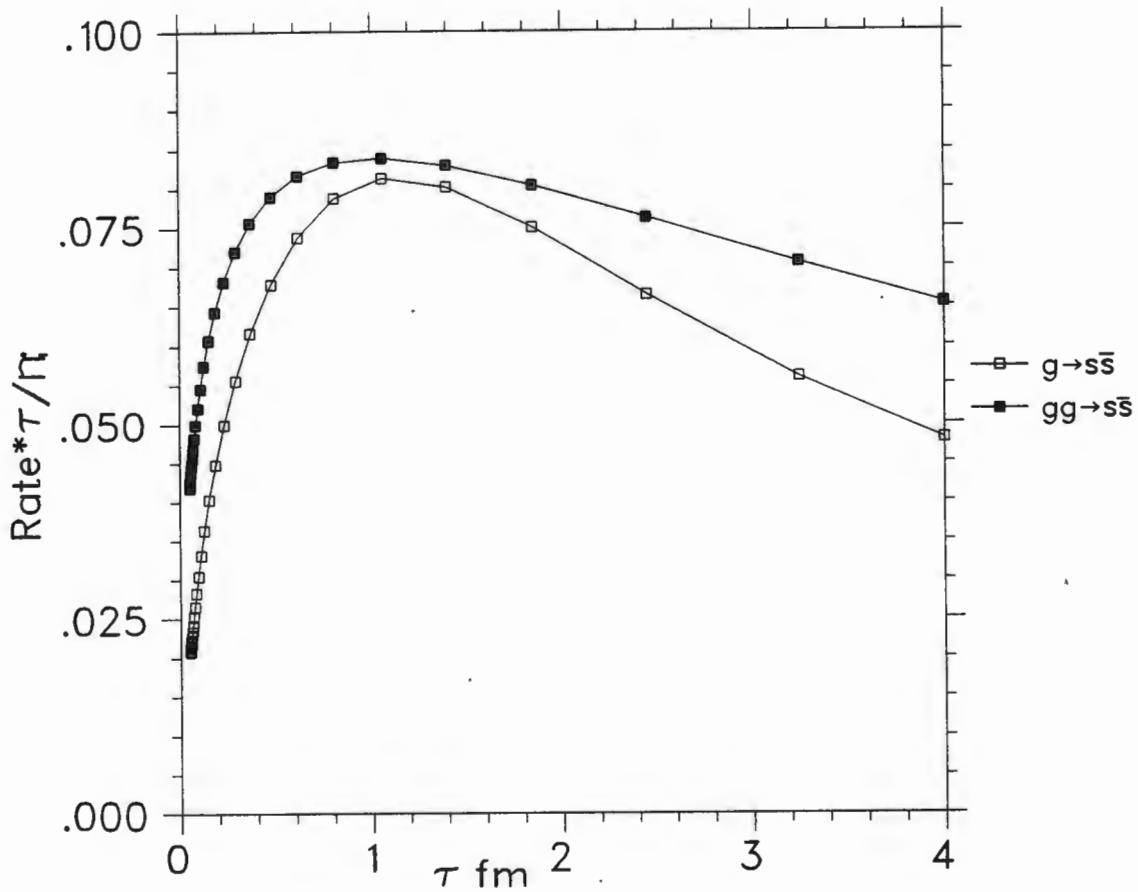


Figure 4.1.5: $\frac{\delta R(\tau)\times\tau}{n_0(\tau)}$ versus $\tau$

**Conclusion for the strange quark simulation:** Expanding the simulation to include more quarks is the next step. Unfortunately we are not able to give any reliable simulation for the bottom and top quark and even the numerical simulation which we give for the charmed quark is questionable (this is given in section 4.5.3).

We would like to confirm the plot of Altherr and Seibert, [7]. We have already concluded in the section of the Heavy Quark Approximation and using Table 4.2 that the expected graphs for bottom and top are unrealistic.

We have found that the strange quarks tend more rapidly to equilibrium than indicated in [7]. Finally, we will find that the up and down quarks reach chemical equilibrium very rapidly indeed. This is in contrast to [7] in which the charm and bottom quarks behave similarly to the strange quark.

The questions to be addressed now are to determine the effects of the up and down quarks on the preceding result. We will explicitly include the baryon number being not equal to zero. The numerical stability of this result in terms of dependence on boundary

conditions and numerical parameters is also examined.

### 4.5.2 Up, Down and Strange quark/anti-quarks

There are three cases we are going to consider:

- **Case 1:** We are going to pick initial chemical potentials to start with as few quarks as (numerically) possible.
- **Case 2:** We will start with three quarks that are initially more abundant than the previous case.
- **Case 3:** By picking slightly different chemical potentials for up and anti-up, and down and anti-down, we can maintain a small positive excess of baryons.

**Case 1:** $\mu_u^o = \mu_{\bar{u}}^o, \mu_{\bar{d}}^o = \mu_d^o \to -\infty$

The initial conditions used are $\tau^o = 0.050$fm, $T^o = 950.00MeV$, $\mu_u^o = \mu_{\bar{u}}^o = -28105$MeV, $\mu_d^o = \mu_{\bar{d}}^o = -28105$MeV and $\mu_s^o = \mu_{\bar{s}}^o = -28105$MeV.

The final values at $\tau = 4$.fm are $T = 172.78$MeV and $\mu_u = \mu_{\bar{u}}^o = 1.94$MeV, $\mu_d = \mu_{\bar{d}}^o = 0.93$MeV and $\mu_s = \mu_{\bar{s}}^o = -94.45$ MeV respectively. It is noticeable that the temperature has decreased. This is due to the up and down quarks being very rapidly produced by gluon decay, which leads to them contributing significantly to the energy and pressure densities. The chemical potentials for the up and down quarks are seen to overshoot zero, but they then return asymptotically to this limit. This overshooting is due to the slightly different masses of the light quarks..

| $\log y =$ | a | b | $-1 \leq r \leq 1$ |
|---|---|---|---|
| $\log T$ | -0.39756 | 5.64936 | -0.99913 |
| $\log \varepsilon$ | -1.33227 | 25.09514 | -1. |
| $\log p$ | -1.33527 | 23.98857 | -1. |
| $\log -\mu_u$ | -1.98965 | 2.42009 | -0.97784 |
| $\log n_u$ | 0.38194 | 16.18314 | 0.13160 |
| $\log -\mu_d$ | -2.02977 | 2.56953 | -0.98590 |
| $\log n_d$ | 0.46451 | 16.08273 | 0.16144 |
| $\log -\mu_s$ | -0.99151 | 5.69211 | -0.97549 |
| $\log n_s$ | 0.60095 | 15.07788 | 0.21826 |

Table 4.14: Up, down and strange quarks: $\delta R \neq 0$, Case 1 - No light quarks initially

We include $n_{u,d,s}$, despite the correlation indicating complete non-linearity. Again, the vertical line for the number density at $\tau = 0.05$fm is purely numerical - we have no way of studying the pre-thermal equilibrium condition.

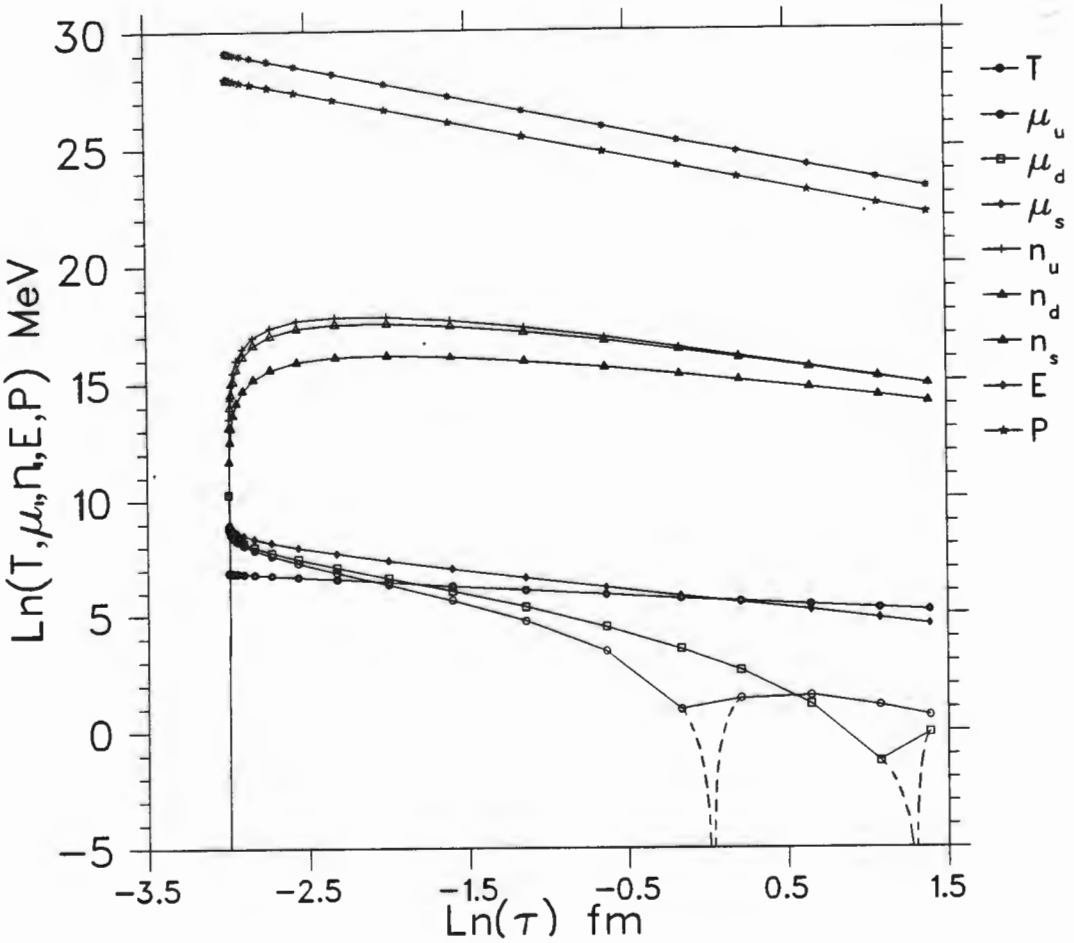


Figure 4.2.1 : Log $(T, n, \varepsilon, p$ and $\mu)$ versus $\log \tau$ - Case 1

The peculiar 'bouncing behaviour' in Figure 4.2.1 of the up and down chemical potential

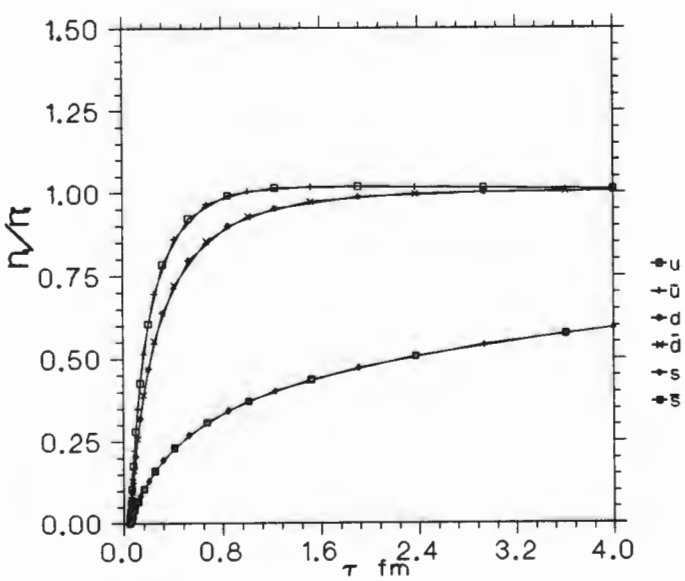


Figure 4.2.2: $\frac{n}{n_0}$ versus $\tau$ - Case 1

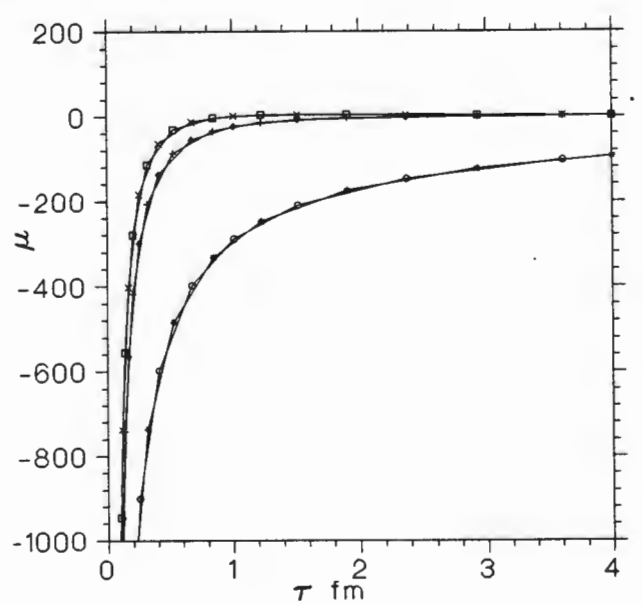


Figure 4.2.3: $\mu$ versus $\tau$ - Case 1

is due to them overshooting $\mu = 0$, and then tending back towards it. This may be purely numerical; the chemical potentials may tend asymptotically to 0. We draw a dotted line to indicate how it probably behaves. The number density of the up and down quarks is very similar.

The plot of the ratio of the number density to the equilibrium value is once again of interest, and is plotted in Figure 4.2.2.

We notice that the addition of the light quarks has led to a reduction in $\gamma_S$ to 0.54.

In Figure 4.2.3 we plot $\mu$ versus $\tau$. From the figure we can estimate the light quark chemical equilibration time to be $\tau \simeq 1$fm.

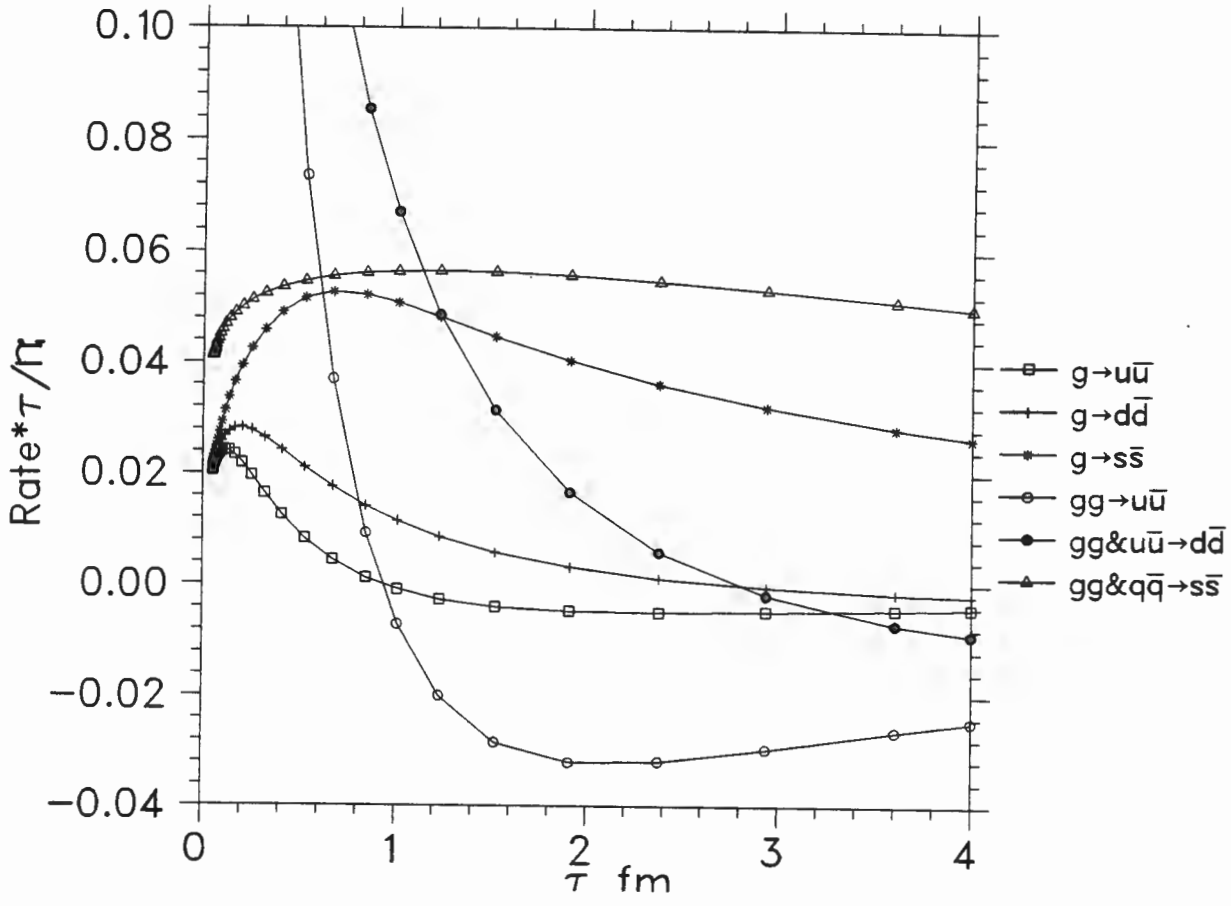


Figure 4.2.4: $\frac{\delta R(\tau)\times\tau}{n_0(\tau)}$ versus $\tau$ - Case 1

Figure 4.2.4 turns out to be very interesting. It takes some explanation. The obvious similarity with Figure 4.1.5 is the $g \rightarrow s\bar{s}$, and $gg \rightarrow s\bar{s}$. The discrepancy arises solely from the more negative chemical potential of the u-d-s simulation. The up and down quark production 'overshoots'. The discrepancy between the gluon decay and gluon fusion processes is due to the fact that at high temperatures they differ. (See Figure 4.1.4 and note the $T^4$ scaling.)

As we observe $\mu_u, \mu_{\bar{u}}, \mu_d$ and $\mu_{\bar{d}}$ overshoot zero. We expect this for reasons best seen in the Figure 4.2.4. At $\tau = 0.05$fm the prominent channels for up and down quark production is gluon fusion. Initially more up than down quarks are produced but by about 0.2 fm $u\bar{u}$ begin producing $d\bar{d}$ quarks as well, and the rate of production of $d\bar{d}$ then begins to exceed $u\bar{u}$. The up quark production overshoots because initially there are only two channels producing up quarks (gluon decay and fusion) but three channels depleting the up quark population (gluon decay, gluon fusion and $u\bar{u} \rightarrow d\bar{d}$. Once the down phase space is complete, this third channel disappears, and the graph returns to zero.

**Case 2:** $\mu_u^o = \mu_{\bar{u}}^o, \mu_d^o = \mu_{\bar{d}}^o \sim 0$ **and** $\mu_s^o, \mu_{\bar{s}}^o \rightarrow -\infty$

It is of interest to see what happens if we start with smaller initial chemical potentials for the light quarks. The corresponding initial conditions are $\tau^o = 0.050$fm, $T^o = 950.00MeV$, $\mu_u^o = \mu_{\bar{u}}^o = -1105$MeV, $\mu_d^o = \mu_{\bar{d}}^o = -1105$MeV and $\mu_s^o = \mu_{\bar{s}}^o = -28105$MeV.

| $\log y =$ | a | b | $-1 \leq r \leq 1$ |
|---|---|---|---|
| $\log T$ | -0.37360 | 5.72507 | -0.99956 |
| $\log \varepsilon$ | -1.33240 | 25.44906 | -1. |
| $\log p$ | -1.33515 | 24.34318 | -1. |
| $\log -\mu_u$ | -1.62641 | 2.04587 | -0.94610 |
| $\log n_u$ | -0.83674 | 16.49754 | -0.99369 |
| $\log -\mu_d$ | -1.65366 | 2.13425 | -0.97652 |
| $\log n_d$ | -0.83432 | 16.46578 | -0.99629 |
| $\log -\mu_s$ | -0.97220 | 5.76256 | -0.97712 |
| $\log n_s$ | 0.65367 | 15.23918 | 0.24380 |

Table 4.15: Up, down and strange quarks: $\delta R \neq 0$, Case 2 - More light quarks initially

The final values at $\tau = 4.0$fm are $T = 188.38$MeV and $\mu_{u,d,s} = 1.82, 2.00, -96.73$ MeV respectively.

In Figure 4.3.1 we see that the change in the chemical potential changes the energy and pressure densities at early proper times, but the final values are close to those of Case 1. $T$ and $\mu_s$ (and therefore $n_s$) are virtually identical in Case 1 and Case 2. More up and down quarks in Case 2 mean that $\varepsilon$, $p$, $n_u$ and $n_d$ are larger than in Case 2.

Judging where the vertical asymptotes on the chemical potential of figure 4.3.1 lie, it is evident that the system approaches chemical equilibrium faster with more light quarks initially.

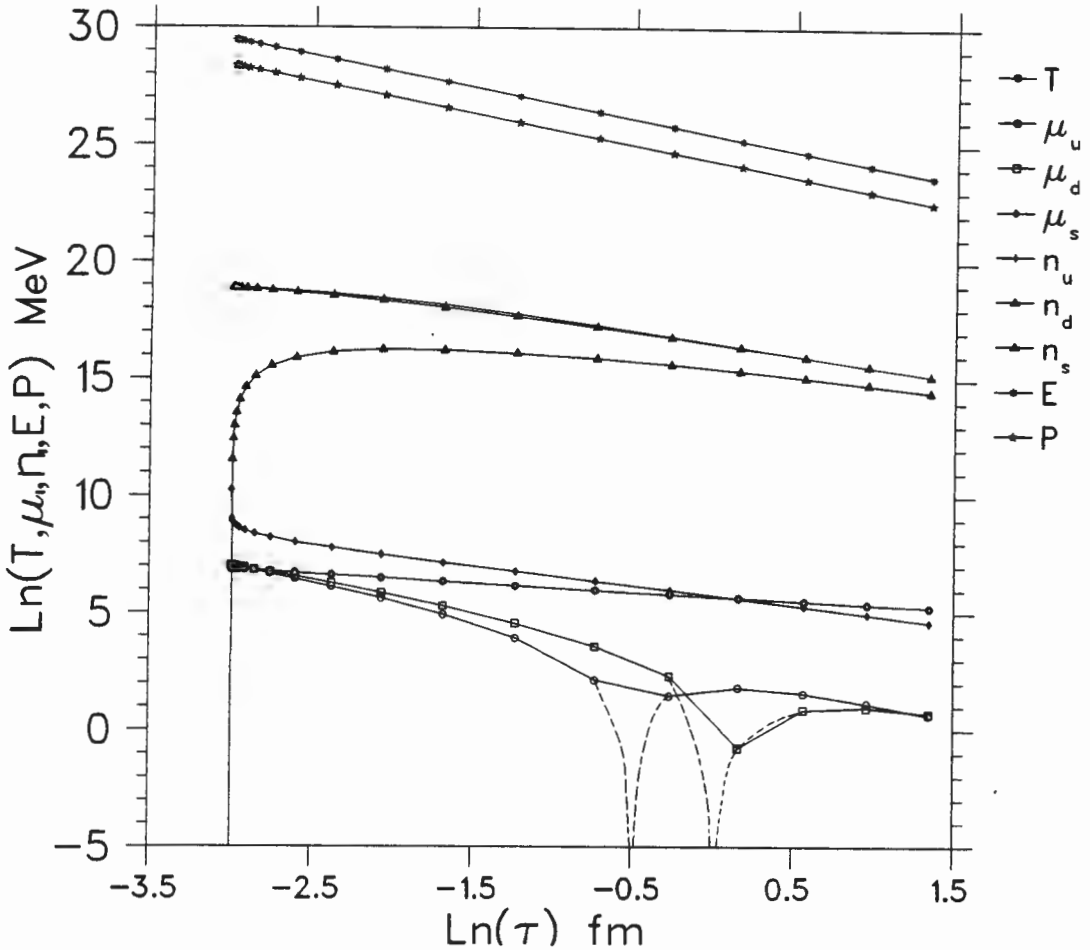


Figure 4.3.1 : Log $(T, n, \varepsilon, p$ and $\mu)$ versus $\log \tau$ - Case 2

For the graphs of the chemical potential and equilibrium number density (Figures 4.3.2 and 4.3.3) we see that the system is not sensitive to its initial values, and seems to be able

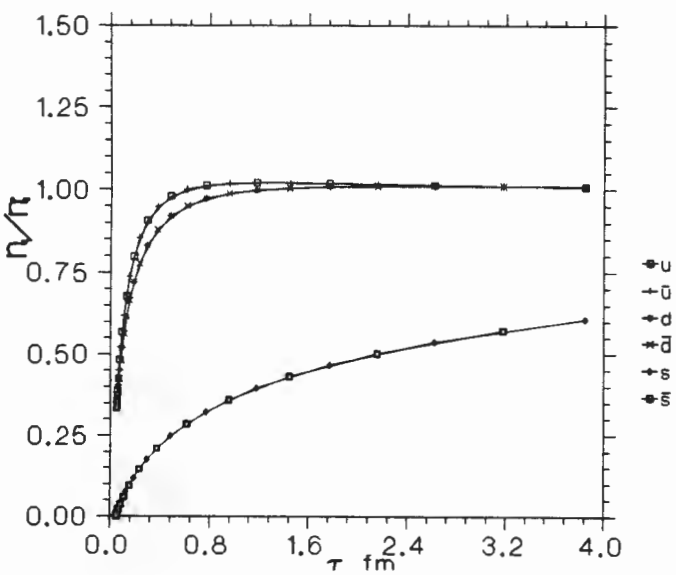


Figure 4.3.2: $\frac{n}{n_0}$ versus $\tau$ - Case 2

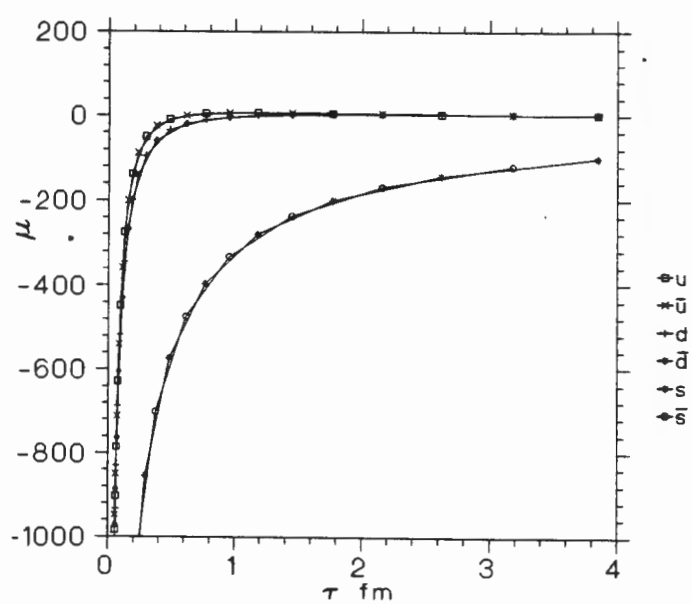


Figure 4.3.3: $\mu$ versus $\tau$ - Case 2

to 'forget' them. The quarks go to chemical equilibrium faster than the previous case. Here we read off $\gamma_S = 0.55$.

The graphs in Figure 4.3.4 go through zero at exactly where $\mu = 0$. We see then that the lighter quarks reach chemical equilibrium more rapidly than in the previous case.

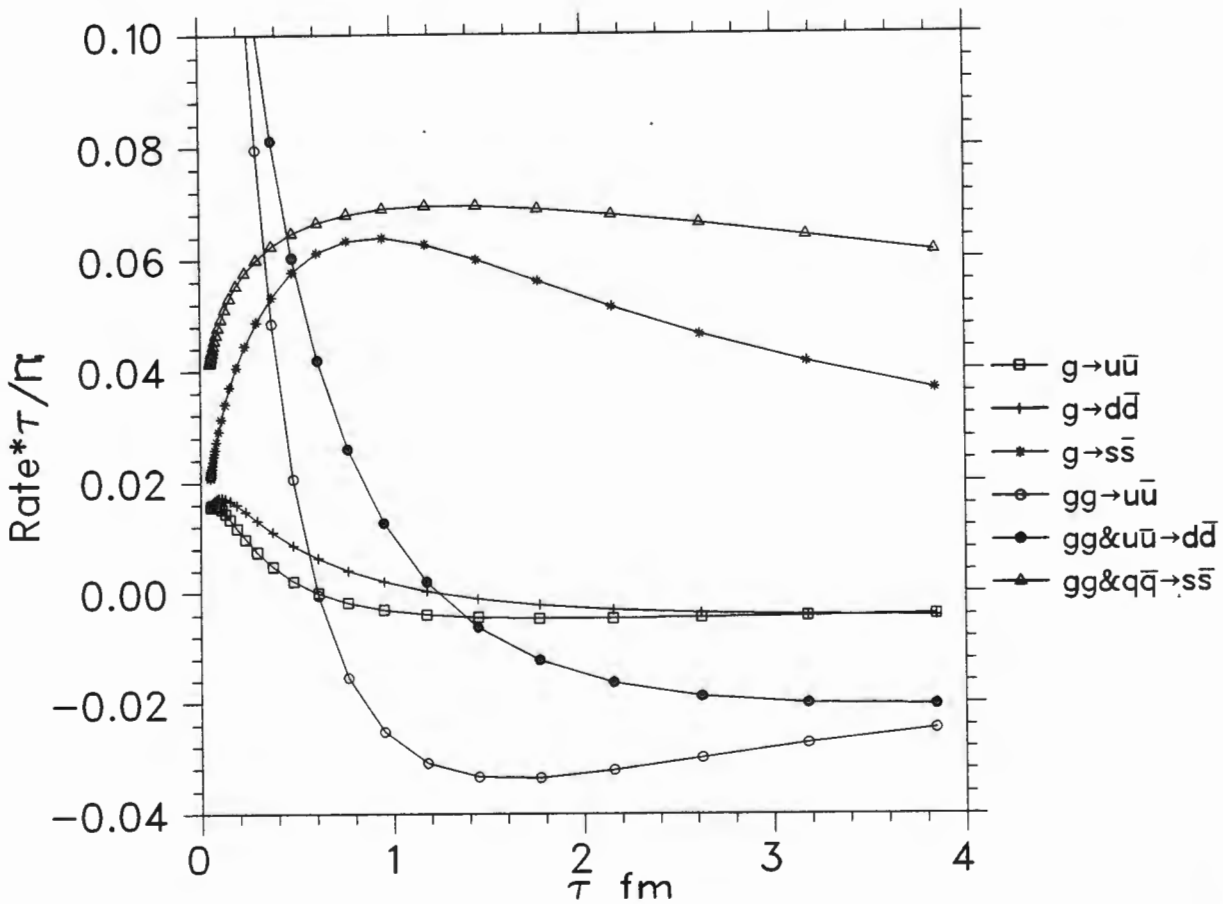


Figure 4.3.4: $\frac{\delta R(\tau)\times\tau}{n_0(\tau)}$ versus $\tau$ - Case 2

### Case 3: Positive Baryon Excess

We can repeat the above, explicitly differentiating between up(down) and anti-up(down) quarks. This gives us another way to test the accuracy of our numerical solutions. As mentioned earlier we would expect $n_{u,d} - n_{\bar{u},\bar{d}}$ multiplied by a suitable volume element to remain constant.

It is interesting to note that in this case we have more up quarks than anti-up quarks. This means that quark fusion will be affected. Our program has been written to take the different chemical potentials of up and anti-up and down and anti-down quarks in the QCD rates into account.

Initial Conditions : $\tau^o = 0.050$fm, $T^o = 950.00 MeV$, $\mu_u^o = -1105$ MeV, $\mu_{\bar{u}}^o = -28105$MeV,

$\mu_d^o = -1105\text{MeV}$,$\mu_{\bar{d}}^o = -28105\text{MeV}$, $\mu_s^o = -28105\text{MeV}$ and $\mu_{\bar{s}}^o = -28105\text{MeV}$.

| $\log y =$ | a | b | $-1 \leq r \leq 1$ |
|---|---|---|---|
| $\log T$ | -0.38603 | 5.68430 | -0.99922 |
| $\log \varepsilon$ | -1.33236 | 25.28763 | -1. |
| $\log p$ | -1.33516 | 24.18163 | -1. |
| $\log -\mu_u$ | -0.72113 | 4.37703 | -0.77457 |
| $\log n_u$ | -0.79451 | 16.65005 | -0.98973 |
| $\log -\mu_{\bar{u}}$ | -1.14477 | 4.75505 | -0.94480 |
| $\log n_{\bar{u}}$ | 0.34938 | 16.04735 | 0.11800 |
| $\log -\mu_d$ | -0.76910 | 4.31743 | -0.81843 |
| $\log n_d$ | -0.79269 | 16.60883 | -0.99399 |
| $\log -\mu_{\bar{d}}$ | -1.13915 | 4.90635 | -0.95891 |
| $\log n_{\bar{u}}$ | 0.43551 | 15.95839 | 0.14837 |
| $\log -\mu_s$ | -0.97918 | 5.73031 | -0.97406 |
| $\log n_s$ | 0.63852 | 15.19356 | 0.22614 |
| $\log -\mu_{\bar{s}}$ | -0.97918 | 5.73031 | -0.97406 |
| $\log n_{\bar{s}}$ | 0.63852 | 15.19356 | 0.22614 |

Table 4.16: Up, down and strange quarks: $\delta R \neq 0$, Case 3 - Baryon Excess

Final Values at $\tau = 4\text{fm}$ are $T = 180.13\text{MeV}$ and $\mu_{u,\bar{u},d,\bar{d},s,\bar{s}} = 61.06$, $-57.89$, $60.98$, $-57.68$, $-97.68$ and $-97.68$ MeV respectively.

When considering Figure 4.4.1 the choice of initial conditions in Case 2 becomes apparent. The graph plotted is now a 'mixture' of Case 1 and Case 2. We find that $\varepsilon$ and $p$ and therefore $T$ are the same as in Case 1. Also $\mu_s$ and therefore $n_s$ are the same as in Case 1. The up and down quarks appear to reach chemical equilibrium quickly. This assumption is spurious, as we shall see in Figures 4.4.2 and 4.4.3.

In the Figure 4.4.2 we see that the anti-up and down never tend to a positive limit. This is because the number of 'valence quarks' being non-zero leads to the quark and anti-quark chemical potentials to reach some other constant. This we can see in Figure 4.4.3.

It seems that while the up and down quarks tend to an equilibrium value asymptotically, the anti-up and down quarks overshoot, before tending to an asymptotic limit. The chemical potentials have the opposite feature.

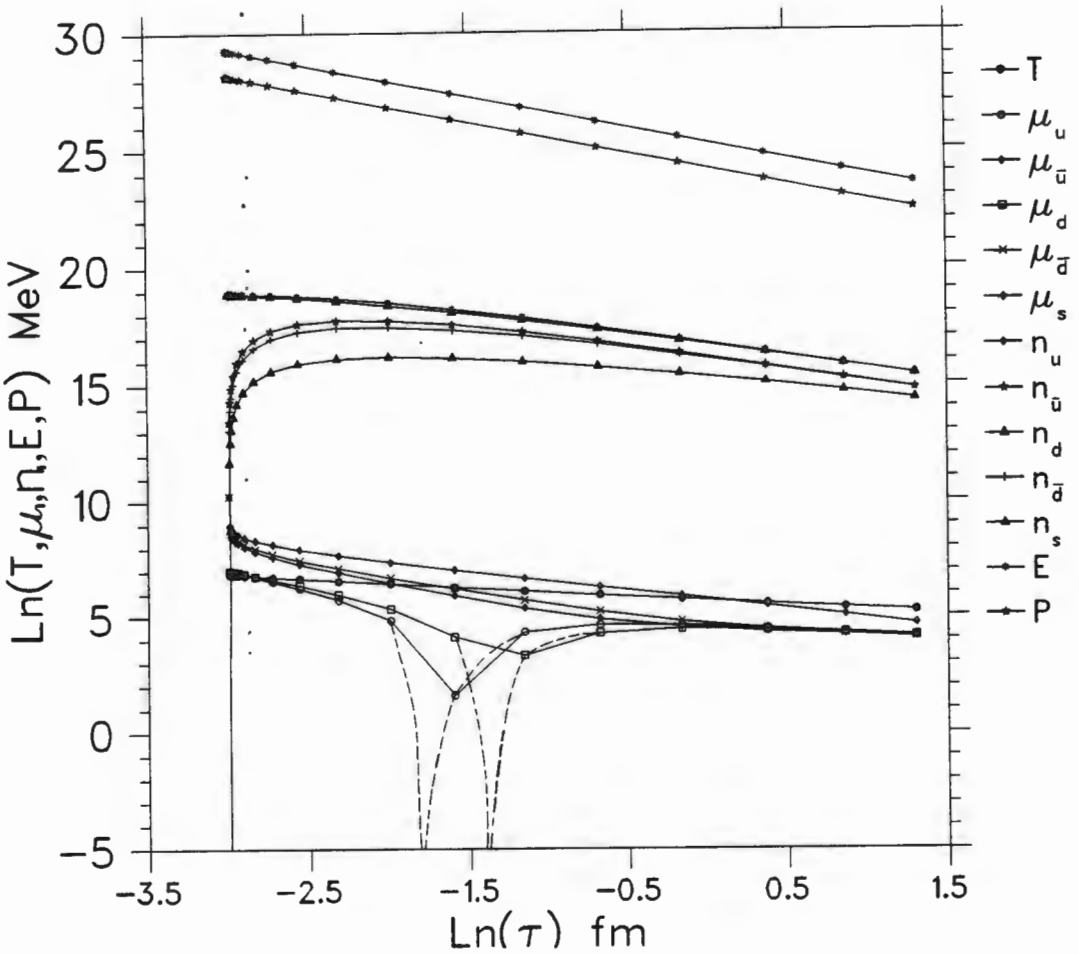


Figure 4.4.1 : Log $(T, n, \varepsilon, p$ and $\mu)$ versus $\log \tau$ - Case 3

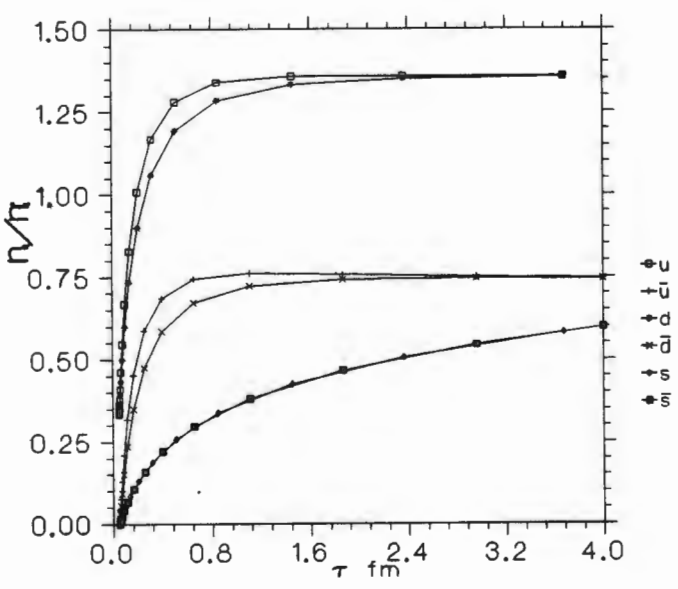


Figure 4.4.2: $\frac{n}{n_0}$ versus $\tau$ - Case 3

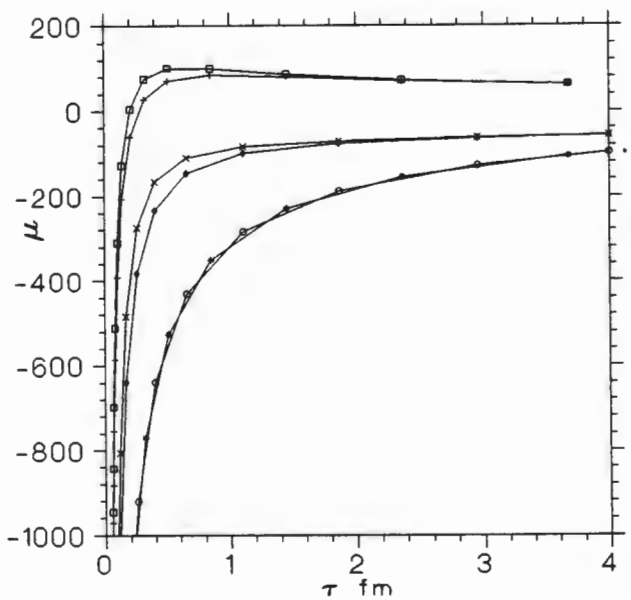


Figure 4.4.3: $\mu$ versus $\tau$ - Case 3

In the light of the explanations of the previous graphs of $\frac{\delta R(\tau) \times \tau}{n_0(\tau)}$ Figure 4.4.4 is nothing

new. The up and down production is suppressed. The strange production is enhanced.

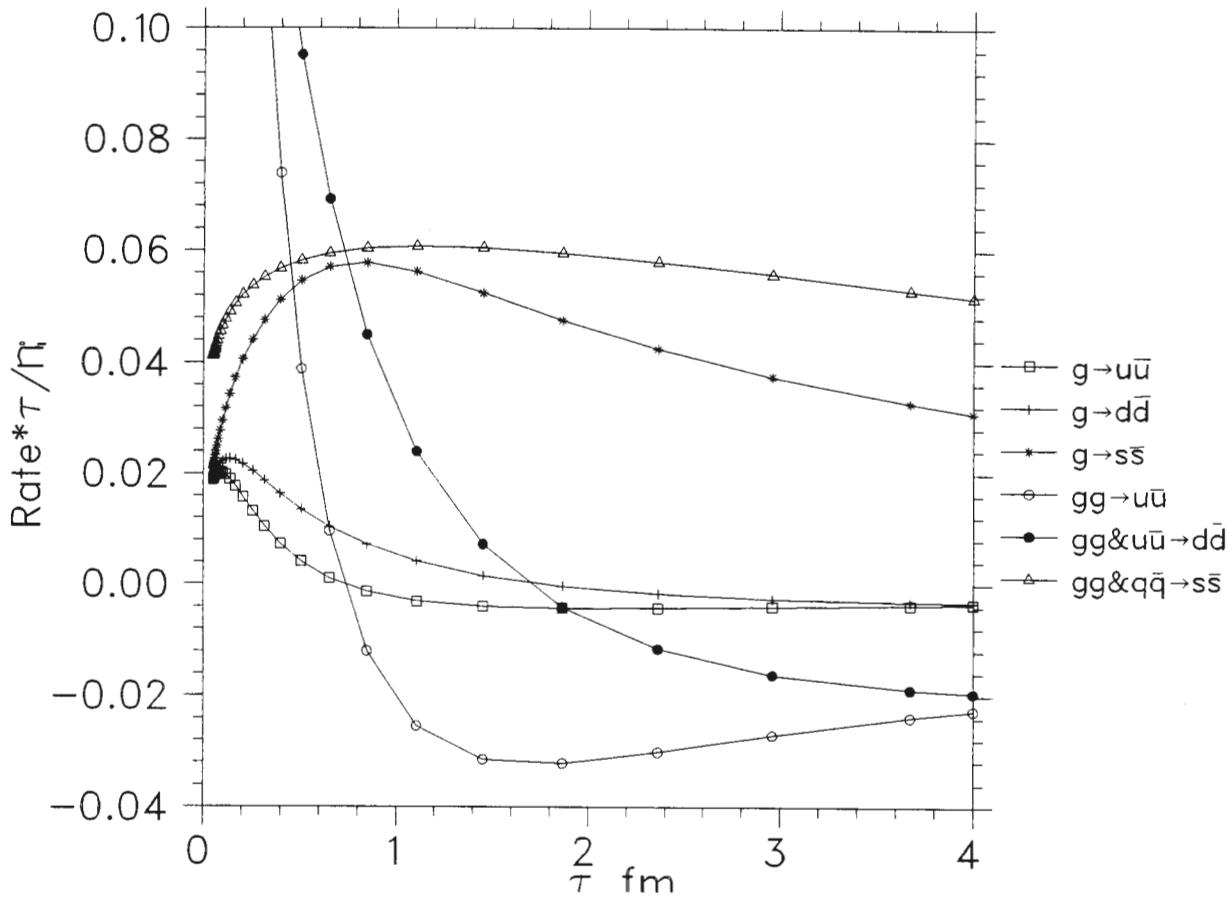


Figure 4.4.4: $\frac{\delta R(\tau)\times\tau}{n_0(\tau)}$ versus $\tau$ - Case 3

There is an amusing observation that can be made using equation 1.4 to 1.7

$$\mu_B = \frac{3}{2}(\mu_u + \mu_d) \text{ and } \mu_S = \frac{1}{3}\mu_B - \mu_s.$$

Reading off the final chemical potentials of up and down quarks and anti-quarks we find $\mu_B \simeq 183$MeV and $\mu_{\bar{B}} \simeq 171$MeV. Hence these two chemical potentials are not equal (the discrepancy is intrinsic in the initial values, and decrease with time). Also $\mu_S \simeq 156$MeV. Although these quantities are not identical to those in chapter 1, they are remarkably close considering that this simulation was for $S$-$S$. Ideally $n_s/n_s(0)$ will tend to some value less than one (and $\mu_S$ will be smaller). This will clearly be the $\gamma_S$ introduced in quark models.

### 4.5.3 Up, Down, Strange and Charm quark/anti-quarks

Including the charmed quarks is now done despite knowing that they are not in thermal equilibrium using our initial conditions. This is due to the initial gluonic and quark thermal equilibrium times of Table 4.2 being quite long. To include heavier quarks some time dependent distribution function should be used obtained from the Fokker-Plank equation.

| $\log y =$ | a | b | $-1 \leq r \leq 1$ |
|---|---|---|---|
| $\log T$ | -0.39304 | 5.66280 | -0.99913 |
| $\log \varepsilon$ | -1.31683 | 25.14240 | -1. |
| $\log p$ | -1.32037 | 24.03424 | -1. |
| $\log -\mu_u$ | -2.12434 | 2.06323 | -0.95717 |
| $\log n_u$ | 0.37388 | 16.16896 | 0.13013 |
| $\log -\mu_d$ | -2.13699 | 2.32807 | -0.97445 |
| $\log n_d$ | 0.45609 | 16.06761 | 0.16012 |
| $\log -\mu_s$ | -0.98221 | 5.71822 | -0.97541 |
| $\log n_s$ | 0.59400 | 15.06658 | 0.21788 |
| $\log -\mu_c$ | -0.86923 | 6.47787 | -0.98045 |
| $\log n_c$ | 0.14886 | 10.99488 | 0.06188 |

Table 4.17: Up, down, strange and charm quarks: $\delta R \neq 0$

Initial conditions at $\tau^o = 0.050$fm are $T^o = 950.00 MeV$, $\mu_u^o = \mu_{\bar{u}}^o = -28105$MeV, $\mu_d^o = \mu_{\bar{d}}^o = -28105$MeV and $\mu_s^o = \mu_c^o = -28105$MeV.

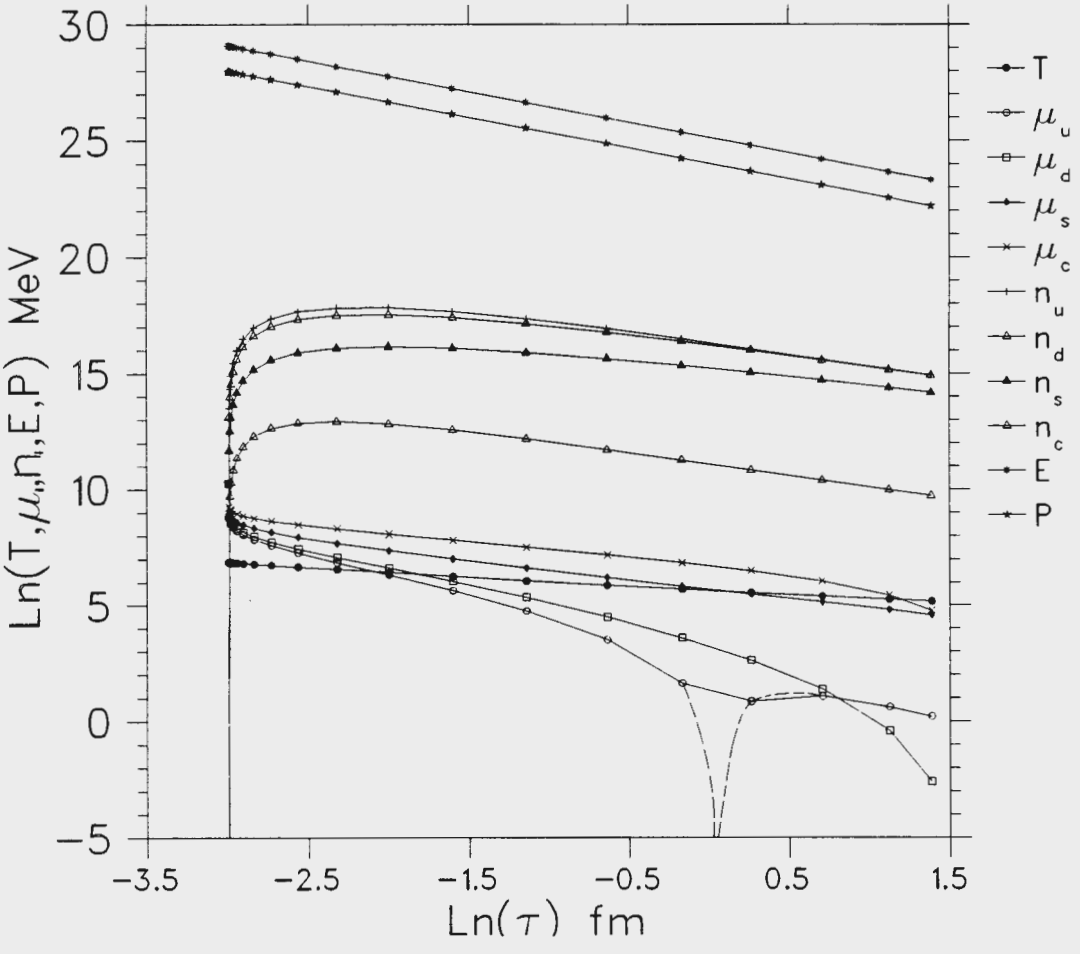


Figure 4.5.1 : Log $(T, n, \varepsilon, p$ and $\mu)$ versus $\log \tau$

The final values at $\tau = 4$fm, $T = 175.62$MeV and $\mu = 1.24$, 1.24, 0.07, 0.07, $-97.56$ and

$-118.64$MeV respectively.

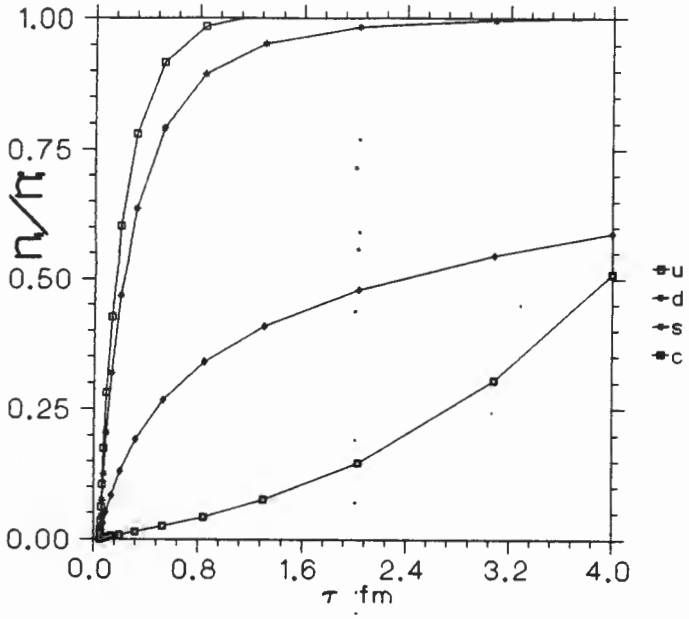


Figure 4.5.2: $\frac{n}{n_0}$ versus $\tau$

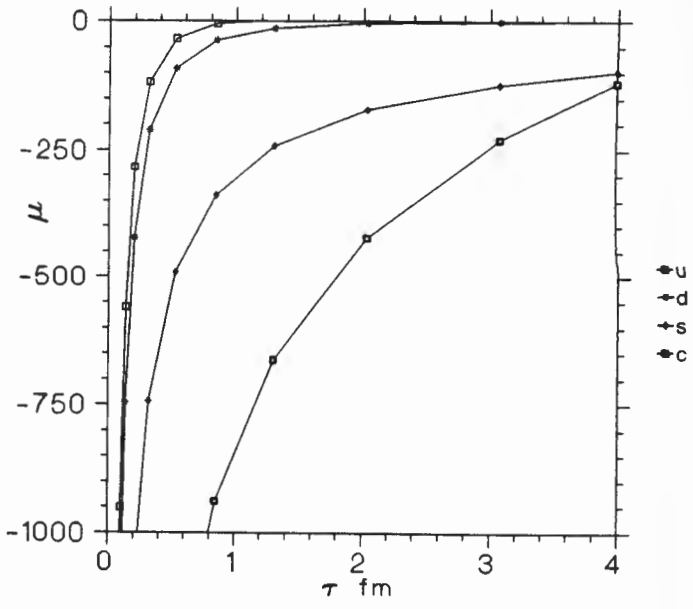


Figure 4.5.3: $\mu$ versus $\tau$

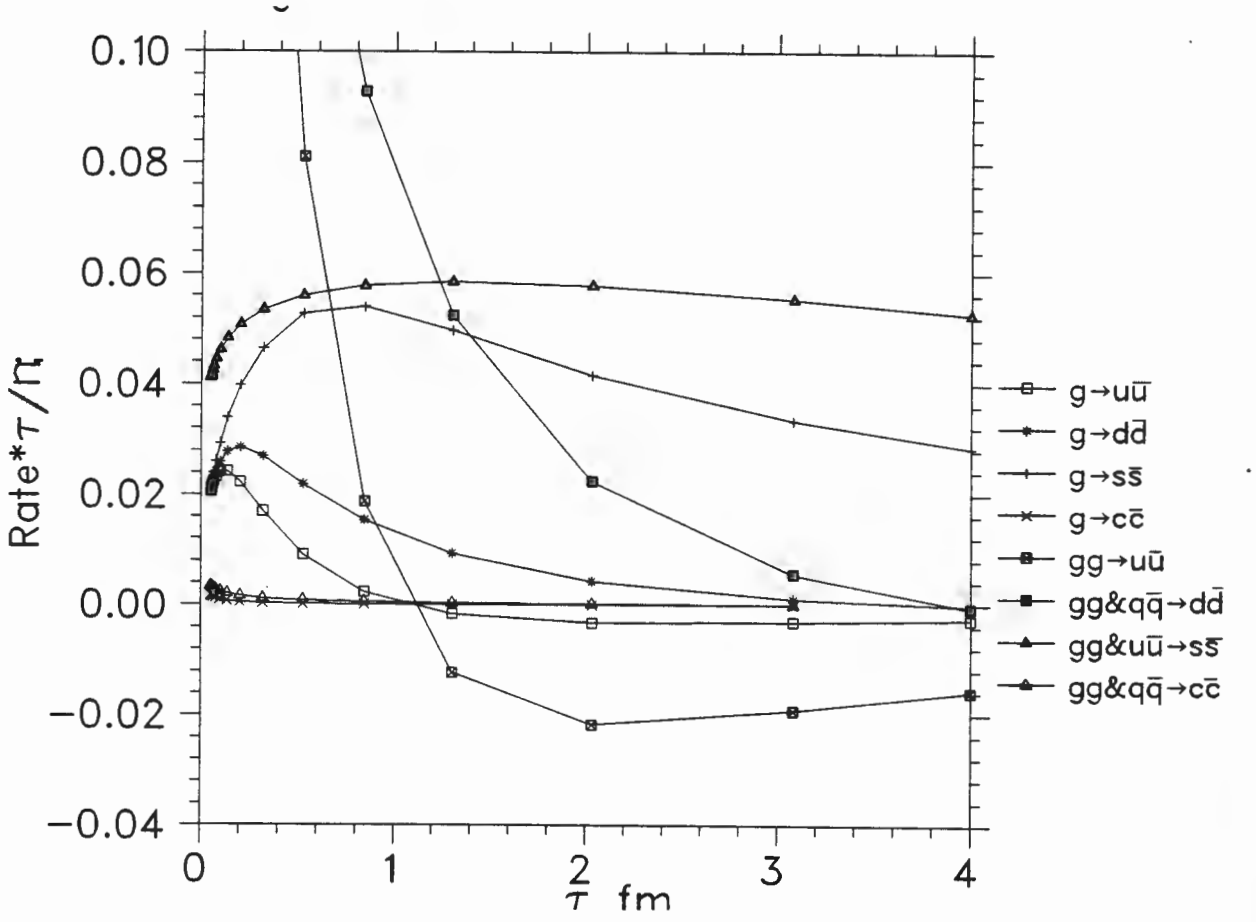


Figure 4.5.4: $\frac{\delta R(\tau) \times \tau}{n_0(\tau)}$ versus $\tau$

## 4.6 Discussion

We have shown that within our model, and according to our quark creation mechanisms, that the strangeness phase space is undersaturated. We further conclude that without substantial modifications to the quark distribution functions, quarks heavier than charm can not be realistically incorporated. We also see that the model breaks down for early times (high temperature), but that the final values are not sensitive to the bad numerical behaviour.

# Chapter 5

# Conclusion

We have demonstrated that in the baryon sector the strangeness phase space is undersaturated. We did this by first showing that it is needed to explain the experimental data, then by showing its thermodynamic consistency, and finally through the microscopic evolution of a gluon gas, we find that this feature persists.

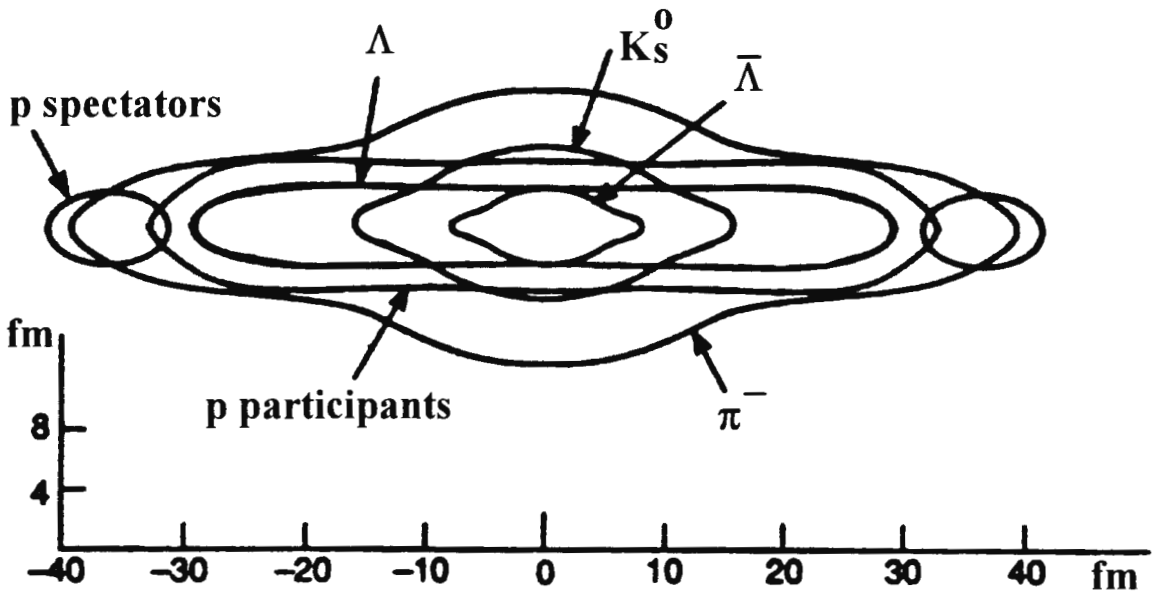


Figure 5.1: The spatial distribution of hadronisation. This is obtained from NA35 data [3]. pg 194. The reason for this plot is to demonstrate the spatial (and temporal) dependence of the number density that is not considered in our model.

This is not to say that strangeness production is a signature of a quark gluon plasma. There are some questions that must still be answered: transverse effects must be taken into account (or, more generally the spacial and temporal evolution of the plasma must be understood and be reliably modelled); a detailed model of the evolution from a quark-gluon plasma to a hadron gas (assuming the phase transition exists) is needed. Further, it would be instructive to know the initial conditions, or, physically speaking, to know how two nuclei disintegrate into a gluon gas, with the knowledge of the temporal evolution).

In Figure 5.1 we display the non-trivial spatial evolution of the remnants of a RHIC.

Undoubtedly, this picture will change, but it illustrates the complexity of the quark-gluon plasma.

This thesis has not addressed the question as to whether an exotic mechanism like a quark-gluon plasma is needed to produce strangeness or whether sufficient strange quarks are produced in the hadronic sector. This question is discussed in [95, 96].

For this thesis my research has been limited to 'Strangeness production in Quark-Gluon plasmas'. A number of interesting question need to be discussed further. Specifically the gauge dependence of the coupling constant [61], the absence of Ward identities (although Ward-like relations exist between integrals) and the regulation of divergences in the production of heavy quarks from light (massless) quarks are all problems worth studying. The damping rate is another quantity susceptible to finite temperature field theory that is important, but little understood. The next order of diagrams in TFT should be calculated, and these corrections should also be added.

Returning briefly to the coupling constant $\alpha_S = g^2/(4\pi)$. It is argued that the logarithmic decrease of $\alpha_S$ at high density due to asymptotic freedom leads to the idea of a quark-gluon plasma at high $T$. This problem has been studied within the formalism of Braaten-Pisarski [61].

It would be interesting to extend Bjorken's hydrodynamic scenario to include temperature dependent coupling constant and masses. More difficult improvements would be including transverse corrections as well as imposing better initial conditions. (Problems such as thermodynamic consistency have not been adequately addressed.)

We find that the results are slightly susceptible (less than 5) percent to the numerical parameters that have to be set in the program.

The program was written with the intention to be expanded.

- **Including temperature dependent masses:** Concerns over thermodynamic consistency led us to decide not to allow temperature dependent quark masses. Implementing this would mean that in taking the temperature derivative of energy which depends on mass, which is algebraically complicated. Also, since gluons would also rightfully have to have temperature dependent masses, and so, considerable more CPU time would be used in evaluating the gluon thermodynamic functions.

- **FORTRAN 77 into FORTAN 90 or $C^{++}$:** Fortran is very useful when developing code, but it is a nightmare to maintain. It would be useful to rewrite the programs in a language that has tighter control over the variables.

- **Thermal distribution functions:** It would be useful to find the behavior of the heavier quarks in the plasma. There have been some claims as to their strange behaviour [4, 65]. Care will have to be taken to maintaining Bjorken's assumptions.

- **g depend on T:** We assumed that g was constant. However we know that g is a function of temperature. How this affects the thermodynamic consistency needs to be considered. Also, temperature derivatives of g are also made in the energy, if temperature dependent masses are included.

- **Transverse Flow:** Transverse flow has been neglected due to the constraints of this model. It would be useful to see if it can be included.

- **Next order corrections to $\delta R$:** Including thermal corrections of the next order (ie thermally dependent quark and gluon fusion) can easily be included in this program. A faster computer would be needed though.

- We should do all the **hadronic gas** scenarios for all the data, all the tables and include isospin.

- Investigate the **masses greater than 2GeV** in the hadron gas scenario. Specifically the idea that the continuum could be described with fractals.

- Continue the hydrodynamic model into the **hadron sector** and **preequilibrium sectors**.

- Redo the hydrodynamic simulation but for *Pb-Pb* and at higher energies. This should be compared to parton models.

# Appendix A

# Notation and key Theorems

Here is a list of notation used in this thesis. This list sometimes has duplicate entries, especially when working with fermions, but by the context of the symbol, the definition should be clear. We use the standard fermion gamma matrices, see for example the appendices of Bjorken and Drell [32] and Appendix C1.
With regard to Feynman diagrams, the gluon color is labeled by $a$, $b$, $c$, ..., the quark color by $k$, $l$, ... and the Dirac gamma matrices have Greek indices $\alpha$, $\beta$, $\gamma$ ... and labels $\mu$, $\nu$ .... Also $\hbar = k = c = 1$. With respect to thermodynamic quantities, $E$,$N$,$S$ and $P$ refer to the energy, numbers, entropy and pressure. $\varepsilon$, $n$, $s$ and $p$ energy density, number density, entropy density and pressure density.

## A.1 Symbols

| Symbol | Meaning | Definition |
|---|---|---|
| $\beta$ | Inverse temperature | $\beta = 1/T$ |
| $\Delta$ | Generic Propagator | |
| $\epsilon_\mu(\zeta, k)$ | Polarisation vector | $\zeta$ = spin,$k$ = momentum |
| $\varepsilon$ | Energy density | |
| $\gamma_S$ | Deviation from chemical equilibrium | |
| $\gamma$ | Damping | |
| $\lambda$ | Mean free path | |
| $\Lambda_\mu$, $\Lambda_{\mu\nu}$, $\Lambda_{\mu...}$ | n-point vertices | |
| ${}^*\Lambda_\mu$, ${}^*\Lambda_{\mu\nu}$, ${}^*\Lambda_{\mu...}$ | resummed n-point vertices | |
| $\mu$ | Chemical potential | |
| $\Pi_{\mu\nu}$ | Polarisation Tensor | |
| $\Sigma$ | Self Energy | |
| $\rho$ | Density | |
| $\theta(x)$ | Step function | $\theta(x) = \begin{cases} 0 \text{ if } x > 0 \\ 1 \text{ if } x < 0 \end{cases}$. |
| $\mathcal{C}$ | The complex plain isomorphic to $\Re^2$ | |
| $D_{\mu\nu}$ | Gluon Propagator | |
| $f_{BE}$, $f_+$ | Bose Einstein statistics | |

| | | |
|---|---|---|
| $f_{FD}$, $f_-$ | Fermi Dirac statistics | |
| $F$, $F_>$, $F_<$ | Generic n-point functions (cutting rules) | |
| Im | The imaginary component of a C number | |
| $k$ | $k = \|\vec{k}\|$ | |
| $K^\mu$ | Internal 4-momentum vector | $K^\mu = (\omega, \vec{k})$ |
| $m_g$ | Non-perturbative gluon mass | |
| $m_s$ | Strange quark mass | |
| $\mathcal{M}$ | $\mathcal{M}_{ij} = (2\pi)^4 \delta^4(P_{initial} - P_{final}) <j\|T\|i>$ | |
| $n$ | Number density | |
| $N_\pi$, $N_N$ | Number of pions or nucleons | |
| $N_C$ | Number of colors | |
| $N_f$ | Number of flavors | |
| $p$ | Pressure | |
| $P, p$ | External 4-momentum,3-momentum | |
| $P_{\mu\nu}$ | Transverse Projection Operator | |
| $Q_{\mu\nu}$ | Longitudinal Projection Operator | |
| $R_{x\to y}$ | Rate of formation of $y$ from $x$ | |
| $\delta R_{x\leftrightarrow y}$ | Rate of formation and annihilation | $\delta R_{x\leftrightarrow y} = R_{x\to y} - R_{y\to x}$ |
| Re | The real component of a C number | |
| $s$ | Invariant mass | $s^2 = k^\mu k_\mu = \omega^2 - q^2$ |
| $<i\|S\|j>$ | S-matrix | Transition amplitude |
| $T$ | Temperature | |
| $<f\|T\|i>$ | T-matrix | $S = 1 - T$ |
| $T_f$ | Freeze-out Temperature | |
| $T_H$ | Hagedorn Temperature | |
| Tr | Trace of a matrix | |
| $V$ | Volume | |

In general we use $k_{1\ldots n}$ for internal momenta and $p_{1\ldots n}$ for external momenta. The Feynman diagrams have time running from left to right. The incoming momenta are labeled sequentially from 1. The outgoing momenta are labeled sequentially from the last internal momentum. Covariant and contravariant notation is used throughout, with the usual Einstein summing convention of repeated indices is employed.

The notation throughout the thesis is standard, and found in the references [32, 77, 138].

## A.2 Laboratory and Centre of Mass frames

The relativistically invariant energy, $s$, is defined as $s = q^\mu q_\mu$ where $q^\mu = q_1^\mu + q_2^\mu$.

There are two frames of interest - the laboratory and centre of mass frames.

In the laboratory frame $q_1^\mu = (m_1, 0)$ and $q_2^\mu = (E_{lab}, \vec{p})$. The mass shell condition is obviously $E_{lab}^2 = m_2^2 + \vec{p}^2$.

In the centre of mass frame $q_1^\mu = (E_1, \vec{p})$ and $q_2^\mu = (E_2, -\vec{p})$. If we are considering two equally massive nuclei $m_1 = m_2 = m$ then $E_1 = (m^2 + \vec{p}^2)^{\frac{1}{2}} = E_2 = (m^2 + \vec{p}^2))^{\frac{1}{2}} = E_{cm}$.

From the above

$$\sqrt{s} = 2E_{cm}$$

and

$$s \simeq 2E_{lab}m.$$

## A.3 Mandelstam Variables

For the case of two incoming momenta, $p_1$ and $p_2$, and two outgoing momenta, $p_3$ and $p_4$, we are able to parameterise the matrix elements according to the Mandelstam variables.

$$s = (p_1 + p_2)^2 = (p_3 + p_4)^2,$$

$$t = (p_3 - p_1)^2 = (p_4 - p_2)^2$$

and

$$u = (p_3 - p_2)^2 = (p_4 - p_1)^2.$$

Conservation of energy gives

$$s + t + u = \sum_{i=1}^{4} m_i^2.$$

## A.4 Kinematics - Unitarity

If two particles scatter, we can graphically express this as

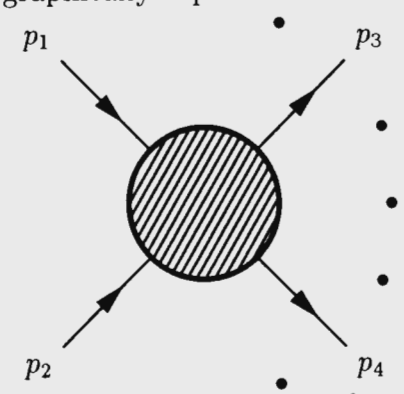


We are only interested in the case of two products, with momenta $p_3$ and $p_4$ respectively. Unitarity imposes on the $S$ matrix that $\sum |< f|S|i >|^2 = 1$. If we define a scattering matrix as $< f|S|i >= \delta_{fi} + i(2\pi)^4\, \delta^4(P_f - P_i)\mathcal{N} < f|T|i >$ then after some algebra we obtain

$$\mathrm{Im}[< f|T|i >] = \frac{1}{2}(2\pi)^4 \sum_a \mathcal{N}^2 < f|T|a >< a|T^*|i >\ \delta^4(P_i - P_f).$$

$\mathcal{N}$ is a normalisation constant. Of particular interest is when $|f>=|i>$, because then, choosing a normalisation factor $\mathcal{N}$ to make the expression relativistically invariant, we get

$$\begin{aligned}\mathrm{Im}[<i|T|i>] &= \frac{1}{2}\frac{1}{(2\pi)^{3(n-2)-4}}\int dp_3\delta(p_3^2-m_3^2)\theta(p_3)\ldots\int dp_n \times \\ &\quad \delta(p_n^2-m_n^2)\theta(p_n)|<p_3\ldots p_n|T^*|i>|^2\delta^4(P_i-P_f) \qquad \text{(A.1)}\end{aligned}$$

where $n-2$ is the number of outgoing particles considered here, and the sum over '$a$' goes over all physical states $|a>$ and the integration is over 4-momentum $d^4p$. Now this is related to the cross section which can be shown to be

$$\begin{aligned}\sigma_{2\to n-2} &= \frac{(2\pi)^4}{4\left[(p_1\cdot p_2)^2-m_1^2m_2^2\right]^{\frac{1}{2}}}\int d\tilde{p}_3\ldots d\tilde{p}_n \\ &\quad |<p_3,\ldots,p_n|T|p_1,p_2>|^2\,\sigma^4(p_1+p_2-p_3-\cdots-p_n) \qquad \text{(A.2)}\end{aligned}$$

where $d\tilde{p}=d^3p/(2p^0)\,(2\pi)^3=d^4p\delta(p^2-m^2)\theta(p)$ is the invariant measure.

Using $<f|T|i>=(2\pi)^4\,\delta^4(P_i-P_f)\mathcal{M}_{fi}$ and expressing the invariant multiplication factor as a function often appearing in kinematics, $\lambda(x,y,z)=x^2+y^2+z^2-2xy-2yz-2xz$, we have for two incoming and outgoing particles

$$\sigma_{2\to2}=\frac{(2\pi)^4\delta^4(P_i-P_f)}{2\lambda(s,m_2^2,m_1^2)^{\frac{1}{2}}}\sum_{spin}|\mathcal{M}_{fi}|^2\frac{dp_3}{(2\pi)^3}\delta(p_1^2-m_1^2)\theta(p_1)\frac{dp_4}{(2\pi)^3}\delta(p_4^2-m_4^2)\theta(p_4) \qquad \text{(A.3)}$$

from which

$$\sigma_{TOT}=\frac{\mathrm{Im}<i|T|i>}{\lambda(s,m_2^2,m_1^2)^{\frac{1}{2}}} \qquad \text{(A.4)}$$

is obtained. The above relation is called the Optical Theorem.

Finally, in this work we are interested in the rates. Loosely speaking the rate is related to the cross sections by integrating over the initial momenta. This means graphically that we must join the incoming and outgoing lines. However, we do not need to worry about the flux which produces the $\lambda$ function. We get the startlingly simple expression for the rate

$$\mathrm{Rate}=\mathrm{Im}<i|T|i>\,. \qquad \text{(A.5)}$$

All the integrals are contained in the above expression because we join the external lines. In this thesis we recognise that this rate may not be defined (because we are integrating over infinite incoming energies) but we include thermal distribution functions to settle this problem.

# Appendix B

# Experiment

## B.1 Experimental Variables

The 4-momentum can be parameterised as $p^\mu = (m_\perp \cosh y, \vec{p}_\perp, m_\perp \sinh y)$ where the rapidity, $y$ and transverse mass $m_\perp$ are the new variables. These are related to the usual parameterization by $m_\perp = \sqrt{\vec{p}_\perp^2 + m^2}$, $\vec{p}_\perp = (p_x, p_y)$ and $y = \operatorname{arcoth}\frac{p_o}{p_z} = \frac{1}{2}\ln\left(\frac{p_o+p_z}{p_o-p_z}\right)$. We are interested in

$$\frac{E\,dn}{d^3p} = \frac{dn}{p_\perp\,d\phi\,dp_\perp\,dy} = \frac{dn}{m_\perp\,d\phi\,dm_\perp\,dy},$$

from this we obtain $dn/dy$ which allows us to calculate the collision products in the beam, target or central regions, and $1/m^{\frac{3}{2}}\,dn/dm_\perp$ yielding the temperature of the system.

In these variables the Boltzman distribution looks like

$$\frac{E\,dn}{d^3p} = \frac{1}{(2\pi)^3} m_\perp \cosh y \exp\left(-\beta m_\perp \cosh y\right).$$

Boosting the distribution is particularly simple if it is along the $z$ axis. We however give a radial boost, $\rho$, as well as a longitudinal boost $y_B$ to obtain

$$\frac{dn}{p_\perp\,d\phi\,dp_\perp\,dy\,dy_B\,d\Phi_B} = \frac{1}{(2\pi)^3} E \exp(-\beta \sinh\rho \cosh y_B \cos(\phi+\Phi_B) + m_\perp R \cosh(\xi + y_B))$$

where $R = \cosh^2 y \sinh^2\rho + 1$, $\tan\xi = -\frac{\tanh y}{\cosh\rho}$ and $E = \cosh(y_B + \xi)$.

We can integrate out the longitudinal rapidity (this corresponds to the sum of baryon clouds boosted along the $z$ axis in arbitrary directions)

$$\frac{dn}{p_\perp\,d\phi\,dp_\perp\,dy} = \frac{1}{(2\pi)^3} m_\perp \cdot I_o(\beta\, p_\perp \cosh y \sinh\rho) \cdot K_1(\beta\, m_\perp\, R \cosh\xi)$$

A typical cross section looks like Figure A.1. However, the emerging new data seems to question nuclear transparency, and so this figure may well be partially incorrect.

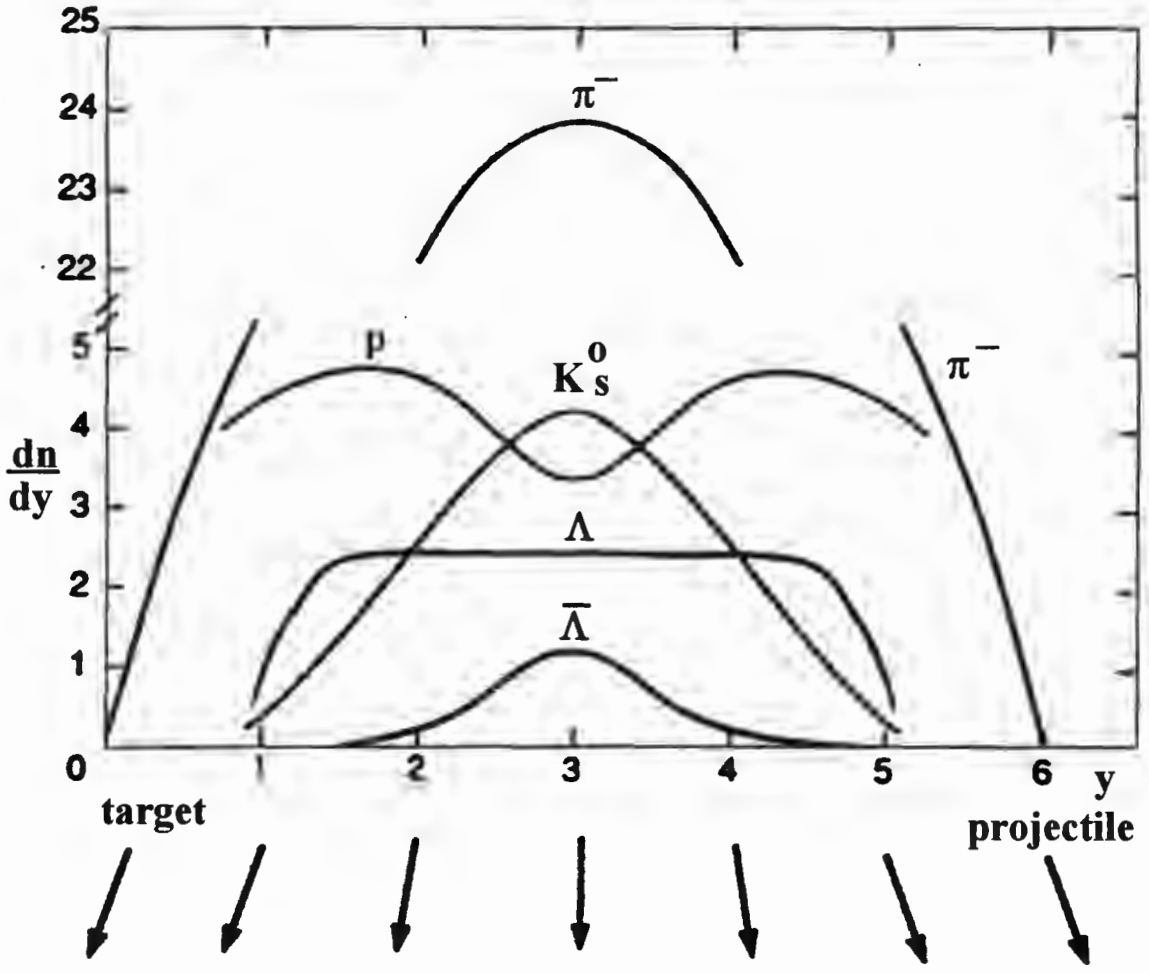


Figure A.1: Rapidity distribution from NA35. $\frac{dn}{dy}$ from [3], pg 194.

## B.2 Acceptance

Experimental data is normally measured within a certain rapidity interval. A $k$-factor is defined to extrapolate it to full phase space. Using the date from WA85 as an example we have : $2.3 \leq y \leq 3.0$ and $1.0 \leq p_\perp \leq 2.0$GeV. Using

$$\frac{E\,dn}{d^3p} = \frac{dn}{dp_\perp\, p_\perp\, dy\, d\phi} = \frac{dn}{dm_\perp\, m_\perp\, dy\, d\phi} = \frac{1}{(2\pi)^3} m_\perp \cosh y\, \exp\left(-\beta\, m_\perp \cosh y\right)$$

and integrating out $\phi$ and $y$ variables we get

$$\frac{dn}{dm_\perp} = 2\pi\, m_\perp^2\, K_1\left(\beta\, m_\perp\right) \tag{B.1}$$

which can be approximated for $T \to \infty$ as

$$\frac{dn}{dm_\perp} = 2\pi\, m_\perp^2 \left(\frac{\pi}{2\,\beta\, m_\perp}\right)^{\frac{1}{2}} \exp\left(-\beta\, m_\perp\right). \tag{B.2}$$

This is the equation used in the log-plot of $\frac{dn}{dm_\perp}\frac{1}{(m_\perp)^{\frac{3}{2}}}$ verses $m_\perp$ to determine the temperature parameter. The fact that $T$ does not tend to infinity and that to obtain B.1 we integrated the rapidity from negative to positive infinity are generally ignored because the approximation seems to be adequate. However the finite transverse mass domain is explicitly corrected for with the k-factor. To determine $n$ we integrate out $m_\perp$ in B.1 After changing variable with $m^2 + p_\perp^2 = m_\perp^2$ we get

$$dn = \frac{2}{(2\pi)^2} m_\perp^2 \frac{dp_\perp}{(\beta\, m_\perp)^{\frac{1}{2}}} \exp\left(-\beta\sqrt{m^2 + p_\perp^2}\right) \tag{B.3}$$

Various forms of equation B.3 are used in evaluating experimental data. To good approximation, the half integer power of $m_\perp$ is replaced with a fraction.

The experimental ratios must now be extrapolated to full phase space. This is done with a k-factor defined for the this example as

$$k_{xy} = \frac{1 + \frac{\int_0^1 x\, m_\perp \exp\left(-\beta\sqrt{m_x^2+x^2}\right) dx}{\int_1^2 x\, m_\perp \exp\left(-\beta\sqrt{m_x^2+x^2}\right) dx}}{1 + \frac{\int_0^1 x\, m_\perp \exp\left(-\beta\sqrt{m_y^2+x^2}\right) dx}{\int_1^2 x\, m_\perp \exp\left(-\beta\sqrt{m_y^2+x^2}\right) dx}}.$$

Accordingly

$$\frac{N_x}{N_{y\ Full\_Phase\_Space}} = \frac{N_x}{N_{y\ p_\perp\_cut}} \times k_{xy}$$

## B.3 Experimental ratios for strange hadrons

### B.3.1 $p-p$ and $p-A$ data

It is important to clearly show the onset of a QGP plasma by contrasting $A-A$ data with $p-p$ and $p-A$ data. Unfortunately there are in general no corresponding data from $p-p$ or $p-A$ collisions. Reliable estimates in the central rapidity regime have been extrapolated ([120], Kachelhoffer and Geist) from incomplete $p-A$ data, summarised in Table B.1.

| $\overline{\Lambda}/\Lambda$ | $\overline{\Xi^-}/\Xi^-$ | $\Omega^-/\Xi^-$ | $\overline{\Omega^-}/\overline{\Xi^-}$ | $\overline{\Omega^-}/\Omega^-$ |
|---|---|---|---|---|
| $0.647 \pm 0.03$ | $0.62 \pm 0.05$ | $0.042 \pm 0.002$ | $0.056 \pm 0.004$ | $0.55 \pm 0.15$ |

Table B.1: Extrapolated p-p and p-A data

For the above table $1.0 < y < 5.0$ GeV/c and $T = 194$ MeV.

### B.3.2 NA35

This experiment analyzed the collisions of $^{16}O$ and $^{32}S$ with targets ranging from $C$ to $Pb$ at 200 GeV/c per nucleon. We are specifically interested in $^{32}S$ projectiles colliding with $S$,

*Ag* and *Au* targets, from which the following data is taken ([120],pg 190). This experiment was one of the first experiments, and counts the a number of strange particles, $\Lambda$'s and kaons (and their anti-particles), but not the ratios. This experiment has a broad rapidity region.

| | $\overline{\Lambda}$ | $\Lambda$ | $\overline{\Lambda}/\Lambda$ |
|---|---|---|---|
| S-S | $1.5 \pm 0.4$ | $8.2 \pm 0.9$ | $0.18 \pm 0.13$ |
| S-W | $0.57 \pm 0.2$ | $2.05 \pm 0.2$ | $0.18 \pm 0.05$ |

Table B.2: Strangeness particle ratios from NA35 data

The last data is from [120] and has $2 < y < 3$.

### B.3.3 NA36

This experiment is about five years old. This experiment analyzed the collisions of $S + S$, $S + Ag$ and $S + Pb$ at 200 GeV/c per nucleon. Below is a table of $S - Pb$ data ([3], pg19 and [114], pg221c). Rapidity in target fragmentation region.

| | $\overline{\Lambda}/\Lambda$ | $\overline{\Xi^-}/\Xi^-$ | $\Xi^-/\Lambda$ | $\overline{\Xi^-}/\overline{\Lambda}$ |
|---|---|---|---|---|
| Cut 1 | $0.207 \pm 0.014$ | $0.276 \pm 0.108$ | $0.066 \pm 0.013$ | $0.127 \pm 0.022$ |
| Cut 2 | $0.117 \pm 0.011$ | $0.276 \pm 0.108$ | $0.066 \pm 0.013$ | $0.127 \pm 0.022$ |

Table B.3: Strangeness particle ratios from NA36 data

For the Cut-1 data,
$\overline{\Lambda}/\Lambda$ data was measured in $1.5 < y < 3.0$GeV/c and $0.6 < p_\perp < 1.6$GeV/c,
$\overline{\Xi^-}/\Xi^-$ in $2.0 < y < 2.5$GeV/c and $0.8 < p_\perp < 1.8$GeV/c,
$\Xi^-/\Lambda$ in $1.5 < y < 2.5$GeV/c and $0.8 < p_\perp < 1.8$GeV/c and
$\overline{\Xi^-}/\overline{\Lambda}$ $2.0 < y < 3.0$GeV/c and $0.6 < p_\perp < 1.8$GeV/c This data is *S-Pb* at 200·A GeV. It was obtained from [113], pg 221 and 327.

The last line has
$\overline{\Lambda}/\Lambda$ data was measured in $2 < y < 2.5$GeV/c and $0.6 < p_\perp < 1.6$GeV/c,
$\overline{\Xi^-}/\Xi^-$ in $2 < y < 2.5$GeV/c and $0.8 < p_\perp < 1.8$GeV/c and
$\Xi^-/\Lambda$ in $1.5 < y < 3.5$GeV/c and $0.8 < p_\perp < 1.8$GeV/c.

It is interesting to note that the degree of saturation of strangeness phase space is calculated to be $\gamma_s = 0.48 \pm 0.13$.

### B.3.4 WA85

The kinematic region for this data is narrow. The data listed is $S$-$W$ at 200·A GeV. This data was from the 1990 run. There was a 1987 run with $^{32}S$. Data for $p-W$ and $S-W$ hyperon ratios at 200 GeV per nucleon was obtained from ([120], pg 231), ([114], pg 230) and ([113], pg 309). The ratios with
$\mathrm{Cut}_1$ ($m_\perp > 1.9$GeV in the rapidity window $2.3 < y_{LAB} < 2.8$ GeV/c),
$\mathrm{Cut}_1.1$ ($1¡p_\perp < 2$GeV in the rapidity window $2.3 < y_{LAB} < 2.8$ GeV/c), and for
$\mathrm{Cut}_2$ ($1.2 < p_\perp < 3.0$GeV for $2.3 < y_{LAB} < 3.0$ GeV/c) are shown below: The data is from

| | $\overline{\Lambda}/\Lambda$ | $\overline{\Xi^-}/\Xi^-$ | $\Xi^-/\Lambda$ | $\overline{\Xi^-}/\overline{\Lambda}$ | $\overline{\Omega^-}/\Omega^-$ |
|---|---|---|---|---|---|
| $Cut_1$ pW | $0.19 \pm 0.02$ | $0.48 \pm 0.07$ | $0.13 \pm 0.01$ | $0.31 \pm 0.03$ | |
| $Cut_1$ SW | $0.20 \pm 0.01$ | $0.41 \pm 0.05$ | $0.19 \pm 0.01$ | $0.40 \pm 0.04$ | |
| $Cut_1.1$ SW | $0.20 \pm 0.01$ | $0.41 \pm 0.05$ | $0.09 \pm 0.01$ | $0.20 \pm 0.03$ | |
| $Cut_2$ pW | $0.19 \pm 0.012$ | $0.47 \pm 0.06$ | $0.064 \pm 0.005$ | $0.15 \pm 0.02$ | |
| $Cut_2$ SW | $0.20 \pm 0.01$ | $0.45 \pm 0.05$ | $0.095 \pm 0.006$ | $0.21 \pm 0.02$ | $0.57 \pm 0.41$ |

Table B.4: Strangeness particle ratios from WA85 data

[3] pg 231 and 240 and [113] pg 230c and 327c.

### B.3.5 WA94

This is $S$-$S$ at 200·A GeV. $2.5 < y_{LAB} < 3$. The data is from [3] pg 265. This experiment measured $S-S$ at 200 GeV. The table was obtained from ([120], pg264) and ([113], pg. 322). $\mathrm{Cut}_3 = 1.2 < p_\perp < 3.0$GeV. $\mathrm{Cut}_4 = 1. < p_\perp < 2.0$GeV and $\mathrm{Cut}_5 = m_\perp > 1.9$GeV

| | $\overline{\Lambda}/\Lambda$ | $\overline{\Xi^-}/\Xi^-$ | $\Xi^-/\Lambda$ | $\overline{\Xi^-}/\overline{\Lambda}$ |
|---|---|---|---|---|
| $\mathrm{Cut}_3$ | $0.23 \pm 0.01$ | $0.55 \pm 0.07$ | $0.09 \pm 0.01$ | $0.21 \pm 0.02$ |
| $\mathrm{Cut}_4$ | $0.24 \pm 0.01$ | $0.58 \pm 0.07$ | $0.08 \pm 0.01$ | $0.20 \pm 0.02$ |
| $\mathrm{Cut}_5$ | $0.22 \pm 0.01$ | $0.54 \pm 0.06$ | $0.18 \pm 0.01$ | $0.44 \pm 0.04$ |

Table B.5: Strangeness particle ratios from WA94 data

# Appendix C

# Feynman Rules and Definitions

## C.1 QCD

### C.1.1 Overall Factors

For every **closed loop** with loop momentum $k$ we need $\frac{1}{(2\pi)^4}\int d^4k$. Closed **fermion loops** get an additional $-1$. Between graphs with **identical fermion** lines interchanged a multiplicative factor of $-1$ is needed. By **convention** an overall $-i$ is used. Finally there is a **symmetry factor** to avoid overcounting identical boson states in closed loops of $\frac{1}{S}$, where $S$ is a combinatorial factor.

### C.1.2 Traces and Contractions

We use covariant and contravariant notation. The metric is $g^{\mu\nu} = \text{diag}[1, -1, -1, -1]$.

#### Gamma Matrices

For convenience we list the Dirac gamma relations.

$$\gamma^\mu\gamma^\nu + \gamma^\nu\gamma^\mu = 2g^{\mu\nu} \tag{C.1}$$

$$\gamma^o\gamma^\nu\gamma^o = \gamma^{\mu\dagger} \tag{C.2}$$

$$g^{\mu\nu}g_{\mu\nu} = \gamma^\mu\gamma_\mu = \text{Tr}[1] = 4 \tag{C.3}$$

$$\text{Tr}(\gamma^\mu\gamma^\nu) = 4g^{\mu\nu} \tag{C.4}$$

$$\text{Tr}(\gamma^\mu\gamma^\nu\gamma^\rho\gamma^\sigma) = 4(g^{\mu\nu}g^{\rho\sigma} - g^{\mu\rho}g^{\nu\sigma} + g^{\mu\sigma}g^{\nu\rho}) \tag{C.5}$$

### Spinors

Certain combinations of spinors are useful.

$$\overline{u} = u^{\dagger}\gamma^{o} \tag{C.6}$$

$$\Lambda^{-}(k) = -\sum_{\alpha=1,2} v_{\epsilon}^{(\alpha)}(k) \otimes \overline{v}_{\kappa}^{(\alpha)}(k) = -\sum_{\alpha=1,2} v_{\epsilon}^{(\alpha)}(k)\overline{v}_{\kappa}^{(\alpha)}(k) = (-\not{k} + m)_{\epsilon\kappa} \tag{C.7}$$

$$\Lambda^{+}(k) = \sum_{\alpha=1,2} u_{\epsilon}^{(\alpha)}(k) \otimes \overline{u}_{\kappa}^{(\alpha)}(k) = \sum_{\alpha=1,2} u_{\epsilon}^{(\alpha)}(k)\,\overline{u}_{\kappa}^{(\alpha)}(k) = (\not{k} + m)_{\epsilon\kappa} \tag{C.8}$$

### Polarisation Vectors

Polarisation vectors relate to gluons and photons.

$$\varepsilon(k,\lambda)\cdot\varepsilon(k,\lambda') = -\delta(\lambda,\lambda') \text{ where } \lambda,\lambda' = 1,2. \tag{C.9}$$

Assuming transversality, then

$$\sum_{\lambda} \varepsilon_{\mu}(k,\lambda)\cdot\varepsilon_{\nu}(k,\lambda)^{*} = -g_{\mu\nu}. \tag{C.10}$$

If transversality does not hold then we refer the reader to the end of section 3.1.2.

### Color

We use the convention that 'color' refers to a concept analogous to charge, and is distinct from 'colour'.

$$T^{a} = \frac{\lambda_{a}}{2} \text{ where } \lambda \text{ are the Gell-Mann matrices,} \tag{C.11}$$

$$\sum_{a} T^{a}_{ij}\,T^{a}_{kl} = \frac{1}{2}(\delta_{il}\,\delta_{jk} - \frac{1}{3}\delta_{ij}\delta_{kl}), \tag{C.12}$$

$$\left(\sum_{a} T^{a}_{ij}\,T^{a}_{kl}\right)^{2} = 2, \tag{C.13}$$

$$\sum_{a} T^{a}_{ij}\,T^{a}_{kl}\,T^{a}_{il}\,T^{a}_{kj} = -\frac{2}{3}, \tag{C.14}$$

$$Tr(T^{a}) = 0, \tag{C.15}$$

$$Tr(T^{a}\,T^{b}) = \frac{1}{2}\delta^{ab}, \tag{C.16}$$

$$Tr(T^{a}\,T^{b}\,T^{a}\,T^{c}) = -\frac{1}{12}\delta^{bc}, \tag{C.17}$$

$$Tr(f^{abc}\, f^{dbc}) = 3\,\delta^{ad},\, f_{abb} = 0 \text{ and } f^{abc} = f^{cab} = -f^{acb} = -f^{cba}. \qquad \text{(C.18)}$$

Unless we state otherwise, we work in the Feynman gauge. The shadowed part of the graph lies to the right of the cut. Propagators in the shadows are obtained by replacing $i$ by $-i$.

### C.1.3 Vertices

See Table C.1.

| | | |
|---|---|---|
| Quark-gluon vertex | $g(\gamma^\mu)_{\alpha\beta}\, T^a_{ji}\, (2\pi)^4\, \delta^4(p - p' - k)$ | 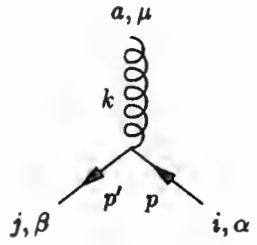  |
| Ghost-gluon vertex | $-g\, C_{abc} (2\pi)^4\, \delta^4(p + k - q) p_\mu$ | 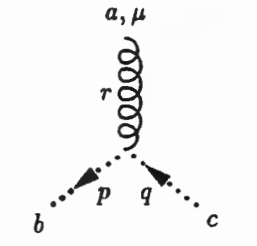  |
| Three gluon vertex | $g\,(2\pi)^4\, \delta^4(p + q + r)\, C_{abc} (g_{\mu\nu}\,(p - q)_\rho$ $+ g_{\nu\rho}\,(q - r)_\mu + g_{\rho\mu}\,(r - p)_\nu)$ | 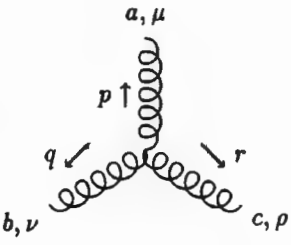  |

Table C.1: Feynman Rules for Vertices

### C.1.4 Spinors

See Table C.2.

### C.1.5 Propagators

See Table C.3.

| | | |
|---|---|---|
| Incoming Fermion | $u(p,\sigma)$ | 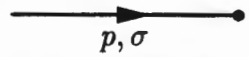  |
| Incoming Antifermion | $\overline{v}(p,\sigma)$ | 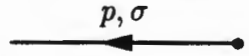  |
| Outgoing Fermion | $\overline{u}(p,\sigma)$ | 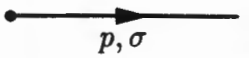  |
| Outgoing Antifermion | $v(p,\sigma)$ | 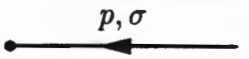  |
| Incoming Vector Particle | $\epsilon^{\mu}(p,\lambda)^*$ | 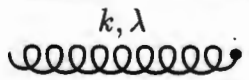  |
| Outgoing Vector Particle | $\epsilon^{\mu}(p,\lambda)$ | 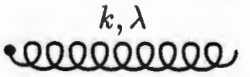  |

Table C.2: Feynman Rules for Incoming or Outgoing Lines

## C.2 Feynman Rules - Real Time Formalism

As mentioned in section 2.2 various choice of contour linking $\tau$ to $\tau - i\beta$ are possible. Normally the contour is chosen to run from $\tau$ to $-\tau$ to $-\tau - i\sigma$ to $\tau - i\sigma$ to $-\tau - i\beta$. We use $\sigma = \frac{1}{2}\beta$, but it is often left as a parameter (this is Thermal Field Dynamics).

The propagator emerges in a complicated form, and are generally simplified, using

$$V(\beta,k,\mu) = \begin{bmatrix} \cos\theta(k,\mu) & -\varepsilon(p_0)\, e^{-\beta\mu/2} \sin(2\,\theta(k,\mu)) \\ \varepsilon(p_0)\, e^{\beta\mu/2} \sin(\theta(k,\mu)) & \cos\theta(k,\mu) \end{bmatrix}$$

where

$$\cos\theta(k,\mu) = \frac{\theta(k_0)\exp(\frac{x}{4}) + \theta(-k_0)\exp(\frac{-x}{4})}{\sqrt{\exp(\frac{x}{2}) + \exp(\frac{-x}{2})}},$$

$$\sin\theta(k,\mu) = \frac{\theta(k_0)\exp(\frac{x}{4}) - \theta(-k_0)\exp(\frac{-x}{4})}{\sqrt{\exp(\frac{x}{2}) + \exp(\frac{-x}{2})}}$$

and $x = \beta(k_0 + \mu)$. Also

$$U(\beta,k) = \begin{bmatrix} \cosh\theta(k,\alpha) & -e^{\alpha/2} \sinh(2\theta(k,\alpha)) \\ e^{-\alpha/2} \sinh(2\theta(k,\alpha)) & \cosh\theta(k,\alpha) \end{bmatrix}$$

where

$$\cosh\theta(k,\alpha) = \frac{\theta(k_0)\exp(\frac{x}{4}) + \theta(-k_0)\exp(\frac{-x}{4})}{\sqrt{\exp(\frac{x}{2}) + \exp(\frac{-x}{2})}},$$

$$\sinh\theta\,(k,\alpha) = \frac{\theta(k_0)\exp(\frac{x}{4}) - \theta(-k_0)\exp(\frac{-x}{4})}{\sqrt{\exp(\frac{x}{2}) + \exp(\frac{-x}{2})}}.$$

and $x = \beta\,(k_0 - \mu)$.

The $\theta$ function is defined as follows

$$\theta(x) = \int_{-\infty}^{\infty} d\tau\, \frac{e^{i\tau\, x}}{\tau - i\epsilon}.$$

The topology of $T = 0$ and $T > 0$ Feynman diagrams is the same except for an extra-label on the vertices. To evaluate a diagram one must sum over all possible vertices on internal lines. Finite temperature does not affect the color, spin or tensor structure of the vertices or propagators. However, there are new expressions for the propagators. Accordingly, the rules of section C.1 holds, except that the following propagators must be used. We have also included the cut propagators, and a translation from the generic notation $(i\Delta_{ij})$ to the specific case $iD^{ab}, iD^{ab}_{\mu\nu}$ and $iS^{ab}$.

### C.2.1 Propagators

$a$ and $b$ are used to label the vertices the propagator is linking. In consistency with the literature we use, for example, $S^*$ to denote that we conjugate only the $i$'s and not any of the $\gamma$ matrices.

**Spin Zero Fields: L=$\frac{1}{2}\,(\partial_\mu\varphi)^2 - \frac{1}{2}m^2\varphi^2$**

$$iD^{ab}(\beta,p) = U(\beta,p) \begin{bmatrix} \Delta(p,m) & 0 \\ 0 & \Delta^*(p,m) \end{bmatrix} U(\beta,p).$$

$$iD^{ab}(\beta,p) = \begin{bmatrix} \Delta(p,m) & 0 \\ 0 & \Delta^*(p,m) \end{bmatrix} + \begin{bmatrix} 1 & \exp(\beta\,|p_0|/2) \\ \exp(\beta\,|p_0|/2) & 1 \end{bmatrix} \frac{2\pi\,\delta(p^2-m^2)}{\exp(\beta\,|p_0|)-1}.$$

Here $\Delta(p,m) = \frac{i}{p^2-m^2+i\varepsilon}$. For the cut propagators we get $i\Delta_{11} = -i\Delta^*_{22} = iD^{ab}_{11}$, $i\Delta_{12} = i\Delta_{21} = iD^{ab}_{12}$ and $i\Delta^{\pm} = 2\pi\,\delta(p^2-m^2)\,(\theta(\pm p_0) + n_B(p))$ where $n_B(p) = \frac{1}{\exp(\beta\,|p_0|)-1}$.

**Gauge Fields: L=-$\frac{1}{4}\,(F_{\mu\nu})^2 - \frac{1}{2}\alpha\,(\partial\cdot A)^2$**

We use the propagator of the previous section ($m = 0$) to obtain
$iD^{ab}_{\mu\nu}(\beta,p) = \left(-g_{\mu\nu} + \frac{1-\alpha}{\alpha} p_\mu\, p_\nu\, \frac{\partial^2}{\partial p^2}\right) iD^{ab}(\beta,p)$.
For the cut propagators we get $i\Delta_{11} = -i\Delta^*_{22} = iD^{ab,\mu\nu}_{11}$, $i\Delta_{12} = i\Delta_{21} = iD^{ab,\mu\nu}_{12}$ and
$i\Delta^{\pm} = 2\pi\,\delta(p^2-m^2)\,\left(-g_{\mu\nu} + \frac{1-\alpha}{\alpha} p_\mu\, p_\nu\, \frac{\partial}{\partial p^2}\right)(\theta(\pm p_0) + n_B(p))$ where $n_B(p) = \frac{1}{\exp(\beta\,|p_0|)-1}$.

**Fermion spin $\frac{1}{2}$ Fields: L=$\overline{\psi}\,(i\gamma\cdot\partial - m)\,\psi$**

$$\begin{aligned} iS^{ab}(p,m) &= V(\beta,p,\mu) \begin{bmatrix} S(p,m) & 0 \\ 0 & S^*(p,m) \end{bmatrix} V(\beta,p,\mu) \\ &= \begin{bmatrix} S(p,m) & 0 \\ 0 & S^*(p,m) \end{bmatrix} - \\ &\quad 2\pi\,(\not{k} + m) \begin{bmatrix} \sin^2\theta & \frac{1}{2}\varepsilon(p_0)\, e^{-\beta\mu}\sin(2\theta) \\ -\frac{1}{2}\varepsilon(p_0)\, e^{\beta\mu/2}\sin(2\theta) & \sin^2\theta \end{bmatrix} \delta(p^2-m^2) \end{aligned}$$

where $S(p,m) = \frac{i}{\not{k}-m+i\varepsilon}$. For $\mu = 0$ we have

$$iS^{ab}(p,m) = \begin{bmatrix} S(p,m) & 0 \\ 0 & S^*(p,m) \end{bmatrix} - 2\pi\,(\not{k}+m) \begin{bmatrix} 1 & \frac{1}{2}\varepsilon(p_0)\exp\frac{\beta|p_0|}{2} \\ -\frac{1}{2}\varepsilon(p_0)\exp\frac{\beta|p_0|}{2} & 1 \end{bmatrix} \frac{\delta(p^2-m^2)}{\exp(\beta\,|p_0|)-1}$$

For the cut propagators we get $i\Delta_{11} = -i\Delta_{22}^* = iS_{11}^{ab}$, $i\Delta_{12} = -i\exp(\beta\mu)\,\Delta_{21} = iS_{12}^{ab}$ and $i\Delta^{\pm} = 2\pi\,(\not{p}+m)\;\delta(p^2-m^2)\;[\theta(\pm p_0) - (\theta(p_0)\;n_F(x) + \theta(-p_0)\,n_F(-x))]$
where $n_F(x) = \frac{1}{\exp x+1}$. We also have $x = \beta(k_0+\mu)$.
For $\mu = 0$ we get $i\Delta^{\pm} = 2\pi\,(\not{p}+m)\;\delta(p^2-m^2)\;(\theta(\pm p_0) - n_F(p))$.

**Ghost Fields**

This includes Gauge Fields like gluons ($m^2 = 0$) and photons:

$$iD^{ab} = \begin{bmatrix} \frac{i}{p^2+i\varepsilon} & 0 \\ 0 & \frac{-i}{p^2-i\varepsilon} \end{bmatrix} + \begin{bmatrix} 1 & \exp(\beta\,|p_0|/2) \\ \exp(\beta\,|p_0|/2) & 1 \end{bmatrix} \frac{2\pi\,\delta(p^2)}{\exp(\beta\,|p_0|)-1}$$

For the cut propagators we get $i\Delta_{11} = -i\Delta_{22}^* = iD_{11}^{ab}$, $i\Delta_{12} = i\Delta_{21} = iD_{12}^{ab}$ and
$i\Delta^{\pm} = 2\pi\,\delta(p^2-m^2)\,(\theta(\pm p_0) + n_B(p))$ where $n_B(p) = \frac{1}{\exp(\beta\,|p_0|)-1}$.

### C.2.2 Vertices

The Feynman rules for zero temperature are exactly the same, except that we have two different kinds of internal vertices. Type 1 vertices are the same as the zero temperature case. Type-2 vertices have a $-1$ attached to them. They only sit on internal vertices. We have to sum over all different types of internal vertex.

For vertices in "the shade" of a cut diagram, they get a $-1$.

## C.3 Cutkosky rules

In coordinate space

- leave $i\Delta(x-y)$ unchanged if neither $x$ nor $y$ is underlined;
- replace $i\Delta(x-y)$ by $\Delta^+(x-y)$ if $x$ but not $y$ is underlined;
- replace $i\Delta(x-y)$ by $\Delta^-(x-y)$ if $y$ but not $x$ is underlined;
- replace $i\Delta(x-y)$ by $\Delta^*(x-y)$ if $x$ and $y$ are underlined;
- Reverse the sign of the vertex when it is underlined.

In momentum space these rules are

- leave $i\Delta(k)$ unchanged if neither of the vertices are circled;
- replace $i\Delta(k)$ by $\Delta^+(k)$ if $k$ flows from an uncircled vertex to a circled one;
- replace $i\Delta(k)$ by $i\Delta^-(k)$ if $k$ flows from a circled vertex to an uncircled one;
- replace $i\Delta(k)$ by $i\Delta^*(k)$ if $k$ both vertices are circled;
- Reverse the sign of the vertex when it is underlined.

Expressions for $\Delta^+, \Delta^-$ and $\Delta^*$ are given in the previous appendix, where $\Delta$ can be identified with $D^{ab}_{\mu\nu}$, $S^{ab}$ and $D_{ab}$.

| | | |
|---|---|---|
| $D^{ab}_{\mu\nu}$ Gluon | $\Delta = i\frac{1}{p^2+i\epsilon}\, g_{\mu\nu}\, \delta_{ab}$ | 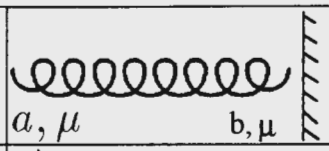  |
| Gluon* | $\Delta^* = -i\frac{1}{p^2-i\epsilon}\, g_{\mu\nu}\, \delta_{ab}$ | 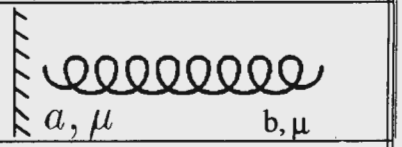  |
| Cut Gluon | $\Delta^{\pm} = -2\pi\, \theta(p_0)\, \delta(p^2)\, g_{\mu\nu}\, \delta_{ab}$ | 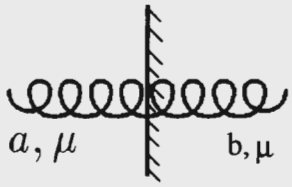  |
| $S^{ab}$ - Quark | $\Delta = \left(i\frac{\not{p}+m}{p^2-m^2+i\epsilon}\right)_{\beta\alpha} \delta_{ij}$ | 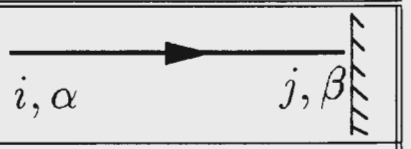  |
| $S^{ab}$ - Quark | $\left(\Delta^* = -i\frac{\not{p}+m}{p^2-m^2-i\epsilon}\right)_{\beta\alpha} \delta_{ij}$ |   |
| Cut Quark | $\Delta^+ = -2\pi\, \theta(p_0)\, \delta(p^2-m^2)\, (\not{p}+m)_{\beta\alpha}\, \delta_{ij}$ |   |
| Cut Quark | $\Delta^- = -2\pi\, \theta(p_0)\, \delta(p^2-m^2)\, (\not{p}+m)_{\beta\alpha}\, \delta_{ij}$ |   |
| $D^{ab}$ Ghost | $\Delta = \left(i\frac{1}{p^2+i\epsilon}\right) \delta_{ab}$ | 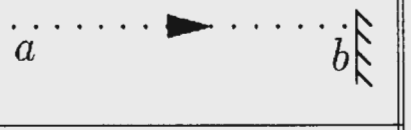  |
| $D^{ab}$ Ghost | $\Delta^* = -\left(i\frac{1}{p^2-i\epsilon}\right) \delta_{ab}$ |   |
| Cut Ghost | $\Delta = -2\pi\, \theta(p_0)\, \delta(p^2)\, \delta_{ab}$ | 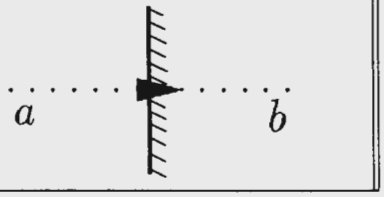  |

Table C.3: Feynman Rules for Propagators

# Appendix D

# QCD matrix elements

## D.1 $q\bar{q} \rightarrow s\bar{s}$

Evaluating the traces of equation 3.2 gives the numerator of the square of the invariant matrix element

$$4^2 \left[p_1^\mu p_2^\nu - p_1 \cdot p_2\, g^{\mu\nu} + p_1^\nu p_2^\mu - g^{\mu\nu} m^2 M^2\right] \left[p_\mu^3 p_\nu^4 - p_3 \cdot p_4\, g_{\mu\nu} + p_\mu^3 p_\nu^4 - g_{\mu\nu} m^2 M^2\right].$$

The lighter quarks have masses $m$ and strange quark $M$. Multiplying out the above gives

$$2 \cdot 16 \left[p_1 \cdot p_4\, p_3 \cdot p_2 + p_1 \cdot p_3\, p_4 \cdot p_2 + m^2 \left(p_1 \cdot p_2 + p_3 \cdot p_4\right) + 2m^2 M^2\right]. \qquad \text{(D.1)}$$

This can be reexpressed using a combination of the Mandelstam variables:

$$\begin{aligned} s &= 2m^2 + 2p_1 \cdot p_2 = 2M^2 + 2p_3 \cdot p_4, \\ u &= m^2 + M^2 - 2p_3 \cdot p_2 = m^2 + M^2 - 2p_1 \cdot p_4 \text{ and} \\ t &= m^2 + M^2 - 2p_3 \cdot p_1 = m^2 + M^2 - 2p_2 \cdot p_4. \end{aligned}$$

Hence equation D.1 becomes

$$8\left[\left(m^2 + M^2 - t\right)^2 + \left(m^2 + M^2 - u\right)^2 + 2s\left(m^2 + M^2\right)\right].$$

Next the following substitutions are needed

$$Q = p_1 + p_2.\ P = \frac{1}{2}\left(p_1 - p_2\right),\ Q' = p_3 + p_4,\ \text{and}\ P' = \frac{1}{2}\left(p_3 - p_4\right). \qquad \text{(D.2)}$$

The inverse is

$$p_1 = \frac{1}{2}\left(Q + 2P\right),\ p_3 = \frac{1}{2}\left(Q' + 2P'\right),\ p_2 = \frac{1}{2}\left(Q - 2P\right)\ \text{and}\ \ p_4 = \frac{1}{2}\left(Q' - 2P'\right). \qquad \text{(D.3)}$$

This has the property that

$$dp_1\, dp_2\, dp_3\, dp_4 = dP\, dP'\, dQ\, dQ'$$

and that

$$\begin{aligned} s &= Q^2 = Q'^2, \\ u &= (P' + P)^2 \text{ and} \\ t &= (P' - P)^2 . \end{aligned}$$

Now parameterising the above, we define

$$\begin{aligned} Q_\mu &= (q_0, 0, 0, q), \\ P_\mu &= (p_0, p\sin\theta, 0, p\cos\theta) \text{ and} \\ P'_\mu &= (p'_0, p'\sin\phi\sin\chi, p'\sin\phi\cos\chi, p'\cos\phi). \end{aligned}$$

It will be noticed that there are two products of delta functions that emerges through the cutting. One of the products is for example

$$\delta\left(\frac{q_0^2}{4} - \frac{q^2}{4} + q_0p_0 - pq\cos\theta + p_0^2 - p^2 - m^2\right)\delta\left(\frac{q_0^2}{4} - \frac{q^2}{4} - q_0p_0 + pq\cos\theta + p_0^2 - p^2 - m^2\right).$$

This we develop using $\delta\left(A(x) - B(x)\right)\delta\left(A(x) - B(x)\right) = \frac{1}{2}\delta\left(A(x)\right)\delta\left(B(x)\right)$

$$\delta\left(\frac{q_0^2}{4} - \frac{q^2}{4} + p_0^2 - p^2 - m^2\right)\delta\left(q_0p_0 - pq\cos\theta\right)$$

which becomes

$$\frac{1}{pqp}\delta\left(p - \sqrt{\frac{q_0^2}{4} - \frac{q^2}{4} + p_0^2 - m^2}\right)\delta\left(\frac{q_0p_0}{pq} - \cos\theta\right)$$

The kinematic constraints are obtained as follows:

$$q_0 = p_0^1 + p_0^2 > 2M$$

and

$$\begin{aligned} -1 \quad \leq \quad & \frac{q_0p_0}{pq} \leq 1 \Longrightarrow (q_0p_0)^2 \leq (pq)^2 \\ \Longrightarrow \quad & p_0^2 \leq \frac{q^2}{q_0^2}\left(\frac{q_0^2}{4} - \frac{q^2}{4} + p_0^2 - m^2\right) \\ \Longrightarrow \quad & p_0^2\left(1 - \frac{q^2}{q_0^2}\right) \leq \frac{q^2}{q_0^2}\left(\frac{s}{4} - m^2\right) \\ \Longrightarrow \quad & p_0^2 \leq \frac{q^2}{4}\left(1 - \frac{4m^2}{s}\right) \end{aligned}$$

and similarly for

$$p_0'^2 \leq \frac{q^2}{4}\left(1 - \frac{4M^2}{s}\right)$$

The integration over the delta functions can be performed, as well as the trivial integration. This leaves four remaining integrations that have to be done numerically. This leads to the final reparameterisation of the integration variables

$$\begin{aligned} q_0 &= -T \ln v + 2m, \\ q &= \left(q_0^2 - 4m^2\right)^{\frac{1}{2}} u, \\ p_0 &= \frac{q}{2}\left(1 - \frac{4m^2}{s}\right)^{\frac{1}{2}} x \text{ and} \\ p_0' &= \frac{q}{2}\left(1 - \frac{4M^2}{s}\right)^{\frac{1}{2}} y. \end{aligned}$$

Here $v$, $u$, $x$ and $y$ run between 0 and 1. The singular point at $v = 0$ is shielded by the Jacobian

$$dq_0\, dq\, dp_0\, dp_0' = \frac{-u^2}{4}\frac{T}{v}\left(1 - \frac{4m^2}{s}\right)^{\frac{1}{2}}\left(1 - \frac{4M^2}{s}\right)^{\frac{1}{2}}\left(q_0^2 - 4m^2\right)^{\frac{3}{2}} dv\, du\, dx\, dy.$$

Quite a substantial amount of work is required to convert the matrix elements into these new variables. We record an important intermediate result

few intermediate results

$$\begin{aligned} & \int d\chi \left(m^2 + M^2 - t\right)\left(m^2 + M^2 - u\right) \\ = & \int d\chi \frac{1}{4}\left[\left(s - 4p_0p_0' + 4\vec{p}\cdot\vec{p}'\right)^2 + \left(s + 4p_0p_0' - 4\vec{p}\cdot\vec{p}'\right)^2\right] \\ = & \int d\chi 2[\left(\frac{s}{2} - 2q_0p_0'\right)^2 + \frac{4}{q^4}((p_0p_0's)^2 \\ + & \; 2p_0p_0's\sqrt{-p_0'^2 s - q^2M^2 + \frac{s}{4}q^2}\sqrt{-p_0'^2 s - q^2m^2 + \frac{s}{4}q^2}\sin\chi \\ & + \left(\sqrt{-p_0'^2 s - q^2M^2 + \frac{s}{4}q^2}\sqrt{-p_0'^2 s - q^2m^2 + \frac{s}{4}q^2}\sin\chi\right)^2)] \\ = & \; 4\pi[\left(\frac{s}{2} - 2q_0p_0'\right)^2 + \frac{4}{q^4}((p_0p_0's)^2 + \frac{s^2}{2}\left(\frac{q^2}{4} - \frac{q^2M^2}{s} + p_0^{2'}\right)\left(\frac{q^2}{4} - \frac{q^2m^2}{s} + p_0^2\right))] \end{aligned}$$

Here we use

$$\vec{p}\cdot\vec{p}' = pp'\left(\sin\phi\sin\theta + \cos\theta\cos\phi\right)pp',$$

$$\vec{p}'\cdot\vec{q} = qp\cos\theta = q_0p_0,$$

$$\vec{p}\cdot\vec{q} = qp'\cos\phi = q_0p_0'$$

and

$$\cos\theta = \frac{q_op_o}{qp} \text{ and } \cos\phi = \frac{q_op_o'}{qp'}.$$

# Appendix E

# Particle Data Tables

## E.1 Table 0

This is simply the lowest lying meson octet and baryon decouplet. It can be obtained from either of the following two tables by taking the first 8 mesons and 10 baryons.

## E.2 Table 1

The following branching ratios were obtained from [107] and edited by the author and Jean Cleymans.

### E.2.1 Lowest lying mesons

| g | mass | s | S | B | $\Pi^+$ | $K^+$ | $K^-$ | $\bar{\Lambda}$ | $\Lambda$ | $\bar{\Sigma}$ | $\Sigma$ | $\rho^+$ | $\Xi^-$ |
|---|---|---|---|---|---|---|---|---|---|---|---|---|---|
| 3. | 0.139 | -1. | 0.0 | 0.0 | 0.333 | 0.000 | 0.000 | 0.000 | 0.000 | 0.000 | 0.000 | 0.000 | 0.000 |
| 1. | 0.549 | -1. | 0.0 | 0.0 | 0.286 | 0.000 | 0.000 | 0.000 | 0.000 | 0.000 | 0.000 | 0.000 | 0.000 |
| 9 | 0.770 | -1. | 0.0 | 0.0 | 0.666 | 0.000 | 0.000 | 0.000 | 0.000 | 0.000 | 0.000 | 0.330 | 0.000 |
| 3 | 0.782 | -1. | 0.0 | 0.0 | 0.910 | 0.000 | 0.000 | 0.000 | 0.000 | 0.000 | 0.000 | 0.000 | 0.000 |
| 1. | 0.958 | -1. | 0.0 | 0.0 | 0.441 | 0.000 | 0.000 | 0.000 | 0.000 | 0.000 | 0.000 | 0.300 | 0.000 |
| 1. | 0.975 | -1. | 0.0 | 0.0 | 0.390 | 0.110 | 0.110 | 0.000 | 0.000 | 0.000 | 0.000 | 0.000 | 0.000 |
| 3. | 0.980 | -1. | 0.0 | 0.0 | 0.008 | 0.013 | 0.013 | 0.000 | 0.000 | 0.000 | 0.000 | 0.000 | 0.000 |
| 3. | 1.020 | -1. | 0.0 | 0.0 | 0.134 | 0.495 | 0.495 | 0.000 | 0.000 | 0.000 | 0.000 | 0.040 | 0.000 |
| 3. | 1.170 | -1. | 0.0 | 0.0 | 0.025 | 0.000 | 0.000 | 0.000 | 0.000 | 0.000 | 0.000 | 0.000 | 0.000 |
| 9. | 1.235 | -1. | 0.0 | 0.0 | 0.995 | 0.025 | 0.025 | 0.000 | 0.000 | 0.000 | 0.000 | 0.030 | 0.000 |
| 9. | 1.260 | -1. | 0.0 | 0.0 | 0.900 | 0.000 | 0.000 | 0.000 | 0.000 | 0.000 | 0.000 | 0.330 | 0.000 |
| 5. | 1.270 | -1. | 0.0 | 0.0 | 0.550 | 0.021 | 0.021 | 0.000 | 0.000 | 0.000 | 0.000 | 0.000 | 0.000 |
| 3. | 1.285 | -1. | 0.0 | 0.0 | 0.482 | 0.055 | 0.055 | 0.000 | 0.000 | 0.000 | 0.000 | 0.000 | 0.000 |
| 3. | 1.300 | -1. | 0.0 | 0.0 | 0.000 | 0.000 | 0.000 | 0.000 | 0.000 | 0.000 | 0.000 | 0.000 | 0.000 |
| 15. | 1.320 | -1. | 0.0 | 0.0 | 0.898 | 0.025 | 0.025 | 0.000 | 0.000 | 0.000 | 0.000 | 0.230 | 0.000 |
| 1. | 1.400 | -1. | 0.0 | 0.0 | 0.465 | 0.035 | 0.035 | 0.000 | 0.000 | 0.000 | 0.000 | 0.000 | 0.000 |
| 3. | 1.420 | -1. | 0.0 | 0.0 | 0.021 | 0.013 | 0.013 | 0.000 | 0.000 | 0.000 | 0.000 | 0.000 | 0.000 |
| 5. | 1.525 | -1. | 0.0 | 0.0 | 0.000 | 0.450 | 0.450 | 0.000 | 0.000 | 0.000 | 0.000 | 0.000 | 0.000 |
| 15. | 1.670 | -1. | 0.0 | 0.0 | 0.775 | 0.020 | 0.020 | 0.000 | 0.000 | 0.000 | 0.000 | 0.110 | 0.000 |

| | | | | | | | | | | | | | |
|---|---|---|---|---|---|---|---|---|---|---|---|---|---|
| 21. | 1.690 | -1. | 0.0 | 0.0 | 0.842 | 0.027 | 0.027 | 0.000 | 0.000 | 0.000 | 0.000 | 0.000 | 0.000 |
| 9. | 1.700 | -1. | 0.0 | 0.0 | 0.000 | 0.000 | 0.000 | 0.000 | 0.000 | 0.000 | 0.000 | 0.000 | 0.000 |
| 5. | 1.680 | -1. | 0.0 | 0.0 | 0.020 | 0.190 | 0.190 | 0.000 | 0.000 | 0.000 | 0.000 | 0.000 | 0.000 |
| 2. | 0.494 | -1. | 1.0 | 0.0 | 0.000 | 0.500 | 0.000 | 0.000 | 0.000 | 0.000 | 0.000 | 0.000 | 0.000 |
| 6. | 0.892 | -1. | 1.0 | 0.0 | 0.333 | 0.500 | 0.000 | 0.000 | 0.000 | 0.000 | 0.000 | 0.000 | 0.000 |
| 6. | 1.270 | -1. | 1.0 | 0.0 | 0.685 | 0.507 | 0.000 | 0.000 | 0.000 | 0.000 | 0.000 | 0.000 | 0.000 |
| 6. | 1.400 | -1. | 1.0 | 0.0 | 0.664 | 0.504 | 0.000 | 0.000 | 0.000 | 0.000 | 0.000 | 0.000 | 0.000 |
| 8. | 1.430 | -1. | 1.0 | 0.0 | 0.566 | 0.849 | 0.000 | 0.000 | 0.000 | 0.000 | 0.000 | 0.000 | 0.000 |
| 10. | 1.430 | -1. | 1.0 | 0.0 | 0.695 | 0.498 | 0.000 | 0.000 | 0.000 | 0.000 | 0.000 | 0.000 | 0.000 |
| 6. | 1.715 | -1. | 1.0 | 0.0 | 0.537 | 0.500 | 0.000 | 0.000 | 0.000 | 0.000 | 0.000 | 0.000 | 0.000 |
| 10. | 1.770 | -1. | 1.0 | 0.0 | 0.582 | 0.367 | 0.000 | 0.000 | 0.000 | 0.000 | 0.000 | 0.000 | 0.000 |
| 14. | 1.780 | -1. | 1.0 | 0.0 | 0.573 | 0.505 | 0.000 | 0.000 | 0.000 | 0.000 | 0.000 | 0.000 | 0.000 |
| 2. | 0.494 | -1. | -1.0 | 0.0 | 0.000 | 0.000 | 0.500 | 0.000 | 0.000 | 0.000 | 0.000 | 0.000 | 0.000 |
| 6. | 0.892 | -1. | -1.0 | 0.0 | 0.333 | 0.000 | 0.500 | 0.000 | 0.000 | 0.000 | 0.000 | 0.000 | 0.000 |
| 6. | 1.270 | -1. | -1.0 | 0.0 | 0.685 | 0.000 | 0.507 | 0.000 | 0.000 | 0.000 | 0.000 | 0.000 | 0.000 |
| 6. | 1.400 | -1. | -1.0 | 0.0 | 0.664 | 0.000 | 0.504 | 0.000 | 0.000 | 0.000 | 0.000 | 0.000 | 0.000 |
| 8. | 1.430 | -1. | -1.0 | 0.0 | 0.566 | 0.000 | 0.849 | 0.000 | 0.000 | 0.000 | 0.000 | 0.000 | 0.000 |
| 10. | 1.430 | -1. | -1.0 | 0.0 | 0.695 | 0.000 | 0.498 | 0.000 | 0.000 | 0.000 | 0.000 | 0.000 | 0.000 |
| 6. | 1.715 | -1. | -1.0 | 0.0 | 0.537 | 0.000 | 0.500 | 0.000 | 0.000 | 0.000 | 0.000 | 0.000 | 0.000 |
| 10. | 1.770 | -1. | -1.0 | 0.0 | 0.582 | 0.000 | 0.367 | 0.000 | 0.000 | 0.000 | 0.000 | 0.000 | 0.000 |
| 14. | 1.780 | -1. | -1.0 | 0.0 | 0.573 | 0.000 | 0.505 | 0.000 | 0.000 | 0.000 | 0.000 | 0.000 | 0.000 |

### E.2.2 Lowest lying baryons

| g | mass | s | S | B | $\Pi^+$ | $K^+$ | $K^-$ | $\bar{\Lambda}$ | $\Lambda$ | $\bar{\Sigma}$ | $\Sigma$ | $\rho^+$ | $\Xi^-$ |
|---|---|---|---|---|---|---|---|---|---|---|---|---|---|
| 4. | 0.939 | 1. | 0. | 1. | 0.000 | 0.000 | 0.000 | 0.000 | 0.000 | 0.000 | 0.000 | 0.000 | 0.000 |
| 4. | 1.440 | 1. | 0. | 1. | 0.446 | 0.000 | 0.000 | 0.000 | 0.000 | 0.000 | 0.000 | 0.000 | 0.000 |
| 8. | 1.520 | 1. | 0. | 1. | 0.483 | 0.000 | 0.000 | 0.000 | 0.000 | 0.000 | 0.000 | 0.000 | 0.000 |
| 4. | 1.535 | 1. | 0. | 1. | 0.203 | 0.000 | 0.000 | 0.000 | 0.000 | 0.000 | 0.000 | 0.000 | 0.000 |
| 4. | 1.650 | 1. | 0. | 1. | 0.390 | 0.040 | 0.000 | 0.000 | 0.080 | 0.000 | 0.000 | 0.000 | 0.000 |
| 12. | 1.675 | 1. | 0. | 1. | 0.534 | 0.000 | 0.000 | 0.000 | 0.000 | 0.000 | 0.000 | 0.000 | 0.000 |
| 12. | 1.680 | 1. | 0. | 1. | 0.441 | 0.000 | 0.000 | 0.000 | 0.000 | 0.000 | 0.000 | 0.000 | 0.000 |
| 8. | 1.700 | 1. | 0. | 1. | 0.566 | 0.000 | 0.000 | 0.000 | 0.000 | 0.000 | 0.000 | 0.000 | 0.000 |
| 4. | 1.710 | 1. | 0. | 1. | 0.291 | 0.105 | 0.000 | 0.000 | 0.150 | 0.000 | 0.020 | 0.000 | 0.000 |
| 8. | 1.720 | 1. | 0. | 1. | 0.525 | 0.043 | 0.000 | 0.000 | 0.050 | 0.000 | 0.020 | 0.000 | 0.000 |
| 16. | 2.190 | 1. | 0. | 1. | 0.000 | 0.000 | 0.000 | 0.000 | 0.000 | 0.000 | 0.000 | 0.000 | 0.000 |
| 20. | 2.220 | 1. | 0. | 1. | 0.000 | 0.000 | 0.000 | 0.000 | 0.000 | 0.000 | 0.000 | 0.000 | 0.000 |
| 20. | 2.250 | 1. | 0. | 1. | 0.000 | 0.000 | 0.000 | 0.000 | 0.000 | 0.000 | 0.000 | 0.000 | 0.000 |
| 24. | 2.600 | 1. | 0. | 1. | 0.000 | 0.000 | 0.000 | 0.000 | 0.000 | 0.000 | 0.000 | 0.000 | 0.000 |
| 16. | 1.232 | 1. | 0. | 1. | 0.331 | 0.000 | 0.000 | 0.000 | 0.000 | 0.000 | 0.000 | 0.000 | 0.000 |
| 8. | 1.620 | 1. | 0. | 1. | 0.582 | 0.000 | 0.000 | 0.000 | 0.000 | 0.000 | 0.000 | 0.000 | 0.000 |
| 16. | 1.700 | 1. | 0. | 1. | 0.615 | 0.000 | 0.000 | 0.000 | 0.000 | 0.000 | 0.000 | 0.000 | 0.000 |
| 8. | 1.900 | 1. | 0. | 1. | 0.033 | 0.000 | 0.000 | 0.000 | 0.000 | 0.000 | 0.000 | 0.000 | 0.000 |
| 24. | 1.905 | 1. | 0. | 1. | 0.516 | 0.010 | 0.000 | 0.000 | 0.000 | 0.000 | 0.000 | 0.000 | 0.000 |
| 8. | 1.910 | 1. | 0. | 1. | 0.552 | 0.000 | 0.000 | 0.000 | 0.000 | 0.000 | 0.000 | 0.000 | 0.000 |

| | | | | | | | | | | | | | |
|---|---|---|---|---|---|---|---|---|---|---|---|---|---|
| 16. | 1.920 | 1. | 0. | 1. | 0.058 | 0.025 | 0.000 | 0.000 | 0.000 | 0.000 | 0.000 | 0.000 | 0.000 |
| 24. | 1.930 | 1. | 0. | 1. | 0.050 | 0.000 | 0.000 | 0.000 | 0.000 | 0.000 | 0.000 | 0.000 | 0.000 |
| 32. | 1.950 | 1. | 0. | 1. | 0.386 | 0.000 | 0.000 | 0.000 | 0.000 | 0.000 | 0.000 | 0.000 | 0.000 |
| 48. | 2.420 | 1. | 0. | 1. | 0.030 | 0.000 | 0.000 | 0.000 | 0.000 | 0.000 | 0.000 | 0.000 | 0.000 |
| 2. | 1.115 | 1. | -1. | 1. | 0.000 | 0.000 | 0.000 | 0.000 | 1.000 | 0.000 | 0.000 | 0.000 | 0.000 |
| 2. | 1.405 | 1. | -1. | 1. | 0.333 | 0.000 | 0.000 | 0.000 | 0.000 | 0.000 | 0.330 | 0.000 | 0.000 |
| 4. | 1.520 | 1. | -1. | 1. | 0.195 | 0.000 | 0.225 | 0.000 | 0.100 | 0.000 | 0.130 | 0.000 | 0.000 |
| 2. | 1.600 | 1. | -1. | 1. | 0.117 | 0.000 | 0.125 | 0.000 | 0.000 | 0.000 | 0.120 | 0.000 | 0.000 |
| 2. | 1.670 | 1. | -1. | 1. | 0.133 | 0.000 | 0.100 | 0.000 | 0.250 | 0.000 | 0.130 | 0.000 | 0.000 |
| 4. | 1.690 | 1. | -1. | 1. | 0.325 | 0.000 | 0.125 | 0.000 | 0.250 | 0.000 | 0.170 | 0.000 | 0.000 |
| 2. | 1.800 | 1. | -1. | 1. | 0.142 | 0.000 | 0.406 | 0.000 | 0.000 | 0.000 | 0.000 | 0.000 | 0.000 |
| 2. | 1.810 | 1. | -1. | 1. | 0.142 | 0.000 | 0.406 | 0.000 | 0.000 | 0.000 | 0.080 | 0.000 | 0.000 |
| 6. | 1.820 | 1. | -1. | 1. | 0.263 | 0.000 | 0.166 | 0.000 | 0.060 | 0.000 | 0.050 | 0.000 | 0.000 |
| 6. | 1.830 | 1. | -1. | 1. | 0.142 | 0.000 | 0.406 | 0.000 | 0.130 | 0.000 | 0.200 | 0.000 | 0.000 |
| 4. | 1.890 | 1. | -1. | 1. | 0.047 | 0.000 | 0.150 | 0.000 | 0.000 | 0.000 | 0.020 | 0.000 | 0.000 |
| 8. | 2.100 | 1. | -1. | 1. | 0.142 | 0.000 | 0.406 | 0.000 | 0.000 | 0.000 | 0.020 | 0.000 | 0.000 |
| 6. | 2.110 | 1. | -1. | 1. | 0.142 | 0.000 | 0.406 | 0.000 | 0.000 | 0.000 | 0.080 | 0.000 | 0.000 |
| 10. | 2.350 | 1. | -1. | 1. | 0.142 | 0.000 | 0.406 | 0.000 | 0.000 | 0.000 | 0.030 | 0.000 | 0.000 |
| 6. | 1.192 | 1. | -1. | 1. | 0.000 | 0.000 | 0.000 | 0.000 | 0.000 | 0.000 | 0.330 | 0.000 | 0.000 |
| 12. | 1.385 | 1. | -1. | 1. | 0.333 | 0.000 | 0.000 | 0.000 | 0.880 | 0.000 | 0.040 | 0.000 | 0.000 |
| 6. | 1.660 | 1. | -1. | 1. | 0.050 | 0.000 | 0.100 | 0.000 | 0.000 | 0.000 | 0.000 | 0.000 | 0.000 |
| 12. | 1.670 | 1. | -1. | 1. | 0.183 | 0.000 | 0.050 | 0.000 | 0.100 | 0.000 | 0.150 | 0.000 | 0.000 |
| 6. | 1.750 | 1. | -1. | 1. | 0.025 | 0.000 | 0.125 | 0.000 | 0.000 | 0.000 | 0.120 | 0.000 | 0.000 |
| 18. | 1.775 | 1. | -1. | 1. | 0.240 | 0.000 | 0.245 | 0.000 | 0.280 | 0.000 | 0.040 | 0.000 | 0.000 |
| 18. | 1.915 | 1. | -1. | 1. | 0.037 | 0.000 | 0.050 | 0.000 | 0.000 | 0.000 | 0.000 | 0.000 | 0.000 |
| 12. | 1.940 | 1. | -1. | 1. | 0.058 | 0.000 | 0.121 | 0.000 | 0.000 | 0.000 | 0.000 | 0.000 | 0.000 |
| 24. | 2.030 | 1. | -1. | 1. | 0.250 | 0.000 | 0.236 | 0.000 | 0.030 | 0.000 | 0.060 | 0.000 | 0.000 |
| 4. | 1.320 | 1. | -2. | 1. | 0.000 | 0.000 | 0.000 | 0.000 | 0.000 | 0.000 | 0.000 | 0.000 | 0.500 |
| 8. | 1.530 | 1. | -2. | 1. | 0.333 | 0.000 | 0.000 | 0.000 | 0.000 | 0.000 | 0.000 | 0.000 | 1.000 |
| 8. | 1.820 | 1. | -2. | 1. | 0.317 | 0.000 | 0.475 | 0.000 | 0.000 | 0.000 | 0.000 | 0.000 | 0.033 |
| 4. | 1.672 | 1. | -3. | 1. | 0.000 | 0.000 | 0.000 | 0.000 | 0.680 | 0.000 | 0.000 | 0.000 | 0.090 |

## E.3 Table 2

The following branching ratios were obtained from [107] and edited by the author and Neven Bilić.

### E.3.1 Lowest lying mesons

| g | mass | s | S | B | $\Pi^+$ | $K^+$ | $K^-$ | $\bar{\Lambda}$ | $\Lambda$ | $\bar{\Sigma}$ | $\Sigma$ | $\rho^+$ | $\Xi^-$ |
|---|---|---|---|---|---|---|---|---|---|---|---|---|---|
| 3 | 0.139 | 0.0 | 0 | 0 | 0.333 | 0.000 | 0.000 | 0.000 | 0.000 | 0.000 | 0.000 | 0.000 | 0.000 |
| 1 | 0.547 | 0.0 | 0 | 0 | 0.285 | 0.000 | 0.000 | 0.000 | 0.000 | 0.000 | 0.000 | 0.000 | 0.000 |
| 9 | 0.768 | 1.0 | 0 | 0 | 0.667 | 0.000 | 0.000 | 0.000 | 0.000 | 0.000 | 0.000 | 0.333 | 0.000 |
| 3 | 0.782 | 1.0 | 0 | 0 | 0.910 | 0.000 | 0.000 | 0.000 | 0.000 | 0.000 | 0.000 | 0.000 | 0.000 |

| | | | | | | | | | | | | | |
|---|---|---|---|---|---|---|---|---|---|---|---|---|---|
| 1 | 0.958 | 0.0 | 0 | 0 | 0.953 | 0.000 | 0.000 | 0.000 | 0.000 | 0.000 | 0.000 | 0.000 | 0.000 |
| 1 | 0.974 | 0.0 | 0 | 0 | 0.521 | 0.110 | 0.110 | 0.000 | 0.000 | 0.000 | 0.000 | 0.000 | 0.000 |
| 3 | 0.983 | 0.0 | 0 | 0 | 0.206 | 0.167 | 0.167 | 0.000 | 0.000 | 0.000 | 0.000 | 0.000 | 0.000 |
| 3 | 1.019 | 1.0 | 0 | 0 | 0.157 | 0.491 | 0.491 | 0.000 | 0.000 | 0.000 | 0.000 | 0.043 | 0.000 |
| 3 | 1.170 | 1.0 | 0 | 0 | 1.000 | 0.000 | 0.000 | 0.000 | 0.000 | 0.000 | 0.000 | 0.333 | 0.000 |
| 9 | 1.232 | 1.0 | 0 | 0 | 1.243 | 0.000 | 0.000 | 0.000 | 0.000 | 0.000 | 0.000 | 0.000 | 0.000 |
| 9 | 1.260 | 1.0 | 0 | 0 | 1.000 | 0.000 | 0.000 | 0.000 | 0.000 | 0.000 | 0.000 | 0.333 | 0.000 |
| 5 | 1.275 | 2.0 | 0 | 0 | 0.691 | 0.023 | 0.023 | 0.000 | 0.000 | 0.000 | 0.000 | 0.000 | 0.000 |
| 3 | 1.282 | 1.0 | 0 | 0 | 1.022 | 0.059 | 0.059 | 0.000 | 0.000 | 0.000 | 0.000 | 0.127 | 0.000 |
| 1 | 1.295 | 0.0 | 0 | 0 | 0.912 | 0.083 | 0.083 | 0.000 | 0.000 | 0.000 | 0.000 | 0.000 | 0.000 |
| 3 | 1.300 | 0.0 | 0 | 0 | 1.000 | 0.000 | 0.000 | 0.000 | 0.000 | 0.000 | 0.000 | 0.167 | 0.000 |
| 15 | 1.318 | 2.0 | 0 | 0 | 0.957 | 0.025 | 0.025 | 0.000 | 0.000 | 0.000 | 0.000 | 0.234 | 0.000 |
| 3 | 1.394 | 1.0 | 0 | 0 | 1.000 | 0.000 | 0.000 | 0.000 | 0.000 | 0.000 | 0.000 | 0.333 | 0.000 |
| 1 | 1.400 | 0.0 | 0 | 0 | 0.624 | 0.037 | 0.037 | 0.000 | 0.000 | 0.000 | 0.000 | 0.000 | 0.000 |
| 3 | 1.426 | 1.0 | 0 | 0 | 0.333 | 0.500 | 0.500 | 0.000 | 0.000 | 0.000 | 0.000 | 0.000 | 0.000 |
| 1 | 1.420 | 0.0 | 0 | 0 | 0.789 | 0.167 | 0.167 | 0.000 | 0.000 | 0.000 | 0.000 | 0.000 | 0.000 |
| 9 | 1.465 | 1.0 | 0 | 0 | 0.666 | 0.000 | 0.000 | 0.000 | 0.000 | 0.000 | 0.000 | 0.000 | 0.000 |
| 3 | 1.512 | 1.0 | 0 | 0 | 0.333 | 1.000 | 1.000 | 0.000 | 0.000 | 0.000 | 0.000 | 0.000 | 0.000 |
| 5 | 1.525 | 2.0 | 0 | 0 | 0.159 | 0.356 | 0.356 | 0.000 | 0.000 | 0.000 | 0.000 | 0.000 | 0.000 |
| 1 | 1.587 | 0.0 | 0 | 0 | 0.762 | 0.000 | 0.000 | 0.000 | 0.000 | 0.000 | 0.000 | 0.000 | 0.000 |
| 3 | 1.594 | 1.0 | 0 | 0 | 0.858 | 0.000 | 0.000 | 0.000 | 0.000 | 0.000 | 0.000 | 0.111 | 0.000 |
| 7 | 1.668 | 3.0 | 0 | 0 | 1.288 | 0.000 | 0.000 | 0.000 | 0.000 | 0.000 | 0.000 | 0.167 | 0.000 |
| 15 | 1.670 | 2.0 | 0 | 0 | 0.983 | 0.058 | 0.058 | 0.000 | 0.000 | 0.000 | 0.000 | 0.103 | 0.000 |
| 3 | 1.680 | 1.0 | 0 | 0 | 0.333 | 1.000 | 1.000 | 0.000 | 0.000 | 0.000 | 0.000 | 0.000 | 0.000 |
| 21 | 1.691 | 3.0 | 0 | 0 | 1.118 | 0.027 | 0.027 | 0.000 | 0.000 | 0.000 | 0.000 | 0.000 | 0.000 |
| 9 | 1.700 | 1.0 | 0 | 0 | 1.333 | 0.000 | 0.000 | 0.000 | 0.000 | 0.000 | 0.000 | 0.333 | 0.000 |
| 1 | 1.709 | 0.0 | 0 | 0 | 0.333 | 0.250 | 0.250 | 0.000 | 0.000 | 0.000 | 0.000 | 0.000 | 0.000 |
| 7 | 1.854 | 3.0 | 0 | 0 | 0.167 | 0.750 | 0.750 | 0.000 | 0.000 | 0.000 | 0.000 | 0.000 | 0.000 |
| 5 | 2.011 | 2.0 | 0 | 0 | 0.313 | 0.982 | 0.982 | 0.000 | 0.000 | 0.000 | 0.000 | 0.086 | 0.000 |
| 9 | 2.049 | 4.0 | 0 | 0 | 0.568 | 0.000 | 0.000 | 0.000 | 0.000 | 0.000 | 0.000 | 0.000 | 0.000 |
| 5 | 2.297 | 2.0 | 0 | 0 | 0.313 | 0.982 | 0.982 | 0.000 | 0.000 | 0.000 | 0.000 | 0.086 | 0.000 |
| 5 | 2.339 | 2.0 | 0 | 0 | 0.313 | 0.982 | 0.982 | 0.000 | 0.000 | 0.000 | 0.000 | 0.086 | 0.000 |
| 2 | 0.494 | 0.0 | +1 | 0 | 0.000 | 0.500 | 0.000 | 0.000 | 0.000 | 0.000 | 0.000 | 0.000 | 0.000 |
| 6 | 0.892 | 1.0 | +1 | 0 | 0.333 | 0.500 | 0.000 | 0.000 | 0.000 | 0.000 | 0.000 | 0.000 | 0.000 |
| 6 | 1.270 | 1.0 | +1 | 0 | 0.686 | 0.491 | 0.000 | 0.000 | 0.000 | 0.000 | 0.000 | 0.140 | 0.000 |
| 6 | 1.402 | 1.0 | +1 | 0 | 0.668 | 0.501 | 0.000 | 0.000 | 0.000 | 0.000 | 0.000 | 0.010 | 0.000 |
| 6 | 1.412 | 1.0 | +1 | 0 | 0.589 | 0.458 | 0.000 | 0.000 | 0.000 | 0.000 | 0.000 | 0.017 | 0.000 |
| 2 | 1.429 | 0.0 | +1 | 0 | 0.310 | 0.465 | 0.000 | 0.000 | 0.000 | 0.000 | 0.000 | 0.000 | 0.000 |
| 10 | 1.430 | 2.0 | +1 | 0 | 0.543 | 0.489 | 0.000 | 0.000 | 0.000 | 0.000 | 0.000 | 0.029 | 0.000 |
| 6 | 1.714 | 1.0 | +1 | 0 | 0.538 | 0.500 | 0.000 | 0.000 | 0.000 | 0.000 | 0.000 | 0.105 | 0.000 |
| 10 | 1.768 | 2.0 | +1 | 0 | 0.876 | 0.489 | 0.000 | 0.000 | 0.000 | 0.000 | 0.000 | 0.029 | 0.000 |
| 14 | 1.770 | 3.0 | +1 | 0 | 0.569 | 0.498 | 0.000 | 0.000 | 0.000 | 0.000 | 0.000 | 0.150 | 0.000 |
| 18 | 2.045 | 4.0 | +1 | 0 | 0.340 | 0.217 | 0.000 | 0.000 | 0.000 | 0.000 | 0.000 | 0.020 | 0.000 |
| 2 | 0.494 | 0.0 | −1 | 0 | 0.000 | 0.000 | 0.500 | 0.000 | 0.000 | 0.000 | 0.000 | 0.000 | 0.000 |
| 6 | 0.892 | 1.0 | −1 | 0 | 0.333 | 0.000 | 0.500 | 0.000 | 0.000 | 0.000 | 0.000 | 0.000 | 0.000 |
| 6 | 1.270 | 1.0 | −1 | 0 | 0.686 | 0.000 | 0.491 | 0.000 | 0.000 | 0.000 | 0.000 | 0.140 | 0.000 |

| | | | | | | | | | | | | | |
|---|---|---|---|---|---|---|---|---|---|---|---|---|---|
| 6 | 1.402 | 1.0 | −1 | 0 | 0.668 | 0.000 | 0.501 | 0.000 | 0.000 | 0.000 | 0.000 | 0.010 | 0.000 |
| 6 | 1.412 | 1.0 | −1 | 0 | 0.589 | 0.000 | 0.458 | 0.000 | 0.000 | 0.000 | 0.000 | 0.017 | 0.000 |
| 2 | 1.429 | 0.0 | −1 | 0 | 0.310 | 0.000 | 0.465 | 0.000 | 0.000 | 0.000 | 0.000 | 0.000 | 0.000 |
| 10 | 1.430 | 2.0 | −1 | 0 | 0.543 | 0.000 | 0.489 | 0.000 | 0.000 | 0.000 | 0.000 | 0.029 | 0.000 |
| 6 | 1.714 | 1.0 | −1 | 0 | 0.538 | 0.000 | 0.500 | 0.000 | 0.000 | 0.000 | 0.000 | 0.105 | 0.000 |
| 10 | 1.768 | 2.0 | −1 | 0 | 0.876 | 0.000 | 0.489 | 0.000 | 0.000 | 0.000 | 0.000 | 0.029 | 0.000 |
| 14 | 1.770 | 3.0 | −1 | 0 | 0.569 | 0.000 | 0.498 | 0.000 | 0.000 | 0.000 | 0.000 | 0.150 | 0.000 |
| 18 | 2.045 | 4.0 | −1 | 0 | 0.340 | 0.000 | 0.217 | 0.000 | 0.000 | 0.000 | 0.000 | 0.020 | 0.000 |

### E.3.2 Lowest lying baryons

| g | mass | s | S | B | $\Pi^+$ | $K^+$ | $K^-$ | $\bar{\Lambda}$ | $\Lambda$ | $\bar{\Sigma}$ | $\Sigma$ | $\rho^+$ | $\Xi^-$ |
|---|---|---|---|---|---|---|---|---|---|---|---|---|---|
| 4 | 0.939 | 0.5 | 0 | 1 | 0.000 | 0.000 | 0.000 | 0.000 | 0.000 | 0.000 | 0.000 | 0.000 | 0.000 |
| 4 | 1.440 | 0.5 | 0 | 1 | 0.450 | 0.000 | 0.000 | 0.000 | 0.000 | 0.000 | 0.000 | 0.000 | 0.000 |
| 8 | 1.520 | 1.5 | 0 | 1 | 0.483 | 0.000 | 0.000 | 0.000 | 0.000 | 0.000 | 0.000 | 0.067 | 0.000 |
| 4 | 1.535 | 0.5 | 0 | 1 | 0.381 | 0.000 | 0.000 | 0.000 | 0.000 | 0.000 | 0.000 | 0.017 | 0.000 |
| 4 | 1.650 | 0.5 | 0 | 1 | 0.383 | 0.035 | 0.000 | 0.000 | 0.070 | 0.000 | 0.000 | 0.033 | 0.000 |
| 12 | 1.675 | 2.5 | 0 | 1 | 0.513 | 0.000 | 0.000 | 0.000 | 0.000 | 0.000 | 0.000 | 0.017 | 0.000 |
| 12 | 1.680 | 2.5 | 0 | 1 | 0.450 | 0.000 | 0.000 | 0.000 | 0.000 | 0.000 | 0.000 | 0.033 | 0.000 |
| 8 | 1.700 | 1.5 | 0 | 1 | 0.633 | 0.001 | 0.000 | 0.000 | 0.002 | 0.000 | 0.000 | 0.033 | 0.000 |
| 4 | 1.710 | 0.5 | 0 | 1 | 0.421 | 0.075 | 0.000 | 0.000 | 0.150 | 0.000 | 0.000 | 0.050 | 0.000 |
| 8 | 1.720 | 1.5 | 0 | 1 | 0.555 | 0.035 | 0.000 | 0.000 | 0.070 | 0.000 | 0.000 | 0.167 | 0.000 |
| 16 | 2.190 | 3.5 | 0 | 1 | 0.322 | 0.002 | 0.000 | 0.000 | 0.003 | 0.000 | 0.000 | 0.100 | 0.000 |
| 20 | 2.220 | 4.5 | 0 | 1 | 0.053 | 0.000 | 0.000 | 0.000 | 0.000 | 0.000 | 0.000 | 0.000 | 0.000 |
| 20 | 2.250 | 4.5 | 0 | 1 | 0.039 | 0.002 | 0.000 | 0.000 | 0.003 | 0.000 | 0.000 | 0.000 | 0.000 |
| 24 | 2.600 | 5.5 | 0 | 1 | 0.027 | 0.000 | 0.000 | 0.000 | 0.000 | 0.000 | 0.000 | 0.000 | 0.000 |
| 16 | 1.232 | 1.5 | 0 | 1 | 0.331 | 0.000 | 0.000 | 0.000 | 0.000 | 0.000 | 0.000 | 0.000 | 0.000 |
| 16 | 1.600 | 1.5 | 0 | 1 | 0.607 | 0.000 | 0.000 | 0.000 | 0.000 | 0.000 | 0.000 | 0.043 | 0.000 |
| 8 | 1.620 | 0.5 | 0 | 1 | 0.583 | 0.000 | 0.000 | 0.000 | 0.000 | 0.000 | 0.000 | 0.093 | 0.000 |
| 16 | 1.700 | 1.5 | 0 | 1 | 0.617 | 0.000 | 0.000 | 0.000 | 0.000 | 0.000 | 0.000 | 0.133 | 0.000 |
| 8 | 1.900 | 1.5 | 0 | 1 | 0.067 | 0.000 | 0.000 | 0.000 | 0.000 | 0.000 | 0.000 | 0.000 | 0.000 |
| 24 | 1.905 | 2.5 | 0 | 1 | 0.633 | 0.001 | 0.000 | 0.000 | 0.000 | 0.000 | 0.001 | 0.250 | 0.000 |
| 8 | 1.910 | 0.5 | 0 | 1 | 0.590 | 0.000 | 0.000 | 0.000 | 0.000 | 0.000 | 0.000 | 0.050 | 0.000 |
| 16 | 1.920 | 1.5 | 0 | 1 | 0.043 | 0.010 | 0.000 | 0.000 | 0.000 | 0.000 | 0.007 | 0.000 | 0.000 |
| 24 | 1.930 | 2.5 | 0 | 1 | 0.050 | 0.000 | 0.000 | 0.000 | 0.000 | 0.000 | 0.000 | 0.000 | 0.000 |
| 32 | 1.950 | 3.5 | 0 | 1 | 0.327 | 0.004 | 0.000 | 0.000 | 0.000 | 0.000 | 0.002 | 0.017 | 0.000 |
| 48 | 2.420 | 5.5 | 0 | 1 | 0.033 | 0.003 | 0.000 | 0.000 | 0.000 | 0.000 | 0.002 | 0.000 | 0.000 |
| 2 | 1.115 | 0.5 | −1 | 1 | 0.000 | 0.000 | 0.000 | 0.000 | 1.000 | 0.000 | 0.000 | 0.000 | 0.000 |
| 2 | 1.405 | 0.5 | −1 | 1 | 0.000 | 0.000 | 0.000 | 0.000 | 0.000 | 0.000 | 0.333 | 0.000 | 0.000 |
| 4 | 1.520 | 1.5 | −1 | 1 | 0.073 | 0.000 | 0.225 | 0.000 | 0.108 | 0.000 | 0.143 | 0.000 | 0.000 |
| 2 | 1.600 | 0.5 | −1 | 1 | 0.000 | 0.000 | 0.115 | 0.000 | 0.000 | 0.000 | 0.117 | 0.000 | 0.000 |
| 2 | 1.670 | 0.5 | −1 | 1 | 0.071 | 0.000 | 0.100 | 0.000 | 0.250 | 0.000 | 0.133 | 0.000 | 0.000 |
| 4 | 1.690 | 1.5 | −1 | 1 | 0.300 | 0.000 | 0.125 | 0.000 | 0.250 | 0.000 | 0.167 | 0.000 | 0.000 |
| 2 | 1.800 | 0.5 | −1 | 1 | 0.220 | 0.000 | 0.275 | 0.000 | 0.194 | 0.000 | 0.082 | 0.000 | 0.000 |
| 2 | 1.810 | 0.5 | −1 | 1 | 0.150 | 0.000 | 0.400 | 0.000 | 0.000 | 0.000 | 0.083 | 0.000 | 0.000 |

| | | | | | | | | | | | | |
|---|---|---|---|---|---|---|---|---|---|---|---|---|
| 6 | 1.820 | 2.5 | −1 | 1 | 0.053 | 0.000 | 0.300 | 0.000 | 0.070 | 0.000 | 0.040 | 0.000 | 0.000 |
| 6 | 1.830 | 2.5 | −1 | 1 | 0.127 | 0.000 | 0.225 | 0.000 | 0.000 | 0.000 | 0.183 | 0.000 | 0.000 |
| 4 | 1.890 | 1.5 | −1 | 1 | 0.300 | 0.000 | 0.290 | 0.000 | 0.264 | 0.000 | 0.035 | 0.000 | 0.000 |
| 8 | 2.100 | 3.5 | −1 | 1 | 0.095 | 0.000 | 0.270 | 0.000 | 0.060 | 0.000 | 0.017 | 0.000 | 0.000 |
| 6 | 2.110 | 2.5 | −1 | 1 | 0.307 | 0.000 | 0.250 | 0.000 | 0.226 | 0.000 | 0.088 | 0.000 | 0.000 |
| 10 | 2.350 | 4.5 | −1 | 1 | 0.000 | 0.000 | 0.060 | 0.000 | 0.000 | 0.000 | 0.033 | 0.000 | 0.000 |
| 6 | 1.192 | 0.5 | −1 | 1 | 0.000 | 0.000 | 0.000 | 0.000 | 0.000 | 0.000 | 0.333 | 0.000 | 0.000 |
| 12 | 1.385 | 1.5 | −1 | 1 | 0.293 | 0.000 | 0.000 | 0.000 | 0.880 | 0.000 | 0.040 | 0.000 | 0.000 |
| 6 | 1.660 | 0.5 | −1 | 1 | 0.133 | 0.000 | 0.100 | 0.000 | 0.400 | 0.000 | 0.133 | 0.000 | 0.000 |
| 12 | 1.670 | 1.5 | −1 | 1 | 0.033 | 0.000 | 0.050 | 0.000 | 0.100 | 0.000 | 0.150 | 0.000 | 0.000 |
| 6 | 1.750 | 0.5 | −1 | 1 | 0.110 | 0.000 | 0.125 | 0.000 | 0.300 | 0.000 | 0.137 | 0.000 | 0.000 |
| 18 | 1.775 | 2.5 | −1 | 1 | 0.190 | 0.000 | 0.223 | 0.000 | 0.258 | 0.000 | 0.041 | 0.000 | 0.000 |
| 18 | 1.915 | 2.5 | −1 | 1 | 0.153 | 0.000 | 0.050 | 0.000 | 0.426 | 0.000 | 0.135 | 0.000 | 0.000 |
| 12 | 1.940 | 1.5 | −1 | 1 | 0.341 | 0.000 | 0.217 | 0.000 | 0.282 | 0.000 | 0.074 | 0.000 | 0.000 |
| 24 | 2.030 | 3.5 | −1 | 1 | 0.284 | 0.000 | 0.207 | 0.000 | 0.288 | 0.000 | 0.048 | 0.000 | 0.000 |
| 4 | 1.320 | 0.5 | −2 | 1 | 0.500 | 0.000 | 0.000 | 0.000 | 0.000 | 0.000 | 0.000 | 0.000 | 0.500 |
| 8 | 1.530 | 1.5 | −2 | 1 | 0.333 | 0.000 | 0.000 | 0.000 | 0.000 | 0.000 | 0.000 | 0.000 | 1.000 |
| 8 | 1.823 | 1.5 | −2 | 1 | 0.000 | 0.000 | 0.500 | 0.000 | 0.800 | 0.033 | 0.033 | 0.000 | 0.025 |
| 12 | 2.025 | 2.5 | −2 | 1 | 0.000 | 0.000 | 0.500 | 0.000 | 0.200 | 0.000 | 0.267 | 0.000 | 0.000 |
| 4 | 1.672 | 1.5 | −3 | 1 | 0.000 | 0.000 | 0.678 | 0.000 | 0.678 | 0.000 | 0.000 | 0.000 | 0.086 |

# Bibliography


[1] T. Abbot and the E802 Collaboration, Phys. Rev. C 50, 1024 (1994).

[2] J. Alam, S. Raha and B. Sinha, Phys. Rev. Lett. 73, 1895-1898 (1994).

[3] *Strangeness and Quark Matter*, eds. G. Vassiliadis, A.D. Panagiotou, S. Kumar and J. Madsen, Conference Proceedings (1-5 September 1994), World Scientific, ISBN 981-02-2269-6.

[4] T. Altherr and D. Seibert, Phys. Lett. 313B, 149-154 (1993) ; Erratum Phys. Lett. 316B, 633 (1993).

[5] T. Altherr, E. Petitgirard and T. del Río Gaztelurrutia, CERN-TH-7044/93 and ENSLAPP-A-441/93.

[6] T. Altherr, E. Petitgirard and T.del Río Gaztelurrutia, Phys. Rev. D47, 703 (1993).

[7] T. Altherr and D. Seibert, Phys. Rev. C49, 1684-1692 (1994).

[8] T. Altherr and P. Salati, Nucl. Phys. B421,662-682 (1994).

[9] T. Altherr, *Thermal Field Theories and their applications.* Proceedings, 3rd Workshop and summer school, Banff, Canada, 463-468 (1993). Edited by F.C. Khanna, H. Umezawa, R. Kobes, G. Kunstatter. World Scientific (1994).

[10] T. Altherr, Int.J.Mod.Phys. A8, 5605-5628 (1993).

[11] T. Altherr, Annals of Physics 207, 374-393 (1991).

[12] R. Anishetty, P. Koehler and L. McLerran, Phys. Rev. D 22, 2793-2804 (1980).

[13] M. N. Asprouli and A. D. Panagiotou, Phys. Rev. C51 (1995).

[14] P. Aurenche and T. Becherrawy, Nucl. Phys. B379, 259-303 (1992).

[15] R. Baier, H. Nakkagawa and A. Niégawa, Can. J. Phys. 71, 205 (1993).

[16] R. Baier, *Thermal Field Theories and their applications*. Proceedings, 3rd Workshop and summer school, Banff, Canada, 417-427 (1993). Edited by F.C. Khanna, H. Umezawa, R. Kobes, G. Kunstatter. World Scientific (1994).

[17] R. Baier, S. Peigne and D. Schiff, Z. Phys. C62, 337-342 (1994).

[18] R. Baier, H. Nakkagawa, A. Niégawa and K. Redlich, Z. Phys. C 53, 433-438 (1992).

[19] R. Baier and A. Niégawa, Phys. Rev. D49, 4107-4112 (1994).

[20] G. Baym B.L. Friman, J.-P. Blaizot, M. Soyeur and W. Czyż, Nucl. Phys. A407, 541-570 (1983).

[21] M. Le Bellac and D. Poizat, Z.Phys. C 47,125-131 (1990).

[22] N. Bilić, J. Cleymans, I. Dadić and D. Hislop, Phys. Rev. C52, 401-407 (1995).

[23] N. Bilić, J. Cleymans, E. Suhonen and D.W. von Oertzen, Phys. Lett. B311, 266-272 (1993).

[24] A. Billoire, G. Lazarides and Q. Shafi, Phys. Lett. 103B, 450 (1981).

[25] T. S. Biró and J. Zimányi, Phys. Lett. 113B, 6-10 (1982).

[26] T. S. Biró, P. Lévai and B. Müller, Phys. Rev. D42, 3078-3087 (1990).

[27] T. S. Biró and B. Müller, Nucl. Phys. A561, 477-500 (1993).

[28] T. S. Biró, Int.J.Mod.Phys., E1, 39-72 (1992).

[29] T. S. Biró, B. Müller and Xin-Nian Wang, Phys. Lett. B283, 171-173 (1992).

[30] T. S.Biró, E. van Doorn, B. Müller and X.-N. Wang, Phys. Rev. C 48, 1275-1284 (1993).

[31] J.D. Bjorken, Phys. Rev. D 27, 140-151 (1983).

[32] J.D. Bjorken and S.D. Drell, Relativistic Quantum Field Theory (1967).

[33] E. Braaten, Can. J. Phys. 71, 215-218 (1993).

[34] E. Braaten, R. D. Pisarski and Tzu Chiang Yuan, Phys. Rev. Lett. 64, 2242 (1990).

[35] E. Braaten and Tzu Chiang Yuan, Phys. Rev. Lett. 66, 2183-2186 (1991).

[36] E. Braaten and R. D. Pisarski, Nucl. Phys. B337, 569-634 (1990).

[37] E. Braaten and R. Pisarski, Phys. Rev. D 45, R1827-R1830 (1992).

[38] E. Braaten and R.D. Pisarski, Phys. Rev. D 42, ,2156-2160 (1990).

[39] E. Braaten and R.D. Pisarski, Nucl. Phys. B339, 311-324 (1989).

[40] P. Braun-Munzinger et al, Phys. Rev. Lett. B344, 43-48 (1995).

[41] C.P. Burgess and A.L. Marini, Phys. Rev. D 45, R17- 20 (1992).

[42] E. Byckling and K. Kajantie, *Particle Kinematics,* John Wiley and Sons.

[43] J. Cleymans, M.I. Gorenstein, J. Stålnake and E.Suhonen, Physica Scripta, 48, 277-280 (1993).

[44] J. Cleymans, E. Suhonen and G.M. Weber, Z. Phys. C 53, 485-491 (1992).

[45] J. Cleymans, Talk presented at the 25th Annual Seminar on Theoretical Physics, July 1990, Port Elizabeth, South Africa.

[46] J. Cleymans and D. W. von Oertzen, Phys. Lett. B 249, 511-513 (1990).

[47] J. Cleymans, V.V. Goloviznin and K. Redlich, BI-TP-94-48 (1994).

[48] J. Cleymans, R.V. Gavai and E. Suhonen, Physics Reports 130, 217-292 (1986).

[49] J. Cleymans, M.I. Gorenstein , J.Staålnacke and E. Suhonen, Phys.Scr. 48, 277-280, (1993).

[50] J. Cleymans and H. Satz, Z.Phys. C57, 135-147 (1993).

[51] J. Cleymans, K. Redlich, H. Satz and E. Suhonen, Z. Phys. C58, 347-356 (1993).

[52] *Phase Structure of Strongly Interacting Matter*, Ed J. Cleymans, Springer-Verlag ISBN 3-540-53138-6/ISBN 0-387-53138-6.

[53] F. Cooper, G. Frye and E. Schonberg, Phys. Rev. D 11, 192-213 (1975).

[54] B.L. Combridge, Nucl. Phys. B151, 429-456 (1979).

[55] R.E. Cutkosky, J. Math. Phys. 1, 429 (1960).

[56] P. Danielewicz and M. Gyulassy, Phys. Rev. D31, 53-62 (1985).

[57] N.J. Davidson, H.G.Miller, R.M.Quick and J.Cleymans, Phys. Lett. B255, 1, 105-109 (1991).

[58] D.W. von Oertzen, N.J. Davidson, R.A. Ritchie and H.G.Miller, Phys. Lett. B274, 128-132 (1992).

[59] T. A. DeGrand and D. Toussaint, Phys. Rev. D25, 526-530 (1982).

[60] L. Dolan and R. Jackiw, Phys. Rev. D9, 3320-3341 (1974).

[61] P. Elmfors and R. Kobes, Phys. Rev. D51, 774-780 (1995).

[62] J. Cleymans, D. Elliott, H. Satz and R.L. Thews, CERN-TH/95-298, AZPH-TH/95-26, BI-TP 95/35, UCT-TP 95/225.

[63] T.S. Evans, Phys. Rev. D 47, R4196-4198 (1993).

[64] A.L. Fetter and J.D. Walecka, *Quantum Theory of many particle systems,* New York, McGraw-Hill 1971.

[65] K. Geiger, Nucl. Phys. A566, 257c-268c (1994).

[66] K. Geiger, Phys. Rev. D46, 4965-4985 (1992).

[67] K. Geiger, Phys. Rev. D46, 4986-5005 (1992).

[68] K. Geiger and J.I. Kapusta, Phys. Rev. D47, 11, 4905-4819 (1993).

[69] V. Goloviznin and H. Satz, Z. Phys. C57, 671-676 (1993).

[70] M. I. Gorenstein and Yu.M. Sinyukov, Phys. Rev. Lett. 142B, 425-551 (1984) .

[71] B. Grossman et al, Nucl. Phys. B417, 289-306 (1994).

[72] R. Hagedorn and K. Redlich, Z. Phys. C27, 541-551 (1985).

[73] P.A. Henning R. Sollacher and H. Weigert, GSI-Preprint 94-56 and hep-ph 9409280 , Submitted to Phys. Rev. D.

[74] HELIOS Collaboration, CERN-PPE/92-130 (1992)

[75] U. Heinz, P. Koch, K.S. Lee, E. Schnedermann and H. Weigert, article in *Phase Structure of Strongly Interacting Matter* ed:J. Cleymans, Springer-Verlag Berlin, Heidelberg (1990).

[76] U. Heinz, K.S. Lee and M Rhoades-Brown, Phys. Rev. Lett. 58, 2292-2295 (1987).

[77] C. Itzykson and J.-B. Zuber, *Quantum Field Theory*, New York, Mcgraw-hill (1980).

[78] J. Joubert and J. Cleymans, Talk presented at the 25th Seminar on Theoretical Physics, July 1990, Port Elizabeth, South Africa.

[79] J. Joubert, PhD thesis, UCT 1992, *Finite Temperature Field Theory and the Structure Function of the Nucleon.*

[80] U. Kalmbach, T. Vetter, T.S. Biró and U. Mosel, Nucl. Phys. A563, 584-604 (1993).

[81] K. Kajantie, M. Kataja and P.V. Ruuskanen, Phys. Lett. B 179, (1986).

[82] U.M. Heller, F. Karsch, J. Rank, BI-TP 95/21, FSU-SCRI-95-53 (1995).

[83] R. L. Kobes and G. W. Semenoff, Nucl. Phys. B260, 714-747 (1985).

[84] R. L. Kobes and G. W. Semenoff, Nucl. Phys. B272, 329-364 (1986).

[85] R. Kobes, G. Kunstatter and K.W. Mak, Z. Phys. C 45 129-140 (1989).

[86] R. Kobes, Phys. Rev. D 42, 562-572 (1990).

[87] R.L. Kobes, G.W. Semenoff and N. Weiss, Z. Phys. C 29, 371-380 (1985).

[88] R. Kobes, Phys. Rev. Lett. 67, 1384-1387 (1991).

[89] P. Koch, B. Müller and J. Rafelski, Physics Reports, 142, 4, (1986).

[90] A. Kocić, Phys. Rev. D33, 1785-1794 (1986).

[91] V.V. Lebedev and A.V. Smilga, Phys. Lett. B 253, 12, 3 (1991).

[92] V.V. Lebedev and A.V. Smilga, Ann. Phys. 202, 229-270 (1990).

[93] K.S. Lee, M.J. Rhoades-Brown and U. Heinz, Phys. Rev. C37, 1452-1462 (1987).

[94] K.S. Lee, M.J. Rhoades-Brown and U. Heinz, Phys. Rev. C37, 1462-1472 (1987).

[95] J. Letessier, A. Tounsi, U. Heinz, J. Sollfrank and J. Rafelski, Phys. Rev. Lett. 70, 3530-3533 (1993).

[96] J. Letessier, A. Tounsi, U. Heinz, J. Sollfrank and J. Rafelski, Phys. Rev. D51, 3408-3435 (1995).

[97] W.J. Marciano, Phys. Rev. D12, 15 (1975).

[98] T. Matsui, B. Svetitsky and L. D. McLerran, Phys. Rev. D34, 783-793 (1986).

[99] T. Matsui, B. Svetitsky and L. D. McLerran, Phys. Rev. D34, 2047-2060 (1986).

[100] P. Braun-Munzinger, J. Stachel, J.P. Wessels, N. Xu, Phys. Lett. B344, 43-48 (1995).

[101] P. Braun-Munzinger, J. Stachel, J.P. Wessels, N. Xu, Phys. Lett. B365, 1-6 (1996).

[102] B. Müller, Rep. Prog. Phys. 58, 611-636 (1995).

[103] NA35 Collaboration, Z. Phys. C48, 191-200 (1990).

[104] NA36 Collaboration, Nucl. Phys. A553, 817c-820c (1993)

[105] NA35 Collaboration, Phys. Rev. Lett. 74. 1303-1306 (1995)

[106] W. H. Press, B. P. Flannery, S. A. Teukolsky and W. T. Vetterling *Numerical Recipes in Fortran.*

[107] *Review of Particles Properties*, Phys. Rev. D 50, 1173 (1994).

[108] G. Peressutti and B.-S. Skagerstam, Phys. Rev. Lett. 110B, 406-410 (1982).

[109] R. D. Pisarski, Phys. Rev. Lett. 63, 1129-1133 (1989).

[110] R. Pisarski, *Hot summer daze: QCD at nonzero temperature and density* Proceedings: BNL summer study 1991. Edited by By A. Gocksch, R. Pisarski. World Scientific (1992).

[111] R. D. Pisarski, Phys. Rev. D47, 5589 (1989).

[112] D. Prorork and L. Turko, Z.Phys C61, 109-114 (1994).

[113] *Proceedings of the Eleventh International Conference on Ultra-Relativistic Nucleus-Nucleus Collisions*, Nucl. Phys. A 590 (1995).

[114] *Proceedings of the Tenth International Conference on Ultra-Relativistic Nucleus-Nucleus Collisions*, Nucl. Phys. A 566 (1994).

[115] P.A. Henning and E. Quack, Phys. Rev. Lett. 75, 2811-2814 (1995).

[116] J. Rafelski and B. Müller, Phys. Rev. Lett. 48, 1066-1069 (1982) .

[117] J. Rafelski, Nucl. Phys. A418, 215c (1984).

[118] J. Rafelski, Nucl. Phys. A544, 279c-292 (1992).

[119] J. Rafelski, Phys. Rev. 88, 331-347 (1982).

[120] Ed. J. Rafelski, AIP Conference Proceedings 340, DOE CONF-950172 (1995).

[121] J. Rafelski, J. Letessier and A. Tounsi, Invited lecture at the 4th International Workshop on Relativistic Apects of Nuclear Physics (Rio de Janiero, Brazil, August 28-30, 1995).

[122] K. Redlich, J. Cleymans, H. Satz and E. Suhonen, Quark Matter 93, Nucl. Phys. A566 (1994), 391-394.

[123] K. Redlich, J. Cleymans, H. Satz and E. Suhonen, Z. Phys. C58, 347-356 (1993).

[124] D. H. Rischke, Y. Pürsün, J. A Maruhn, H. Stöcker and W. Greiner, CU-TP-695, nucl-th/9505014, (May 1995).

[125] L. H. Ryder, *Quantum Field Theory.*

[126] H. Satz, *Quark Matter and Nuclear Collisions - An Introduction to the Thermodynamics of Strongly Interacting Systems* (Draft) (1989).

[127] H. Satz, Phys. Rev. D19, 1912-1916 (1979).

[128] S. Schramm and W. Greiner, Int.J.Mod.Phys E, 1, 1, 73-94 (1992).

[129] D. Seibert and T. Altherr, Phys. Rev. D48, 3386-3387 (1993).

[130] D. Seibert and G. Fai, Phys. Rev. C50, 2532-2539 (1994).

[131] A. Shor, Phys. Lett. B215, 375 (1988).

[132] D. Srivastava, Private communication through B Sinha. Submitted to Annals of Physics.

[133] E. Shuryak, Phys. Rev. Lett. 68, 22, 3270-3272 (1992).

[134] C. Slotta, J. Sollfrank and U. Heinz, *Rapidity Dependence of Strange Particle Ratios in Nuclear Collisions* TPR-95-04, Preprint hep-ph/9504225 (1995).

[135] J. Sollfrank, M. Gaździcki, U. Heinz and J. Rafelski, Z. Phys. C61, 659-666, (1994).

[136] J.Sollfrank and U. Heinz, To be published in Quark Gluon Plasma 2, R.C. Hwa, editor, World Scientific, Preprint nucl-th/9505004.

[137] A. V. Smilga, Phys.Atom.Nucl 57, 519-531 (1994).

[138] G. Sterman, *Quantum Field Theory,.*

[139] NA35 Collaboration, Nucl. Phys. A525, 59c-66c, (1991).

[140] J.C. Taylor, Phys. Rev. D47, 15 (1993).

[141] M.H. Thoma, Phys. Lett. B269, 144-148 (1991).

[142] M.H. Thoma, Nucl. Phys. B 351, 491-506 (1991).

[143] L. Turko, Lectures given at NATO Advanced Study Workshop on Hot Hadronic Matter: Theory and Experiment (1994). Preprint hep-ph/9411346.

[144] G. 't Hooft and M. Veltman, *Diagrammar*, CERN yellow report (1973).

[145] G. 't Hooft, *"Diagrammar" and Dimensional Renormalisation* (1973).

[146] WA85 Collaboration, Phys. Lett. B270, 123-127 (1991).

[147] WA85 Collaboration, Phys. Lett. B316, 615-619 (1993).

[148] H.A. Weldon, Phys. Rev. D26 1394-1407 (1982).

[149] H.A. Weldon, Phys. Rev. D26, 2789 (1982).

[150] H.A. Weldon, Phys. Rev. D28, 2007-2015 (1983).

[151] H.A. Weldon, Phys. Rev. D 26, 2789-2796 (1982).

[152] H.A. Weldon, Phys. Rev. D 26, 1394-1407 (1982).

[153] H.A. Weldon, Phys. Rev. D47, 2759 (1983).

[154] H.A. Weldon, Phys. Rev. Lett. 66,3 (1991).

[155] H.A. Weldon, Phys. Rev. D 45, 352-355 (1992).

[156] H.A. Weldon, Phys. Rev. D 47, 594-600 (1992).

[157] H.A. Weldon, Phys. Lett. B 174, 427-428 (1986).

[158] H.A. Weldon, Phys. Rev. D 40, 2410-2420 (1989).

[159] H.A. Weldon, Ann.Phys. 228, 43-51 (1993).

[160] Ch. G. van Weert, *Thermal Field Theories and their applications.* Proceedings, 3rd Workshop and summer school, Banff, Canada, 1-25 (1993). Edited by F.C. Khanna, H. Umezawa, R. Kobes, G. Kunstatter. World Scientific (1994).

[161] S.M.H. Wong, Z. Phys. C 53, 465-477 (1992).

[162] D0 Collaboration Phys. Rev. Lett. 74, 2632-2637 (1995)

[163] CDF Collaboration Phys. Rev. Lett. 74, 2626-2631 (1995)

[164] E. Fermi, Progr. Theor. Phys. 5 (1950) 570.

[165] E. Fermi, Phys. Rev. 81 (1951) 683.

[166] L.D. Landau, in : D. Ter Haar (Editor) "Collected Papers of L.D. Landau", page 665, Gordon and Breach, New York , 1965. Original papers : Izv. Akad. Nauk. SSSR 17, 51 (1953); S. Belenkij and L.D. Landau, Ups. Fiz. Nauk. 56, 309, (1955) and Novo Cimento Suppl 3, 15 (1956).

[167] I. Pomeranchuk, Dokl. Akad. Nauk. SSR, 78 (1951) 889.

[168] R. Hagedorn, in "Hot Hadronic Matter", Eds. J. Letessier, H.H. Gutbrod and J. Rafelski, Rafelskilenum Press, 1994.

[169] For references to Silin see references in [9].

[170] For references to Klimov see references in [9].

[171] N. Bilić, J. Cleymans, I. Dadić and D. Hislop *Perspectives in Particle Physics* Proceedings of the 7th Aduatic Meeting on Particle Physics Brijuni, Croatia, Editors D. Klabucar, I. Picek and D. Tadić, World Scientific, 1995